



Prifysgol
Abertawe
Swansea
University

Enzymes-encapsulated hydrogels for Electrochemiluminescence (ECL) sensing applications.

by

Lucia Simona Ferraraccio

Thesis

Submitted to Swansea University

For the degree of

Doctor of Philosophy

Supervisor: Dr. Paolo Bertoncello

Department of Chemical Engineering

School of Engineering and Applied Science

Swansea University, February 2022



Ysgoloriaethau Sgiliau Economi Gwybodaeth
Knowledge Economy Skills Scholarships



Ysgoloriaeth Sgiliau Economi Gwybodaeth (KESS) yn Gymru gyfan sgiliau lefel uwch yn fenter a arweinir gan Brifysgol Bangor ar ran y sector AU yng Nghymru. Fe'i cyllidir yn rhannol gan Gronfeydd Cymdeithasol Ewropeaidd cydgyfeirio ar gyfer Gorllewin Cymru a'r Cymoedd.

Knowledge Economy Skills Scholarships (KESS) is a pan-Wales higher level skills initiative led by Bangor University on behalf of the HE sectors in Wales. It is part funded by the Welsh Government's European Social Fund convergence programme for West Wales and the Valleys.

This work is part funded by the Welsh Government's European Social Fund convergence programme for West Wales and the Valleys.



PERPETUUS
advanced materials

Summary

Nowadays, the development of innovative biosensors based on non-invasive techniques for a reliable and precise real time detection of vital parameters has become the new frontier for the scientific research. In this thesis, a novel prototype of ECL-based biosensor involving different enzymes is proposed.

The primary aim of this project was to determine the possibility to apply an ECL approach to encapsulated and immobilised enzymes for the detection of their activity. Particular attention has been placed on the encapsulation of enzymes to maintain their catalytic properties unaffected. Alginate hydrogels and cryogels have been used as matrices for the encapsulation and the development of an amperometric ECL-based biosensor. Both the entrapment processes have been deeply described and their characterisation is reported.

The first ECL-based biosensor examined regards the oxidase enzymes and luminol system. It is well established that the oxidase activity can be determined by measuring the amount of H_2O_2 produced by the redox reaction between the encapsulated enzyme and its corresponding substrate. The utilisation of luminol is determinant for the ECL emission by reacting with the produced hydrogen peroxide, hence for the investigation of the enzymatic reaction. Different aspects of the oxidase-luminol system have been deepened, including the statistical analysis, Michaelis-Menten study, limits of detection and quantification, interferences, and real sample analysis.

The second system disclosed in this thesis regards the ECL-based biosensor concerning the employment of dehydrogenase enzymes, $[\text{Ru}(\text{bpy})_3]^{2+}$ and NAD^+ . These enzymes have been successfully encapsulated into alginate hydrogel matrices following the same procedure adopted for the encapsulation on the oxidase group. Likewise, the electrochemical analysis is reported showing the cyclic voltammetry and ECL results, the statistical analysis obtained from the study of mean and standard deviation of three repetitions for each enzyme leading to the final considerations regarding Michaelis-Menten parameters, limits of detection and quantification.

The last section of this work is dedicated to the improvement of the proposed biosensors by examining the electro-polymerisation of the two luminophores. Firstly, the electro-polymerisation of the luminol for the generation of polyluminol is proposed with particular attention on the development of a bilayer system composed of a first layer of ECL-active

polymer on the GCE surface and a second layer obtained with the deposition of the encapsulated enzyme to be analysed. Different essential aspects for a successful electro-polymerisation have been discussed namely different scan rates, number of scans, supporting electrolytes and electrolytic solution. The electrochemical analysis is also reported showing a very efficient detection of the different enzymatic activities (glucose oxidase, lactate oxidase, Horseradish peroxidase and cholesterol oxidase) through the generation of H_2O_2 and the consequent reaction with the polyluminol film. The statistical analysis of the bilayer systems is brought showing the promising results of this novel ECL-biosensor.

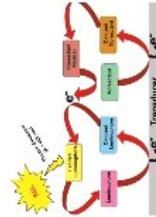
Finally, preliminary results are mentioned regarding the development of a new ECL-active film, not yet reported in literature, gained by applying the electro-polymerisation to $[Ru(bpy)_3]^{2+}$. In like manner, the main features have been investigated to achieve a highly performant ECL-active film on the GCE surface such as different scan rates effect, number of scans and very determinant the supporting electrolyte and solvent used to form the ideal electrolytic solution for the generation of the here named Poly- $[Ru(bpy)_3]^{2+}$. The UV and FTIR characterisation are proposed leading to the discovery of the oligomeric nature of the electro-polymerised film. Preliminary electrochemical tests have been performed by building a bilayer system with the Poly- $[Ru(bpy)_3]^{2+}$ layer and the superimposed alginate hydrogels containing dehydrogenase enzymes. Multiple aspects of this newfound material still need to be investigated and further explored.

Chapter 1	Chapter 2	Chapter 3	Chapter 4	Chapter 5	Chapter 6	Chapter 7	Chapter 8	Chapter 9
-----------	-----------	-----------	-----------	-----------	-----------	-----------	-----------	-----------

Introduction

Theory:

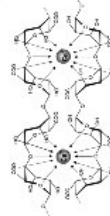
1. Electrochemistry
2. Mass transfer
3. Electrical double layer
4. ECL pathways
5. Electron transfer reaction
6. Cyclic voltammetry
7. Workstation
8. Biosensors



Encapsulation techniques

Hydrogels

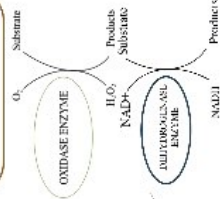
1. Immobilisation techniques
2. Microspheres
3. Layer-by-layer process
4. Alginate hydrogels as biomaterials



ECL main features

Features

1. Enzymes: Oxidase & Dehydrogenase
2. Luminophores: Luminol & $[Ru(bpy)_3]^{2+}$
3. Co-reactants
4. Electrochemical cell: 3-electrodes configuration



Experimental approaches and methods

Methods and materials

1. Chemicals
2. Cleaning process of GCE
3. Enzymes encapsulation in alginate hydrogel procedure
4. Characterisation of alginate hydrogels

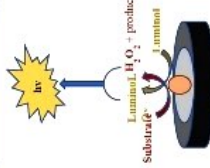


Experimental results

Luminol-H₂O₂ systems
Hydrogels

Hydrogel Systems

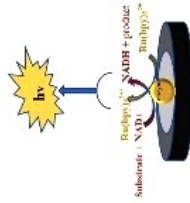
1. HRP-H₂O₂
 2. Gox-Glucose
 3. Lox-Lactic Acid
 4. ChOX-Cholesterol
- ❖ ECL-CV
 - ❖ Michaelis-Menten
 - ❖ LOD&LOQ
 - ❖ Interferences
 - ❖ Real sample



[Ru(bpy)₃]²⁺ and dehydrogenase system
Cryogels

Cryogel systems

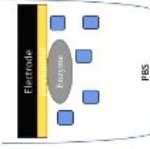
- ❖ Fabrication & characterisation of Cryogels (collaboration University of Cardiff)
- ❖ Electrochemical experiments with Oxidase enzymes



Electro-polymerisation

Technique

1. General principles
2. Poly-luminol process
3. Electrochemical characterisation
4. Preliminary: Poly-Ru(bpy)
5. Electrochemical tests



Conclusions


Abstract

Nowadays, the need of real time self-monitoring of physiological parameters such as glucose, cholesterol and lactic acid has become the new frontier in the research field. Multiple types of tests are used for the diagnosis of diseases such as diabetes, hypercholesterolemia, and cancer throughout blood testing. Self-monitoring of body fluids such as saliva, sweat and urine represents a novel non-invasive method for the control and prevention of pathological conditions. The main objective of this thesis is to develop an electrochemical biosensor to help the patient in self-monitor key health analytes in order to control and even prevent potential disorders. As such, it has become inevitable to develop an efficient biosensor, applicable to a range of biological recognition element (enzyme). Therefore, the development of an electrochemiluminescent (ECL) biosensor is described in this thesis, utilising the two traditional luminol and $[\text{Ru}(\text{bpy})_3]^{2+}$ luminophores. ECL has been largely used as a detection approach of biological molecules of interest because of its high sensitivity and sensitivity, good signal to noise ratio, control over space and time of the reaction. These benefits have allowed the use of this technique over other detection techniques for the development of a range of ECL-based sensors. The biosensor was successfully applied for the detection of glucose, lactic acid, cholesterol, and ethanol at clinically appropriate concentrations and tested in semi-real samples (contact lenses liquid and artificial sweat solution). For this sensor, modified glassy carbon electrodes with alginate hydrogels and cryogels were prepared and tested throughout the use of voltammetric and electrochemiluminescence detection methods. Alginate hydrogels and cryogels were chosen as immobilisation matrices for their properties of biocompatibility, biodegradability, low cost, mild gelation conditions and simplicity of realisation. With the encapsulation technique described also in this thesis, the enzymatic bioactivity, stability and specificity were retained showing a good ECL signal as result of the redox reactions occurring between the immobilised enzyme and the corresponding substrate. Moreover, to test the specificity of the sensor, the different enzymes were investigated in the presence of different interferent species that are present in human fluids such as ascorbic acid, and uric acid. Finally, the performances of the biosensor were improved by depositing a film of luminophore on the electrode surface using the electropolymerisation technique. Previous works used the same method to obtain a

polyluminol film on different electrodes (screen printed electrode, indium tin oxide, platinum electrode) and tested its ECL properties in the presence of hydrogen peroxide. In addition to the polyluminol, a novel polymerisation of $[\text{Ru}(\text{bpy})_3]^{2+}$ is proposed obtaining an ECL-active thin film of the electrode surface.

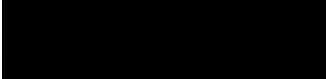
Declaration

This work has not previously been accepted in substance for any degree and is not being concurrently submitted in candidature for any degree.

Signed 

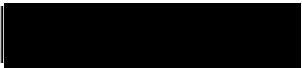
Date 08-02-2022

This thesis is the result of my own investigations, except where otherwise stated. Other sources are acknowledged by footnotes giving explicit references. A bibliography is appended.

Signed 

Date 08-02-2022

I hereby give consent for my thesis, if accepted, to be available for photocopying and for inter-library loan, and for the title and summary to be made available to outside organizations.

Signed 

Date 08-02-2022

The University's ethical procedures have been followed and, where appropriate, that ethical approval has been granted.

Signed 

Date 08-02-2022

Table of contents

Summary	3
Abstract	6
Declaration	8
Table of contents	9
List of tables	12
List of figures	13
Abbreviation	21
Acknowledgements	24
Publications	26
Conferences attended	27
Chapter 1: Introduction	28
1. State of art	28
1.2 Fundamentals of electrochemistry	30
1.3 Mass Transfer	33
1.3.1 Diffusion	35
1.3.2 Migration.....	36
1.3.3 Convection	37
1.4 Electrode-solution interface: electrical double layer	38
1.5 Type of luminescence	40
1.6 Electrogenerated chemiluminescence (ECL)	43
1.6.1 Pathways of ECL	45
1.6.2 Electron transfer reaction	52
1.6.3 Fundamentals of ECL.....	58
1.7 Cyclic voltammetry	61
1.8 Biosensors	65
1.8.1 Amperometric biosensors	66
1.9 Conclusions	69
Chapter 2: Encapsulation of enzymes into alginate hydrogels	70
2.1 Enzymes encapsulation techniques: literature review	70
2.2 Encapsulation techniques	72
2.2.1 Entrapment	73
2.2.2 Encapsulation	74
2.2.3 Cross-Linking	75
2.2.4 Covalent Bonding	76
2.2.5 Adsorption	77
2.3 CaCO₃ microspheres	78
2.4 Alginate hydrogels as biomaterial	80
2.5 Conclusions	82
Chapter 3: ECL main features	83
3.1 Enzymes	83

3.1.1 Enzyme Kinetics.....	86
3.1.2 Oxidase.....	90
3.1.3 Dehydrogenase	91
3.2 Luminophores.....	93
3.2.1. Luminol	93
3.2.2. Tris(bipyridine)ruthenium(II) chloride.....	95
3.3 Co-reactant	98
3.4 Working electrode	99
5. Conclusions.....	102
<u>Chapter 4: Experimental approaches and methods.....</u>	<u>103</u>
4.1 Chemicals.....	103
4.2 Cleaning process of GCE	105
4.3 Enzyme-encapsulation in alginate hydrogels procedure.....	106
4.3.1 Characterisation of the alginate hydrogels	109
4.4 Electrochemical experiments	111
4.4.1. Workstation.....	111
4.4.2. Measurements protocol.....	117
4.5 Conclusions	118
<u>Chapter 5: Luminol – H₂O₂ system</u>	<u>119</u>
5.1 Luminol- H₂O₂ system: introduction	119
5.2 Description of the system.....	124
5.3 Role of pH in electrochemical measurements	126
5.4 Characterisation of the biosensor: Randless-Sevcik equation.....	129
5.5 Result and discussion	133
5.4.1. HRP-luminol-H ₂ O ₂ system	133
5.4.2 GOx -luminol-glucose system.....	137
5.4.3 LOx-lumino-L-lactic acid system	141
5.4.4 ChOx-luminol-cholesterol system	146
5.5 Michaelis-Menten kinetics study	152
5.6 Limit of detection and limit of quantification study	155
5.7 Interference’s study.....	157
5.8 Real sample tests	159
5.9 Conclusions.....	163
<u>Chapter 6: Luminol and oxidase encapsulated into cryogels.....</u>	<u>164</u>
6.1 Cryogels: introduction	164
6.2 Description of the system.....	166
6.3 Characterisation of the material	168
6.4 Characterisation of the biosensor: Randles-Sevcik equation	171
6.5 Results and discussion.....	173
6.5.1 HRP-luminol-H ₂ O ₂ cryogel system.....	173
6.5.2 GOx -luminol-glucose cryogel system	175

6.5.3 LOx-luminol-lactic acid cryogel system.....	177
6.5.4 ChOX-luminol-cholesterol cryogel system.....	179
6.6 Michaelis-Menten kinetics study	181
6.7 Limit of detection and limit of quantification study	182
6.8 Study of the duration	183
6.9 Real sample study	184
6.10 Conclusions	188
<u>Chapter 7: [Ru(bpy)3]2+ and dehydrogenase system</u>	<u>189</u>
7.1 [Ru(bpy)3] 2+-NADH system: introduction.....	189
7.2 Description of the system.....	192
7.3 Characterisation of the biosensor: Randles-Sevcik equation	196
7.4 Results and discussion.....	198
7.4.1 ADH-[Ru(bpy)3]2+-NADH system	198
7.4.2 GDH-[Ru(bpy)3]2+-NADH system.....	203
7.4.3 LDH-[Ru(bpy)3]2+-NADH system.....	206
7.4.4 ChDH-[Ru(bpy)3]2+-NADH system	209
7.5 Michaelis-Menten kinetics study	213
7.6 Limit of detection and limit of quantification study	215
7.7 Conclusions.....	216
<u>Chapter 8: Electro-polymerisation</u>	<u>217</u>
8.1 General principles	217
8.2 Modified GCE with polyluminol.....	224
8.2.1 Luminol electro-polymerisation	225
8.3 Polyluminol: Results and Discussion	236
8.3.1 HRP-polyluminol-H2O2 hydrogel bilayer system.....	237
8.3.2 GOx-polyluminol-glucose hydrogel bilayer system	238
8.3.3 LOx-polyluminol-lactic acidhydrogel bilayer system.....	239
8.3.4 ChOx-polyluminol-cholesterol hydrogel bilayer system	240
8.3.5 Comparison luminol-polyluminol.....	241
8.3.6 HRP-polyluminol-H2O2 cryogel bilayer system	243
8.3.7 GOx-polyluminol-glucose cryogel bilayer system.....	244
8.3.8 LOx-polyluminol- L-lactic acid cryogel bilayer system	245
8.3.9 ChOx-polyluminol- cholesterol cryogel bilayer system	246
8.3.10 Comparison luminol-polyluminol cryogel bilayer system	247
8.4 Modified GCE with Poly-[Ru(bpy)3]2+	248
8.4.1 [Ru(bpy)3]2+ electro-polymerisation	249
8.4.2 Characterisation of the material: polymer or oligomer?	252
8.5 Poly-[Ru(bpy)3]2+ -dehydrogenase system: Preliminary results.....	255
8.6 Conclusions.....	257
<u>Chapter 9: Conclusions and further investigations.....</u>	<u>259</u>

List of tables

TABLE 1: DIFFERENT TYPES OF LUMINESCENCE WITH THE CORRESPONDING REACTIONS THAT TRIGGER THE EMISSION OF LIGHT	34
TABLE 2: LIST OF THE DIFFERENT GROUPS OF ENZYMES AND THEIR CORRESPONDING ACTIVITY	77
TABLE 3: SUMMARY OF THE OXIDASE ANALYSED IN THIS WORK SPECIFYING THE SOURCE AND THE REACTION WITH THE CORRESPONDING SUBSTRATE	81
TABLE 4: DEHYDROGENASE ENZYMES ANALYSED IN THIS WORK.	83
TABLE 5: COMMONLY USED WORKING ELECTRODES WITH THEIR ADVANTAGES AND DISADVANTAGES LISTED.....	92
TABLE 6: LIST OF SOLVENTS AND CHEMICALS USED DURING THE EXPERIMENTAL ACTIVITY.....	94
TABLE 7: VALUES OF THE CHOLESTEROL RANGE OBTAINED FROM THE NATIONAL CHOLESTEROL EDUCATION PROGRAM.....	135
TABLE 8 VALUES OF THE MICHAELIS-MENTEN APPARENT FOR THE SYSTEMS STUDIED.....	142
TABLE 9 THEROETICAL VALUES OF LOD AND LOQ OF THE FOUR SYSTEMS ANALYSED USING THE OXIDASE ENZYMES ENCAPSULATED INTO ALGINATE HYDROGELS.....	144
TABLE 10 THEORETICAL VALUES FOR THE LOQ AND LOD FOR EACH ENZYME ENCAPSULATED INTO CRYOGELS MATRICES.....	168
TABLE 11 MICHAELIS-MENTEN MODEL STUDIED FOR THE DEHYDROGENASE ENZYMES SYSTEM	197
TABLE 12 THEORETICAL LIMIT OF DETECTION AND LIMIT OD QUANTIFICATION STUDY FOR THE DEHYDROGENASE SYSTEMS STUDIED. ... 199	
TABLE 13 COMBINATION OF SOME SUPPORTING ELECTROLYTE WITH MEDIUMS MERISATION.....	203

List of figures

FIGURE 1: PROTOTYPE OF THE FIRST FUEL CELL PROPOSED BY GROVE IN 1839[7].....	24
FIGURE 2: SCHEMATIC REPRESENTATION OF THE STEPS THAT ESTABLISH AN ELECTRODE REACTION: (1) MASS TRANSPORT, (2) CHEMICAL REACTION BETWEEN THE SPECIES, (3) SURFACE REACTIONS AND (4) ELECTRON TRANSFER REACTION.....	25
FIGURE 3: MOLECULAR PROCESS OF ELECTRON TRANSFER REACTION AT THE ELECTRODE SURFACE.....	27
FIGURE 4: REPRESENTATION OF THE THREE MODES OF MASS TRANSFER [16].	28
FIGURE 5: REPRESENTATION OF THE DIFFUSION PROFILES DEPENDING ON THE ELECTRODE SIZE: THE PLANAR DIFFUSION HAPPENING AT MACROELECTRODE (LEFT) AND THE RADIAL DIFFUSION FOR ULTRAMICROELECTRODES (RIGHT).	30
FIGURE 6: HELMHOLTZ MODEL SHOWING A RIGID INTERACTION BETWEEN THE TWO PHASES (A), GOUY-CHAPMAN MODEL WITH THE FORMATION OF THE DIFFUSE-LAYER (B) AND STERN'S MODEL WITH THE COMBINATION OF THE HELMHOLTZ LAYER AT THE ELECTRODE SURFACE AND THE DIFFUSION-LAYER IN THE BULK SOLUTION (C).	33
FIGURE 7: SCHEMATIC REPRESENTATION OF THE GRAHAME MODEL OF THE ELECTRICAL DOUBLE LAYER (A) AND THE BOCKRIS, DEVANATHAN AND MULLEN CONSIDERING THE PARTIALLY ADSORBED ION ON THE ELECTRODE SURFACE (B).....	33
FIGURE 8: CHEMILUMINESCENT OF LUMINOL OBTAINED BY REACTING WITH THE HYDROGEN PEROXIDE. (HTTPS://PHYSICOPENLAB.ORG/2019/02/06/LUMINOL-2/ . ACCESSED 15 JUNE 2021).	35
FIGURE 9: SCHEMATIC REPRESENTATION OF THE ABSORPTION BY INCREASING THE ENERGY LEVEL OF A PHOTON (A) AND THE EMISSION OF A PHOTON AFTER A DECREASE OF ENERGY LEVEL FROM E_2 TO E (B).	35
FIGURE 10: SCHEMATIC DESCRIPTION OF THE ENERGY LEVELS FOR ELECTRON IN ATOMS.	36
FIGURE 11: SCHEMATIC REPRESENTATION OF THE GENERAL PRINCIPLES FOR A) CHEMILUMINESCENCE AND B) ELECTROCHEMILUMINESCENCE [24].	37
FIGURE 12: MIAO'S TIMELINE OF THE ECL PROGRESS AS REPORTED IN THE LITERATURE [23].....	38
FIGURE 13: SCHEMATIC DIAGRAM OF THE DIFFERENT PATHWAYS ADOPTED TO PRODUCE ECL SIGNALS.	39
FIGURE 14: STRUCTURE OF $[Ru(BPY)_3]^{2+}$ AND ANNIHILATION MECHANISM FOR $[Ru(BPY)_3]^{3+}/[Ru(BPY)_3]^{2+}$ [44].	41
FIGURE 15: SCHEMATIC REPRESENTATION OF THE ELECTRON-TRANSFER REACTION BETWEEN THE ELECTROGENERATED RADICAL IONS FOR S-ROUTE ANNIHILATION	42
FIGURE 16: SCHEMATIC REPRESENTATION OF A POSSIBLE CONFIGURATION OF THE TRIPLET STATE FORMATION. "T-ROUTE" ANNIHILATION PATHWAY.	42
FIGURE 17: SCHEME FOR THE CO-REACTANT MECHANISM OF $[Ru(BPY)_3]^{2+}/TPRA$ SYSTEM [50].	44
FIGURE 18: SCHEMATIC REPRESENTATION OF THE CO-REACTANT PATHWAY TO PRODUCE ECL.....	45
FIGURE 19: SCHEMATIC PERRIN-JABLONSKY DIAGRAM. REPRESENTATION OF ENERGY LEVELS AND MOLECULAR ORBITALS DURING THE ABSORPTION AND EMISSION OF RADIATION [51].	46
FIGURE 20: POSSIBLE SCENARIO WITH THE ABSORPTION (PURPLE LINE), INTERNAL CONVERSION (GREEN LINE) AND VIBRATIONAL RELAXATION (BLUE LINE) PROCESSES [51].	47
FIGURE 21: POSSIBLE SCENARIO WITH THE ABSORPTION (PURPLE LINE), INTERNAL CONVERSION (GREEN LINE), VIBRATIONAL RELAXATION (BLUE LINE) AND FLUORESCENCE (RED LINE) PROCESSES [51].	47
FIGURE 22: POSSIBLE SCENARIO WITH THE ABSORPTION (PURPLE LINE), INTERNAL CONVERSION (GREEN LINE), VIBRATIONAL RELAXATION (BLUE LINE), INTERSYSTEM CROSSING (BROWN LINE) AND PHOSPHORESCENCE (PINK LANE) PROCESS [51].	48
FIGURE 23: SCHEMATIC REPRESENTATION OF (A) REDUCTION AND (B) OXIDATION REACTIONS WITH THE LUMO AND HOMO CONFIGURATION.	50
FIGURE 24: TYPICAL CYCLIC VOLTAMMOGRAM FOR A REVERSIBLE REDOX COUPLE THAT FORMS STABLE REDUCED AND OXIDIZED IONS WITH THE APPLICATION OF A SUITABLE POTENTIAL AT THE WORKING ELECTRODE.	51
FIGURE 25: MOLECULAR ORBITAL DIAGRAM REPRESENTING THE TWO ELECTRON TRANSFER REACTION ROUTES. ROUTE A LEADS TO THE FORMATION OF THE EXCITED STATE, MEANWHILE ROUTE B FORMS TWO GROUND STATE MOLECULES. ADAPTED FROM [57, 58].	53
FIGURE 26: CYCLIC VOLTAMMETRY TRIANGULAR WAVEFORM (TOP) AND THE CORRESPONDING VOLTAMMOGRAM SHOWING THE OXIDATION AND REDUCTION CURVES (BOTTOM) [63].	56
FIGURE 27: CYCLIC VOLTAMMETRY OF 10 mM POTASSIUM FERRICYANIDE IN KCl AT 0.05 V/S SCAN RATE. THE OXIDATION AND REDUCTION PEAKS ARE AT 0.18 V AND 0.27 V RESPECTIVELY.	57
FIGURE 28: VOLTAMMOGRAMS SHOWING HOW THE DIFFERENCE SCAN RATES AFFECT THE PEAK CURRENTS [67].	58
FIGURE 29: MAIN COMPONENTS OF A GENERAL BIOSENSOR.	59
FIGURE 30: CLASSIFICATION OF THE DIFFERENT BIOSENSORS DEPENDING ON THE TYPE OF TRANSDUCER.	59
FIGURE 31: SCHEMATIC REPRESENTATION OF THE WORKING PRINCIPLE OF THE FIRST GENERATION OF BIOSENSORS [76].	61

FIGURE 32: SECOND GENERATION OF THE AMPEROMETRIC BIOSENSOR SHOWING THE MEDIATOR ACTING AS ELECTRONS CARRIER FOR THE ELECTRON TRANSFER REACTION [76].	61
FIGURE 33: THIRD GENERATION OF BIOSENSORS WHERE THE ELECTRONS ARE DIRECTLY TRANSFERRED FROM THE ENZYME TO THE ELECTRODE SURFACE [76].	62
FIGURE 34: SCHEME OF THE DIFFERENT ENZYME IMMOBILISATION STRATEGIES, (COPYRIGHT CREATIVE ENZYMES®) [111].	66
FIGURE 35: ENZYME IMMOBILISATION STRATEGY: ENTRAPMENT.	66
FIGURE 36: ENZYME IMMOBILISATION STRATEGY: ENCAPSULATION.	67
FIGURE 37: ENZYME IMMOBILISATION STRATEGY: CROSS-LINKING	68
FIGURE 38: ENZYME IMMOBILISATION STRATEGY: COVALENT BONDING.	69
FIGURE 39: ENZYME IMMOBILISATION STRATEGY: ADSORPTION.	69
FIGURE 40: STRUCTURES OF THE THREE POLYMORPHS OF CALCIUM CARBONATE, A) ARAGONITE, B) VATERITE AND C) CALCITE. (REPRINTED, COPYRIGHT ELSEVIER) [133].	71
FIGURE 41: CHEMICAL STRUCTURE OF THE TWO MONOMERS AND OF THE BLOCK'S DISTRIBUTION FOR THE OBTAINMENT OF THE ALGINATE SALT. (COPYRIGHT JOURNAL AND BIOLOGICAL ENGINEERING) [141].	72
FIGURE 42: ENCAPSULATION FOR THE Ca^{2+} CATION INTO THE POLYMERIC CHAIN OF ALGINATE FORMING THE HYDROGELS BY CROSS-LINKING PROCESS [139].	73
FIGURE 43: REPRESENTATION OF THE ENZYME-CATALYSED EXOTHERMIC REACTIONS (LEFT) AND ENDOTHERMIC REACTIONS (RIGHT) WITH THE RELATIONSHIP BETWEEN THE ACTIVATION ENERGY AND THE ENTHALPY (ΔH) [143].	75
FIGURE 44: ENERGY DIAGRAM OF REDOX REACTIONS COUPLING AN EXOTHERMIC AND ENDOTHERMIC REACTION AND OBTAINING A FINAL EXOTHERMIC SPONTANEOUS REACTION [143].	76
FIGURE 45: SATURATION CURVE OF THE ENZYME-SUBSTRATE REACTION SHOWING THE MICHAELIS-MENTEN CONSTANT AT THE 50% OF THE REACTION RATE.	78
FIGURE 46: LINEWEAVER-BURK PLOT FOR THE CALCULATION OF THE KINETICS PARAMETERS.	80
FIGURE 47: SCHEMATIC REACTION BETWEEN OXIDASE ENZYMES AND THEIR SPECIFIC SUBSTRATE TO PRODUCE HYDROGEN PEROXIDE AND THE PRODUCTS OF THE REACTION	81
FIGURE 48: REACTION BETWEEN NAD^+ AND $NADH$ [159].	83
FIGURE 49: STRUCTURE OF LUMINOL $C_8H_7N_3O_2$. ADAPTED FROM [168].	84
FIGURE 50: TYPICAL BLUE COLOUR OF THE CHEMILUMINESCENCE OF LUMINOL WHEN IN CONTACT WITH AN OXIDIZING REAGENT LIKE HYDROGEN PEROXIDE. (© ROYAL SOCIETY OF CHEMISTRY 2022).	85
FIGURE 51: CHEMILUMINESCENCE OF LUMINOL [171].	86
FIGURE 52: STRUCTURE OF $[Ru(BPY)_3]^{2+}$.	87
FIGURE 53: SCHEME REPRESENTING THE REDUCTIVE-OXIDATION PROCESS OF RUTHENIUM USING $S_2O_8^{2-}$ AS CO-REACTANT. ADAPTED FROM [178].	88
FIGURE 54: DESCRIPTION OF THE OXIDATIVE-REDUCTION AND ANNIHILATION PROCESSES WITH THE USE OF TPRA AS CO-REACTANT. ADAPTED FROM [178].	89
FIGURE 55: CO-REACTANT ECL FOR THE TWO SYSTEMS ANALYSED IN THIS THESIS. $NADH$ FOR THE $[Ru(BPY)_3]^{2+}$ SYSTEM (LEFT) AND HYDROGEN PEROXIDE (RIGHT) FOR THE LUMINOL SYSTEM.	90
FIGURE 56: MOST USED WORKING ELECTRODE MATERIALS (WITH PERMISSION OF IJ CAMBRIA).	91
FIGURE 57: MECHANICAL POLISHING PROCEDURE USING THE FIGURE-EIGHT MOTION IN ORDER TO REMOVE EVENLY ALL THE PARTICLES ON THE ELECTRODE SURFACE[190].	97
FIGURE 59: CHEMICAL STRUCTURE OF THE ANIONIC CHARGED POLYMER PDDA (LEFT) AND THE CATIONIC CHARGED POLYMER PSS (RIGHT) USED FOR THE LAYER-BY-LAYER PROCESS [132].	98
FIGURE 60: ENZYME ENCAPSULATED INTO MICROSPHERES CORES AND LAYER-BY-LAYER PROCEDURE BY ALTERNATING THE PSS AND PDDA OBTAINING THE FINAL CATIONIC CHARGED LAYER.	98
FIGURE 61: MODIFIED GCE WITH THE DEPOSITION OF ALGINATE HYDROGELS. A) FIRST DRYING AT ROOM TEMPERATURE FOR 1 HOUR OF THE DEPOSITED GEL; B) CROSS-LINKING PROCESS STARTED BY DEPOSITION OF GDL ON THE HYDROGELS; C) SECOND DRYING AT ROOM TEMPERATURE FOR 12 HOURS.	99
FIGURE 62: CONFOCAL IMAGING WAS ACQUIRED WITH LEICA TCS SP5 TANDEM DMI6000 (LEICA MICROSYSTEMS CMS, MANNHEIM, GERMANY) INVERTED CONFOCAL LASER SCANNING MICROSCOPE COUPLED WITH LEICA IRAPO 25x, 0.95 NA WATER IMMERSION OBJECTIVE AND LEICA 63xPL APO1.4 NA IMMERSION OBJECTIVE AND LEICA 63xPL APO1.4 NA IMMERSION OBJECTIVE AND LEICA 63xPL APO1.4 NA OIL IMMERSION OBJECTIVE (LEICA MICROSYSTEMS, MANNHEIM, GERMANY). SCALE BAR: 4 μm .	100

FIGURE 63: A) MAX INTENSITY PROJECTION OF 500 MM Z-STACK OF MICROCAPSULES EMBEDDED INTO ALGINATE HYDROGEL; B) MAX INTENSITY PROJECTION OF 300 MM Z-STACK OF MICROCAPSULES EMBEDDED INTO ALGINATE HYDROGEL; C) MAX INTENSITY PROJECTION OF A SINGLE MICROCAPSULE EMBEDDED INTO ALGINATE HYDROGEL. SCALE BAR: 4 MM.	101
FIGURE 64: A) VOLUMETRIC REPRESENTATION (XYZ) OF MICROCAPSULES DISPERSION INTO ALGINATE HYDROGEL (z= 500 MM), B) VOLUMETRIC REPRESENTATION (XYZ) OF MICROCAPSULES DISPERSION INTO ALGINATE HYDROGEL (z= 300 MM).	101
FIGURE 65: SCHEMATIC REPRESENTATION OF THE THREE-ELECTRODES CONFIGURATION OF AN ELECTROCHEMICAL CELL USED FOR THE ECL EXPERIMENTS. (COPYRIGHT 2017 THE AMERICAN CHEMICAL SOCIETY AND DIVISION OF CHEMICAL EDUCATION, INC.) [63].	102
FIGURE 66: A) GLASSY CARBON ELECTRODE USED AS WE, B) Ag/AgCl REFERENCE ELECTRODE AND C) PLATINUM WIRE AS CE. SCHEMATIC REPRESENTATION OF THE THREE-ELECTRODE ELECTROCHEMICAL CELL (LEFT), ELECTROCHEMICAL GLASS CELL USED FOR THE ECL TESTS (RIGHT).	103
FIGURE 67: CH INSTRUMENT POTENTIOSTAT 705E MODEL USED FOR THE ELECTROCHEMICAL TESTS.	104
FIGURE 68: SCHEMATIC REPRESENTATION OF THE ELECTRIC CIRCUIT REGULATING THE POTENTIOSTAT.	105
FIGURE 69: ECL WORKSTATION COMPOSED OF THE POTENTIOSTAT CHI 705E, DC POWER SUPPLY, PHOTOMULTIPLIER AMPLIFIER AND PMT POWER SUPPLIER.	106
FIGURE 70: PHOTOMULTIPLIER TUBE USED FOR THE DETECTION OF PHOTONS DURING THE ECL EMISSION (LEFT) AND SCHEMATIC REPRESENTATION OF THE WORKING PRINCIPLE OF THE DEVICE (RIGHT) [196].	107
FIGURE 71: SCHEMATIC REPRESENTATION OF THE CONNECTIONS BETWEEN THE DEVICES OF THE ECL WORKSTATION.	107
FIGURE 72: SCHEMATIC DESCRIPTION OF THE CHEMILUMINESCENT REACTION BETWEEN THE CATALYST AND THE REAGENT TO GENERATE HYDROGEN PEROXIDE. ADAPTED FROM [205].	111
FIGURE 73: SCHEMATIC REPRESENTATION OF A POTENTIOMETRIC SENSORS WITH THE POTENTIAL RUNNING BETWEEN THE WE AND THE RE WHEN A CONSTANT CURRENT IS APPLIED. ADAPTED FROM [205].	112
FIGURE 74: SCHEMATIC REPRESENTATION OF AN AMPEROMETRIC SENSOR WITH THE CURRENT RUNNING BETWEEN THE WE AND THE RE WHEN A CONSTANT POTENTIAL IS APPLIED. ADAPTED FROM [205].	113
FIGURE 75: SCHEMATIC REPRESENTATION OF THE LUMINOL-OXIDASE-H ₂ O ₂ SYSTEM WITH IMMOBILISED ENZYME ON THE GLASSY CARBON ELECTRODE SURFACE.	115
FIGURE 76: INTERMEDIATES OF LUMINOL FORMED DURING THE REACTION WITH THE H ₂ O ₂ . AFTER THE EMISSION OF PHOTONS, THE EXCITED FORM OF LUMINOL DECAY TO THE GROUND STATE [226].	116
FIGURE 77: STUDY OF THE ECL SIGNAL FOR DIFFERENT CONCENTRATIONS OF LUMINOL OBTAINING THE CALIBRATION CURVE SHOWING AN INITIAL INCREASE OF THE SIGNAL REACHING THE HIGHEST SIGNAL AT 0.3 mM IN THE PRESENCE OF 22 mM OF HYDROGEN PEROXIDE IN 0.01 M PH 12. ERROR BARS REPRESENT TRIPPLICATE DATA POINTS.	117
FIGURE 78: STUDY OF THE BEHAVIOUR OF LUMINOL AT DIFFERENT PH. ERROR BARS REPRESENT TRIPPLICATE DATA POINTS.	118
FIGURE 79: DESCRIPTION OF THE DEPENDENCE OF THE CURRENT PEAK FROM THE SCAN RATE (LOW RATES) A) AND FROM THE SQUARE ROOT OF THE SCAN RATES (HIGH RATES) B) APPLIED DURING THE CYCLES OF CYCLIC VOLTAMMETRY. THE LINEAR RANGE OF THE SQUARE ROOT OF THE SCAN RATES HAS ALSO BEEN PLOTTED C). ERROR BARS REPRESENT TRIPPLICATE DATA POINTS.	121
FIGURE 80: DEPENDENCE OF THE CURRENT PEAK FROM THE DIFFERENT SCAN RATES APPLIED TO THE WORKING ELECTRODE HOSTING AN EMPTY ALGINATE HYDROGEL. HIGHER VALUES OF STANDARD ERROR HAVE BEEN RECORDED IN THIS CASE. ERROR BARS REPRESENT TRIPPLICATE DATA POINTS.	122
FIGURE 81: STRUCTURE OF HORSERADISH PEROXIDE (HRP) OBTAINED BY PDB DATABASE (BERGLUND, G.I., CARLSSON, G.H., HAJDU, J., SMITH, A.T., SZOKE, H., HENRIKSEN, A. (2002), 10.2210/PDB1HCH/PDB).	123
FIGURE 82: ECL PERFORMANCES OF THE HRP/H ₂ O ₂ SYSTEM AT DIFFERENT PH SHOWING THAT THE BEST RESULTS ARE OBTAINED AT 0.01 M PBS PH 9.0. SCAN RATE 0.05 V s ⁻¹ . ERROR BARS REPRESENT TRIPPLICATE DATA POINTS.	125
FIGURE 83: CALIBRATION CURVE OF THE HRP-LUMINOL-H ₂ O ₂ SYSTEM A). ERROR BARS REPRESENT TRIPPLICATE DATA POINTS. STUDY OF THE LINEAR RANGE B). CV AND ECL PLOTS SHOWING THE INCREASING OF THE OXIDATION PEAK C) AND THE ECL EMISSION D). E) CV AND ECL SCANS AT 44 mM H ₂ O ₂ IN 0.01 M PBS PH 9.0 WITH 0.2 MMOL OF LUMINOL IN SOLUTION. SCAN RATE 0.05 V s ⁻¹	126
FIGURE 84: STRUCTURE OF GLUCOSE OXIDASE (GOX) OBTAINED BY PDB DATABASE. (PDB: 1GPE; GOODSSELL D. (MAY 2006). "MOLECULE OF THE MONTH: GLUCOSE OXIDASE". RCSB PROTEIN DATA BANK. DOI: 10.2210/RCSB_PDB/MOM_2006_5).	127
FIGURE 85: ECL PERFORMANCES OF THE GOX-GLUCOSE SYSTEM AT DIFFERENT PH. SCAN RATE 0.05 V s ⁻¹ . ERROR BARS REPRESENT TRIPPLICATE DATA POINTS.	129

FIGURE 86: A) CALIBRATION CURVE FOR THE GOX-GLUCOSE SYSTEM IN 0.01 M PBS AT PH 9, AND STUDY OF LINEAR RANGE AND REGRESSION EQUATION B). ERROR BARS REPRESENT TRIPLICATE DATA POINTS. C) CVs OF THE GLUCOSE-GOX-LUMINOL SYSTEM, D) ECL FOR DIFFERENT CONCENTRATIONS OF GLUCOSE. E) CV AND ECL SCANS AT 5 mM GLUCOSE IN 0.01MOL PBS PH 9.0 WITH 0.2MMOL OF LUMINOL IN SOLUTION. SCAN RATE 0.05 V s ⁻¹	130
FIGURE 87: STRUCTURE OF LACTATE 2-MONOXYGENASE OR LACTATE OXIDASE (LOX) OBTAINED FROM PDB DATABASE. (H.M. BERMAN, J. WESTBROOK, Z. FENG, G. GILLILAND, T.N. BHAT, H. WEISSIG, I.N. SHINDYALOV, P.E. BOURNE. (2000) THE PROTEIN DATA BANK NUCLEIC ACIDS RESEARCH, 28: 235-242.)	132
FIGURE 88: A) CALIBRATION CURVE OF THE L-LACTATE-LOX SYSTEM AND STUDY OF THE LINEAR RANGE B). ERROR BARS REPRESENT TRIPLICATE DATA POINTS. C) CVs SHOWING THE OXIDATION PEAK INCREASING WITH THE INCREASE OF THE SUBSTRATE IN SOLUTION. ECL CURVES B). E) CV AND ECL SCANS AT 30 mM L-LACTIC ACID IN 0.01 M PBS PH 7.4 WITH 0.2 MMOL OF LUMINOL IN SOLUTION. SCAN RATE 0.05 V s ⁻¹	134
FIGURE 89: REPRESENTATION OF THE PATHWAY FOR THE CHOLESTEROL-CHOLESTEROL OXIDASE SYSTEM [278].	135
FIGURE 90: STRUCTURE OF CHOLESTEROL OXIDASE (CHOX). (JAWAHAR SWAMINATHAN AND MSD STAFF AT THE EUROPEAN BIOINFORMATICS INSTITUTE HTTP://WWW.EBI.AC.UK/).....	136
FIGURE 91: PH STUDY FOR THE CHOLESTEROL/CHOX SYSTEM. INCREASING THE ALKALINITY OF THE PH OF THE ELECTROLYTIC SOLUTION ALSO THE ECL INTENSITY INCREASES. SCAN RATE 0.05 V s ⁻¹ . ERROR BARS REPRESENT TRIPLICATE DATA POINTS.	138
FIGURE 92: A) CALIBRATION CURVE OF ECL RESULTS. ERROR BARS REPRESENT TRIPLICATE DATA POINTS. B) LINEAR RANGE AND REGRESSION EQUATION STUDY FOR THE LUMINOL-CHOX-CHOLESTEROL SYSTEM. C) CYCLIC VOLTAMMETRY AND ECL FOR DIFFERENT CONCENTRATIONS OF CHOLESTEROL IN SOLUTION D). E) CV AND ECL SCANS AT 15 mM OF CHOLESTEROL IN 0.01 M PBS PH 9.0 WITH 0.2 mM OF LUMINOL. SCAN RATE 0.05 V s ⁻¹	139
FIGURE 93: MICHAELIS-MENTEN PREDICTION OF THE REACTION RATE AS A FUNCTION OF THE SUBSTRATE CONCENTRATION.	140
FIGURE 94: MICHAELIS-MENTEN BEHAVIOURS OF THE ENZYMES ANALYSED IN THIS CHAPTER. ERROR BARS REPRESENT TRIPLICATE DATA POINTS.	142
FIGURE 95: SCHEME REPRESENTING THE THEORETICAL NORMAL DISTRIBUTION RESPECT THE BLANK OF THE LOD AND THE LOQ.	144
FIGURE 96: A) VOLTAMMOGRAMS AND B) ECL OF GLUCOSE BIOSENSORS WITH THE ADDITION OF 0.1 mM OF AA TO TEST THE SPECIFICITY OF GOX FOR THE SUBSTRATE. C) CALIBRATION CURVE SHOWING THE RELATION BETWEEN THE ECL INTENSITY AND THE DIFFERENT CONCENTRATIONS OF GLUCOSE IN SOLUTION IN PRESENCE OF 0.1 mM OF AA. SCAN RATE 0.05 V s ⁻¹ . ERROR BARS REPRESENT TRIPLICATE DATA POINTS.	145
FIGURE 97: HISTOGRAMS SHOWING THE ECL SIGNALS OBTAINED FOR EACH BIOSENSOR IN THE PRESENCE OF DIFFERENT INTERFERENTS ADDED IN 0.01 M PBS ELECTROLYTIC SOLUTION. ERROR BARS REPRESENT TRIPLICATE DATA POINTS.....	146
FIGURE 98: CV AND ECL OF HRP-H ₂ O ₂ -LUMINOL SYSTEM FOR DIFFERENT CONCENTRATIONS OF CONTACT LENSES LIQUID ADDED TO THE 0.01 M PBS ELECTROLYTIC SOLUTION. SCAN RATE 0.05 V s ⁻¹ . ERROR BARS REPRESENT TRIPLICATE DATA POINTS.	147
FIGURE 99: ELECTROCHEMICAL STUDY OF THE GOX-GLUCOSE-LUMINOL BIOSENSORS WITH ARTIFICIAL SWEAT SOLUTION. A) VOLTAMMOGRAMS SHOWING THE OXIDATION PEAK OF LUMINOL AND B) ECL RESULTS SHOWING AN INCREASE OF THE INTENSITY WITH THE ADDITION OF DIFFERENT ALIQUOTS OF SAMPLE. SCAN RATE 0.05 V s ⁻¹ . ERROR BARS REPRESENT TRIPLICATE DATA POINTS.	148
FIGURE 100: ELECTROCHEMICAL STUDY OF THE LOX-LUMINOL BIOSENSORS WITH ARTIFICIAL SWEAT SOLUTION. A) VOLTAMMOGRAMS SHOWING THE OXIDATION PEAK OF LUMINOL AND B) ECL RESULTS SHOWING AN INCREASE OF THE INTENSITY WITH THE ADDITION OF DIFFERENT ALIQUOTS OF SAMPLE. SCAN RATE 0.05 V s ⁻¹ . ERROR BARS REPRESENT TRIPLICATE DATA POINTS.	149
FIGURE 101: EMPTY TEMPLATE (LEFT) AND FILLED (RIGHT) WITH CRYOGELS FOR THE REALIZATION OF 1 MM DIAMETER AND 0.5 MM THICKNESS CRYOGELS.	153
FIGURE 102: CRYOGELS DEPOSITED ON THE GCE SENSITIVE AREA.	154
FIGURE 103: THREE-ELECTRODES CONFIGURATION ELECTROCHEMICAL CELL WITH THE MODIFIED-GCE IMMERSED INTO THE SUPPORTING ELECTROLYTE AND THE PHOTOMULTIPLIER POSITIONED TO DETECT PHOTONS RESULTING FOR THE CHEMICAL REACTION.	154
FIGURE 104: MICROSCOPIC IMAGING OBTAINED IN CARDIFF UNIVERSITY OF THE CRYOGELS. SCALE BAR REPRESENTS 300 MM.	155
FIGURE 105: SEM IMAGING. 100X MAG, WD = 32.36 MM EHT = 15 kV, I PROBE = 250 pA. SCALE BARS = 100 MM.	156
FIGURE 106: A) DEPENDENCE OF THE CURRENT PEAK FROM DIFFERENT SCAN RATES. B) COMPARISON BETWEEN ALGINATE HYDROGELS, CRYOGELS AND BARE GCE. SCAN RATE IN AN EMPTY CRYOGELS C), SQUARE ROOT OF THE SCAN RATE D) INTO AN EMPTY CRYOGELS, BARE GCE E) AND F) LINEAR RANGE THE CRYOGEL MATRIX G) AND ON THE BARE GCE H). ERROR BARS REPRESENT TRIPLICATE DATA POINTS.	158

FIGURE 107: A) CVs AND B) ECL OF HRP-CRYOGEL-LUMINOL SYSTEM IN 0.01 M PBS AT PH 9.0 WITH 0.2 mM C) CALIBRATION CURVE OBTAINED WITH DIFFERENT CONCENTRATIONS OF H ₂ O ₂ . LINEAR RANGE OF THE CURVE SHOWING A R ² VALUE OF 0.99 D). E) COMPARISON BETWEEN THE CALIBRATION CURVES OF THE HRP INTO CRYOGELS AND ALGINATE HYDROGELS. F) ECL AND CV SCANS FOR 44 MM OH H ₂ O ₂ . SCAN RATE 0.05 V s ⁻¹ . ERROR BARS REPRESENT TRIPPLICATE DATA POINTS.....	160
FIGURE 108: A) CVs AND B) ECL OF GOX-CRYOGEL-LUMINOL SYSTEM IN 0.01 M PBS AT PH 9.0 WITH 0.2 MM LUMINOL. C) CALIBRATION AT DIFFERENT CONCENTRATIONS OF GLUCOSE ADDED IN THE SOLUTION CONTAINING 0.2 MM LUMINOL. D) LINEAR RANGE OF THE CURVE SHOWING A R ² VALUE OF 0.99. E) COMPARISON OF THE CALIBRATION CURVES OF GOX IN ALGINATE HYDROGEL AND CRYOGELS. F) ECL AND CV SCANS FOR 6,72 MM OF GLUCOSE. SCAN RATE 0.05 V s ⁻¹ . ERROR BARS REPRESENT TRIPPLICATE DATA POINTS.	162
FIGURE 108: A) CVs AND B) ECL OF LOX-CRYOGEL-LUMINOL SYSTEM IN 0.01 M PBS AT PH 7.4 WITH 0.2 MM LUMINOL. C) CALIBRATION CURVE OF THREE REPETITIONS OF ECL TESTS AT DIFFERENT CONCENTRATIONS OF L-LACTIC ACID ADDED. D) LINEAR RANGE AND R ² VALUE OF 0.97. E) ECL AND CV SCANS FOR 30 MM OF L-LACTIC ACID. SCAN RATE 0.05 V s ⁻¹ . ERROR BARS REPRESENT TRIPPLICATE DATA POINTS.	164
FIGURE 110: A) CVs AND B) ECL OF CHOx-CRYOGEL-LUMINOL SYSTEM IN 0.01 M PBS AT PH 9.0 WITH 0.2 MM LUMINOL. C) CALIBRATION CURVE OBTAINED FROM THREE REPETITIONS AT DIFFERENT CONCENTRATIONS OF CHOLESTEROL. D) LINEAR RANGE AND R ² VALUE. E) ECL AND CV SCANS FOR 15 MM OF CHOLESTEROL. SCAN RATE 0.05 V s ⁻¹ . ERROR BARS REPRESENT TRIPPLICATE DATA POINTS.	166
FIGURE 111: MICHAELIS-MENTEN STUDY FOR THE OXIDASE ENZYMES ENCAPSULATED INTO CRYOGELS. A) HRP-H ₂ O ₂ -LUMINOL SYSTEM, B) GOX-GLUCOSE-LUMINOL SYSTEM, C) LOX-L-LACTIC ACID-LUMINOL SYSTEM, D) CHOx-CHOLESTEROL-LUMINOL SYSTEM. ERROR BARS REPRESENT TRIPPLICATE DATA POINTS.	167
FIGURE 112: CALIBRATION CURVES OBTAINED WITH THE ADDITION OF DIFFERENT CONCENTRATIONS OF HYDROGEN PEROXIDE FOR HRP ENCAPSULATED INTO CRYOGELS. THREE REPETITIONS HAVE BEEN PERFORMED TO STUDY THE STATISTICAL ANALYSIS. ERROR BARS REPRESENT TRIPPLICATE DATA POINTS.	169
FIGURE 113: REAL SAMPLE ANALYSIS OF THE HRP ENCAPSULATED INTO CRYOGELS. A) CV AT DIFFERENT CONCENTRATIONS OF CONTACT LENSES LIQUID ADDED TO 0.01 M PBS PH 9.0 B) ECL SIGNAL INCREASES WITH THE INCREMENT OF THE ALIQUOTS OF REAL SAMPLE IN SOLUTION. C) CALIBRATION CURVE OBTAINED FROM THE STATISTICAL ANALYSIS OF THREE REPETITIONS OF MEASUREMENTS. SCAN RATE 0.05 V s ⁻¹ . ERROR BARS REPRESENT TRIPPLICATE DATA POINTS.....	170
FIGURE 114: REAL SAMPLE ANALYSIS OF THE GOX ENCAPSULATED INTO CRYOGELS. A) CV AT DIFFERENT ALIQUOTS OF ARTIFICIAL SWEAT ADDED TO 0.01 M PBS PH 9.0 B) ECL SIGNAL C) CALIBRATION CURVE OBTAINED FROM THE STATISTICAL ANALYSIS OF THREE REPETITIONS OF MEASUREMENTS. SCAN RATE 0.05 V s ⁻¹ . ERROR BARS REPRESENT TRIPPLICATE DATA POINTS.	171
FIGURE 115: REAL SAMPLE ANALYSIS OF THE LOX ENCAPSULATED INTO CRYOGELS. A) CV AT DIFFERENT ALIQUOTS OF ARTIFICIAL SWEAT ADDED TO 0.01 M PBS PH 7.4 B) ECL SIGNAL C) CALIBRATION CURVE OBTAINED FROM THE STATISTICAL ANALYSIS OF THREE REPETITIONS OF MEASUREMENTS. SCAN RATE 0.05 V s ⁻¹ . ERROR BARS REPRESENT TRIPPLICATE DATA POINTS.	172
FIGURE 116: STRUCTURE OF THE TRIS(2-2'-BIPYRIDYL) RUTHENIUM (II) [174].	175
FIGURE 117: STRUCTURES OF TRIPROPYLAMINE (LEFT) AND NICOTINAMIDE ADENINE NUCLEOTIDE (RIGHT) SHOWING THE TERTIARY AMINE IN BOTH THE STRUCTURES. (EDITED BY ROBERT E. LENG. THE SIGMA-ALDRICH LIBRARY OF CHEMICAL SAFETY DATA. [MILWAUKEE, WIS., USA]: SIGMA-ALDRICH CORP., 1988).	175
FIGURE 118: ELECTROCHEMILUMINESCENCE MECHANISM OF [RU(BPY) ₃] ²⁺ WITH NAD ⁺ AND DEHYDROGENASE ENZYMES [329].	176
FIGURE 119: CHEMICAL STRUCTURE OF NAD ⁺ AND NADH. (N. R. GOUGH, ANTI-AGING SUPPLEMENTS: THE BASIS FOR BASIS. BIOSERENDIPITY (11 JUNE 2018) HTTPS://WWW.BIOSERENDIPITY.COM/ANTI-AGING-SUPPLEMENTS-THE-BASIS-FOR-BASIS/).....	177
FIGURE 120: CALIBRATION CURVE OF [RU(BPY) ₃] ²⁺ AT DIFFERENT CONCENTRATION OF NADH 3MMOL IN SOLUTION (A) AND STUDY OF THE LINEAR RANGE AND R ² VALUE (B). CALIBRATION CURVE FOR [RU(BPY) ₃] ²⁺ AT DIFFERENT CONCENTRATIONS OF TPRA 0.1MOL IN SOLUTION (C) AND STUDY OF THE LINEAR RANGE AND R VALUE (D). SCAN RATE 0.05 V s ⁻¹ . ERROR BARS REPRESENT TRIPPLICATE DATA POINTS.	179
FIGURE 121: SCHEMATIC REPRESENTATION OF THE DEHYDROGENASE/[RU(BPY) ₃] ²⁺ /NADH SYSTEM	179
FIGURE 122: STUDY OF THE BEHAVIOR OF [RU(BPY) ₃] ²⁺ AT DIFFERENT PH LEVELS WITH 1.5 MM OF NADH IN SOLUTION. SCAN RATE 0.05 V s ⁻¹ . ERROR BARS REPRESENT TRIPPLICATE DATA POINTS.	180
FIGURE 123: DEPENDENCE OF THE CURRENT PEAK FROM THE DIFFERENT SCAN RATES A) AND SQUARE ROOT OF THE SCAN RATE B) INTO AN EMPTY AGINATE HYDROGEL AND THE SAME STUDY HAS BEEN DONE FOR A BARE GCE C), D). STUDY OF THE LINEAR RANGE AND R ² VALUE FOR THE [RU(BPY) ₃] ²⁺ DIFFUSED INTO THE ALGINATE HYDROGEL MATRIX E) AND ON THE BARE GCE F). ERROR BARS REPRESENT TRIPPLICATE DATA POINTS.	181

FIGURE 124: STRUCTURE OF ADH [333].	182
FIGURE 125: EFFECT OF DIFFERENT PH VALUES FOR THE ADH-[Ru(BPY) ₃] ²⁺ -NADH SYSTEM IN 0.01 M PBS. SCAN RATE 0.05 V S ⁻¹ . ERROR BARS REPRESENT TRIPPLICATE DATA POINTS.	184
FIGURE 126: EFFECT OF DIFFERENT CONCENTRATIONS OF NAD ⁺ FOR THE ADH-[Ru(BPY) ₃] ²⁺ -NADH SYSTEM IN 0.01 M PBS AT PH 7.5. SCAN RATE 0.05 V S ⁻¹ . ERROR BARS REPRESENT TRIPPLICATE DATA POINTS.	185
FIGURE 127: A) CALIBRATION CURVE OF THE ADH-ETHANOL-[Ru(BPY) ₃] ²⁺ SYSTEM IN 0.01 M PBS WITH 1 mM NAD ⁺ AT PH 7.5. ERROR BARS REPRESENT TRIPPLICATE DATA POINTS. B) AND STUDY OF THE REGRESSION EQUATION IN THE LINEAR RANGE BETWEEN 15-30 mM OF ETHANOL. ELECTROCHEMICAL RESULTS: CVs AND ECL (D) OBTAINED BY ADDING ETHANOL IN 0.01 M PBS AT PH 7.5 IN THE PRESENCE OF 1 mM NAD ⁺ AND 2.5 mM [Ru(BPY) ₃] ²⁺ . SCAN RATE 0.05 V S ⁻¹ .	186
FIGURE 128: STRUCTURE OF GLUCOSE DEHYDROGENASE OBTAINED BY PDB DATABASE [336].	187
FIGURE 129: EFFECT OF PH FOR 1 mM NAD ⁺ , 2.5 mM [Ru(BPY) ₃] ²⁺ AND 3.36 mM GLUCOSE IN 0.01 M PBS. SCAN RATE 0.05 V S ⁻¹ . ERROR BARS REPRESENT TRIPPLICATE DATA POINTS.	188
FIGURE 130: CALIBRATION CURVE OF THE GDH-GLUCOSE-[Ru(BPY) ₃] ²⁺ SYSTEM SHOWING THE ECL-EMISSION AT DIFFERENT CONCENTRATIONS OF GLUCOSE ADDED TO 0.01 M PBS WITH 1 mM NAD ⁺ AT PH 8.3 A) AND STUDY OF THE REGRESSION EQUATION IN THE LINEAR RANGE BETWEEN 2-4.2 mM OF GLUCOSE B). ERROR BARS REPRESENT TRIPPLICATE DATA POINTS. ELECTROCHEMICAL RESULTS: CVs C) AND ECL D) OBTAINED BY ADDING GLUCOSE. SCAN RATE 0.05 V S ⁻¹ .	189
FIGURE 131: LACTATE DEHYDROGENASE MOLECULAR STRUCTURE (BIOLOGYDICTIONARY.NET EDITORS. "LACTATE DEHYDROGENASE." BIOLOGY DICTIONARY, BIOLOGYDICTIONARY.NET, 08 APR. 2018, HTTPS://BIOLOGYDICTIONARY.NET/LACTATE-DEHYDROGENASE/).	190
FIGURE 132: EFFECT OF THE PH ON THE LDH ACTIVITY IN THE PRESENCE OF 2.5 mM [Ru(BPY) ₃] ²⁺ , 1 mM NAD ⁺ AND 10 mM L-LACTIC ACID. SCAN RATE 0.05 V S ⁻¹ . ERROR BARS REPRESENT TRIPPLICATE DATA POINTS.	191
FIGURE 133: CALIBRATION CURVE OF THE LDH-L-LACTIC ACID-[Ru(BPY) ₃] ²⁺ SYSTEM WITH THE ECL-EMISSION AT DIFFERENT CONCENTRATIONS OF L-LACTIC ACID ADDED TO 0.01 M PBS WITH 1mM NAD ⁺ AT PH 7.4 (A) AND STUDY OF THE REGRESSION EQUATION IN THE LINEAR RANGE BETWEEN 5-20 mM OF L-LACTIC ACID (B). ELECTROCHEMICAL RESULTS: CVs (C) AND ECL (D) OBTAINED BY ADDING THE SUBSTRATE IN SOLUTION. SCAN RATE 0.05 V S ⁻¹ . ERROR BARS REPRESENT TRIPPLICATE DATA POINTS.	192
FIGURE 134: CRYSTAL STRUCTURE OF CHOLESTEROL DEHYDROGENASE [346].	193
FIGURE 135: PH STUDY FOR THE CHOLESTEROL DEHYDROGENASE IN THE PRESENCE OF 2.5 mM [Ru(BPY) ₃] ²⁺ , 1 mM NAD ⁺ AND 15 mM OF CHOLESTEROL IN 0.01 M PBS. SCAN RATE 0.05 V S ⁻¹ . ERROR BARS REPRESENT TRIPPLICATE DATA POINTS.	195
FIGURE 136: CALIBRATION CURVE OF THE CHDH-CHOLESTEROL-[Ru(BPY) ₃] ²⁺ SYSTEM THE ECL-EMISSION AT DIFFERENT CONCENTRATIONS OF CHOLESTEROL ADDED TO 0.01 M PBS WITH 1 mM NAD ⁺ AT PH 8.5 (A) AND STUDY OF THE REGRESSION EQUATION IN THE LINEAR RANGE BETWEEN 5-20 mM OF CHOLESTEROL (B). ELECTROCHEMICAL RESULTS: CVs (C) AND ECL (D) OBTAINED BY ADDING THE SUBSTRATE IN SOLUTION. SCAN RATE 0.05 V S ⁻¹ . ERROR BARS REPRESENT TRIPPLICATE DATA POINTS.	196
FIGURE 137: OXIDATIVE ELECTRO-POLYMERIZATION OF ANILINE MECHANISM [357].	202
FIGURE 138: CATHODIC ELECTRO-POLYMERIZATION METHOD TO PRODUCE POLY(P-PHENYLENEVINYLENES) (PPVs) [357].	202
FIGURE 139: LSV OF ANILINE IN HClO ₄ /CH ₃ CN ON PGE (LEFT). FORMATION OF THE POLYANILINE FILM IN ACETONITRILE PERFORMING 15 SCANS AT 50 mV S ⁻¹ (RIGHT) [362].	205
FIGURE 140: OXIDATION STATES OF THE ANILINE FORMED DURING THE ELECTRO-POLYMERIZATION PROCESS [388].	206
FIGURE 141: ZHANG AND CHEN ELECTRO-POLYMERIZATION OF LUMINOL IN H ₂ SO ₄ , 50 SCANS WITH 100mVs-1 SCAN RATE SHOWING THE GROWTH OF THE POLYMER (BLACK PEAKS) AND THE DECREASE OF THE MONOMER (RED PEAKS) [402].	208
FIGURE 142: MOLECULAR STRUCTURES OF THE ANILINE AND LUMINOL [403].	209
FIGURE 143: SCHEMATIC REACTION FOR THE ELECTRO-POLYMERIZATION OF LUMINOL WITH THE IMPLICATION OF THE AMINO-GROUP [403].	209
FIGURE 144: VOLTAMMOGRAMS OF 1mM LUMINOL PERFORMED IN 1M H ₂ SO ₄ [404].	210
FIGURE 145:SCHEMATIC REPRESENTATION OF THE CHOLINE BIOSENSOR PROPOSED BY SASSOLAS' GROUP [405].	210
FIGURE 146: SASSOLAS' POLYMERIZATION OF LUMINOL IN 0.1 M PHOSPHATE/0.1 M KCL AT PH 6.0 FOR 10 SCANS AT 100 mV S ⁻¹ SCAN RATE [405].	211
FIGURE 147: CVs SHOWING THE POLYMERIZATION OF LUMINOL ON MODIFIED SCREEN PRINTED GRAPHITE WORKING ELECTRODE PROPOSED BY LECA-BOUVIER ET AL. THE POLYMERIZATION HAS BEEN PERFORMED IN 0.1 M PHOSPHATE/0.1 M KCL AT PH 6.0 IN THE PRESENCE OF 1 mM LUMINOL WITH 20 SCANS AND AT 100 mV S ⁻¹ SCAN RATE [403].	212

FIGURE 148: ELECTRO-POLYMERIZATION OF 1 mM LUMINOL IN 0.1 M PBS/KCL AT PH 8.0. 20 SCANS AT 50 mV s ⁻¹ OF SCAN RATE SHOWING THE THREE PEAKS RELATED TO THE CONSUMPTION OF THE MONOMER (A) AND THE REDOX COUPLE OF THE GROWING POLYMER FILM.	213
FIGURE 149: ECL RESPONSE OF THE MONOLAYER SYSTEM (TOP) AND BILAYER SYSTEM (BOTTOM) SHOWING A COMPLETELY DIFFERENT BEHAVIOUR OF THE POLYLUMINOL. THE TWO CALIBRATIONS CURVES HAVE BEEN OBTAINED FOR DIFFERENT CONCENTRATIONS OF HYDROGEN PEROXIDE ADDED TO THE 0.1 M PBS AT PH 9.0. SCAN RATE 0.05 V s ⁻¹ . ERROR BARS REPRESENT TRIPPLICATE DATA POINTS.	214
FIGURE 150: CALIBRATION CURVES OF BILAYER SYSTEMS OBTAINED FOR DIFFERENT NUMBER OF SCANS. DIFFERENT CONCENTRATIONS OF HYDROGEN PEROXIDE HAVE BEEN ADDED TO TEST THE ECL-PROPERTIES OF THE POLYLUMINOL. SCAN RATE 0.05 V s ⁻¹ . ERROR BARS REPRESENT TRIPPLICATE DATA POINTS.	215
FIGURE 151: CALIBRATION CURVES FOR THE DIFFERENT POLIMERISATIONS PERFORMED AT DIFFERENT PHs OF 0.1 M PBS/0.1 M KCL. THE CURVES HAVE BEEN OBTAINED BY STUDYING THE ECL SIGNAL AT DIFFERENT CONCENTRATIONS OF HYDROGEN PEROXIDE ADDED TO THE ELECTROLYTE SOLUTION. SCAN RATE 0.05 V s ⁻¹ . ERROR BARS REPRESENT TRIPPLICATE DATA POINTS. ...	216
FIGURE 152: HRP BILAYER SYSTEM. A) CV AT DIFFERENT CONCENTRATIONS OF H ₂ O ₂ . B) ECL OF THE POLYLUMINOL DEPOSITED ON THE GCE. C) CALIBRATION CURVE OF THE INCREMENT OF ECL SIGNAL CORRESPONDING TO THE INCREASE OF H ₂ O ₂ PRODUCED. SCAN RATE 0.05 V s ⁻¹ . ERROR BARS REPRESENT TRIPPLICATE DATA POINTS.	219
FIGURE 153: GOX BILAYER SYSTEM. A) CV AT DIFFERENT CONCENTRATIONS OF GLUCOSE IN 0.01 M PBS PH 9.0. B) ECL SIGNAL OF POLYLUMINOL ON THE GCE. C) CALIBRATION CURVE OF THE INCREMENT OF ECL SIGNAL CORRESPONDING TO THE INCREASE OF THE GLUCOSE IN SOLUTION. SCAN RATE 0.05 V s ⁻¹ . ERROR BARS REPRESENT TRIPPLICATE DATA POINTS.	220
FIGURE 154: LOX BILAYER SYSTEM. A) CVs CURVES OBTAINED AT DIFFERENT CONCENTRATIONS OF L-LACTIC ACID ADDED IN 0.1 M PBS AT PH 7.4. B) ECL SIGNAL OBTAINED FROM THE REACTION OF THE HYDROGEN PEROXIDE AND THE POLYLUMINOL FILM DEPOSITED ON THE GCE SURFACE. C) CALIBRATION CURVE OF THE ECL SIGNAL SHOWING AN INCREASE IN THE ECL SIGNAL CORRESPONDING TO THE INCREASE OF THE CORRESPONDING SUBSTRATE ADDED TO THE ELECTROLYTIC SOLUTION. SCAN RATE 0.05 V s ⁻¹ . ERROR BARS REPRESENT TRIPPLICATE DATA POINTS.	221
FIGURE 155: CHOx BILAYER SYSTEM. A) VOLTAMMOGRAMS OBTAINED AT DIFFERENT CONCENTRATIONS OF CHOLESTEROL IN 0.1 M PBS AT PH 8.0. B) ECL SIGNAL OBTAINED FROM THE REACTION OF THE H ₂ O ₂ PRODUCED BY THE REDOX REACTION AND THE POLYLUMINOL FILM DEPOSITED ON THE GCE SURFACE. C) CALIBRATION CURVE OF THE ECL SIGNAL SHOWING AN INCREASE IN THE ECL SIGNAL CORRESPONDING TO THE INCREASE OF THE CHOLESTEROL. SCAN RATE 0.05 V s ⁻¹ . ERROR BARS REPRESENT TRIPPLICATE DATA POINTS.	222
FIGURE 156: SCHEMATIC REPRESENTATION OF THE TWO SYSTEMS DEVELOPED IN THIS RESEARCH. A) REPRESENTATION OF THE ECL-BASED BIOSENSOR WITH THE USE OF LUMINOL IN SOLUTION (YELLOW PARTS); B) REPRESENTATION OF THE ECL-BASED SYSTEM WITH THE USE OF POLYLUMINOL ELECTRO-DEPOSITED ON THE GCE SURFACE.	224
FIGURE 157: COMPARISON BETWEEN THE CALIBRATION CURVES OF THE RESULTS OBTAINED FROM THE LUMINOL IN SOLUTION AND POLYLUMINOL TESTS. SCAN RATE 0.05 V s ⁻¹ . ERROR BARS REPRESENT TRIPPLICATE DATA POINTS.	224
FIGURE 158: CV AND ECL PLOTS OF THE HRP-CRYOGEL-POLYLUMINOL BILAYER SYSTEM AT DIFFERENT CONCENTRATIONS OF HYDROGEN PEROXIDE IN SOLUTION. C) CALIBRATION CURVE STUDYING THE DEPENDENCE OF THE ECL INTENSITY FROM THE SUBSTRATE CONCENTRATIONS. SCAN RATE 0.05 V s ⁻¹ . ERROR BARS REPRESENT TRIPPLICATE DATA POINTS.	225
FIGURE 159: CV AND ECL RESULTS OF THE GOX-CRYOGELS-POLYLUMINOL BILAYER SYSTEM IN 0.01 M PBS AT PH 9.0 (A & B); CALIBRATION CURVE OF THE SYSTEM SHOWING THE DEPENDENCE OF THE ECL SIGNAL FROM THE DIFFERENT CONCENTRATIONS OF GLUCOSE IN SOLUTION. SCAN RATE 0.05 V s ⁻¹ . ERROR BARS REPRESENT TRIPPLICATE DATA POINTS.	226
FIGURE 160: CV AND ECL PLOTS OF THE STUDY OF THE ENZYMATIC ACTIVITY OF LOX ENCAPSULATED INTO CRYOGEL WITH THE PRESENCE OF POLYLUMINOL FILM ON THE GCE SURFACE (A AND B); CALIBRATION CURVE OBTAINED FROM THE STATISTICAL ANALYSIS OF THREE REPETITIONS OF THE ECL TESTS. SCAN RATE 0.05 V s ⁻¹ . ERROR BARS REPRESENT TRIPPLICATE DATA POINTS.	227
FIGURE 161: CV AND ECL RESULTS FOR THE CHOx-CRYOGELS-POLYLUMINOL BILAYER SYSTEM IN 0.01 M PBS AT PH 9.0 (A,B). C) CALIBRATION CURVE OBTAINED FOR DIFFERENT CONCENTRATIONS OF CHOLESTEROL ADDED TO THE SOLUTION. SCAN RATE 0.05 V s ⁻¹ . ERROR BARS REPRESENT TRIPPLICATE DATA POINTS.	228
FIGURE 162: COMPARISONS OF THE CALIBRATION CURVES OBTAINED FROM THE STATISTICAL ANALYSIS OF THE CRYOGEL-LUMINOL SYSTEMS AND CRYOGEL-POLYLUMINOL BILAYER SYSTEMS. A) HRP-CRYOGEL-HYDROGEN PEROXIDE SYSTEMS, B) GOX-CRYOGEL-GLUCOSE SYSTEMS, C) LOX-CRYOGEL-L-LACTIC ACID, D) CHOx-CRYOGEL- CHOLESTEROL SYSTEMS. SCAN RATE 0.05 V s ⁻¹ . ERROR BARS REPRESENT TRIPPLICATE DATA POINTS.	230

FIGURE 163: ECL RESULTS OF THE POLY-[RU(BPY) ₃] ²⁺ OBTAINED FOR DIFFERENT NUMBER OF SCANS (LEFT). CALIBRATION CURVE OF ECL RESULTS OBTAINED FOR THREE REPETITIONS OF EACH NUMBER OF SCANS SHOWING THAT THE BEST SIGNAL IS OBTAINED FOR 20, 30 AND 40 SCANS. SCAN RATE 0.05 V s ⁻¹ . ERROR BARS REPRESENT TRIPLICATE DATA POINTS.....	232
FIGURE 164: ELECTRO-POLYMERIZATION SCANS FOR THE DIFFERENT SCAN RATE FROM 50 TO 400 mVs ⁻¹ ARE REPORTED WITH THE CORRESPONDING ECL SIGNAL. (D) COMPARISON OF THE ECL SIGNALS FOR THE DIFFERENT SCAN RATE SHOWING THE BEST PERFORMANCE FOR 100 mVs ⁻¹	233
FIGURE 165: UVV RESULTS OF THE MONOMER AND FILM DILUTED IN METHANOL ALSO SCANNED AS BACKGROUND.....	234
FIGURE 166: FTIR PLATE WITH THE DEPOSITION OF THE FILM POWDER OBTAINED AFTER THE EVAPORATION OVERNIGHT OF THE SOLVENTS. IT IS POSSIBLE TO NOTICE THAT THE FILM ELECTRO-POLYMERIZED CONSERVED THE RED COLOUR SPECIFIC FOR THE RUTHENIUM COMPOUNDS.	235
FIGURE 167: FTIR CHARACTERISATION OF DIFFERENT SOLVENTS AND MOLECULE WHICH ARE INVOLVED IN THE GENERATION OF THE POLY-RU[(BPY) ₃] ²⁺ FILM ON THE GCE SURFACE.	236
FIGURE 168: COMPARISON OF THE FTIR SPECTRA OF THE MONOMER [RU(BPY) ₃] ²⁺ AND THE OLIGOMERIC FILM ELECTROPOLYMERIZED.....	236
FIGURE 169: RESULTS OBTAINED FOR THE FOUR SYSTEMS OF DEHYDROGENASE ENZYME ENCAPSULATED INTO ALGINATE HYDROGELS AND DEPOSITED ON GCE IN THE PRESENCE OF THE POLY-[RU(BPY) ₃] ²⁺ FILM FORMING A BILAYER SYSTEM. A) ADH-ETHANOL-POLY-[RU(BPY) ₃] ²⁺ SYSTEM IN THE PRESENCE OF 30 MM OF ETHANOL; B) GDH-GLUCOSE- POLY-[RU(BPY) ₃] ²⁺ SYSTEM WITH 20 MM OF GLUCOSE; C) LDH-L-LACTIC ACID- POLY-[RU(BPY) ₃] ²⁺ AND 25 MM OF SUBSTRATE IN SOLUTION AND FINALLY D) CDH-CHOLESTEROL- POLY-[RU(BPY) ₃] ²⁺ AND 25 MM OF CHOLESTEROL. SCAN RATE 0.05 V s ⁻¹	238

Abbreviation

ΔG	Gibbs free energy
AA	Ascorbic acid
ADH	Alcohol dehydrogenase
Ag/AgCl	Silver/Silver Chloride
BSA	Bovine Serum Albumin
CE	Counter electrode
ChDH	Cholesterol dehydrogenase
ChOx	Cholesterol oxidase
CL	Chemiluminescence
CLEA	Cross-linking enzyme aggregate
CLEC	Cross-linking enzyme crystal
CV	Cyclic voltammetry
DA	Dopamine
ECL	Electrochemiluminescence
ECLIA	Electrochemiluminescence immunoassay
E_i	Initial potential
ELISA	Enzyme-linked immunosorbent assay
E_{pa}	Anodic peak potential
E_{pc}	Cathodic peak potential
FAD	Flavin adenine dinucleotide
FTIR	Fourier transform infra-red
GCE	Glassy carbon electrode
GDH	Glucose Dehydrogenase
GDL	D-Glucono-1,5-lactone
GOx	Glucose oxidase
HOMO	Highest occupied molecular orbital
HPLC	High performance liquid chromatography
HRP	Horseradish peroxide

I_{\max}	Maximum current
i_{pa}	Anodic peak current
i_{pc}	Cathodic peak current
ITO	Indium titanium oxide
K_D	Dissociation constant
K_M	Michaelis-Menten constant
K_{Mapp}	Apparent Michaelis-Menten constant
LBL	Layer-by-layer
LDH	Lactate dehydrogenase
LOD	Limit of detection
LOQ	Limit of quantification
LOx	Lactate oxidase
LUMO	Lowest unoccupied molecular orbital
MOI	Molecule of interest
NAD ⁺	Nicotinamide adenine dinucleotide
PBS	Phosphate buffered solution
PDB	Protein data base
PDDA	Poly(diallyldimethylammonium)
PEGDA	Poly (ethylene glycol) diacrylate
PL	Photoluminescence
PLA	Poly(lactic acid)
PMT	Photomultiplier tube
PSS	Poly (sodium 4-styrenesulfonate)
RE	Reference Electrode
Rpm	Revolution per minute
SAMs	Self-assembled monolayers
SCE	Saturated calomel electrode
SEM	Scanning electron microscopy
SHE	Standard hydrogen electrode
SPCE	Screen printed electrode

TPrA	Tri-n-propylamine
UV	Ultraviolet
V_{\max}	Maximum velocity
WE	Working electrode

Acknowledgements

When I first arrived in this country, I never imagined that these three years of PhD would be an adventure between laboratory experiments, lockdowns, fire in the campus, multiple laboratories moving, and again experiments. But here we are, I've done it.

For these reasons, I am extremely grateful to my supervisor, Paolo Bertoncello for his invaluable advice, continuous support, and most of all for his patience. His immense knowledge and plentiful experience have encouraged me to keep studying, improving, and questioning everything, but above all to don't give up.

I would also like to thank all the technicians for their support especially after the fire, their help has been fundamental for the reorganisation of the lab. I would like to thank all the members of KESS for funding my scholarship.

A thank you to the examiners that will spend time reading and evaluating this thesis.

A big thank is for my precious friends Diana and Katie. Without them, it would be impossible for me to finish this PhD without a mental breakdown. We have been supporting each other, gossiping, sharing coffees and dreams. Thanks chicas, I'm so lucky I found you both!

These three years wouldn't be the same without Nick. You've been on my side living every single minute of this research, listening every-time I tried to explain it, being proud when I was successful and supportive when I was down. It has been an honor having you on my side, always. And what about Mia? She came in our home when everything has been stopped by Covid, bringing happiness and energy. I can't imagine my days without you two, so thank you!

During these three years of study, I've been far from my family. Mamma e Papà, I hope I made you proud with this achievement as you make me proud everyday with your dedication and hard-working. Since I started my academic career, I wrote three theses, graduated twice and you have been emotional every time like if it was the first one. I promise, this is the last one! Thanks for giving me the opportunity to be free and make my choices always knowing to have you behind me ready to catch me in case I fall. Grazie!

Moving in UK I left at home my brother and sister, basically all my heart. Shara e Gigi, how much I miss you both is unbelievable. I'm doing all my best to be a good example, but from what I can see you both are so intelligent, courageous, and successful that you are my example to follow, constantly impressing me in all your achievements! I'm proud of both of you.

Publications

In progress: **Enzymes-encapsulated into alginate hydrogels: Bioelectrocatalysis towards sensing applications.**

Lucia Simona Ferraraccio, Laura Pastorino, Paolo Bertoncello.

In progress: **ECL biosensor based on tris(2,2'-bipyridyl) ruthenium (II) and dehydrogenase enzymes encapsulated into alginate hydrogels.**

Lucia Simona Ferraraccio, Paolo Bertoncello.

In progress: **Polyluminol/cryogels biosensor for the Electrochemiluminescent detection of encapsulated oxidase enzymes.**

Lucia Simona Ferraraccio, Benjamin Newland, James Russel, Paolo Bertoncello.

External collaboration: **On the development of electrochemical sensors coated with polycaprolactone.**

Eva Raccosta Leone, Lucia Simona Ferraraccio, Giacomo Damonte, Paola Lova, Paolo Bertoncello, Orietta Monticelli.

Electrochemistry Communications, Volume 129, August 2021.

(<https://doi.org/10.1016/j.elecom.2021.107089>)

Conferences attended

1. *Great Western Electrochemistry* – June 24, 2019, University of Bath (England): presentation and poster “*Electrochemiluminescence (ECL) at enzymes-encapsulated into Alginate Hydrogels*”. The poster has been chosen for the CHEMELECTROCHEM poster award.
2. *Electrochemistry Conference* – September 30 - October 02, 2019, Istanbul (Turkey): presentation “*ECL-based biosensors for the detection of encapsulated Dehydrogenase enzymes into Alginate Hydrogels*”.
3. *72nd Annual meeting of the International Society of Electrochemistry* – August 29 – September 3, 2021, Korea (remote conference): presentation “*Electrochemiluminescence (ECL) at Oxidase and Dehydrogenase enzymes encapsulated into Alginate Hydrogels*”.

Chapter 1: Introduction

The biosensors developed during this PhD project are based on the electrochemiluminescence (ECL) technique, a novel luminescence analysis widely used for analytical applications due to its properties of high sensitivity and selectivity.

In this chapter, the ECL theory and general principles are described. Furthermore, a complete literature review regarding the main applications and the history of the discovery of ECL is offered focussing on the biomedical demand for the development of biosensors.

1. State of art

Electrochemistry is a science based principally on two fundamental events: the electron transfer and the solution/electrode interface. The main purpose of this discipline is the investigation of the relation between the electrical potential represented by a flow of electrons and the chemical changes. In particular, when the chemical reaction is triggered by the application of a potential, it is known as electrochemical reaction [1]. The history of electrochemistry starts with Alessandro Volta and Luigi Galvani with their electricity studies [2, 3] followed by Nicholson and Carlisle in 1800 with the discovery of the water splitting into hydrogen and oxygen through electrolysis[4]. Furthermore, in 1833 Faraday reported studies about electrolysis introducing for the first time the term *electrochemistry* [5]. During his studies, Faraday made two important discoveries leading to the two Faraday's laws of electrochemistry:

- 1) *The electricity passing through the electrochemical cell is directly proportional to the amount of a substance that is deposited on the electrode surface.*
- 2) *The amount of the species deposited by the electricity are proportionally equivalent to their chemical weights.*

Based on these fundamentals, in 1839 the first fuel cell has been produced by William Grove assuming that it is possible to produce current and water by mixing together hydrogen and

oxygen based on the fact that applying an electric current across water, the latter will split into hydrogen and oxygen[6] (Fig. 1).

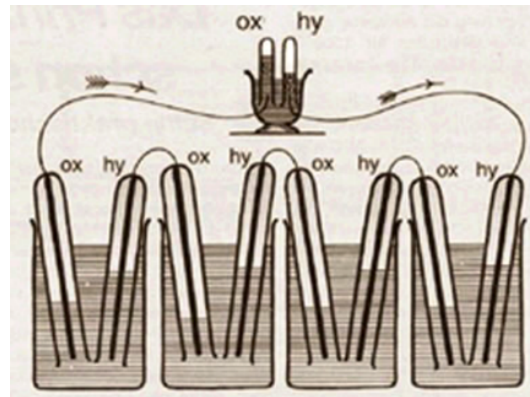


Figure 1: Prototype of the first fuel cell proposed by Grove in 1839[7].

Following the first fuel cell, more aspects have been discovered becoming fundamental for the modern electrochemistry for example the Nernst equation proposed in 1889 by Walther Nernst who demonstrated how the current produced is related to the free energy.

In the 20th century two societies entirely dedicated to Electrochemistry have been founded, The Electrochemical Society (ECS) in 1902 and the International Society of Electrochemistry (ISE) in 1949 which nowadays is hosting every year international conferences to update the latest discoveries[8]. The second half of the century is marked by the development of the quantum electrochemistry proposed by Revaz Dogonadze.

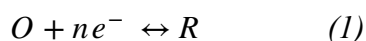
The electrochemical methods belong to the analytical chemistry area based on the study of the potential and current produced in an electrochemical cell containing different species[9-12]. These methods are divided into different categories depending on which parameters of the electrochemical cell is controlled and which one is measured. Specifically, there are three main groups:

- 1) *Potentiometry*: calculation of the potential between two electrodes at 0 net current.
- 2) *Coulometry*: calculation of the number of coulombs to complete a reaction.
- 3) *Voltammetry*: calculation of the cell's current at different cell's potentials for the estimation of oxidation and reduction processes.

Voltammetry is the method adopted for the experiments presented in this thesis as these electrochemical techniques can uncover the electrochemical properties of an analyte by varying the potential in the electrochemical cell and studying the resulting current. Furthermore, voltammetry can be divided as well into two categories of techniques, the *polarography* which use mercury materials as working electrode and the *amperometry*. Amperometry indicates all those electrochemical analyses measuring the current as function of the potential or the time[13].

1.2 Fundamentals of electrochemistry

The redox reactions are electrochemical processes involving the exchange of electrons or ion between species into the electrochemical cell. Considering the reduction reaction (I), the oxidised (O) and the reduced (R) species involved in the reaction, exchange n number of electrons between each other.



The oxidation/reduction reaction at the electrode surface, is composed of different sequences of smaller reactions such as (1) the mass transport of species from the bulk solution to the interface of the electrode, (2) chemical reaction which leads to the formation of the products, (3) reactions taking place at the surface of the electrode such as the absorption of species and finally, the (4) electron transfer reaction (Fig. 2).

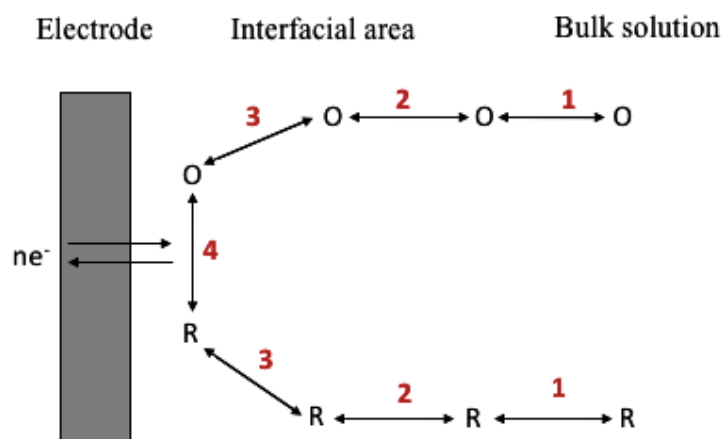


Figure 2: Schematic representation of the steps that establish an electrode reaction: (1) mass transport, (2) chemical reaction between the species, (3) surface reactions and (4) electron transfer reaction.

The application of an external potential to the working electrode can trigger the reactions at its surface, in particular the application of a positive (negative) potential allows the decrease (increase) of the energy of electrons. Hence, by applying positive potential levels to the electrode, the energy of the electrons reduces sufficiently for their transfer to a free energy state on the electrode surface obtaining in this way an *oxidation current*. On the other hand, with the application of negative potentials the energy of the electrons increases sufficiently to move from the electrode to free energy states in the bulk solution with the resulting *reduction current*.

The equation describing the relationship between the concentrations of the two species introduces the concept of free energy ΔG [J mol^{-1}] is:

$$\Delta G = G^0 + RT \ln \frac{[R]}{[O]} \quad (2)$$

Where R is the gas constant ($8.3145 \text{ J mol}^{-1} \text{ K}^{-1}$) and T is the temperature in Kelvin. From the relation between the oxidised and reduced species with the free energy (2) the potential can be extracted following the equation (3) relating the equilibrium potential (E) with the number of electrons exchanged during the reaction and Faraday's constant F ($96,485.3 \text{ C mol}^{-1}$)

$$\Delta G = -nFE \quad (3)$$

Another mathematical equation associating the concentrations of the species with the potential is the Nernst equation which can be applied for the reversible electron transfer reaction studying the relationship between the potential of an electrochemical cell (E), the standard potential of species (E^0) and the oxidised and reduced analytes at the equilibrium:

$$E = E^0 + \frac{RT}{nF} \ln \frac{(Ox)}{(Red)} \quad (4)$$

Where:

R is the gas constant ($J K^{-1} mol^{-1}$).

T is the temperature (K).

F is the Faraday constant ($C mol^{-1}$).

The standard oxidation (reduction) potential E^0 is calculated against the standard hydrogen electrode, also known as SHE, in standard thermodynamic conditions (298K, 1 atm.). Generally, the Nernst equation can be used to determine the concentration of the analyte reduced at the electrode surface at the specific applied potential during the electron transfer reaction. The concentration of the analyte at the electrode changes immediately as the electrode potential changes so the electrons are exchanged reversibly, and the equilibrium determined by the Nernst equation is maintained for the duration of the reaction. Particularly, during a CV with the changing of the potential E , the electrons are transferred between the electrode surface and the analyte[14] (Fig. 3).

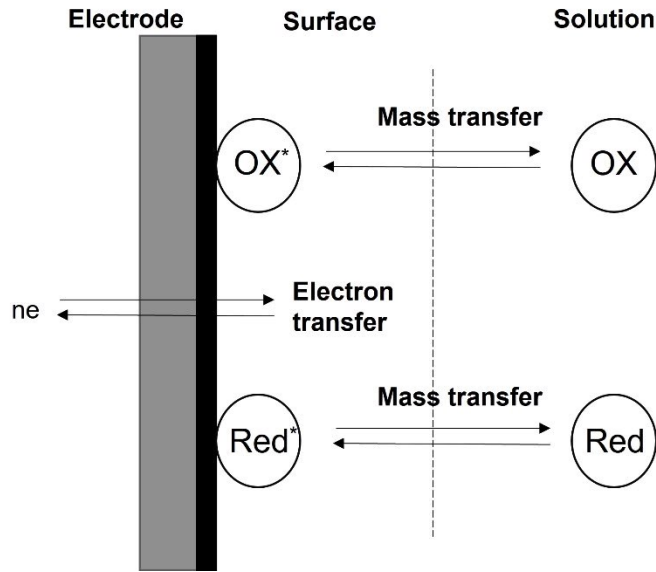


Figure 3: Molecular process of electron transfer reaction at the electrode surface.

1.3 Mass Transfer

The phenomenon of the mass transfer is essential for the electrochemistry reactions allowing the movement of electrons from one species to the another[15]. It can happen in three different ways: *migration* when the charged particles move in an electric field; *diffusion* when the movement of particles goes against the concentration gradient and *convection* obtained by stirring or density gradient (Fig. 4). The diffusion process is the most significant for the electrochemical tests, instead migration and convection could be reduced in the experimental set-up.

These three mass transfer methods are described in the Nernst-Planck equation associating the flux of the species with the movement of the particles:

$$J_i(x) = \underbrace{-D \frac{\delta C_i(x)}{\delta x}}_{1^{\text{st}} \text{ term}} - \underbrace{\frac{z_i F}{RT} D_i C_i \frac{\delta \phi(x)}{\delta x}}_{2^{\text{nd}} \text{ term}} + \underbrace{C_i v(x)}_{3^{\text{rd}} \text{ term}} \quad (5)$$

Where:

D is the diffusion coefficient (SI unit: $\text{m}^2 \text{s}^{-1}$);

$\frac{\delta C_i(x)}{\delta x}$ is the concentration gradient;

z_i is the valence of ionic species;

F denotes the Faraday constant (SI unit: C mol^{-1});

R is the gas constant (SI unit: $\text{J K}^{-1} \text{mol}^{-1}$);

T is the absolute temperature (Kelvin);

C_i is the concentration of the ion i (SI unit: mol m^{-3});

$\frac{\delta \phi(x)}{\delta x}$ is the electric potential;

$v(x)$ is the velocity vector (SI unit: m s^{-1}).

The first term of the equation describes the diffusion also known as Fick's first law; the second is related to the migration process of species in a solution and finally the last term represents the mass transfer by convection considering the rate $v(x)$ at which the particles move in the solution[11].

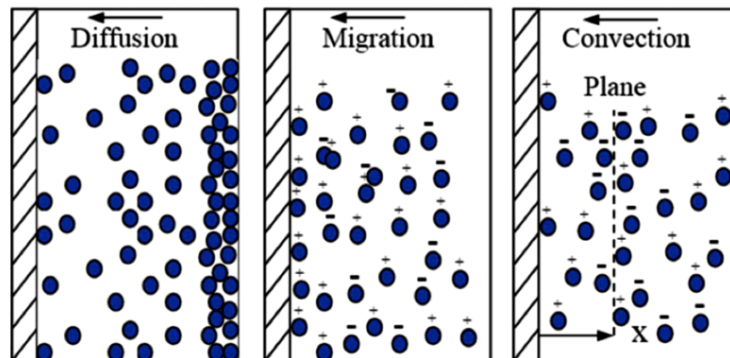


Figure 4: Representation of the three modes of mass transfer [16].

The Cottrell equation that relates in a directly proportional way the concentration of the active species with the current:

$$i = \frac{nFAC^*\sqrt{D}}{\sqrt{\pi t}} \quad (6)$$

Where:

i = the current (A);

n = the number of electrons;

F = Faraday constant (96485 C mol⁻¹);

A = area of the electrode (cm²);

D = diffusion coefficient (cm² s⁻¹);

C^* = initial concentration of the analyte (mol cm⁻³);

t = time (s).

Following this equation, it is possible to establish the time that a particle needs to reach a certain distance, specifically as the current i decreases with the time.

1.3.1 Diffusion

Going more into detail, the diffusion process is represented by Fick's first law

$$J_i(x) = -D \frac{\delta C_i(x)}{\delta x} \quad (7)$$

Where:

D = diffusion coefficient (cm² s⁻¹);

$\frac{\delta C_i(x)}{\delta x}$ = concentration gradient

and describes the movement of particles following the concentration gradient. From equation (7) the flux of the particles J is linearly dependant on the diffusion coefficient D and the concentration gradient $\delta C / \delta x$. The diffusion of a species at the electrode surface depends also on the size of the electrode itself. In fact, in the case of macro-electrodes, like the GCE used for this research with 3 mm dimension, there is a planar diffusion that produces a peak-

shaped voltammogram. With the decrease of the electrode size, the diffusion becomes radial forming a larger diffusion layer which involves also the area around the electrode surface[11] (Fig. 5).

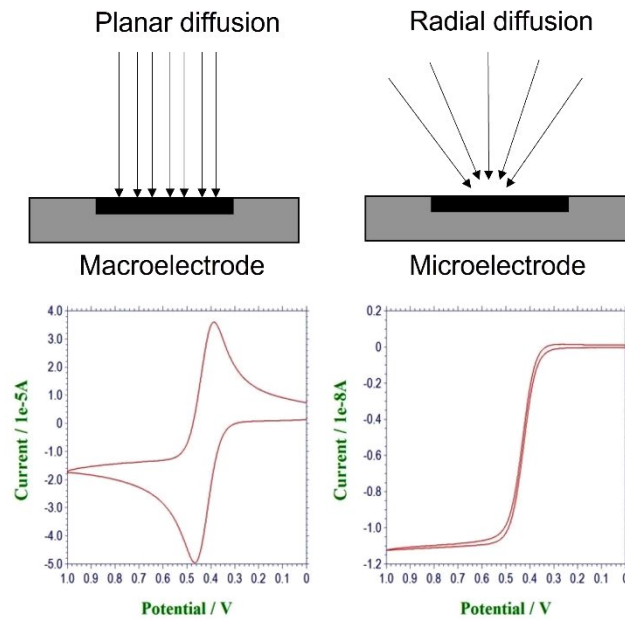


Figure 5: Representation of the diffusion profiles depending on the electrode size: the planar diffusion happening at macro-electrode (left) and the radial diffusion for ultra micro-electrodes (right).

1.3.2 Migration

Differently from the diffusion process, the movement of charges by migration is due to the presence of a potential gradient. This process is described by equation (8) showing the linear dependence of the flux from the electric field:

$$J_i(x) = - \frac{z_i F}{RT} D_i C_i \frac{\delta \phi(x)}{\delta x} \quad (8)$$

Where:

z_i is the valence of ionic species;

F denotes the Faraday constant (SI unit: C mol⁻¹);

R is the gas constant (SI unit: J K⁻¹ mol⁻¹);

T is the absolute temperature (Kelvin);

C_i is the concentration of the ion i (SI unit: mol m⁻³);

$\frac{\delta\phi(x)}{\delta x}$ is the electric potential.

This contribution can be minimised using an inert supporting electrolyte in the electrochemical solution as the migration forces are mostly electrostatic.

For electrochemical experiments, a large amount of supporting electrolyte (almost 100 times higher than the concentration of species involved in the redox process) is used causing the formation of a thinner double layer at the interface enhancing the electron transfer reaction.

1.3.3 Convection

The last contribution for the mass transport comes from the convection which allows the movement of the particles applying mechanical forces such as stirring or by heat transfer at high temperatures.

$$J_i(x) = C_i v(x) \quad (9)$$

Where:

C_i is the concentration of the ion i (SI unit: mol m⁻³);

$v(x)$ is the velocity vector (SI unit: m s⁻¹).

For the experiments performed in this thesis, convection is not considered as the experiments are performed in stable conditions and in a short time so the contribution is negligible compared to the one of the diffusion.

1.4 Electrode-solution interface: electrical double layer

As anticipated, one of the main processes that is investigated in electrochemistry is the interface between the electrode and the solution or in other kind of electrochemical reactions the interface between two liquids. For this thesis, the reactions happen between a glassy carbon electrode (GCE) surface and the species in the supporting electrolyte solution so it is interesting to understand what happens when the two come in contact with each other[17]. In general, an electric double layer is generated when two conducting phases meet at the interface and one of the phases acquires a positive charge on its surface which is balanced with the accumulation of the negative charge on the surface of the other phase[18].

Once the two phases (solid and liquid) meet, a double layer is set up at the interface due to the transfer of charge across this area. For the description of the double layer, few models have been proposed, the first one was the parallel-plate condenser model also known as Helmholtz Model related to the electrode-electrolyte interface[19]. The Helmholtz double layer refers to the accumulation of electrical charge at the interface of an electrode and the electrolyte when they come in contact, representing the combination of two layers of opposite charge. This model describes the interface between two different phases, solid and liquid, not considering important factors such as diffusion and adsorption of charges on the surface. Significant improvements have been made by Gouy and Chapman introducing the diffusion model of the double layer. They suggested that the charges are not rigidly held on the surfaces of the phases as stated with the Helmholtz model, but they tend to diffuse obtaining the so called diffusion double layer. Specifically, this model describes a rigid charged surface and a cloud of opposite charged ions in the solution, the concentration of the opposite charges in the solution decreases with the increase of the distance from the solid surface. Consequently, the potential decreases exponentially with the increase of the distance from the surface of the bulk solution. The Gouy-Chapman model gives a better approximation of charges behaviour in proximity of the interface of the two phases than Helmholtz but it does not consider the possible physical limitations for the ions when approaching the surface[20]. In 1924, Stern proposed a new theory resulting as the combination of Helmholtz and Gouy-Chapman models. The Stern's model assumes that some ions adhere to the surface of the electrode as a result of the attraction of the opposite charges (Helmholtz's idea) obtaining

what is called the Stern's layer, and other charges instead, form the diffuse-layer as Gouy and Chapman proposed[21] (Fig. 6).

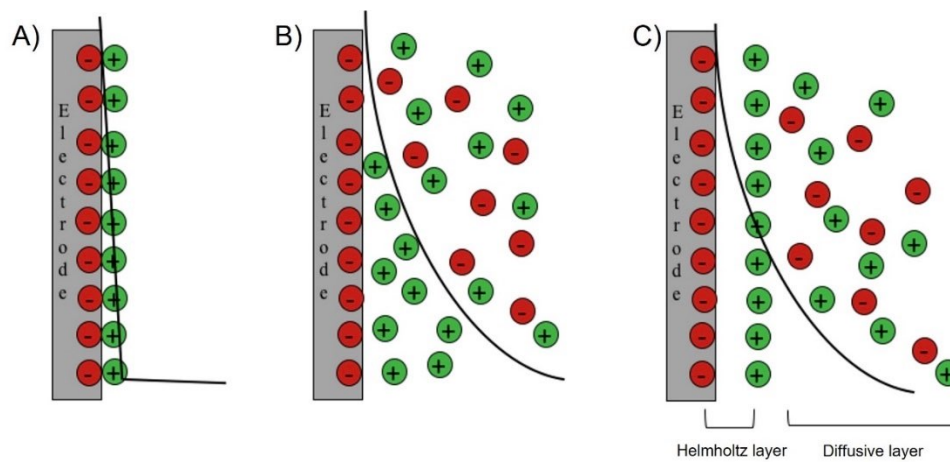


Figure 6: Helmholtz model showing a rigid interaction between the two phases (A), Gouy-Chapman model with the formation of the diffuse-layer (B) and Stern's model with the combination of the Helmholtz layer at the electrode surface and the diffusion-layer in the bulk solution (C).

The Stern's model has some limitations as the ions are considered like charges, so they have a finite size hence the closest distance of the ions from the surface of the electrode is equal to the ionic radius. This model has been modified in 1947 by Grahame who proposed that also other ionic and uncharged species could penetrate the Stern layer. Specifically, Grahame's theory considers three areas known as the inner Helmholtz plane where the ions are adsorbed on the surface, the outer Helmholtz plane where the ions are surrounded by the molecules of the solvent (solvated ions) and the final diffusion layer.

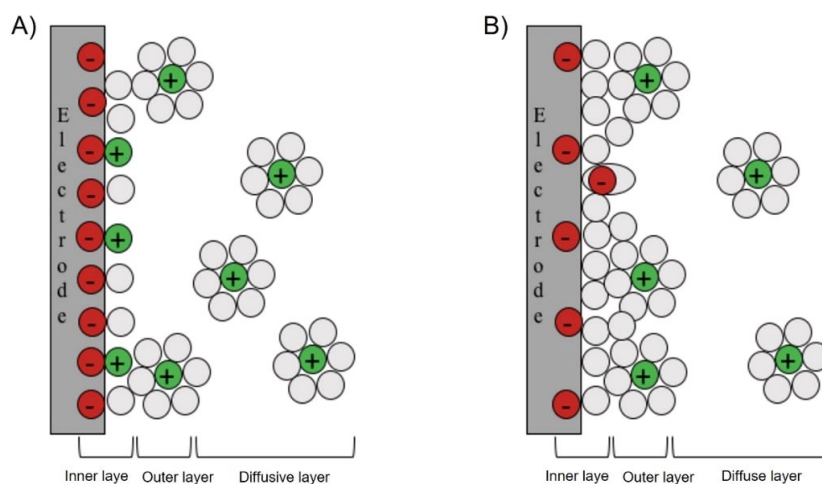


Figure 7: Schematic representation of the Grahame model of the electrical double layer (A) and the Bockris, Devanathan and Mullen considering the partially adsorbed ion on the electrode surface (B).

In 1963, Bockris, Devanathan and Mullen proposed an upgrade of the Grahame’s model considering the influence of the solvent molecules at the interface between the two phases. As for Grahame’s, there are three regions but in the inner layer are also included adsorbed partially solvated ions[18, 22] (Fig. 7).

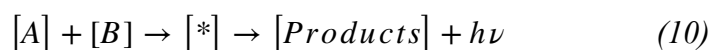
1.5 Type of luminescence

Luminescence is the phenomenon that allows a spontaneous emission of light caused by different kinds of chemical reactions. In table 1, the main categories of luminescence are listed with the corresponding reaction able to trigger the emission of light.

Table 1: Different types of luminescence with the corresponding reactions that trigger the emission of light

<i>Luminescence type</i>	<i>Triggered by</i>
<i>Bioluminescence</i>	Biochemical reaction
<i>Chemiluminescence (CL)</i>	Chemical reaction
<i>Electrochemiluminescence (ECL)</i>	Electrochemical reaction
<i>Fluorescence</i>	Singlet-singlet electronic relaxation
<i>Mechanoluminescence</i>	Mechanical action on a solid
<i>Photoluminescence (PL)</i>	Photon's absorption
<i>Radioluminescence</i>	Ionising radiation
<i>Thermoluminescence</i>	Energy absorbed by heating
<i>Phosphorescence</i>	Radiation of short wavelength

Chemiluminescence is a technique used to produce light after a chemical reaction between two reactants [A] and [B] forming an excited intermediate [*] leading to the final emission of light.



A classic example of chemiluminescent reaction is the luminol-hydrogen peroxide system (Fig. 8):

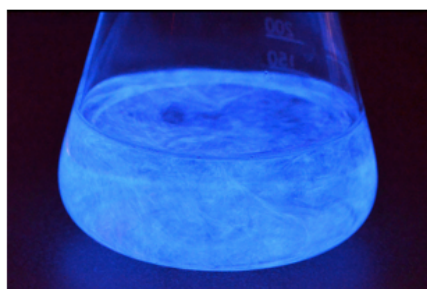
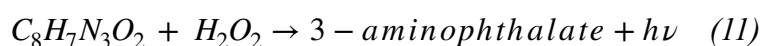


Figure 8: Chemiluminescent of luminol obtained by reacting with the hydrogen peroxide. (<https://physicsopenlab.org/2019/02/06/luminol-2/>. Accessed 15 June 2021).

Generally, when the excited state of a specie decays to a lower energy level it causes the emission of light from an excited electronic state. In fact, the electrons of atoms or molecules can transit by changing their energy level following two different ways: by emitting and by absorbing a photon (Fig. 9).

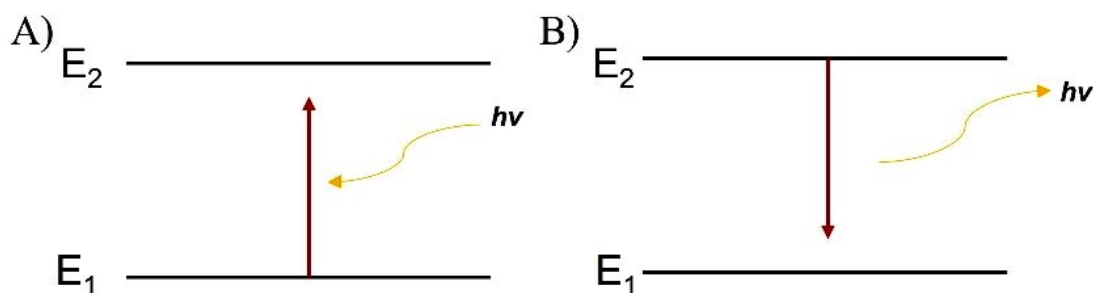


Figure 9: Schematic representation of the absorption by increasing the energy level of a photon (A) and the emission of a photon after a decrease of energy level from E₂ to E₁ (B).

The transition from the ground state (lowest energy level) to an excited one of atoms occurs by absorbing a photon that has an energy equal to the energy difference between the two levels. Instead, the transition by emission of light takes place when the species at the excited state decays to the ground state emitting the photon that has equal energy to the energy difference (Fig. 10).



Figure 10: Schematic description of the energy levels for electron in atoms.

The factor that distinguishes the chemiluminescence from the fluorescence or phosphorescence is that the excited state is achieved as a result of a chemical reaction instead

of the absorption of a photon. In the case of electrochemiluminescence the emission of light is due to an electrochemical initiation obtained by the application of a suitable voltage.

1.6 Electrogenerated chemiluminescence (ECL)

Electrochemiluminescence (ECL), also known as electrogenerated chemiluminescence, is a form of luminescence enabling the emission of light as a result of a chemiluminescent reaction happening after an electrical stimulation at the working electrode hosting the reactions. Different aspects distinguish ECL from chemiluminescence (CL) starting from the different luminescence initiation methods; in fact, in CL the reaction occurs when the reagents are mixed together instead for the ECL the luminescence happens applying and controlling the electrode potential [23] (Fig. 11).

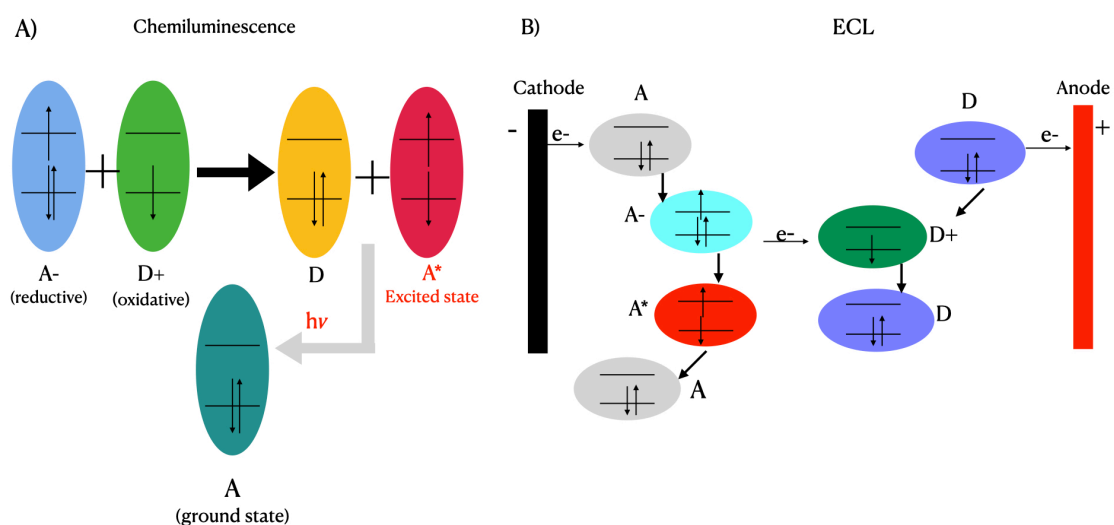


Figure 11: Schematic representation of the general principles for A) chemiluminescence and B) electrochemiluminescence [24].

One of the best advantages of ECL with respect to CL is the possibility to control the time and position of the light-emission [25, 26]. Particularly, by controlling the time, the light emission could be delayed until reactions take place, for example until the enzyme catalyses the reaction with the corresponding substrate. On the other hand, the control over the position can be obtained by limiting the light emission to an area that is located near the photons

detector. By doing so, with the ECL it is possible to improve the sensitivity and so increase the signal to noise ratio [27]. The second advantage of ECL over CL is the high selectivity through the generation of an excited state controlled by varying the working electrode potential levels [28]. Furthermore, ECL is defined as a non-destructive analytical technique because the luminophores, in most cases, can be regenerated at the end of the reaction and used again. Not only ECL is advantageous over CL but also considering general spectroscopy-based methods, ECL does not require any kind of light source so the problems related to scattered light and the presence of luminescent impurities are completely avoided [23].

The first studies of ECL were conducted in the mid-1960 with Hercules and Bard [29, 30] even if the first observations of the light emission during electrolysis by using luminol and Grignard compounds were studied in 1927 with Dufford et al. [31]. The first ECL documented experiments go back to 1964 when the technique was used for different applications like immunoassay, food and water tests and biological warfare detection [31-33] (Fig. 12).

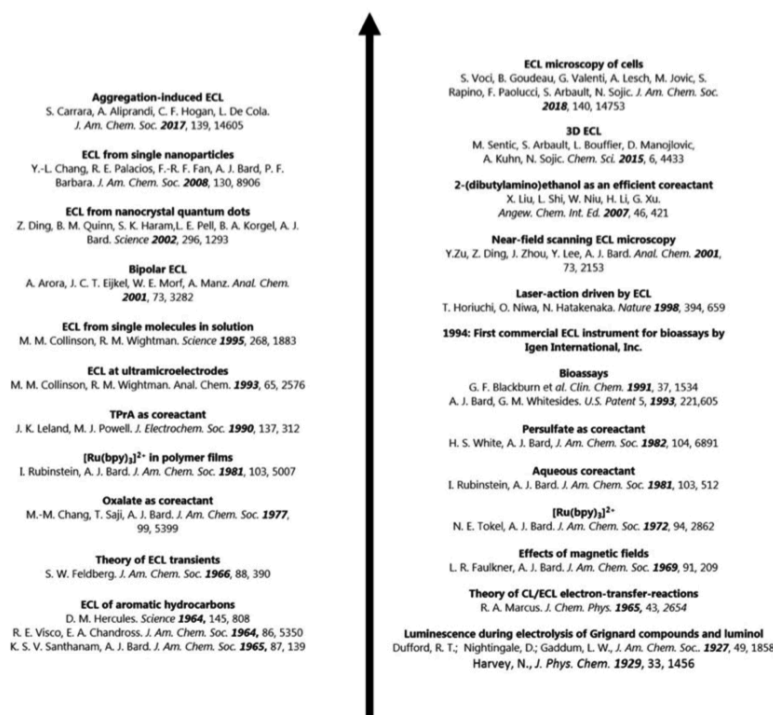


Figure 12: Miao's timeline of the ECL progress as reported in the literature [23]

The most interesting discovery about the electron-transfer excitation started in 1964 with the analysis of reversible ECL systems concerning radical ions annihilation reactions. Hercules et al. reported the ECL from different hydrocarbons in acetonitrile solvents adopting two different configurations; by alternating the current (1) and applying a current (2) at two electrodes in close proximity [29]. With these results, the stability of the electrogenerated species has been underlined. Later on, the same group proposed the annihilation pathway of the ECL strictly related to the CL as they share the same configuration and theoretical fundamentals [32]. Subsequently, Bard and Chandross explored the anodic and cathodic processes using the cyclic voltammetry of aromatic hydrocarbons explaining in this way the annihilation mechanism of ECL [33]. Early in 1970s, the first results of ECL obtained from the electrogenerated species of $[\text{Ru}(\text{bpy})_3]^{2+}$ complex had been reported by Bard and Tokel [34]. The following publications were focused on the theory [35] behind the simple electron-transfer reaction of ECL and CL by Marcus et al. and the ECL emission in aqueous solutions using the main co-reactant tri-n-propylamine (TPrA) [36]. With these latest studies, the ECL has been successfully adopted as a technique for bioassay for clinical diagnostics as shown in the work of Blackburn et al. where the technique has been used for the detection of polymerase chain reaction (PCR) and for the quantification of the HIV1 gag gene [37].

1.6.1 Pathways of ECL

For the production of an efficient ECL signal there are three central factors: an efficient electron-transfer reaction to produce the excited state, a good luminophore and a stable precursor to start the reaction [38]. Two pathways characterise the ECL, the annihilation and the co-reactant. The modern ECL is mainly based on the co-reactant like the experiments performed in this thesis, however, the early ECL studies were mostly based on the ion annihilation method (Fig. 13).

Generally, both pathways come from a previous exergonic electron-transfer reaction in the supporting electrolyte between the redox couple and the luminophore which undergo a homogeneous electron-transfer reaction once a suitable potential is applied to the working electrode. This leads to the production of an excited state and the subsequent emission of

light [27]. Based on the reversibility of the reaction, the luminophore is regenerated by decaying back to the ground state after emission [39].

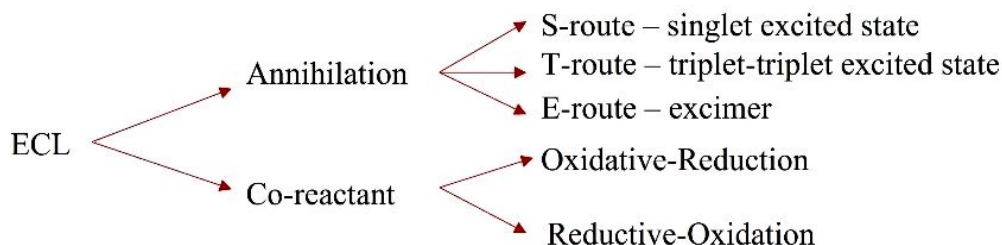
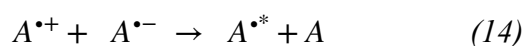


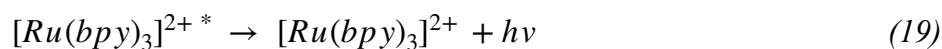
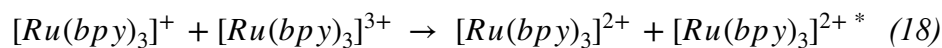
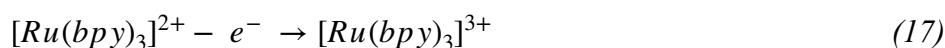
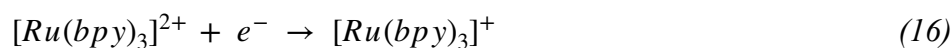
Figure 13: Schematic diagram of the different pathways adopted to produce ECL signals.

The annihilation method involves multiple reactions for the formation of oxidised and reduced forms. Initially, a potential is applied to the working electrode generating radical cations in the diffusion layer around the electrode and anions which instead diffuse away from the electrode surface following Fick's first law. The electrogenerated cations and anions interact forming the excited state which finally decays back to the ground state emitting light [27].



The major advantage of the annihilation pathway is that only solvents and electrolyte are needed for the generation of light obtaining a simple and low-cost system (as no enzymes or other species are involved). On the other hand, this ECL mechanism to produce light in the visible range, 400-700 nm, requires a wide potential window up to 3.3 V to generate radical ions. Moreover, quenching problems related to the dissolved O₂ can significantly affect the ECL emission [40].

An example of annihilation process is the ECL of [Ru(bpy)₃]²⁺ presented for the first time in Bard's work in 1972 [34]. Tris(bipyridine)ruthenium chloride is a luminophore unstable in aqueous solutions, therefore the ECL cannot be achieved in aqueous solutions varying the potential to generate [Ru(bpy)₃]³⁺ and [Ru(bpy)₃]⁺.



Equations (16) and (17) the electro-reduction and the electro-oxidation of the luminophore, respectively. (18) is the electro-transfer reactions at the electrode surface when a potential is applied. Finally the (19) specifies the emission of light from the excited state of the $[Ru(bpy)_3]^{2+*}$ form [41, 42] with a wavelength approximately of 620 nm [43].

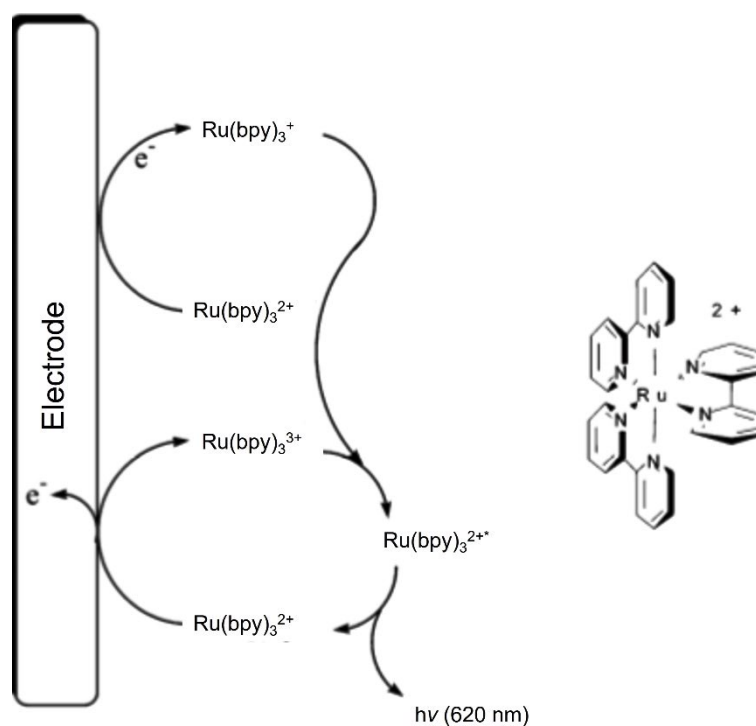


Figure 14: Structure of $[Ru(bpy)_3]^{2+}$ and annihilation mechanism for $[Ru(bpy)_3]^{3+}/[Ru(bpy)_3]^{2+}$ [44].

As shown in Fig.14, the annihilation pathways can be divided in three different “routes” depending on the free energy of the reaction. Briefly, the Gibbs free energy of an annihilation process is calculated from the equation (20):

$$\Delta G = -nF(E_{reduction}^0 - E_{oxidation}^0) \quad (20)$$

where ΔG defined the Gibbs free energy of the system in question, n is the number of electrons transferred, while F represents the Faraday's constant, finally $E_{reduction}^0 - E_{oxidation}^0$ are the reduction and the oxidation potentials, respectively. Depending on ΔG it is possible to distinguishes between the three routes (S-route, T-route, and E-route). If the homogeneous electron-transfer reaction between the electrogenerated species is exergonic, so the system has enough free energy, the annihilation process follows the singlet route also known as "S-route" (Fig. 15).

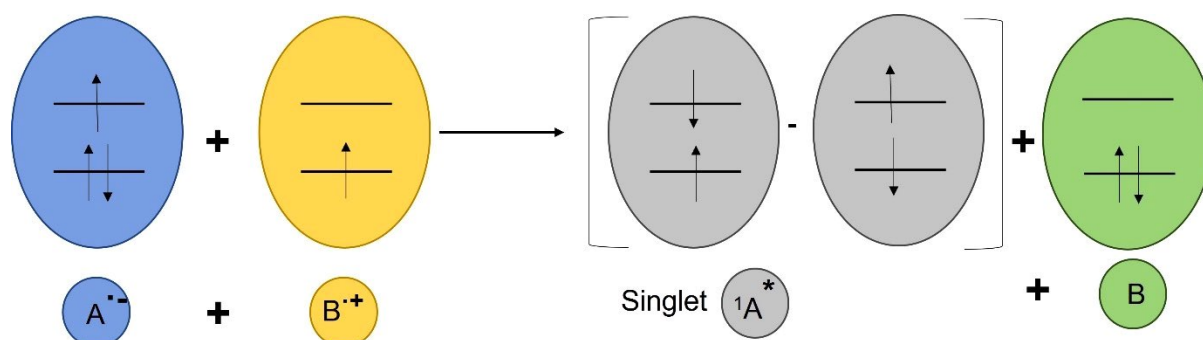


Figure 15: Schematic representation of the electron-transfer reaction between the electrogenerated radical ions for S-route annihilation

However, if the free energy of the system is not sufficient to directly generate the singlet state, the annihilation follows the "T-route" which includes the formation of a triplet state as indicated in equation (21) (Fig. 16).

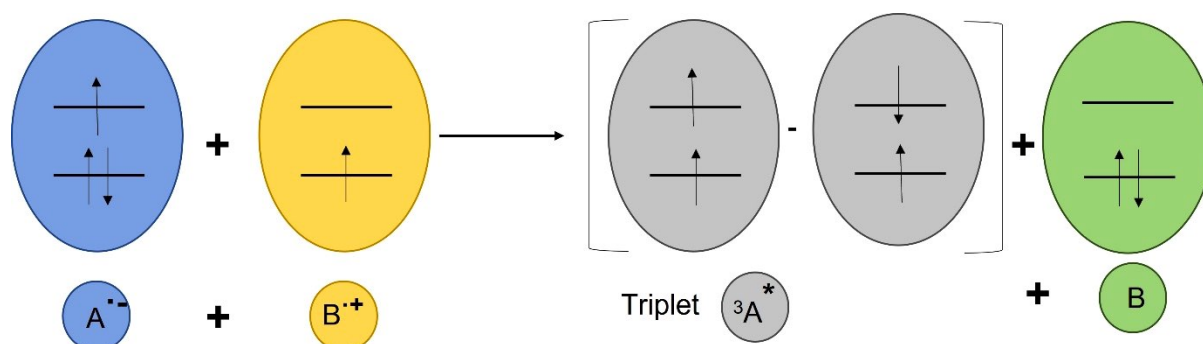
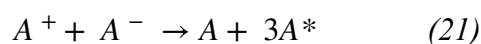
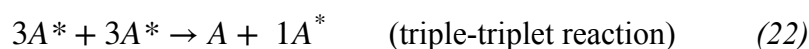


Figure 16: Schematic representation of a possible configuration of the triplet state formation. "T-route" annihilation pathway.

In this kind of “energy deficient system”, after the production of a triplet state, the triplet-triplet recombination allows eventually the singlet emitting state in a second step (22):

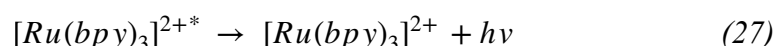
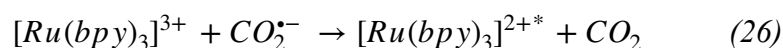
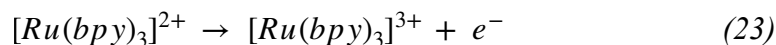


Finally, for a particular kind of systems the emissive species is an excimer, a dimer associated in an electronic state and dissociative in its ground state. One of the typical example of excimer is the pyrene [45]. This compound uses the “*E-route*” to produce ECL at very low energy compared to the monomeric species.

The second method to produce ECL is the co-reactant pathway that has been widely used in several fields thanks to the significant advantage to obtain ECL in aqueous solutions. This procedure opens up the possibility of analysis of a wide range of molecules essential for diagnostics and with a particular biological significance such as enzymes. Contrary to the annihilation process, the co-reactant pathway demands just one-directional potential scanning at the electrode hosting the species to be analysed, and luminophore, reagent and co-reactant as well, in the supporting electrolyte [46].

The co-reactant is a chemical species that, once the electrochemical oxidation or reduction starts, provides the production of an intermediate which in turn reacting with the oxidised or reduced form of the luminophore finally generate the excited state and so the emission of light[47]. During the electrochemical reaction, the co-reactant represents the sacrificial molecule since it is consumed irreversibly after each cycle, instead the luminophore can be regenerated at the electrode surface. Many factors need to be considered for the choice of the ECL co-reactant like the solubility, stability, electrochemical properties, kinetics, quenching effect and ECL background. The co-reactant is the species that undergoes easily to the oxidation or reduction process and provides the necessary energetic radicals able to react with the luminophore and rapidly produce the excited state [23]. This pathway is characterised by two kinds of reactions [42](Fig. 13), the *oxidative-reduction* and the *reductive-oxidation* processes. The first mechanism uses three different reactions to generate the emission of light: (1) the electrochemical oxidation at the electrode surface after the application of the potential, (2) the bond-breaking reaction of the co-reactant creating a strong reducing radical and finally (3) the reduction of the oxidised form of the luminophore by the co-reactant radicals. A classic example of this reaction was offered for the first time in 1977 by Bard et

al. when studying the emission of light from oxalate in acetonitrile [42]. Successively, the same mechanism has been studied in aqueous solutions with the detection of oxalate and $[Ru(bpy)_3]^{2+}$ with an emission of 610nm [41].



The *reductive-oxidation* system is normally achieved by applying a negative potential to the working electrode. In this kind of reactions it is quite difficult to acquire a stable ECL emission in aqueous solutions because of the hydrogen disturbance at very low potential as it undergoes to a reduction interfering with the electrochemical reaction [48]. For this pathway, both luminophore and co-reactant are firstly subjected to reduction; afterwards the reduced co-reactant undergoes a chemical reaction obtaining a strong oxidising radical. This radical is then involved in an electron-transfer reaction with the reduced form of the luminophore producing an excited state and the following ECL emission. A classic example of the co-reactant way to produce ECL is the $[Ru(bpy)_3]^{2+}$ /tripropylamine (TPrA) system (Fig. 17). This network represents the most used common method for the immunoassays in DNA analyses [49].

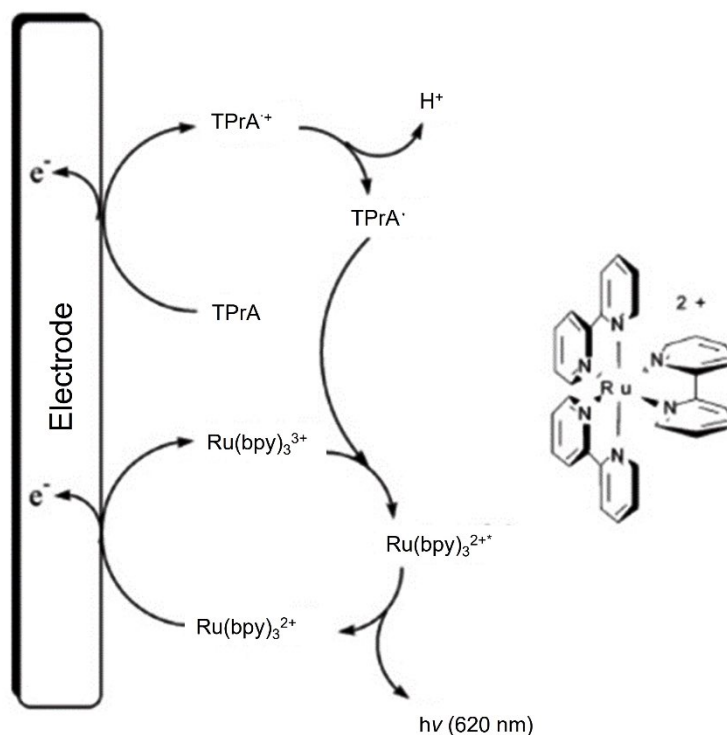
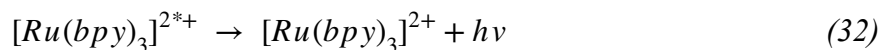
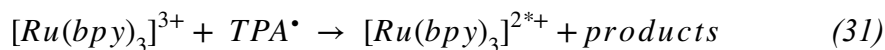
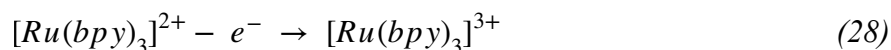


Figure 17: Scheme for the co-reactant mechanism of $[Ru(bpy)_3]^{2+}/TPrA$ system [50].

Both species undergo an oxidation taking place on the electrode surface with the consequent reduction of the $[Ru(bpy)_3]^{3+}$ by TPrA. This reduction allows the generation of an excited state of the luminophore emitting light as the final step of the process as defined in the following equations.



The co-reactant pathway has the important benefit to produce light in aqueous solution where the co-reactant and the luminophore can be oxidised and reduced with a single potential step (Fig. 18). This makes the co-reactant ECL ideal for biomedical applications where it is necessary to maintain a physiological pH to satisfy biocompatibility.

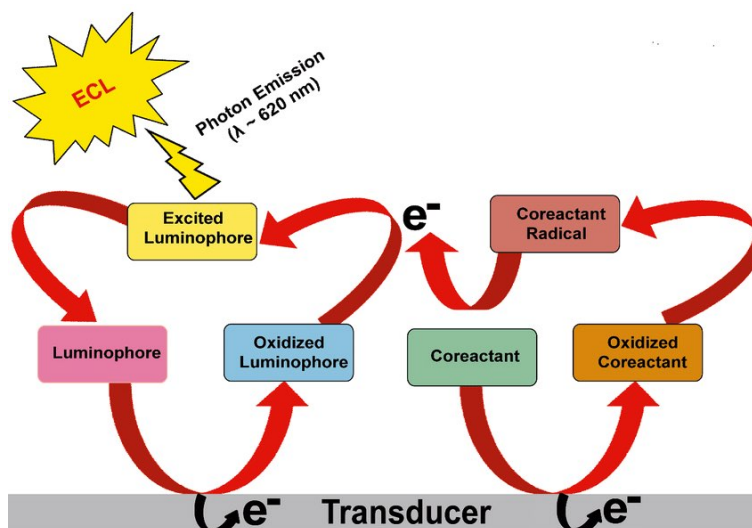


Figure 18: Schematic representation of the co-reactant pathway to produce ECL.

1.6.2 Electron transfer reaction

The electron transfer reactions between the electrogenerated species are essential for the formation of an excited state and the consequent relaxation to a ground state resulting in the ECL emission. Generally, the emission of light is achieved after the transitions from the ground state to the excited state of the species. Considering the Perrin-Jablonsky diagram, two phases define the electronic states of a molecule and the consequent transition between them: absorption, emission divided into fluorescence and phosphorescence [51].

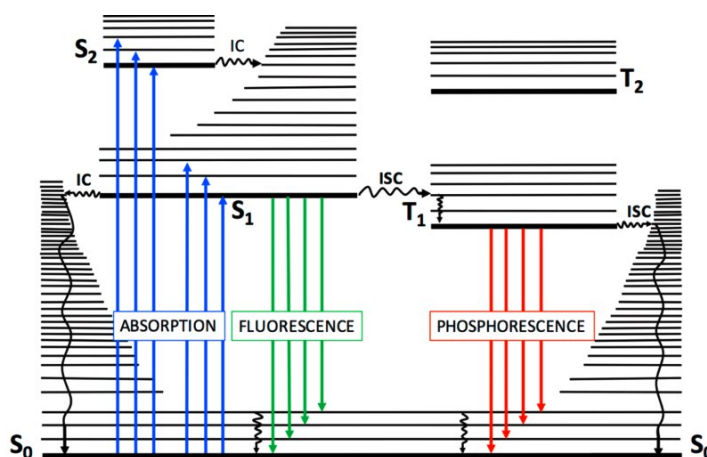


Figure 19: Schematic Perrin-Jablonsky diagram. Representation of energy levels and molecular orbitals during the absorption and emission of radiation [51].

The first transition in Fig.19 concerns the absorption of a photon defined as the method by which the electron is excited from a low energy level to a higher energy level, that means from S_0 to S_1 or S_2 . Once the electron is excited, the energy could be dissipated in different ways such as through a vibrational relaxation that induces to a non-radiative process happening when the photon's energy deposited onto the electron is exposed to other vibrational states as kinetic energy. However, if the vibrational energy levels powerfully overlap the electron energy levels, the excited electron transits from a vibrational level in an electronic state to another vibrational level in a lower electronic state. This second process is defined as internal conversion (Fig.20).

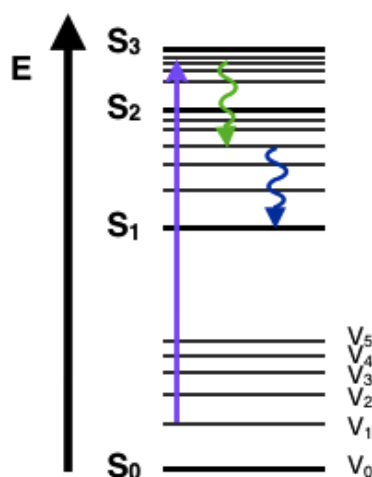


Figure 20: Possible scenario with the absorption (purple line), internal conversion (green line) and vibrational relaxation (blue line) processes [51].

Another pathway for molecules to cope with the energy received from photons is the emission of light, namely fluorescence. With regard to the absorption, the fluorescence is a slow process and often observed between the first excited electron state and the ground state for any molecule because at higher levels it is more likely that energy will be dissipated through internal conversion and vibrational relaxation (Fig.21).

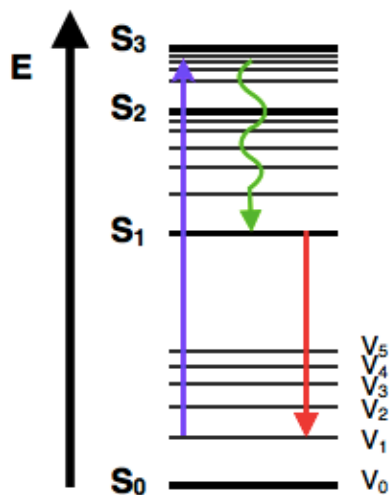


Figure 21: Possible scenario with the absorption (purple line), internal conversion (green line), vibrational relaxation (blue line) and fluorescence (red line) processes [51].

Finally, another path is the dissipation of energy called intersystem crossing happening when the electron changes spin direction from an excited singlet state to an excited triplet state. This is the slowest process represented in the Perrin-Jablonsky diagram. This process leads to several interesting routes back to the ground electronic state and the most frequent is the phosphorescence where a radiative transition occurs from an excited triplet state to a singlet ground state (Fig.22).

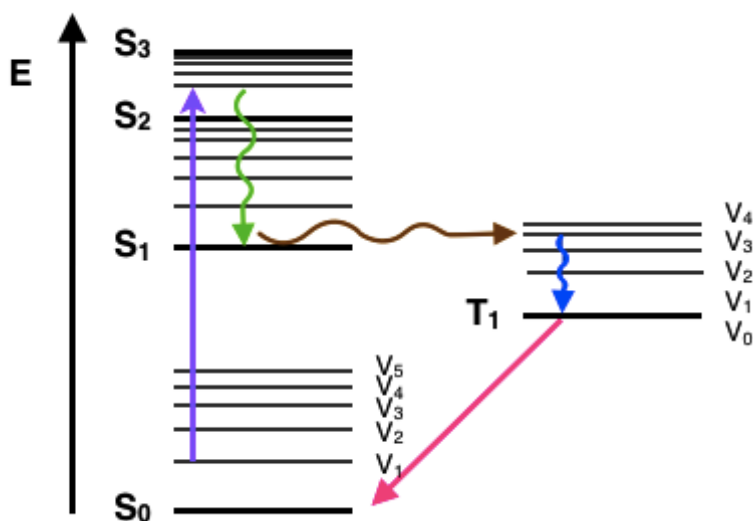


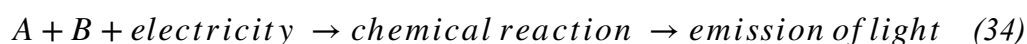
Figure 22: Possible scenario with the absorption (purple line), internal conversion (green line), vibrational relaxation (blue line), intersystem crossing (brown line) and phosphorescence (pink line) process [51].

Electrochemiluminescence (ECL) has received reasonable attention during recent years thanks to innumerable advantages of versatility, effective temporal and spatial control and high sensitivity and selectivity. ECL differs from the traditional chemiluminescence for different aspects, first in the initiation form.

Chemiluminescence [11], is the process where the energy is obtained by the homogeneous chemical reaction between at least two reagents:



In ECL process, the species generated on the electrode surface undergo high-energy electron-transfer reactions to form an excited state which in turn emits light. The generation of species on the electrode is achieved with the application of a suitable potential without which the reaction does not occur [11].



Another important distinction between the two techniques is the generation of two different forms of luminescence; CL emission is yielded in the bulk solution through mixing the species involved, conversely ECL, due to the electrochemical initiation of the species *in situ*, is characterised by an emission in the direct proximity of the electrode surface and not in the solution [23].

In summary, the word ECL explains exactly the main steps implicated in the process, 'E' electrochemical initiation of the reaction, 'C' is related to the chemical step and finally 'L' in the concluding light emission. Furthermore, the production of the ECL light is achieved by the application of an electrical energy to the working electrode providing the excitation of a luminophore in the electrolytic solution. In fact, the initial highly exergonic homogeneous electron-transfer reaction consequently gives generation of the excited state of the luminophore, which in turn, when relaxed to the ground state, provokes the emission of light [52]. The electron-transfer reaction that occur between the redox species involved and electrode surface, is fundamental for the emission of light and in general represents the main

process in electrochemistry [11]. During a redox reaction, two processes are basic: the Fermi level and the frontier molecular orbitals.

Considering the Fermi level, the energy of the electrons is defined by the potential of the electrode, by changing this potential through a potentiostat, the electron energy consequently changes consequently on the electrode. On the other hand, the frontier molecular orbitals like HOMO (highest occupied molecular orbital) and LUMO (lowest unoccupied molecular orbital) are essential to describe the reactivity for the redox processes. The combination of the two has as consequence the formation of the oxidation and reduction reactions of the species involved in the electrochemical reaction (Fig.23).

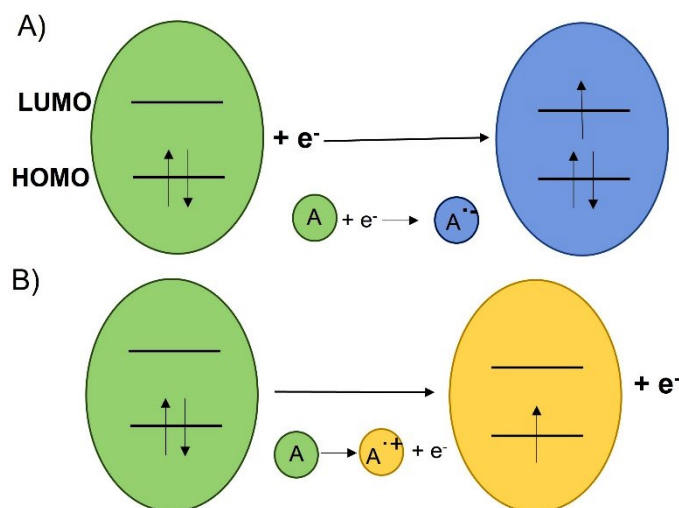


Figure 23: Schematic representation of (A) reduction and (B) oxidation reactions with the LUMO and HOMO configuration.

The reduction reaction, Fig.23A), can be achieved introducing negative potentials to the electrode. Thus, the energy of the electrode increases, and an electron is moved from the electrode to the unoccupied electronic state of the species involved (LUMO). Conversely, applying a more positive potential, its energy decreases and the electron is shifted from the chemical species to the electrode (HOMO) forming the oxidation process, Fig.23B). The application of the potential E to the WE is crucial to determine the type of reaction. Once the electrons cross the electrode, a flow current (i) runs in the solution moving crossing the WE and the counter electrode representing the electrons flow. This current is directly proportional to the number of transformed species during the electrochemical reaction. To study and analyse the electrochemical properties of a redox species, the cyclic voltammetry (CV)

technique represents the best tool providing all the information about the current flow sweeping continuously the applied potential to the working electrode [11]. During CV experiments, the starting potential applied does not produce any electrochemical reaction, then increasing or decreasing the potential, the reduction or oxidation reactions of the redox couple, take place respectively. Once the potential at which the redox reaction occurs is reached, the linear sweep of the voltammogram is reversed and the species can be detected also during the opposite scan depending on their stability as shown in Fig.24. The typical graph of the cyclic voltammetry is a voltammogram representing the current as a function of the electrode potential (i vs. E). During the reversible oxidation waves a cation radical is formed ($A^{\bullet+}$), instead in the reduction process an anion radical ($A^{\bullet-}$).

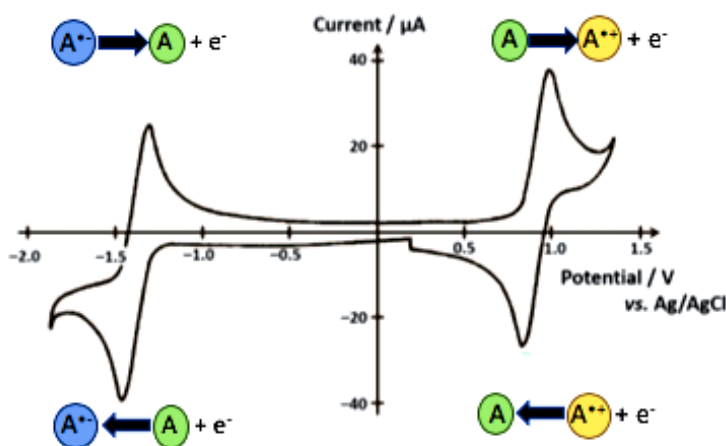


Figure 24: Typical cyclic voltammogram for a reversible redox couple that forms stable reduced and oxidised ions with the application of a suitable potential at the working electrode.

There are several essential parameters necessary for the subsequent interpretation of the data, 1) the scan rate of the potential that controls the scale of the voltametric experiments; 2) the cathodic and anodic potential peak; 3) the cathodic and anodic current peak; 4) the half-peak potential and finally 5) the half-wave potential [53].

In a conventional ECL experiment, the intensity of the emitted light is measured with ECL intensity as function of the potential applied (ECL vs. E). The ECL curve follows the behaviour of the voltammogram curve, and the resulting plot gives information about the stability of the species involved in the electron-transfer reaction, the reactivity of the electrogenerated species and the relation between the species and the equivalent co-reactant.

1.6.3 Fundamentals of ECL

Three essential factors are required for the generation of the ECL emission:

1. Generation of a stable precursors species in the electrochemical cell;
2. Sufficient-energy electron transfer reaction to obtain an excited state;
3. Good photoluminescent properties of the generated excited state.

As described in section 1.6.1, the precursors can be generated following two different pathways, annihilation, and co-reactant [54, 55]. In organic conditions, the precursors can exist in both the forms of oxidised and reduced radical ions. The main factor for the generation of ECL is the kinetics of the electron transfer reaction, essential for the formation of the precursor and so of the excited state [27].

During the annihilation process, the application of a potential at the WE allow the production of a radical cation (or anion) in the diffusion layer in the proximity of the electrode surface. When the potential is switched, the other radical form is produced diffusing from the electrode surface to the solution according to Fick's first law, moving from a region of high concentration to one with lower concentration [11]. The radical species obtained during the first potential applied are reduced at the electrode surface causing a decrease of their concentration. The concentration gradient is formed allowing a back diffusion of the species from the diffusion layer to the electrode surface. Here, the two species interact forming the excited state and the final emission of the ECL signal[56].

For the co-reactant pathway, the use of a reagent (co-reactant) that can be oxidised and reduced during the application of potential is required. Depending on the polarity of the potential applied, the oxidation or reduction reaction involving the luminophore and the co-reactant starts at the electrode surface forming radicals. The electro-generated species of the co-reactant undergoes to a rapid decomposition to form a reducing or oxidising intermediates characterised by a standard redox potential. The oxidised or reduced precursor is rapidly injected into the electrogenerated form of the luminophore generating the excited state and finally the emission of light [39].

The excited state and its relaxation to the ground state are fundamental for the obtainment of the ECL signal. The ECL signal can be observed when the excited state is formed and when it relaxes to the ground state dissipate energy by emitting photons. Therefore, the interaction and the electrons transfer reaction are two essential phenomena for the observation of the ECL signal. However, two different routes, A and B, can be followed after the electron transfer reaction (Fig 25).

- A. Generation of an excited state: an e^- is transferred from the LUMO of the reduced precursor to the LUMO of the oxidised precursor forming a ground state molecule and an excited state molecule. This excited molecule relaxing to the ground state emits a photon.
- B. Generation of two ground state molecules: an e^- is transferred from the LUMO of the reduced precursor to the HOMO of the oxidised precursor forming in this way two ground state molecules.

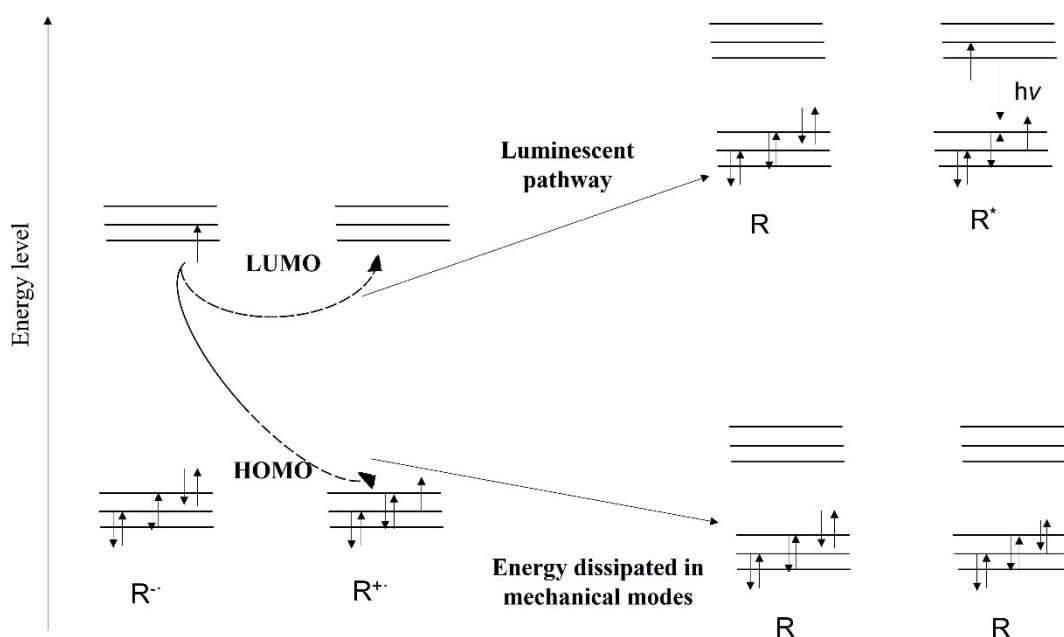


Figure 25: Molecular orbital diagram representing the two electron transfer reaction routes. Route A leads to the formation of the excited state, meanwhile route B forms two ground state molecules. Adapted from [57, 58].

From the thermodynamic point of view, route B is more favourable as two ground state molecules have been formed after the electron transfer reaction resulting in the release of high energy from the system in mechanical modes such as vibrations. This dissipation form is not positive for the system as it can cause disturbances in the system as a large amount of energy has to be dissipated in a short period of time [59]. These considerations are based on the Franck-Condon principle which states that the positions and momenta of the atoms involved in a transition are preserved as the movement of an e^- is exponentially faster than the movement of a nucleus [60]. The formation of two ground states during the route B is more thermodynamically favourable than route A as a large quantity of energy is dissipated from the system with vibrations. Alternatively, the luminescent pathways (route A) by producing an excited state and a ground state molecule, is less thermodynamically favourable so less energy has to be dissipated in a mechanical mode *via* vibrations. For these reasons, the system is more advantageous from the kinetic point of view, therefore the electron transfer reaction is more rapid [61]. Marcus theory of the electron transfer relates the electronic and nuclear considerations with the rate of the reaction according to (35):

$$K_{ET} = \nu e^{\left(-\frac{\Delta G^\ddagger}{RT}\right)} \quad (35)$$

Where:

K_{ET} is the rate of the electron transfer reaction;

ν is the frequency factor;

ΔG^\ddagger is the Marcus free energy of activation;

R is the gas constant (8.3145 J mol⁻¹ K⁻¹);

T is the temperature (K).

The Marcus free energy of activation can also be related to the free energy of the reaction indicated as ΔG^0 as indicated in (36):

$$\Delta G^\ddagger = \frac{(\Delta G^0 + \lambda)^2}{4\lambda} \quad (36)$$

where λ is the total reorganisation energy which consists in the outer sphere component so the reorganisation of the solvent and the media and the inner sphere contribute involving the reorganisation of the molecular geometry of reactants [60, 62].

1.7 Cyclic voltammetry

Cyclic voltammetry is an important tool for the investigation of electrochemical reactions and for the study of the kinetics of the electrode reactions. Specifically, with the CV it is possible to analyse the reversibility of the reactions observing the oxidation and reduction potentials and the diffusion of the species changing the reaction rate [63]. Normally, the system used for recording voltammograms is a three-electrode configuration composed of working, reference and counter electrodes connected to create a circuit able to overcome a drop in the working electrode potential compared to the applied potential as result of the resistance of the electrolyte[53].

The CV study starts after the application of an initial potential, E_i , at the working electrode changing linearly with time following the triangular waveform of the potential versus time. The potential is measured between the working electrode and the reference electrode which has a fixed potential, instead the resulting current is measured between the WE and the CE. During the initial forward scan, the potential increases over time determining the rise of the anodic current describing the oxidation of the analytes in solution. Once the switching potential is reached, the potential starts to decrease obtaining a reverse scan characterising the reduction of the species involved [11]. For the cyclic voltammetry technique, a typical voltammogram, shown in Fig. 26, is obtained by applying a potential which when reaches the potential E_2 it changes direction returning to the initial potential E_1 . The scan rate is an essential parameter which sets the period for the potential sweep. The i - E trace characterising the voltammogram shows the swept potential in terms of oxidation and reduction reactions. In particular, the oxidation process happens when the potential is swept from E_1 to E_2 causing an increase of the diffusion layer and the consequent faradaic current.

The diffusion layer becomes large enough to reduce the flux of particles to the electrode obtaining in this way a slow electron transfer reaction at the electrode surface. This results in an anodic peak current known as i_{pa} at the corresponding E_{pa} . The process happens when the potential is swept back from E_2 to E_1 causing a reduction reaction and so a cathodic peak current i_{pc} at the potential E_{pc} (Fig. 25).

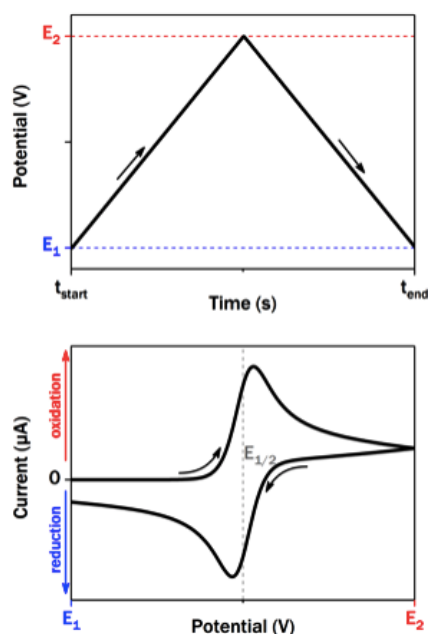


Figure 26: Cyclic voltammetry triangular waveform (top) and the corresponding voltammogram showing the oxidation and reduction curves (bottom) [63].

Two factors characterise the generation of the current, 1) the movement of the redox species near the electrode surface and 2) the electron transfer reaction. In fact, the peaks in the voltammogram are observed at potentials that initiate a chemical reaction in the electrolyte in particular an oxidation for positive potential and a reduction for negative, involving a flow of electrons. For positive potentials, the flow of electrons goes from the solution to the electrode surface obtaining the *oxidative current*, so the energy of the electrons is lowered; instead for negative potentials the electrons rise moving from the electrode to the solution obtaining the *reductive current*. This movement of electrons forms a gradient as a result of the difference of species between the electrode surface and the electrolyte [64]. The movement of these electrons is defined by a diffusion-controlled mass transport as the CV experiments are carried out in a stationary condition (no stirring) [65].

Considering an electrochemical reversible couple, the analyte can be recovered after the forward and reverse scan cycle. The voltammogram is characterised by two Gaussian-shaped peaks, known as duck-shaped, describing the oxidation and the reduction as for the potassium ferricyanide in Fig. 27.

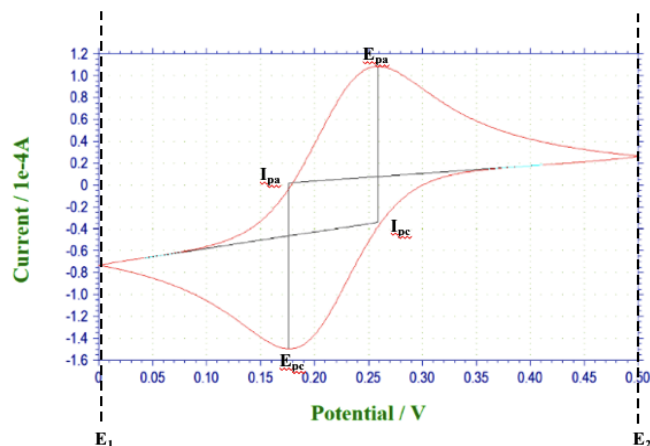


Figure 27: Cyclic voltammetry of 10 mM potassium ferricyanide in KCl at 0.05 V/s scan rate. The oxidation and reduction peaks are at 0.18 V and 0.27 V respectively.

One of the most important aspects is the difference between the two peaks describing the effect of the diffusion rate.

$$\Delta E_p = \left| E_{pa} - E_{pc} \right| > 0 \quad (37)$$

In the ideal case of a reversible couple exchanging one electron, for the conditions predicted by Nernst equation, the ΔE_p value is 57 mV. For systems that exchange n electrons during the process, the ΔE_p could be described by the following:

$$E_{pa} - E_{pc} = \frac{57 \text{ mV}}{n} \quad (38)$$

One of the most important parameters to set for the CV experiments, is the scan rate that controls how fast the potential is applied affecting the resulting peak current [66]. The current i is described as the charge (Coulomb) per unit time, so in cyclic voltammetry the current passing through the electrode is limited by the diffusion of the species involved on the electrode surface. The diffusion is also influenced by the concentration gradient developed

around the same electrode which in turn is affected by the velocity at which the species can diffuse through the electrolytic solution. For high scan rate values there is a decrease of the diffusion layer formed on the electrode surface with the consequent increase of the current [67] (Fig. 28).

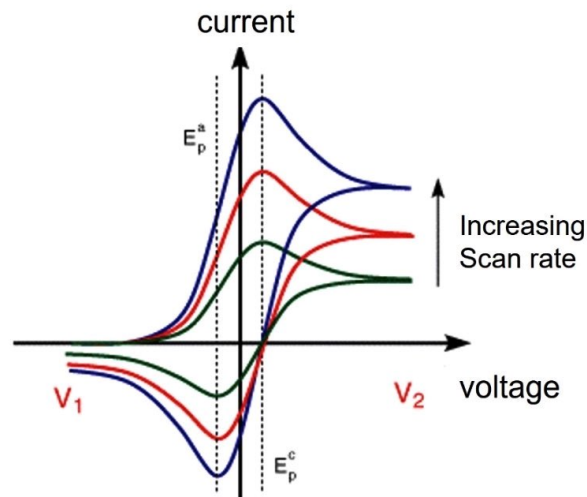


Figure 28: Voltammograms showing how the difference scan rates affect the peak currents [67].

The relationship between scan rate, current and diffusion is described by the Randles-Sevcik equation where the peak current i_p increases linearly with the square root of the scan rate.

$$i_p = 0.446 n F A C \left(\frac{n F v D}{RT} \right)^{1/2} \quad (39)$$

Where:

i_p is the studied peak current (A)

n is the number of electrons transferred during the reactions

F is the Faraday constant (96,4853 C mol⁻¹)

A is the area of the electrode where the reaction occurs (cm²)

C is the concentration of the analyte (mol cm⁻³)

v is the scan rate (V s⁻¹)

D is the diffusion coefficient (cm² s⁻¹)

R is the gas constant (8,314 J K⁻¹ mol⁻¹)

T is the temperature (K).

1.8 Biosensors

The aim of this research was the development of a non-invasive biosensor for the real-time detection of enzyme's activity. In general, a biosensor is an analytical device able to measure a chemical species with the use of a dedicated detector [68, 69].

It is composed of three elements, bio-receptor (such as enzymes, cells, antibodies, aptamers), a transducer or electronic system and a signal processing system[70] (Fig. 29).

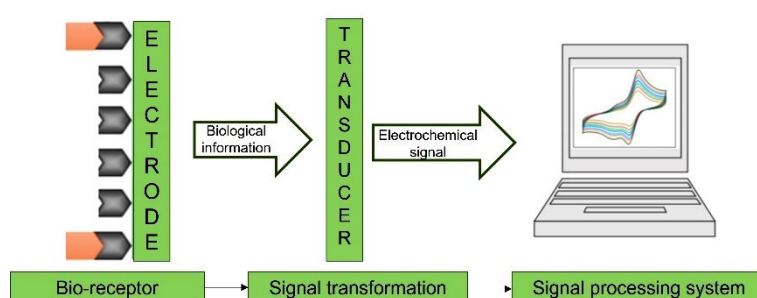


Figure 29: Main components of a general biosensor.

The bio-receptor is the area of the biosensor that hosts the analyte, and it must be characterised by a high selectivity for the specific species amongst the other chemical and biological compounds in the electrochemical cell. Depending on the type of transducer and on the signal obtained, biosensors can be classified as reported in Fig. 30.

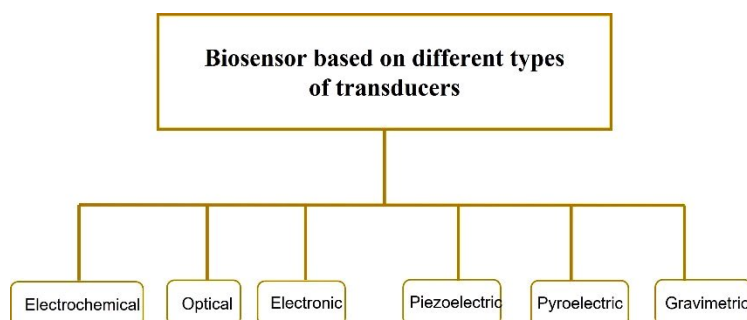


Figure 30: Classification of the different biosensors depending on the type of transducer.

The electrochemical biosensors are based on enzymatic reactions (catalysis) with the production of electrons. The reaction takes place on the electrode area causing either the

transfer of electrons through the double layer (producing current) or contributing to the potential of the double layer (producing voltage) [71]. The electrochemical biosensor here proposed is based on immobilised enzymes on the electrode surface (bio-receptor), after the application of potential the chemical reaction occurs producing a current and an emission of light (electrochemical signal) which can be finally processed. The final signal is produced after an electrochemical stimulation instead of other excitation with light sources minimising in this way the signal-to-noise ratio. This represents one of the advantages of the ECL respect to other photoluminescence methods where it is possible to have light scattering or luminescent background. Furthermore, the use of co-reactants in buffered aqueous solutions operating with positive potentials, oxidative-reduction process, make the ECL-based biosensors ideal for immunoassay analysis [72-75].

1.8.1 Amperometric biosensors

The amperometric biosensors have been divided into three different groups depending on the method used for the detection and how it affects the electrons transfer during the biochemical reaction. Furthermore, criteria such as the transducer, mediators, co-reactants, and enzyme have been crucial for the division of the amperometric sensors. In general, an amperometric sensor can measure the current produced when a potential is applied to an electrochemical cell. The species undergo to the redox reaction with the consequent production of the electrochemical signal.

The *first generation* is known as mediator-less amperometric biosensors as they allow the detection of analytes in the electrochemical solution due to the electrical signal produced by the diffusion of the analyte in the proximity of the electrode surface (Fig. 31). The transducer can be modified with biomolecules like enzymes able to transform a specific substrate in an electroactive molecule giving an electrochemical signal to be processed [74].

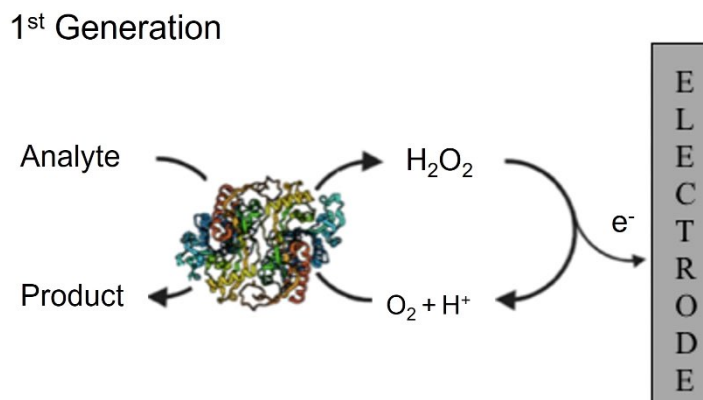


Figure 31: Schematic representation of the working principle of the first generation of biosensors [76].

The *second generation* known as mediator-amperometric biosensors employ mediator as oxidising agents acting as electron carries (Fig. 32). With this kind of biosensors is possible to work at very low potentials without any interferences due to O_2 dependence. Different mediators have been investigated such as ferrocene and ferricyanide, Prussian blue, methylene blue, phenazines, methyl violet, alizarin yellow, and inorganic redox ions. If an enzymatic system is employed, it is suitable to use an electron acceptor able to transfer electrons from the enzymes to the electrode surface. This generation has some drawbacks which do not make it suitable for the electrochemical tests like the difficulty in the immobilisation of the mediators, the possibility to have some leaking of the mediator during the time and the necessity to have a specific and stable behaviour for all the duration of the electrochemical analysis [77].

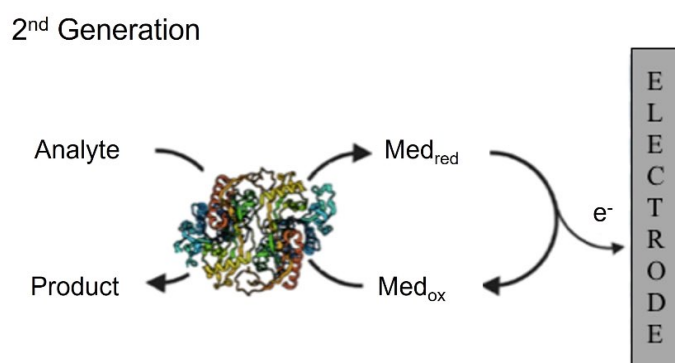


Figure 32: Second generation of the amperometric biosensor showing the mediator acting as electrons carrier for the electron transfer reaction [76].

Finally, the *third generation* is mostly used for the measurements of electron transfer between the electrode surface and the enzyme (Fig. 33). These kind of biosensors are composed of three main components, the bio-recognition element that is normally an enzyme, the electrode surface where the reactions happen and the redox couple that allows the production of the signal [78]. To increase the performance of the biosensor, it is possible to use polymers to connect the center of the redox couple with the electrode surface [79].

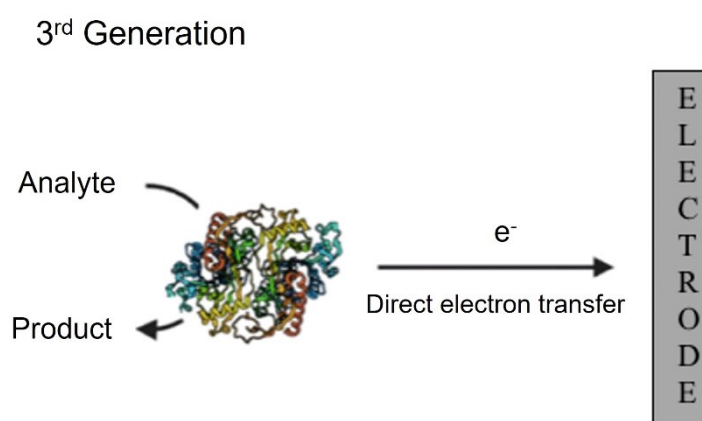


Figure 33: Third generation of biosensors where the electrons are directly transferred from the enzyme to the electrode surface [76].

The biosensor developed for this research involves the use of immobilised enzymes entrapped into the alginate hydrogel on the electrode surface. The specific substrate added to the electrolytic solution reacting with the enzyme allows a direct transfer of the electrons from the center of the redox couple to the electrode surface. This novel biosensor could be in the category of the third generation amperometric biosensors.

1.9 Conclusions

In this chapter the main theoretical aspects characterising the achievement of the ECL signal have been described. The main purpose of the biomedical research is the development of a sensitive, selective, low-cost, and real time biosensors for the monitoring of clinically relevant parameters. Therefore, the ECL technique represents a novel approach such applications due to the high sensitivity, control over time and space of the light-emitting reactions, sensibility. The use of biocompatible materials into these devices has allowed improvements in the use of this experimental technique for a wide range of applications in the healthcare field.

Chapter 2: Encapsulation of enzymes into alginate hydrogels

This chapter is dedicated to the description of the method developed for the encapsulation of the enzymes into alginate hydrogels materials. Firstly, a review of the main works in the literature regarding the enzyme's encapsulation is carried out by considering all the different techniques developed throughout the years, underlying both the advantages and disadvantages. Following the three main steps for the successful encapsulation of the enzyme, 1) the entrapment into microspheres cores, 2) the building of an electroactive external layer and 3) the final encapsulation of the system into alginate hydrogels. To conclude the chapter, the full characterisation of the biomaterial with the imaging of the system obtained through the confocal microscopy is proposed.

2.1 Enzymes encapsulation techniques: literature review

The use of enzymes as biocatalyst has increased during the years due to the several properties of these biomolecules like the biodegradability, catalytic efficiency, and selectivity. To improve these aspects, different techniques have been developed for the enzyme's immobilisation. In fact, compared to a free enzyme in a solution, an immobilised one becomes more resistant and robust to the environmental changes such as pH, temperature and external agents [80]. Additionally, it is possible and easier for an immobilised enzyme to be reused for further tests than an enzyme freely dissolved into a solution.

In the last decade, different techniques have been proposed for the restraining of biological species. Immobilisation is defined as the retention of macromolecules, like cells, enzymes, and proteins, in a specific support or matrix enabling the exchange of medium containing substrate, effector or inhibitor molecules. In the literature it is possible to identify four phases for the development of the different immobilisation techniques. The first rises in the first half of the nineteenth century when microorganisms have been restraint for industrial purposes like waste water treatments [81]. Subsequently, in 1960s a single enzyme has been immobilised for the production of L-amino acids and for the isomerisation of glucose [82]. Between 1985 and 1995, the third age is dated with the multiple enzyme immobilisation, the cofactor regeneration and cell detention. An example is the production of L-amino acids dehydrogenase starting from keto-acids. At last, the fourth age has been traced from 1995 to

the present days where the immobilisation of species is used in a wide range of disciplines with applications for the clinical, industrial, and environmental fields.

These techniques have multiple advantages of higher efficiency, continuous use of the enzyme and so its recovery for further uses, less chance of contamination of the products. Furthermore, the immobilisation protects the enzyme from the external environment and improve the performances under critical conditions regarding acidity, alkalinity, organic solvents and elevated temperatures [83].

In 1916, Nelson and Griffin proposed the first immobilisation by adsorption of the invertase enzymes for the food industry use [84]. This discovery triggered the development of other immobilisation strategies like the different covalent methods developed during the 1950s and 1960s. Thanks to these approaches, few hundred enzymes have been restrained and then used for a wide range of industries [85] like the industrial production of antibiotics or amino acids; food industry to enhance the fermentation [86], baking [87], dairy products [88, 89]. Also, the detergent and paper industry started to use enzymes [90, 91]. Large impact was also detected in the pharmaceutical [92] and chemical manufacture [93]. The immobilisation has been also widely employed in the diagnosis and treatment of many conditions thanks to the specificity of enzymes [94].

In this research, the immobilisation of enzymes is required to study and detect their activity corresponding to different amount of substrates level essential for the monitoring of pathological conditions like diabetes, or high levels of cholesterol and lactic acid.

The matrixes for the immobilisation can be classified in three major categories: (1) natural polymers, (2) synthetic polymers and (3) inorganic materials. Natural polymers are generally defined as macromolecular materials easily obtainable from microorganisms such as bacteria, algae, and fungi instead the more complex polymers are found in animals. These compounds are widely used in industries due to their biodegradability, biocompatibility, and ability to be modified. In fact, collagen, gelatine, chitin, chitosan, alginate and silk fibroin are all natural materials used for different biomedical engineering applications like wound healing [95], bio scaffolding [96], controlled delivery of drugs [97, 98] and implantations [99]. The natural polymer used for this research is the alginate also known as alginic salt derived from the cell wall of brown algae and seaweed. Alginate has several properties like the hydrophilicity, low toxicity, low cost and mild gelation by adding divalent cations like Ca^{2+} [100, 101]. It is

typically used in the form of hydrogels in a three-dimensionally cross-linked network composed of hydrophilic polymers with a very high water content [102] and used in biomedicine for different purposes such as scaffolds for the tissue engineering, wound healing and drug delivery [103].

Other examples of natural polymers are chitosan and chitin, two natural polysaccharides able to build covalent bonds between the different functional groups of the enzymes and the -OH group of the chitin chain to permanently retain the species [104]. This cationic polymer has been widely used in industries like food, cosmetic, biomedical and pharmaceutical due to its biocompatibility [105]. Furthermore, collagen is characterised by an excellent biocompatibility and biodegradability and so widely used for medical applications, especially for drug delivery system, cell culture matrix, sponge for burn and wounds, skin replacement and scaffold for artificial blood vessels and valves [106].

Synthetic polymers instead, are human-made materials characterised by insoluble supports with a very porous surface. This aspect is essential for the entrapment and holding of the enzymes and or whole cells. They are widely used in biomedical and pharmacological industries for the development of prosthetic implants, suture material and drug carriers [107].

Finally, to the category of inorganic materials belong compounds like zeolites with a microporous structures with good adsorbing properties widely used for the enzymes and whole cells immobilisation [108].

2.2 Encapsulation techniques

Depending on the possibility to retrieve or not the enzyme at the end of the immobilisation process, it is possible to distinguish the different encapsulation procedures between two main groups: reversible and irreversible processes [109] depending on the strength of the bond established between the enzyme and the corresponding support (Fig. 34). The most common approach is the irreversible one obtained when building a very strong bond between the matrix and the enzyme itself sacrificing in this way the chance to reuse the enzyme. As a matter of fact, it is very hard to satisfy the stability and reversibility aspects at the same time [110]. The following procedures of immobilisation have been developed

during the years to achieve an higher stability, durability and resistance of the enzymes in different environmental conditions that could otherwise affect the catalyst activity [80].

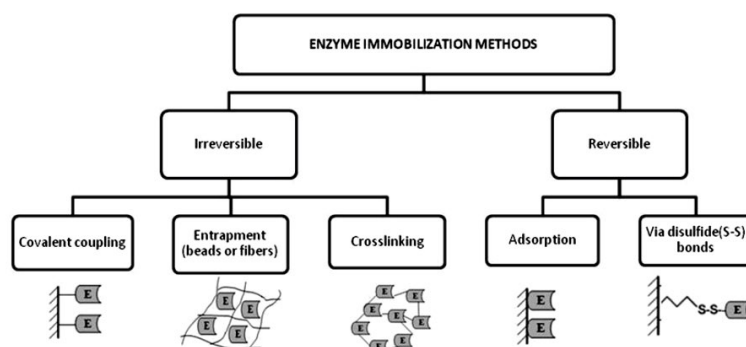


Figure 34: Scheme of the different enzyme immobilisation strategies, (Copyright Creative Enzymes®) [111].

2.2.1 Entrapment

Considering the irreversible methods, the most used procedures are the entrapment, covalent coupling, and cross-linking. In the entrapment, enzymes are immobilised in insoluble beads or microspheres like calcium alginate chains (Fig. 35). This method is largely used for cell detention finding particularly interest also for the enzyme’s immobilisation. Theoretically, the specie is not attached to the polymer chain, but it is free in the matrix. However, very often the enzyme is an integral part of the polymer chain with the formation of covalent and non-covalent bonds. This technique is characterised by several advantages including low cost of the materials and it is a fast and easy method that can be used for sensing applications. On the other hand, several disadvantages affect this method such as a limited pore diffusion and the possibility of leakage of the enzymes through the pores.

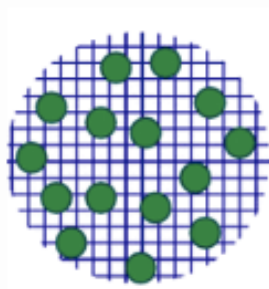


Figure 35: Enzyme immobilisation strategy: entrapment.

The entrapment, also known as inclusion, corresponds literally to the confinement of the species inside the polymer matrix and it is carried out by mixing the biocatalyst into the monomer solution followed by polymerisation initiated by a change in temperature or by a chemical reaction. The size of the pores can be adjusted by changing the polymerisation conditions, for example the drying process can affect the polymer composition allowing a modulation of the porosity. The most used polymer as matrices are polyacrylamide used by Lee and Huang for the immobilisation of trypsin [112], collagen that is a high biocompatible extracellular matrix used to form hydrogels [113].

2.2.2 Encapsulation

A similar technique is the encapsulation used in this research to immobilise the enzymes inside the microspheres cores and subsequently encapsulate the nano-material inside the alginate hydrogel matrix (Fig. 36). This method allows the protection of the enzyme from the external environment, from the change of different conditions such as pH, temperature, and acidic/alkaline solutions. This kind of immobilisation is defined by the enclosure of the species into a capsule made up of different materials. This procedure permits the possibility to immobilise enzymes with a cheap, simple, and fast method.

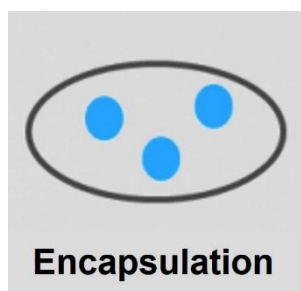


Figure 36: Enzyme immobilisation strategy: Encapsulation.

The main membrane used for this kind of encapsulation is the alginate, a polysaccharide containing blocks of (1,4)-linked-d-mannuroic (M block) and α -l-guluronic (G block) acids [114]. It is commonly used for the encapsulation of therapeutic agents thanks to its biocompatibility like in Lim and Sun paper [115], then alginate has become the most studied material for the encapsulation of living cells [116]. For this research alginate hydrogels have been combined with CaCO_3 microspheres to improve the enzyme response and durability of the system. With the introduction of the microspheres the structure of the biomaterial is more uniform and with an higher mechanical stability[117].

2.2.3 Cross-Linking

The cross-linking method is also known as co-polymerisation and the immobilisation of the enzymes is achieved by a covalent bond between various group of the enzymes through multifunctional reagents (Fig. 37).

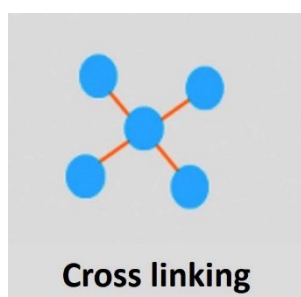


Figure 37: Enzyme immobilisation strategy: Cross-linking

The multifunctional reagent works as linker to connect the enzymes into three dimensional aggregates. In literature, two different way to obtain a cross-linking process are described, (1) the cross linking enzyme aggregate (CLEA) and (2) the cross linking enzyme crystal (CLEC) [118]. For the CLEC-based method, the linking agent used is the glutaraldehyde and the enzymes immobilised show significant improvements in mechanical properties with high stability and efficiency [119]. CLEA method instead, can be applied in aqueous solutions with the addition of salts, organic solvents, or non-ionic polymers to form enzymes aggregates.

2.2.4 Covalent Bonding

Finally, the covalent bonding is one of the most used method due to the stability of the links between the functional groups enzymes molecules and the support matrix. As a result of this great advantage, the leaking of enzyme during the use of the system is heavily reduced (Fig. 38). The main functional group used for the formation of the covalent bond are: amino group, carboxylic group, phenolic group, sulfhydryl group, thiol group, imidazole group, indole group and hydroxyl group [120]. Two steps need to be followed to immobilise the enzyme with the covalent bonding procedure: (1) activation of the surface with a linker molecule like glutaraldehyde or carbodiimide working as a bridge between the surface of the matrix and the enzyme through a covalent bonding, (2) enzyme covalent coupling to the activated support.

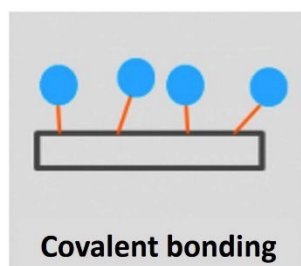


Figure 38: Enzyme immobilisation strategy: Covalent Bonding.

2.2.5 Adsorption

Reversible methods like the adsorption and the entrapment via disulfide bonds are used in case of necessity to retrieve the enzyme. The adsorption is based on the formation of very strong bonds such as Van der Waal's forces, electrostatic and hydrophobic interactions [109] (Fig. 39). The enzyme is diluted in solution and the matrix or support is placed in direct contact with that solution for a period granting its adsorption. This a simple and cheap way of immobilisation, reagent-free and non-destructive for the enzymes.

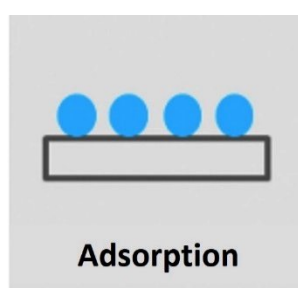


Figure 39: Enzyme immobilisation strategy: Adsorption.

There are three sub-categories of adsorption: (1) physical adsorption, (2) electrostatic binding and (3) hydrophobic adsorption. The physical strategy requires the immersion of the support into the solution that hosts the enzyme for a certain period. In this way the enzymes are adsorbed on the surface of the matrix without involving any kind of reagent but just establishing Van der Waal's forces, hydrophobic interactions and/or hydrogen bonding [121]. The electrostatic binding uses electrostatic forces considering the pH of the reaction solution and the isoelectric point of the enzyme to be immobilised. The enzyme surface can be positive or negative charged depending on the difference between its isoelectric point and the pH value, thus the enzyme could be immobilised on a surface with the opposite charge through ionic and polar interactions. Two common techniques for the electrostatic immobilisation are in place, the layer-by-layer deposition and the electrochemical doping used to define the charge of the enzyme surface. Finally, the hydrophobic adsorption involves hydrophobic interactions between the support and the enzyme. For this method, an entropically driven interaction takes place instead of the formation of a chemical bond.

For this work it has been used a combination of different technique to successfully immobilise the enzyme on the GCE surface. Firstly, the enzyme is entrapped inside microspheres cores where the species are free to move. This nano-material is then subjected to a layer-by-layer process to define the superficial charge and allow the final encapsulation into the alginate hydrogel matrix. The final capsule undergoes to a cross-linking process creating very strong covalent bonds and reduce the pore sizes to maintain the enzyme entrapped in the material. The last process is performed directly on the electrode surface to build a solid final bond between the electrode surface and the external surface of the hydrogel.

2.3 CaCO₃ microspheres

Microspheres are three-dimensional holders typically in a spherical shape able to transport drugs, enzymes, proteins, antibody and vaccines [122]. There are three methods for the obtainment of the cores, from biopolymers, glasses, and ceramics. Polymer-based microspheres have been widely studied during the years for their potential in controlled drug deliveries achieved by degradation of the polymer matrix or due to the leakage of the incorporated drug through the pores of the matrix. For the production of these carries can be used either natural polymers such as collagen [123] and protein [124] suitable for the enzyme degradation, and synthetic polymers like polylactic acid (PLA) which instead undergo hydrolytic degradation [125]. Glass and ceramic based microspheres are more convenient for tissue regeneration, orthopaedic [126] and dental applications due to their crystal configuration, biocompatibility and osteoconductivity [127].

The entrapment of biomolecules, like enzymes, is an advantageous method to protect the molecules from degradation due to the external environment, to achieve a controlled release in the case of drug delivery and to reduce the risk of immune response [128, 129]. During the years several attempts have been made to incapsulate molecules, principally proteins, like spray and freeze drying, encapsulation into polymeric particles and/or liposomes [130, 131], crystallisation [132] finding however problems related to interferences with external agents like reactive cross-linking agents or organic solvents. A new assembly procedure has been introduced by Volodkin in 2014 for the development of porous calcium

carbonate (CaCO_3) vaterite micro-particles using a layer-by-layer process based on the alternation of oppositely charged polyelectrolytes obtaining capsule efficient for bio applications [133]. This method has been followed for the entrapment of the oxidase and dehydrogenase enzymes for the ECL experiments here reported. CaCO_3 presents in nature three different polymorphs namely calcite, aragonite and vaterite which is the most stable due to the porous structure. It is characterised by spherical shape cores suitable for applications based on encapsulation of both small and large biomolecules (Fig. 40).

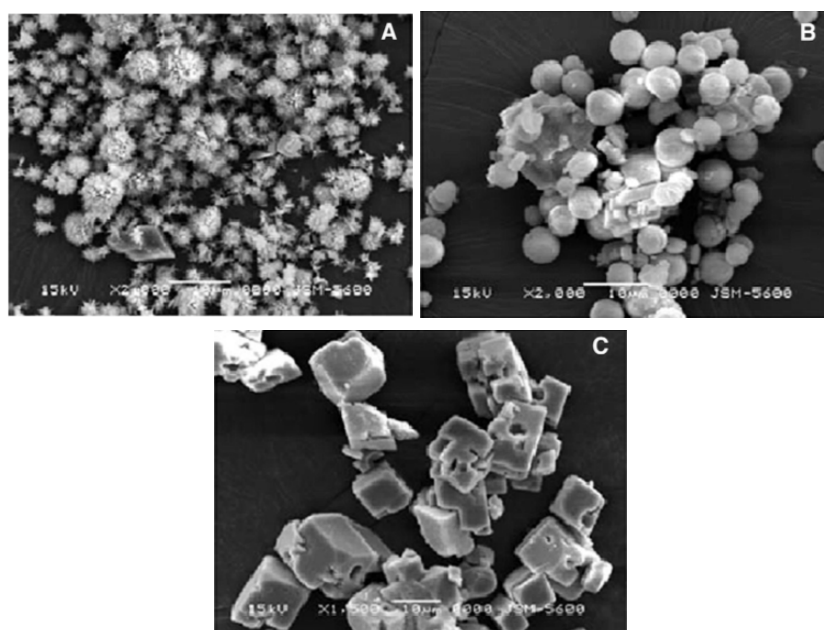


Figure 40: Structures of the three polymorphs of calcium carbonate, A) aragonite, B) vaterite and C) calcite. (Reprinted, Copyright Elsevier) [133].

To obtain a well-defined pore sizes of the polymorph CaCO_3 , the two different salts CaCl_2 and Na_2CO_3 have been vigorously mixed by stirring forming pores with dimensions between 3 and 20 μm [134]. The two salts mixture leads to the formation of nuclei followed by the growth of vaterite crystals characterised by a controlled pore size due to the monitoring of the time and stirring speed. This represents a great advantage of this technique as the formation of microspheres is normally quite expensive due to the different additives introduced to control some of the microsphere's features. With the Volodkin's method instead, insoluble CaCO_3 microspheres are generated without adding any further additives to the two salts solution. Different works reported the obtainment of crystallisation form of calcium carbonate by adding organic additives like citric acid or magnesium [135, 136]. Three

methods to load the macromolecules into the CaCO₃ cores can be used: physical adsorption, co-precipitation, and solvent exchange. The co-precipitation is the technique used for the enzymes encapsulation and it is based on the capture of the molecule of interest (MOI) during the vaterite preparation. This is a single-step procedure providing the encapsulation of MOI in large amount by simply adding them to the salt's solution during the stirring process. The molecules are physical introduced into the interconnected spaces of the calcium carbonate matrices however, it is still not clear how the MOI may affect the internal structure of the microspheres and also how this entrapment mechanism exactly happens [137]. The physical adsorption instead, is driven by electrostatic interactions between the cores surface and proteins. Finally the solvent exchange method, or infiltration, requires an amount of MOI that exceeded that used for the physical adsorption using intermolecular interactions like the protein isoelectric precipitation [134].

2.4 Alginate hydrogels as biomaterial

Alginate hydrogels are three-dimensional network characterised by the ability to swell when they absorb liquids maintaining their initial structure. One of the most used is the sodium alginate obtained from condensation of β -D-mannuronic acid (M) and α -L-guluronic (G) residues which is characteristic to form gels in the presence of multivalent cations and cross-link by exchanging sodium ions with the cations [138, 139]. Due to these properties the alginate hydrogels have been widely used for the immobilisation of different macromolecules, for the controlled release of drugs, for tissue engineering and scaffolding. Looking at the chemical structure of the alginate, there are two blocks M and G which together build a water-soluble polysaccharide naturally extracted from brown algae cell walls and bacteria [140] (Fig. 41).

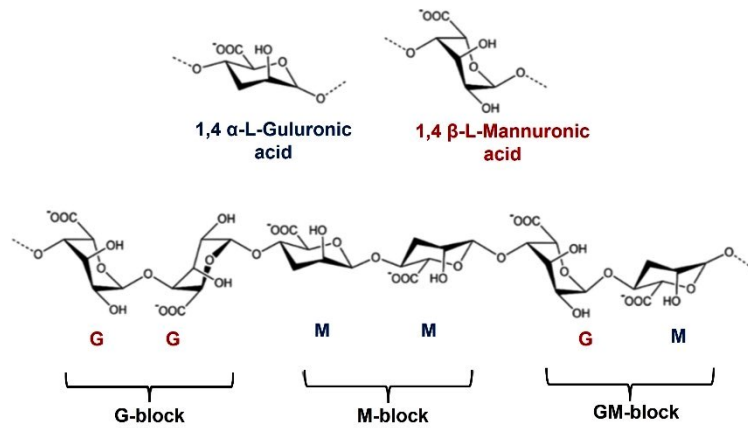


Figure 41: Chemical structure of the two monomers and of the block's distribution for the obtainment of the alginate salt. (Copyright Journal and Biological Engineering) [141].

The gelation process provides the formation of alginate hydrogels and the development of a 3D network with a chemical or physical cross-linking. In particular, the alginate gelation is obtained by substitution of sodium ions Na^+ contained into the alginate polymeric chain, with cations like Ca^{2+} with the role of cross-linking the polymer following the “egg-box” model occurring by incorporation of Ca^{2+} into the structure of the G-block [141] (Fig. 42). The chemical cross-linking can be achieved by using lactones like d-glucono-delta-lactone [142].

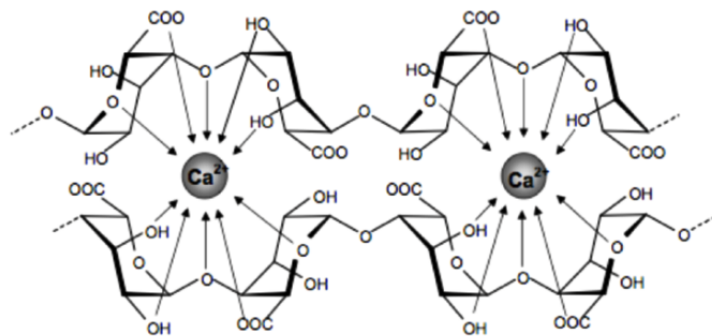


Figure 42: Encapsulation for the Ca^{2+} cation into the polymeric chain of alginate forming the hydrogels by cross-linking process [139].

2.5 Conclusions

A variety of immobilisation techniques and materials are used in a wide range of applications with the main purpose to protect the molecules of interest and preserve their properties. Chapter 2 provided an overview of the main immobilisation methods focussing on the main features used for the encapsulation of enzymes used for this work. The combination of CaCO₃ microsphere, and alginate hydrogels represents a good solution for the immobilisation of biological molecules as they provide biocompatibility, biodegradability, and porosity essential for the diffusion.

Research is constantly continuing to improve methods and materials used for the encapsulation of molecules applicable to different field.

Chapter 3: ECL main features

In chapter 1 the two pathways of the ECL have been described, particularly the co-reactant pathway has been chosen for the study of the enzyme activity detection. The main figures for the co-reactant pathway are luminophore, the co-reactant and the enzymes. An important aspect for the obtainment of reasonable results is the effective cleaning of the glassy carbon electrode which hosts the encapsulated enzymes by modifying its surface. In this chapter, the three features of ECL are described focusing on their properties, furthermore the cleaning process and the modification of the GCE surface are described.

3.1 Enzymes

Enzymes are biocatalysts able to convert a specific substrate into products. Most of the metabolic processes happening in biological cells require an enzymatic catalysis to increase the reaction rate by decreasing the activation energy. This energy is the lowest energy that a compound requires to start a chemical reaction. The catalyst is not consumed during the reaction, maintaining the reactant and product energy constant meanwhile decreasing the activation energy (E_a) and maintaining in this way the equilibrium. To reduce E_a the catalyst must form a transition state releasing energy, called binding energy, creating a bond with the substrate on the active site. The active site is the region where specific bonding is built until the substrate reaches the high-energy transition state with the formation of the so-called activation complex. This complex lasts short period of time ending with the formation of products characterised by an energy level. Depending on the kind of reaction there are two different cases, the products have lower energy than the reactants (exothermic reaction) or the products have higher energy of the reactants (endothermic reaction) [143] (Fig. 43).

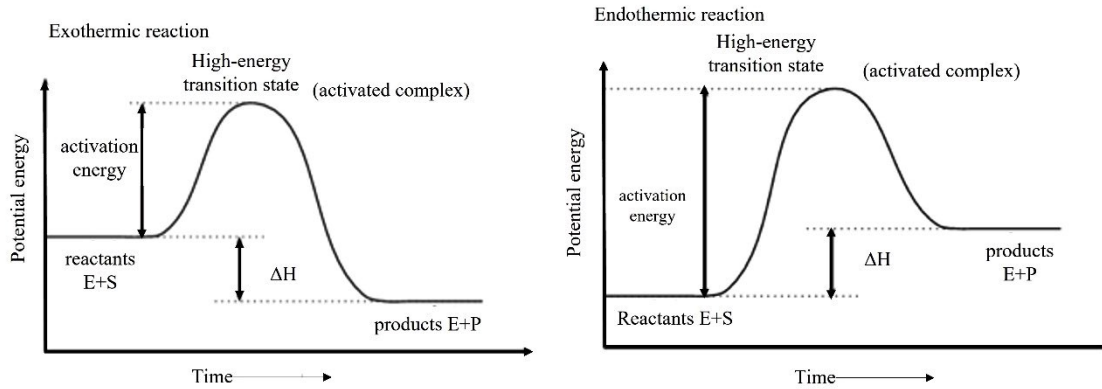


Figure 43: Representation of the enzyme-catalysed exothermic reactions (left) and endothermic reactions (right) with the relationship between the activation energy and the enthalpy (ΔH) [143].

The exothermic reactions can produce energy among the products, and in organisms these reactions are called catabolic reactions able to break down molecules in smaller species by releasing energy. A classic example is the glucose in the cellular respiration. On the other side, the anabolic processes of an organism are energy-absorbing reactions and so endothermic whereby small molecules build up together to form more complex systems such as the synthesis of glucose from glycogen. Enzymes couple exothermic reactions with endothermic in a coupled final reaction that is exothermic overall. A redox reaction involves a complete or partial loss of electrons which is an energy consuming process (oxidation) and a complete or partial gain of electrons (reduction) and so of energy. Knowing that an exothermic process leads to the formation of products with a lower energy level than the reactants (spontaneous reaction) and an endothermic instead has products with a higher energy level and considering that all redox reactions are spontaneous reactions, the conclusion is that these reactions are exothermic (Fig. 44).

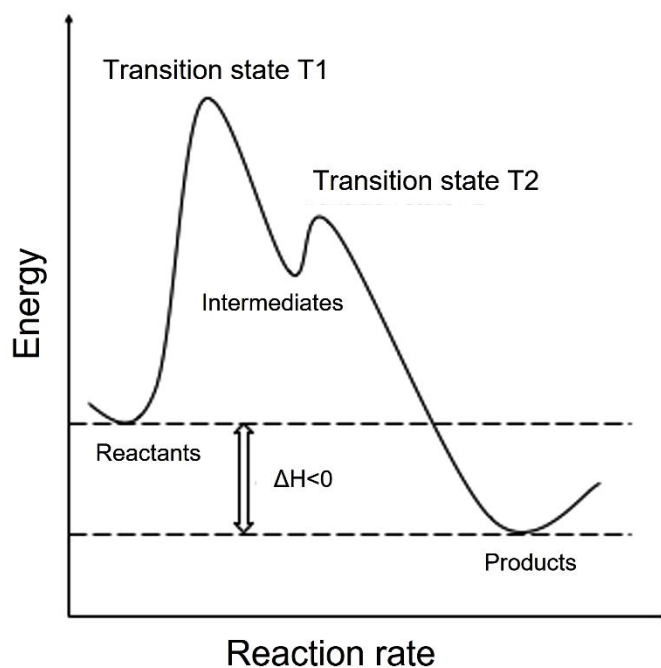


Figure 44: Energy diagram of redox reactions coupling an exothermic and endothermic reaction and obtaining a final exothermic spontaneous reaction [143].

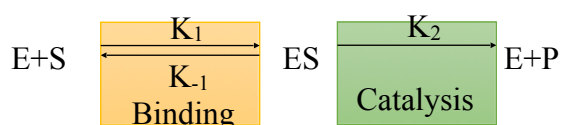
Enzymes can be classified by their enzymatic activity; the type analysed in this research belong to the Oxidoreductase group which catalyse redox reactions indeed (Table 2). These are able to transfer electrons from a reductant molecule (electron-donor) to an oxidant molecule (electron-acceptor) [144]. Depending on the group of donors involved during the reaction the oxidoreductase are divided in 21 subclasses. Particularly, *oxidase* enzymes can oxidise a substrate by using a dioxygen O_2 as electron acceptor and *dehydrogenase* enzymes instead oxidise the substrate with the concomitant reduction of an electron acceptor like NAD^+ or $NADP^+$.

Table 2: List of the different groups of enzymes and their corresponding activity

<i>Group</i>	<i>Reaction</i>
<i>Oxidoreductase</i>	Oxidation/reduction
<i>Transferase</i>	Transfer of functional group
<i>Hydrolase</i>	Hydrolysis of bonds
<i>Lyase</i>	Split various bonds
<i>Isomerase</i>	Isomerization changes
<i>Ligase</i>	Join molecules with covalent bonds
<i>Translocase</i>	Movement of ions and/or molecules

3.1.1 Enzyme Kinetics

The kinetics is an important tool for the study of the rate of the enzyme-catalysed reactions and how the catalyst create a bond with the corresponding substrate obtaining then the products [145]. In 1913 was proposed a quantitative model for the enzyme kinetics by L. Michaelis and M.L. Menten also known as Michaelis-Menten kinetics [146]. With this model, the enzyme reactions are divided into two steps, first the substrate create a reversible bond with the enzyme forming the enzyme-substrate complex, secondly the chemical reaction takes place with the final formation of products [147]. Considering a generic reaction catalysed by an enzyme E, at first the reaction is bimolecular as it happens between the enzyme and the substrate forming the complex ES. During the formation of this complex the rate of the reaction increases and becomes dependant from the ES complex starting a unimolecular reaction which leads to obtainment of final products P.



The reactions catalysed by enzymes are saturable, in fact the relationship between the reaction rate and the substrate concentration are not linear as shown in Fig. 45.

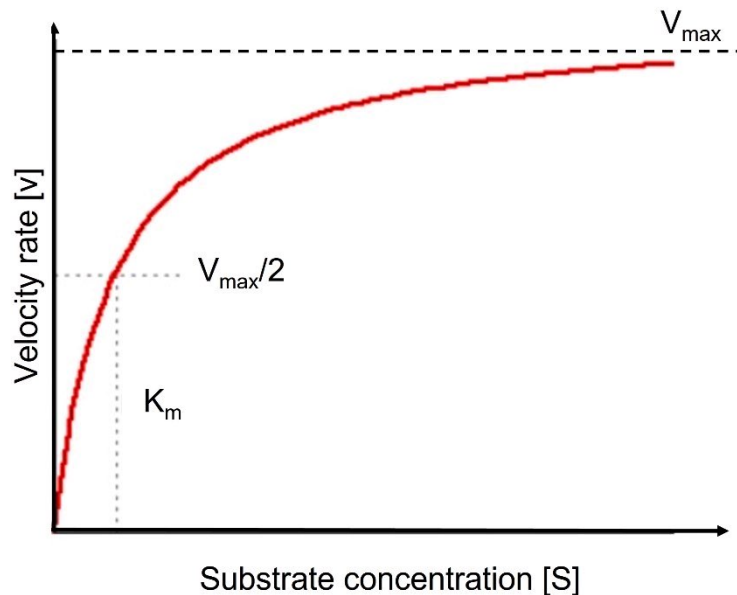


Figure 45: Saturation curve of the enzyme-substrate reaction showing the Michaelis-Menten constant at the 50% of the reaction rate.

At the beginning of the reaction, the rate increases with the increase of the substrate concentrations [S]. For higher concentrations of S, the enzyme reaches the saturation point, and the rate of the reaction achieves the maximum rate V_{max} reaching a plateau. Specifically, when the substrate is added to the reaction in large amounts, just a part of this can form the ES complex with the enzyme. Since the concentration of substrate is low, the enzyme is free to catalyse the reaction and so to increase the reaction rate, but as soon as all the binding sites of the enzyme are filled with the substrate molecule (higher concentration of S) the enzyme reaches the saturation point and the reaction rate ends to increase. The substrate concentration at the 50% of the maximum reaction rate is known as Michaelis constant K_M [148]. Two properties are essential for the study of the enzyme's kinetic, the saturation point of the enzyme for a specific substrate 1) and the maximum reaction rate that an enzyme can achieve 2).

The Michaelis-Menten equation describes the relation between the initial reaction rate depending on the concentration of the substrate:

$$v_0 = \frac{v_{max} [S]}{K_M + [S]} \quad (40)$$

K_M can be experimentally calculated and corresponds to the substrate concentration at which the reaction rate is the 50% of the maximum rate and could be approximated to the dissociation constant [149] of the ES complex.

$$K_M = \frac{K_2 + K_{-1}}{K_1} \approx K_D \quad (41)$$

where K_1 , K_{-1} and K_2 correspond to the rate constants for each reaction during the enzyme-catalysed reaction. K_D and K_M are two parameters which give information regarding the binding relation between the substrate and the enzyme. Specifically, the dissociation constant defines the equilibrium between the substrate (or ligand) free in solution $[S]$ and linked with the enzyme $[ES]$ giving information regarding the affinity that the substrate has for the binding site of the enzyme:



In general, for higher affinity ligands the dissociation constant has lower values and can be defined as an equilibrium constant express as the ratio between the product of the concentrations over the concentration of the ES complex:

$$K_D = \frac{[E][S]}{[ES]} \quad (43)$$

Considering the association and dissociation rate constants which regulate the reaction to form the complex ES,



the equilibrium is achieved when the complex association and dissociation take place at equal rates:

$$K_1[E][S] = K_{-1}[ES] \quad (45)$$

$$K_D = \frac{[E][S]}{[ES]} = \frac{K_{-1}}{K_1} \quad (46)$$

From these equations it is possible to conclude that the dissociation constant K_D is defined as the ratio of the dissociation and the association constant where the dissociation describes a unimolecular reaction and the association instead a bimolecular reaction involving [E] and [S] [150].

Another important tool for the determination of the kinetics parameters is the Lineweaver-Burk plot that is a graphical study first described in 1934 by Hans Lineweaver and Dean Burk. It is characterised by the determination of the reciprocal of the substrate concentration (x-axis) and of the maximum velocity (y-axis):

$$V = \frac{V_{max} + [S]}{K_M[S]} \quad (47)$$

$$\frac{1}{V} = \frac{K_M + [S]}{V_{max} [S]} = \frac{K_M}{V_{max}} \frac{1}{[S]} + \frac{1}{V_{max}} \quad (48)$$

This method was used to determine the K_M and V_{max} before all the computer with the non-linear regression software were available as it is difficult to estimate the two parameters using the hyperbolic plot of Michaelis-Menten where the V_{max} could be achieved at infinite substrate concentrations. For this reason, Michaelis-Menten equation has been transformed in a double reciprocal plot composed of a straight line (Fig. 46).

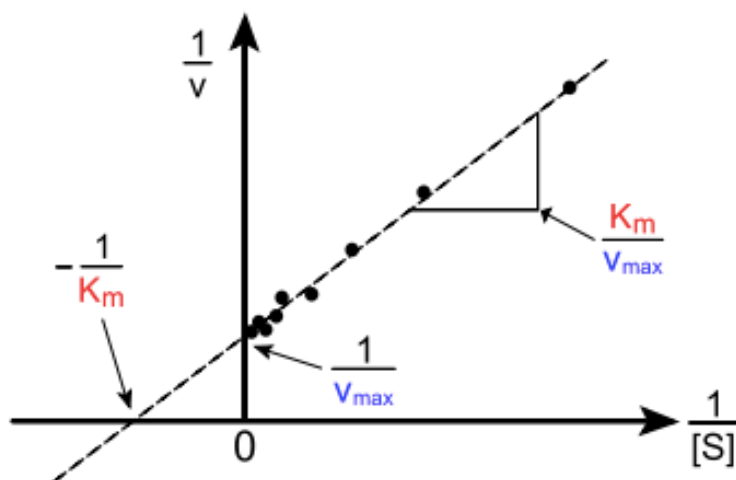


Figure 46: Lineweaver-Burk plot for the calculation of the kinetics parameters.

3.1.2 Oxidase

The first group of enzymes encapsulated into alginate hydrogels and studied with ECL tests is the oxidase (Fig. 47).

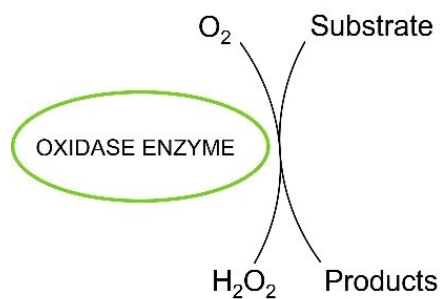


Figure 47: Schematic reaction between oxidase enzymes and their specific substrate to produce hydrogen peroxide and the products of the reaction

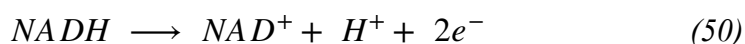
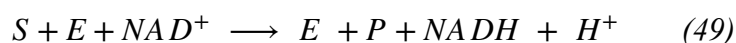
During this reaction, the enzyme oxidises its substrate by reducing the di-oxygen to hydrogen peroxide H_2O_2 by accepting two protons and two electrons. The oxidase enzymes studied in this work are reported in the Table 3:

Table 3: Summary of the oxidase analysed in this work specifying the source and the reaction with the corresponding substrate

<i>Enzyme</i>	<i>Source</i>	<i>Substrate</i>	<i>Products</i>	<i>Ref.</i>
<i>Glucose Oxidase</i>	<i>Aspergillus Niger</i>	B-D-Glucose	D-glucono- δ -lactone + H ₂ O ₂	[151, 152]
<i>Lactate Oxidase</i>	<i>Aerococcus Viridians</i>	L-Lactic Acid	Pyruvate + H ₂ O ₂	[153, 154]
<i>Cholesterol Oxidase</i>	<i>Streptomyces sp</i>	Cholesterol	Cholest-4-en-3-one + H ₂ O ₂	[155, 156]

3.1.3 Dehydrogenase

The dehydrogenase enzymes activity is described as following:



These enzymes (E) oxidise their specific substrate (S) by reducing at the same time the cofactor NAD⁺ obtaining the products (P) of the reaction and the NADH. During the reaction there is the removal of and hydrogen due to the enzyme activity.

The main difference between the two classes of the oxidoreductase enzymes is the type of electron acceptors involved. The oxidases use only oxygen O₂ as electron acceptor coming from the substrate; instead, the dehydrogenase transfer the electrons from the specific substrate to an electron carrier like NAD⁺, FAD and NADP⁺. During this process the electron carriers undergo to a reduction and the substrate instead to an oxidation [157]. The dehydrogenase enzymes Analysed in this work used nicotinamide adenine dinucleotide (NAD⁺) as cofactor. This molecule is composed of two nucleotides, one containing the nicotinamide and the other one the adenine group (Fig. 48). The reduction of this molecule happens when a hydrogen and two electrons are added to the ring of 6 carbon atoms of the nicotinamide. One of the electrons is added to the carbon placed oppositely of the positive

charged nitrogen obtaining a new arrangement of bonds into the ring resulting in the loss of the positive charge due to the new electrons acquired. The second electron instead is obtained from an additional hydrogen and after this transfer the hydrogen ion is left in the solution [158, 159].

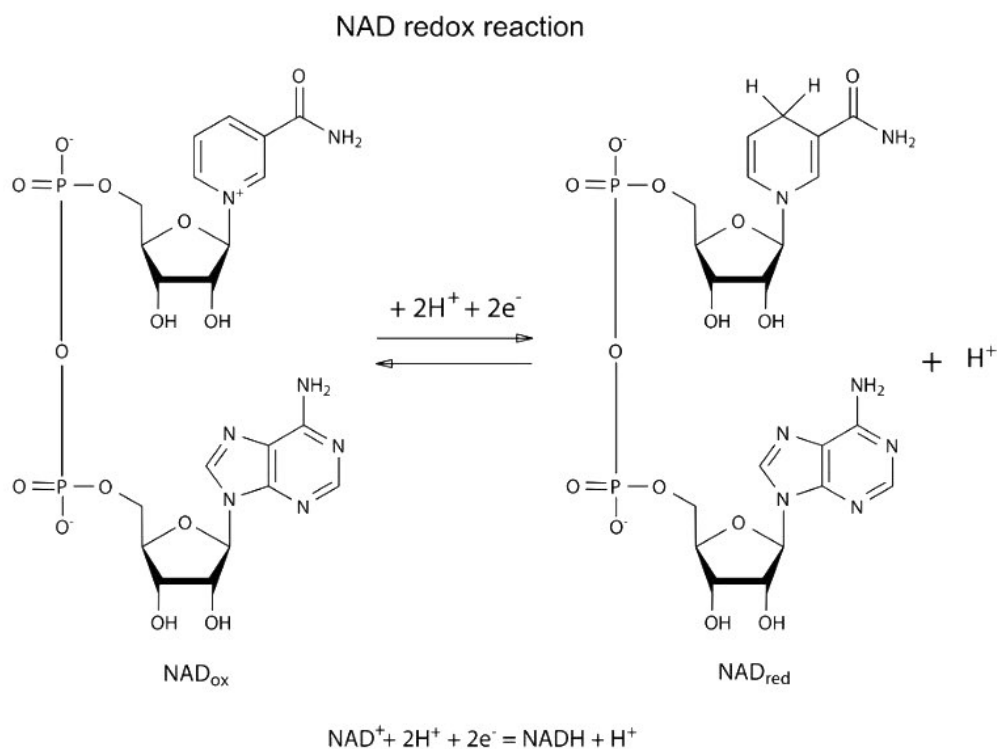


Figure 48: Reaction between NAD^+ and NADH [159].

Table 4: Dehydrogenase enzymes analysed in this work.

<i>Enzyme</i>	<i>Source</i>	<i>Substrate</i>	<i>Products</i>	<i>Ref.</i>
<i>Glucose Dehydrogenase</i>	<i>Aspergillus</i>	Glucose	D-glucono- δ -lactone+NADH	[160,
	<i>Niger</i>			161]
<i>Lactate Dehydrogenase</i>	<i>Escherichia</i>	L-lactic acid	Pyruvate + NADH	[162,
	<i>Coli</i>			163]
<i>Cholesterol Dehydrogenase</i>	<i>Nocardia sp</i>	Cholesterol	Cholest-4-en-3-one+ NADH	[164,
				165]
<i>Alcohol Dehydrogenase</i>	<i>Saccharomyces cerevisiae</i>	Ethanol	Acetaldehyde+NA DH	[166,
				167]

3.2 Luminophores

The main protagonists of the electrochemiluminescence are the luminophores, without the presence of these molecules into the electrolytic solution and/or immobilised on the electrode surface the light emission will not occur.

During an ECL experiments, luminophores reach their excited state after the exergonic electron transfer reaction between the redox couple and the luminophore itself. But the obtainment of an excited state can be achieved also through a reaction able to break bonds. A difference between the two ways of producing an excited state is related to the reversibility of the reaction. In fact, the electron transfer reaction is a reversible process so after the emission of light the luminophore is regenerated ready for a new emission. On the other hand, the bond-breaking reactions are a non-reversible process so the electrochemiluminophore can emit just once. Luminol is a classic example of bond-breaking luminophore instead, $[\text{Ru}(\text{bpy})_3]^{2+}$ represents an example of renewable compound [39]. The first type of luminophore reported in the literature were the Grignard compound [31] and luminol [30]. Currently luminophores can be classified in three main groups, organic like luminol (1), inorganic like $[\text{Ru}(\text{bpy})_3]^{2+}$ (2), and nanoparticles such as quantum dots (3) [23, 27, 52]. This wide range of different luminophores give the possibility to choose the best emission wavelength from the visible region to the infrared.

3.2.1. Luminol

Luminol is an organic luminophore widely used for the ECL and chemiluminescent techniques as it exhibits a blue luminescence when it is mixed with an oxidising precursor (Fig. 49).

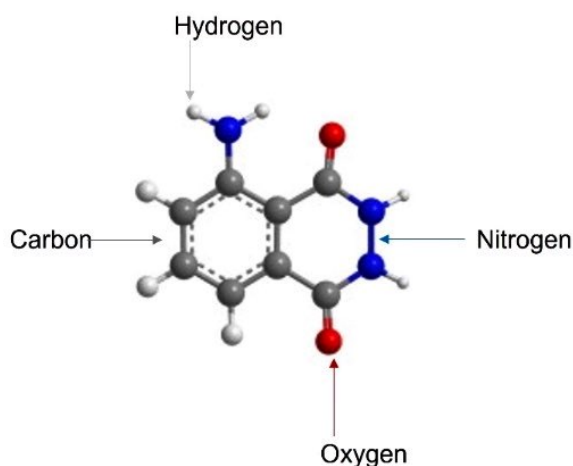


Figure 49: Structure of luminol $C_8H_7N_3O_2$. Adapted from [168].

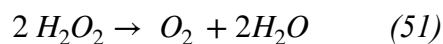
It is a white-to-yellow compound described for the first time in 1928 by Albrecht who found that blood in the presence of other substances can enhance the luminescence of luminol when is in alkaline solutions with hydrogen peroxide [169]. With the chemical formula $C_8H_7N_3O_2$, it is soluble in most polar organic solvents, but not in water. This chemical has been widely studied and used for the forensic investigations to detect blood stains as it reacts with the iron groups present in haemoglobin [170] (Fig. 50). Luminol oxidation is a complex multistep reaction depending on different factors as pH, temperature, species in the solution, metal catalyst, ionic strength of the supporting electrolyte where the reaction happens and the presence of hydroxide ions.



Figure 50: Typical blue colour of the chemiluminescence of luminol when in contact with an oxidising reagent like hydrogen peroxide. (© Royal Society of Chemistry 2022).

To emit light, luminol needs to be activated with an oxidant that usually contains hydrogen peroxide or hydroxide ions in water. For the proposed biosensor, the activator of the luminol is the H_2O_2 produced during the electrochemical reaction under specific conditions for each

enzyme. The hydrogen peroxide in the presence of a catalyst undergoes to a decomposition to form oxygen and water following the reaction (51):



Firstly, luminol is deprotonated in basic conditions and then is oxidised to the anionic radical. Once the luminol reaches the oxidised form, it reacts with the H_2O_2 forming the excited state: 3-aminophthalate (Fig. 51). This highly unstable molecule, when relaxes to the ground state emits light at 425nm of wavelength in the form of a blue light [171].

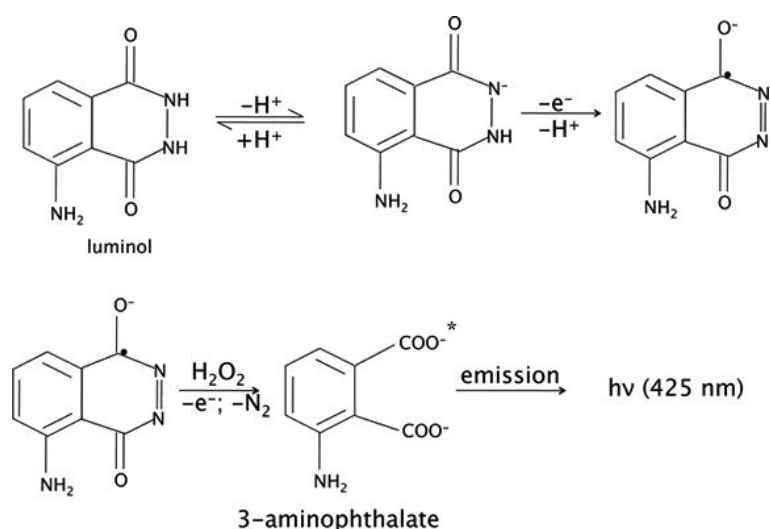


Figure 51: Chemiluminescence of luminol [171].

Thanks to its stability, availability, and high sensitivity, luminol is one of the most used chemiluminescent luminophores for the study of biological systems. One of the factors which plays an essential role for the CL of luminol is the pH of the solution. In fact, at acidic pH, luminol's activity is drastically reduced with no emission of light, while moving at more alkaline pH solutions, also the luminescence sees a significant increase in the intensity.

3.2.2. *Tris(bipyridine)ruthenium(II) chloride*

$[Ru(bpy)_3]^{2+}$ is a polypyridine cation able to absorb visible and ultraviolet light (Fig. 52). The first ECL tests using this luminophore was reported by A. J. Bard in 1972 starting in this way the new era of ECL reactions [34]. These first experiments were restricted to the

annihilation pathway of the ECL using just organic electrolytes and a wide potential range. To reduce the potential window, an addition reagent was added to the solution discovering thus the co-reactant mechanism of the ECL in 1981 always by A. J. Bard group of research [172]. Different co-reactants have been tested with $[\text{Ru}(\text{bpy})_3]^{2+}$ such as oxalate, tri-n-propylamine (TPrA) and NADH, triethylamine (TEA), diethylamine (DEA), ascorbic acid, glutathione and so on [173].

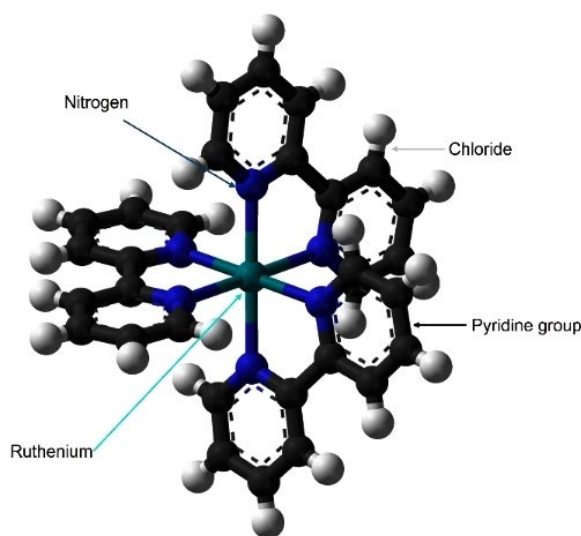


Figure 52: Structure of $[\text{Ru}(\text{bpy})_3]^{2+}$. Adapted from [174].

The co-reactant pathway using $[\text{Ru}(\text{bpy})_3]^{2+}$ has been widely used for clinical diagnostic applications due to the good luminescent characteristics, high solubility in organic and aqueous solution at room temperature, high potential region and superior ECL efficiency [175]. As a result of all these properties, $[\text{Ru}(\text{bpy})_3]^{2+}$ has been used as an ECL probe for DNA detection by detecting its double strand [176], for bio-imaging, metal ions detection and more studies [52].

Three different mechanisms have been studied to produce the ECL of the $[\text{Ru}(\text{bpy})_3]^{2+}$: the *reductive-oxidation* process (1), the one *oxidative-reduction* used for this research (2) and the *annihilation* method (3). The (1) involves the use of selected co-reactants, $\text{S}_2\text{O}_8^{2-}$, H_2O_2 and glutathione, for the ECL of $[\text{Ru}(\text{bpy})_3]^{2+}$. The co-reactant is reduced when the cathodic potential is applied producing a radical intermediate and the luminophore undergoes to a reduction obtaining the anionic form $[\text{Ru}(\text{bpy})_3]^{1+}$. The reduced radical of the co-reactant

and the anionic form of the luminophore reacting together generate the excited form $[\text{Ru}(\text{bpy})_3]^{2+*}$ which then emits light [177] (Fig, 53).

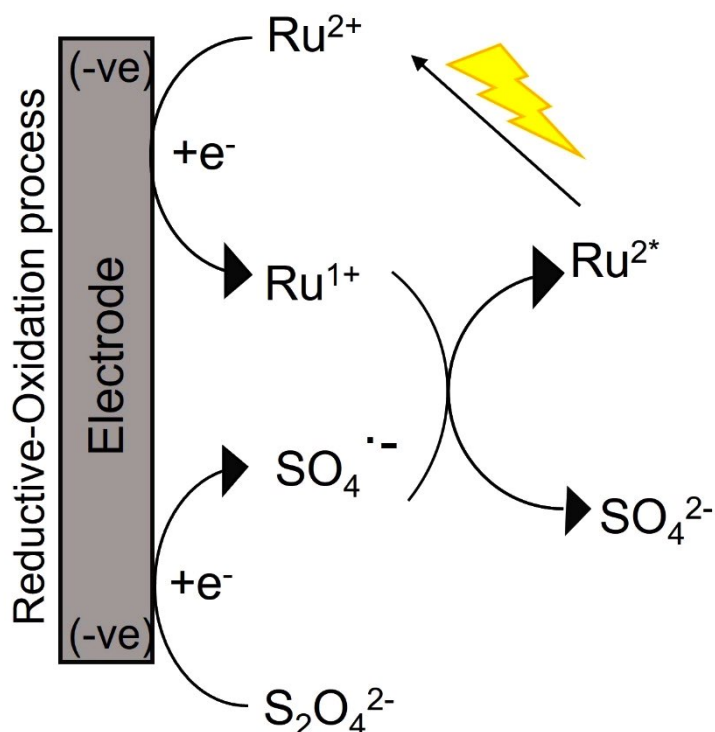


Figure 53: Scheme representing the reductive-oxidation process of Ruthenium using $\text{S}_2\text{O}_8^{2-}$ as co-reactant. Adapted from [178].

Considering TPrA as co-reactant, the *oxidative-reduction* pathway allows the ECL emission of $[\text{Ru}(\text{bpy})_3]^{2+}$ by following a cascade of different steps starting with the oxidation of the TPrA and the production of $[\text{Ru}(\text{bpy})_3]^{3+}$ from $[\text{Ru}(\text{bpy})_3]^{2+}$ through oxidation which then will be reduced to the excited form $[\text{Ru}(\text{bpy})_3]^{2+*}$ [179]. Instead for the (3), $[\text{Ru}(\text{bpy})_3]^{2+}$ becomes $[\text{Ru}(\text{bpy})_3]^{3+}$ via an electrochemical oxidation. The oxidised form of TPrA reacting with $[\text{Ru}(\text{bpy})_3]^{2+}$ forms $[\text{Ru}(\text{bpy})_3]^{1+}$ which undergo then to an electron transfer reaction forming $[\text{Ru}(\text{bpy})_3]^{3+}$ generating the excited state $[\text{Ru}(\text{bpy})_3]^{2+*}$ [180] (Fig. 54).

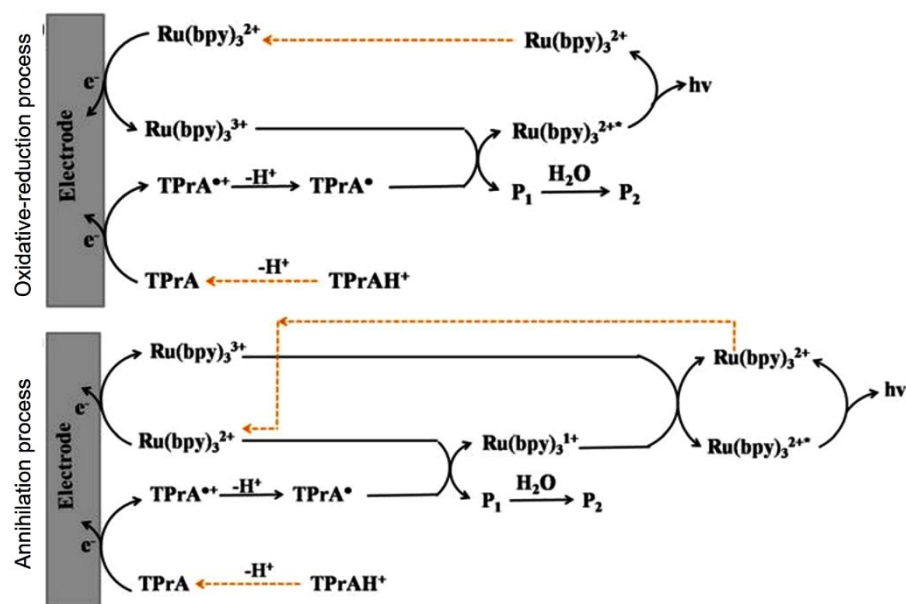


Figure 54: Description of the oxidative-reduction and annihilation processes with the use of TPrA as co-reactant. Adapted from [178].

3.3 Co-reactant

Co-reactants are a sacrificial molecule added to the electrolytic solution to achieve the ECL emission during the exergonic redox reaction in the presence of oxidising and reducing species. After the application of an initial potential, the co-reactant produces a reductant after an oxidation (*oxidative-reduction* process) or an oxidant after the initial reduction (*reductive-oxidation* process). For both the mechanisms, the initial electron-transfer reaction is followed by a chemical reaction which includes the formation of bonds and so is irreversible.

In this work the two systems analysed follow the *oxidative-reduction* process using a co-reactant that is not added to the electrolytic solution at the beginning of the ECL experiments but produced after the initial chemical reaction between the species involved. In this way is assured the specificity of the co-reactants for the luminophore confirmed by the emission of light. For the $[\text{Ru}(\text{bpy})_3]^{2+}$ system the co-reactant involved is NADH and it's produced from the chemical reaction between the immobilised dehydrogenase enzyme and its specific substrate (Fig. 55 left). For the luminol-based ECL instead, the co-reactant is the hydrogen peroxide also chemically generated after the redox reaction (Fig. 55 right).

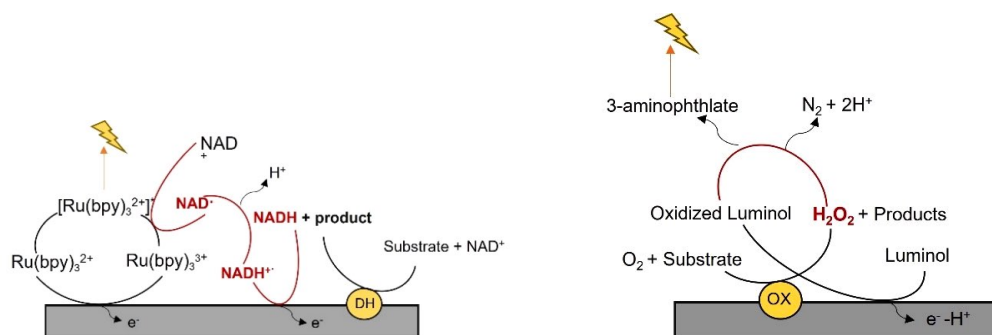


Figure 55: Co-reactant ECL for the two systems analysed in this thesis. NADH for the [Ru(bpy)₃]²⁺ system (left) and hydrogen peroxide (right) for the luminol system.

As listed above, the co-reactant is chemically produced in the solution and creating a bond with the oxidised form of the luminophore allow the formation of the excited state and the consequent emission of light. It is an irreversible reaction, therefore, to have a new ECL emission new substrate must be added in solution to produce new co-reactant. By measuring the intensity of emission of light it is possible to detect the concentration of co-reactant produced and so create a calibration curve that relates the signal obtain with the amount of substrate that allowed that emission.

3.4 Working electrode

In chapter 1 the three-electrode configuration of the electrochemical cell has been described. Particularly, the WE hosts the species to be analysed namely the encapsulated enzymes which once deposited on the electrode surface allow the modification of its surface [24]. Once the initial potential is applied to the WE, the reactions occur on its surface and on the basis of the type of reaction it can be called cathodic electrode if it is a reduction reaction or anodic electrode if an oxidation [10, 11]. There are different materials for the area of the WE, the most common are inert carbon like boron doped diamond, glassy carbon, mercury drop, film electrodes and pyrolytic carbon or inert metals such as gold, silver and platinum [181, 182].

The WE material is an important choice to achieve a good selectivity in organic electrochemical reactions as the material has a fundamental effect of the thermodynamics and kinetics during the electron transfer reaction [183]. Firstly, the material of WE needs to show a good redox behaviour with the analyte allowing a fast and reproducible electron transfer

reaction [184]. Furthermore, the electrode must be characterised by a potential window wide enough to allow the oxidation and reduction of the analyte to happen at its specific potential. Important factors that need to be considered regards the cost of the material, the size of the sensitive area, the geometry, and the toxicity. The most used WE in the literature are platinum, carbon, gold, and mercury (Fig. 56).

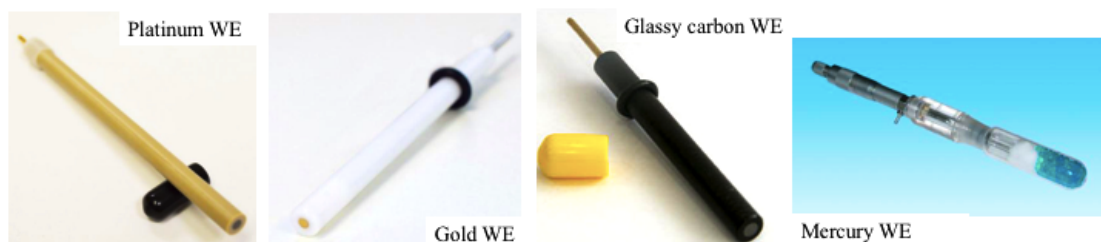


Figure 56: Most used Working Electrode materials (with permission of IJ Cambria).

Platinum WE have been widely used in the literature for the optimal electrochemical inertness. It can be fabricated in different shapes and sizes, but it is highly expensive, moreover a disadvantage consists in the ability to reduce the hydrogen ion forming hydrogen gas at negative potentials when even a small amount of water or acids are present into the electrolytic solution. When the hydrogen evolution occurs into the electrochemical cell, it is not possible to obtain any useful analytical result for that experiment [185].

The gold material used for WE have roughly the same behaviour of the platinum except for the limited utility for positive potentials due to the oxidation of the surface of the electrode. Gold electrodes have been widely used for the development of modified electrodes containing self-assembled monolayers (SAMs) introduced in the first half of 1990s for the detection of several species like metal ions, biomolecules and microorganisms [186].

Mercury material has been used as working electrode in different shapes but the most common is a spherical drop at the end of a glass empty tube where the liquid is allowed to flow. Mercury WE are characterised by a good potential window for the cathodic direction but, as the gold electrode, is limited in the anodic potentials due to the easy oxidation of its surface. An important drawback of this kind of material is the toxicity of mercury for biological species [187]. Finally, carbon electrodes are suitable for electrochemical studies as they allow wide potential window with more negative potentials respect to the platinum and a

large positive window respect gold and mercury as its surface does not suffer of oxidation. The most common used is the glassy carbon electrode (GCE) characterised by a good resistance for high temperature, low electrical resistance, excellent resistance to chemical attack and good impermeability to gasses and liquids [188].

Table 5: Commonly used working electrodes with their advantages and disadvantages listed.

<i>Material</i>	<i>Advantages</i>	<i>Disadvantages</i>
<i>Platinum</i>	Available in different size and shapes	Hydrogen evolution for cathodic potentials; expensive
<i>Gold</i>	Wide range of cathodic potentials; different shapes and sizes	Limited anodic potentials due to surface oxidation; expensive
<i>Carbon</i>	Several configurations, good cathodic and anodic potential range; low electrical resistance; resistance to chemical attack; impermeability	Hard to shape
<i>Mercury</i>	Good cathodic window	Limited anodic window due to the oxidation of the surface; toxic

The electrode materials are encapsulated into a non-conducting shell of inert material like Teflon, Kel-F or PEEK and commonly the electrode is exposed in the shape of a disk with the diameter of 1.0, 3.0 or 10.0 mm able to produce currents in the range from μA to mA for analyte concentrations around 1 mM.

As result of its numerous advantages, the GCE has been used for the electrochemical experiments performed in this work. Especially, due to the possibility to analyse very wide anodic potentials without any problem related to the oxidation of the electrode surface, it was possible to study the oxidation of the species involved during the redox reactions.

3.5. Conclusions

The leading characters of the ECL experiments performed in this thesis are the enzymes, the luminophores and the co-reactant. The electrochemical-enzyme biosensor here proposed is based on the generation of electroactive species that can be detected upon a redox reaction directly at the electrode surface. The advantage of this sensor is that the generated electroactive species have the properties of co-reactant which reacting with the luminophore gives the ECL emission. The enzyme biosensors can detect mainly two bio-products/co-reactant of the enzyme reaction which are H_2O_2 and NADH.

This chapter introduces the three main features essential for the achievement of the emission of light. The combination of the enzyme selectivity towards the substrate and the high sensitivity of the photons detection leads to the development of ECL-based enzyme biosensors characterised by a simple architecture, easy light detection system and a rapid measurement.

Chapter 4: Experimental approaches and methods

4.1 Chemicals

The liquids used for the analysis are aqueous and non-aqueous solutions. All the aqueous solutions used for the ECL experiments reported in chapters 5,6,7 and 8 were prepared using Milli-Q water with resistivity of 18 M Ω cm at 25 °C.

All the chemicals used were weighed with a four-figure analytical balance purchased from Sartorius model TE124S and are listed in Table 6.

Table 6: List of solvents and chemicals used during the experimental activity.

Chemical	Formula	Purity	Supplier
Solvents			
Acetonitrile	C ₂ H ₃ N	≥ 99%	Thermo Scientific
Acetone	CH ₃ COCH ₃	≥ 99.5%	ACS reagent
Methanol	CH ₄ O	≥ 99.8%	ACS reagent
Ethanol	C ₂ H ₅ O	≥ 99.8%	BioUltra
Chemicals for ECL experiments			
Tetrabutylammonium hexafluorophosphate	(CH ₃ CH ₂ CH ₂ CH ₂) ₄ N(PF ₆)	≥ 99.0%	Sigma-Aldrich
Potassium chloride	KCl	99 %	Sigma-Aldrich
Sodium chloride	NaCl	≥ 99%	ACS reagent
Sodium hydroxide	NaOH	≥ 98%	Sigma-Aldrich
Hydrochloric acid	HCl	99.9%	Sigma-Aldrich
Phosphate buffered saline	PBS pH 7.4	--	Sigma-Aldrich
Tris(2,2' — bipyridyl) dichlororuthenium (II) hexahydrate	C ₃₀ H ₂₄ Cl ₂ N ₆ Ru · 6H ₂ O	99.95% trace metal basis	Sigma-Aldrich
Luminol	C ₈ H ₇ N ₃ O ₂	97 %	Sigma-Aldrich
D-(+)-Glucose	C ₆ H ₁₂ O ₆	≥ 99.5%	Sigma-Aldrich

B-Nicotinamide adenine dinucleotide hydrate	C ₂₁ H ₂₇ N ₇ O ₁₄ P ₂ · H ₂ O	≥ 96.5%	Sigma-Aldrich
Tripropylamine	(CH ₃ CH ₂ CH ₂) ₃ N	≥ 98%	Sigma-Aldrich
L-Lactic acid	C ₃ H ₆ O ₃	90 %	Thermo scientific
Hydrogen peroxide	H ₂ O ₂	35 %	SAFC
Cholesterol	C ₂₇ H ₄₆ O	≥ 99%	Sigma-Aldrich
Enzymes			
Type	Molecular weight	Solubility	Supplier
Glucose oxidase from <i>Aspergillus Niger</i>	~ 160 kDa	0.1 M phosphate buffer: 1.0 mg/ml	Sigma-Aldrich
Peroxide from horseradish	~ 44 kDa	0.1 M phosphate buffer: 1.0 mg/ml	Sigma-Aldrich
Lactate oxidase from <i>Aerococcus viridians</i>	80 kDa	0.1 M phosphate buffer: 1.0 mg/ml	Sigma-Aldrich
Cholesterol oxidase from <i>Streptomyces sp.</i>	~ 34 kDa	50 mM potassium buffer: 1.0 mg/ml	Sigma-Aldrich
Alcohol dehydrogenase from <i>Saccharomyces cerevisiae</i>	141-152 kDa	0.1 M phosphate buffer: 1.0 mg/ml	Sigma-Aldrich
Glucose dehydrogenase from <i>Pseudomonas sp.</i>	~ 50 kDa	0.1 M phosphate buffer: 1.0 mg/ml	Sigma-Aldrich
Lactose dehydrogenase	140 kDa	0.1 M phosphate buffer: 1.0 mg/ml	Sigma-Aldrich
Cholesterol dehydrogenase from <i>Nocardia sp.</i>	~ 37 kDa	50 mM potassium buffer: 1.0 mg/ml	Sigma-Aldrich
Alginate hydrogel realisation			
Chemical	Formula	Purity	Supplier
Alginic sodium salt from brown algae	--	--	Sigma-Aldrich

Poly (sodium 4-styrenesulfonate)	$(C_8H_7NaO_3S)_n$	Viscous liquid	Sigma-Aldrich
Poly(diallyldimethylammonium chloride) solution	$(C_8H_{16}ClN)_n$	Viscous liquid	Sigma-Aldrich
Calcium chloride	$CaCl_2$	99.99%	Sigma-Aldrich
Sodium carbonate	Na_2CO_3	$\geq 99.5\%$	Sigma-Aldrich

4.2 Cleaning process of GCE

The working electrode must operate repeatably every time is used. Different factors could affect the reproducibility of the experiments like the cleanliness of the electrode surface, the structure of the material itself and use of chemicals. For these reasons, before the use of the electrode it is imperative to observe a pre-treatment to guarantee that the electrode surface can highly perform during the electrochemical experiment. The polishing procedure is different for each type of material, for carbon and platinum this procedure is mostly a mechanical polishing followed by sonication in pure water to remove the smallest particles [189]. Sometimes it is also suggested to run some scans of cyclic voltammetry across a wide potential range using a normal electrolyte to assure the removal of all the absorbed particles repeating the process until any peak is observed in the voltammogram [190].

Considering the glassy carbon electrode as the WE, once the surface has been polished it becomes very reactive. The electrode surface needs to be polished before and in between each measurement because some impurities from analytes could be absorbed on the electrode surface. All the ECL experiments have been performed after three different procedures: mechanical polishing of the surface (1), sonication in water (2) and modification of the GCE electrode (3). The mechanical polishing procedure consists in the use of two alumina powders with different grades (0.1 and 0.05 mm) deposited on their specific polishing pad. The electrode is repetitively polished in the water-alumina mixture for 15 minutes for each size of powder in a figure-eight motion as in Fig. 57. By using this eight-shape the surface of the electrode is evenly cleaned compared to the classic circle motion where the polishing results uneven and the surface could result tilted [63]. After each powder

treatment, the electrode is washed with deionised water and dried with compressed air to completely remove all the dust particles deposited afterwards. After the mechanical polishing, the electrode is sonicated in pure water for 5 mins to also remove the absorbed particles that could possibly be still on the surface.

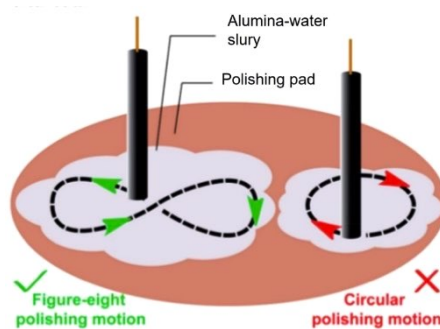
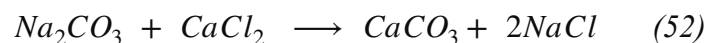


Figure 5758: Mechanical polishing procedure using the figure-eight motion in order to remove evenly all the particles on the electrode surface[190].

4.3 Enzyme-encapsulation in alginate hydrogels procedure

Following Volodkin's method the fabrication of microspheres involves the preparation of a 0.66 M CaCl_2 and 0.33 M Na_2CO_3 solutions. The two salts have been purchased from Sigma and the stock solutions have been prepared with 12 ml of deionised water by dissolving respectively 0.432 g of CaCl_2 and 0.42 g of Na_2CO_3 . The salts solution is prepared by mixing 0.5 ml of CaCl_2 and 1 ml Na_2CO_3 salt for 20 seconds at 900 rpm speed to obtain the calcium carbonate particles in the vaterite form according to (50).



To perform the enzyme entrapment 0.5 ml of enzyme solution (1 mg/ml enzyme solution in 0.1 M PBS pH 7.4) is added during the stirring sequence. The removal of the supernatant is necessary by performing three washes with deionised water followed by a centrifugation at 500 rpm for 60 seconds. At the end of the process the enzyme is completely encapsulated into the CaCO_3 in a final solution of 2 ml. Following this procedure, the physical entrapment of

the enzymes into polymeric matrices is achieved in a rapid and simple way maintaining an high retention of the macromolecule and a good stability [134].

Once the enzymes have been entrapped into the calcium carbonate cores, a polyelectrolyte multi-layered layer-by-layer process has been performed to improve the stability of the biosensor and provide a diffusion barrier for the encapsulated enzymes inside the alginate hydrogels. Due to this process, the leakage of enzymes outside the matrices is reduced increasing the performances of the sensor. The two polymers used for the stabilisation of the CaCO_3 are Poly (sodium 4-styrenesulfonate) (PSS) and Poly(diallyldimethylammonium) (PDDA). They belong to poly-styrene-sulfonate polymers characterised by sulfonate functional groups and a high charge density, in particular anionic charge for PSS and cationic one for PDDA [191] (Fig. 59).

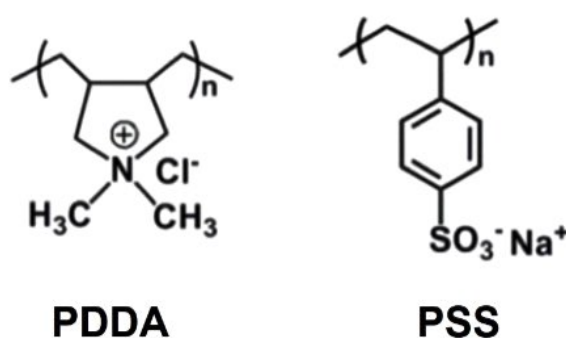


Figure 59:Chemical structure of the anionic charged polymer PDDA (left) and the cationic charged polymer PSS (right) used for the layer-by-layer process [132].

The polymer stock solutions were prepared by mixing 0.4 g powder of PSS in 20 ml of deionised water and 250 μl of PDDA in 25 ml of deionised water. The layer-by-layer procedure was performed by adding 1 ml of one polymer at time into the CaCO_3 microspheres alternating PSS and PDDA at each cycle. The solution was mixed for 15 minutes using the vortex enabling the building of a charged layer around the microsphere matrices. After the vortex mixing the solution is washed three times with deionised water to remove the excess of polymer and prepare the microspheres surface for the next charged polymer layer. The washings were performed using a centrifuge at the speed of 500 rpm for 1 minute for the complete division of the microspheres and the surfactant to be remove. The entire process is repeated 6 time, three for each polymer for the obtainment of a positively

charged final layer ready to create a bond with the negative surface of the alginate hydrogel [192] (Fig. 60).

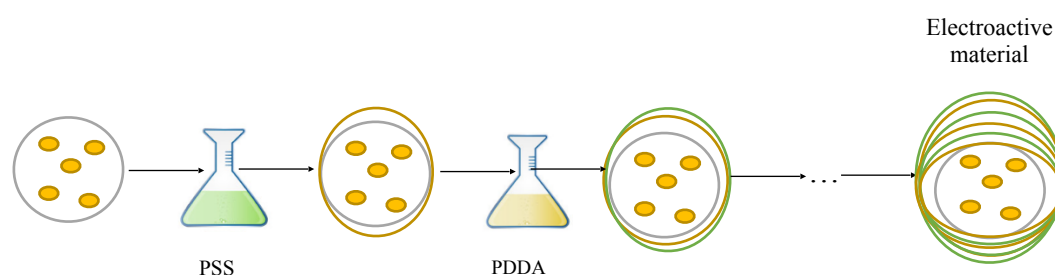


Figure 60: Enzyme encapsulated into microspheres cores and layer-by-layer procedure by alternating the PSS and PDDA obtaining the final cationic charged layer.

For the final step in the enzyme encapsulation, 1 g of alginate sodium salt has been dissolved in 50 ml of deionised water obtaining a 2% of alginic sodium salt solution. Previous work shows that the best ratio consists in two parts of 2% hydrogel solution and 1 part of the microspheres. For the ECL experiments described 4 ml of alginic sodium salt and 2 ml of microspheres were mixed by using a syringe without the needle and then the magnetic stirring [193]. To perform the ECL tests, the GCE has been modified by depositing the hydrogels on its surface. Specifically, after the cleaning of the surface area using different alumina powder and the corresponding polishing pads, 3 μl of the hydrogel solution were drop-casted on the 3 mm surface area of the GCE. After a first drying at room temperature, normally lasted 1 hour, the material was ready for the final cross-linking process. A drop of the cross-linking agent D-Glucono-1,5-lactone (GDL) was deposited on the hydrogel to dissociate the CaCO_3 molecule with the consequently release of Ca^{2+} resulting in the cores dissolution and the cross-linking of the three-dimensional network. A second drying has been performed leaving the electrodes to dry overnight at room temperature (Fig. 61).

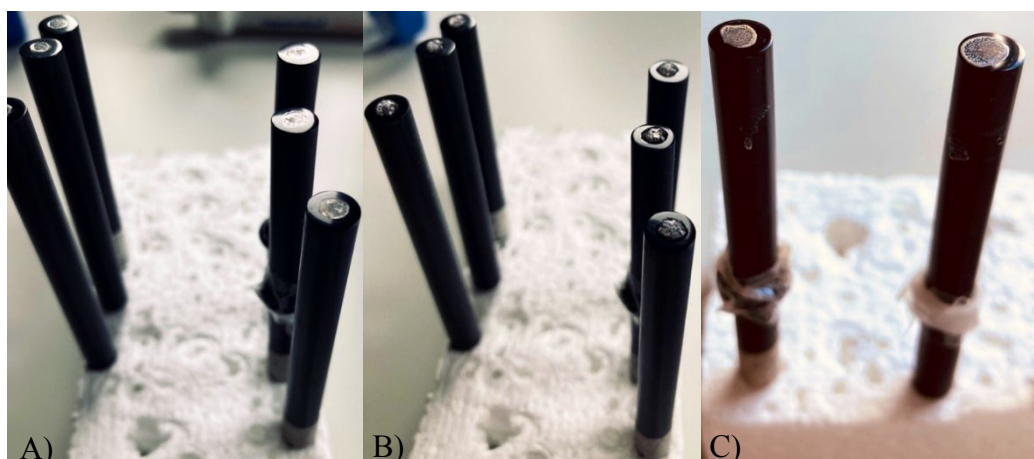


Figure 61: Modified GCE with the deposition of alginate hydrogels. A) First drying at room temperature for 1 hour of the deposited gel; B) cross-linking process started by deposition of GDL on the hydrogels; C) second drying at room temperature for 12 hours.

4.3.1 Characterisation of the alginate hydrogels

The effective encapsulation of the enzymes into the alginate hydrogels is demonstrated by the ECL results. A confocal microscopy study has been carried out to show how the enzyme is retained into the matrix (Fig. 62).

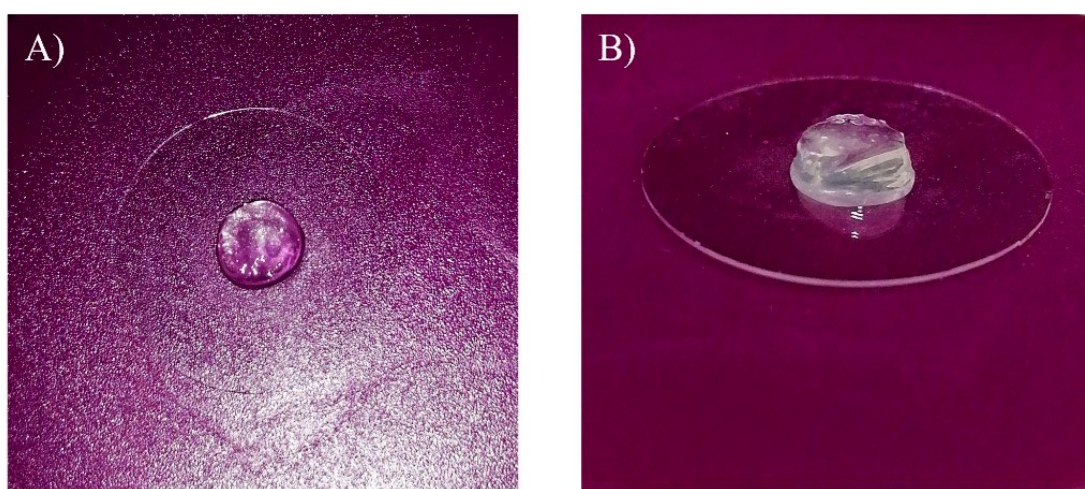


Figure 62: Confocal imaging was acquired with Leica TCS SP5 Tandem DMI6000 (Leica Microsystems CMS, Mannheim, Germany) inverted confocal laser scanning microscope coupled with Leica IRAPO 25x, 0.95 NA water immersion objective and Leica 63×PL APO1.4 NA immersion objective and Leica 63×PL APO1.4 NA oil immersion objective (Leica Microsystems, Mannheim, Germany). Scale bar: 4 μm .

Thanks to a collaboration with Genova University, by coupling the hydrogels with bovine serum albumin (BSA) labelled with Rhodamine B, it was possible to obtain the confocal imaging in Fig. 63 showing the microspheres embedded into the alginate hydrogels.

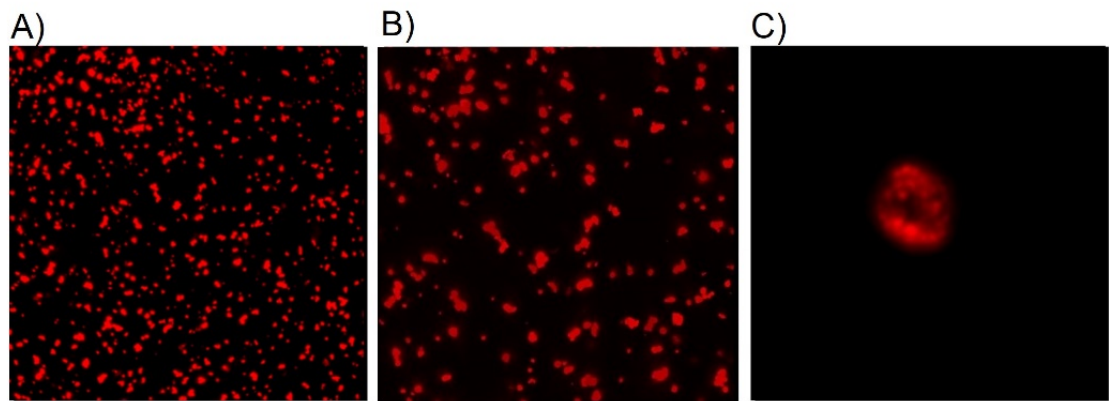


Figure 63: A) Max intensity projection of 500 μm z-stack of microcapsules embedded into alginate hydrogel; B) max intensity projection of 300 μm z-stack of microcapsules embedded into alginate hydrogel; C) Max intensity projection of a single microcapsule embedded into alginate hydrogel. Scale bar: 4 μm .

A final three-dimensional imaging has been acquired showing the dispersion of the microspheres into the alginate hydrogel in a volumetric representation (Fig. 64).

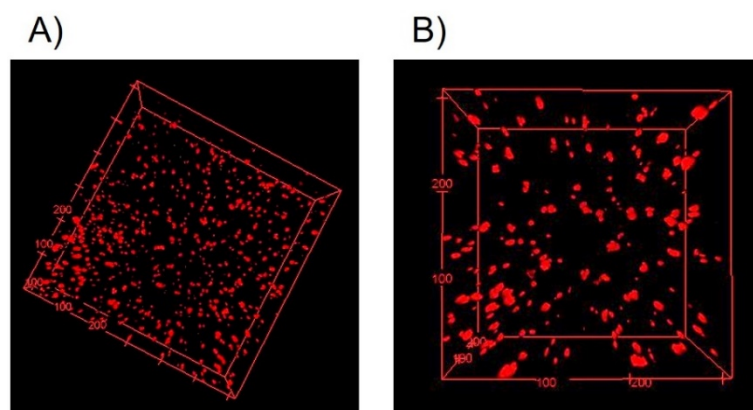


Figure 64: A) volumetric representation (XYZ) of microcapsules dispersion into alginate hydrogel ($z=500\ \mu\text{m}$), B) volumetric representation (XYZ) of microcapsules dispersion into alginate hydrogel ($z=300\ \mu\text{m}$).

4.4 Electrochemical experiments

4.4.1. Workstation

The electrochemical cell can have two different configurations depending on the number of electrodes involved: a *two-electrodes* cell has a working electrode (WE) and a reference/counter electrode all immersed into the electrolytic solution and a *three-electrodes* configuration that has been used for the ECL tests reported in this work. This configuration is chosen for systems which use higher currents with an ohmic drop > 1 mV. By using the third electrode, counter electrode, the flow of current does not pass through the RE avoiding in this way a change in its potential (Fig. 65).

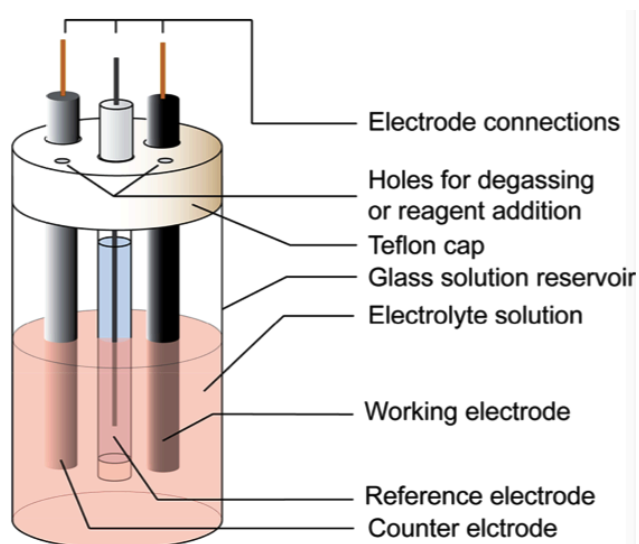


Figure 65: Schematic representation of the three-electrodes configuration of an electrochemical cell used for the ECL experiments. (Copyright 2017 The American Chemical Society and Division of Chemical Education, Inc.) [63].

The electrochemical cell hosts the electrolyte solution and the three electrodes which are working electrode (WE), reference electrode (RE) and counter electrode (CE) all immersed in the same solution. All the electrodes are connected to the potentiostat used to apply the potential and measure the current obtained as result of the chemical reactions on the WE surface. The WE is the electrode that hosts the species to be Analysed, in this case the encapsulated enzymes. It is normally composed of redox-inert materials such as carbon paste, glassy carbon, platinum, and mercury which are the most common working electrodes for the

electrochemical analysis. All the electrochemical reactions happen at the WE surface so it is essential that the electrode is well cleaned by using defined polishing procedure. In particular, with glassy carbon electrode as WE, a mechanical polishing helps to remove all the impurities from the surface allowing the obtainment of a very reactive surface [63]. Impurities on the surface of the electrode during the CV tests could cause modifications of the voltammogram affecting in this way the results.

The RE has a defined potential and is used as reference against the potential applied to working electrode. Ag/AgCl electrodes can keep the potential constant thanks to the action of chloride ions into the reference electrode tube. Different reference electrodes are used for electrochemical analysis, the most common are saturated calomel electrode (SCE), the standard hydrogen electrode (SHE) and the silver/silver chloride (Ag/AgCl) chose for the ECL experiments. The Ag/AgCl is composed of a silver wire immersed in a solution containing an Ag⁺ salt. The reference electrode in question was used with a $E^0 = + 0.22 \text{ V vs. SHE}$.

Finally, the counter electrode closes the electrical circuit favouring the flow of the current. In fact, once the potential is applied to the WE, the electron transfer reaction starts, and the electrons move from the WE to the CE forming a current flow. The CE is an inert material with a very small surface compared to the one of the WE. An example of CE is the platinum wire (Fig. 66).

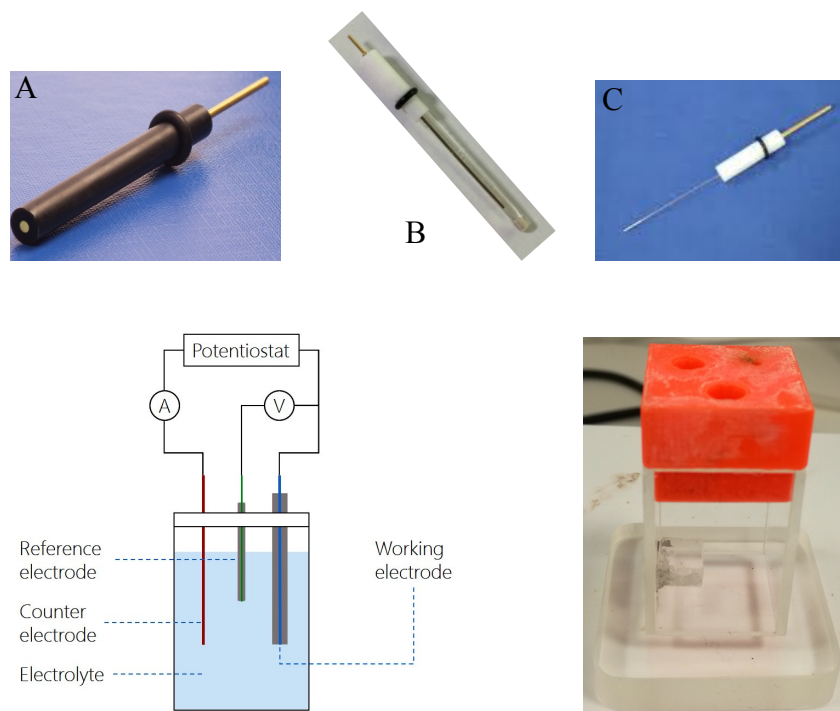


Figure 66: A) Glassy carbon electrode used as WE, B) Ag/AgCl reference electrode and C) platinum wire as CE. Schematic representation of the three-electrode electrochemical cell (left), electrochemical glass cell used for the ECL tests (right).

The main instrument for the electrochemical tests is the potentiostat which has the important role to control the three electrodes cell by applying a potential. The device used for the experiments here reported, was purchased by CH Instrument model 705E in Fig. 67.



Figure 67: CH Instrument potentiostat 705E Model used for the electrochemical tests.

This electronic device is essential for the electrochemical experiments as is capable of maintaining the potential of the WE at a constant value with respect to the RE by modulating the current at the CE [24]. In general, a potentiostat includes an electric circuit dedicated to

the control of the potential across the electrochemical cell by detecting any change in the cell's resistance and modulating the resulting current following the Ohm's law:

$$R = \frac{V}{I} \quad (53)$$

Where:

R is the resistance (Ω);

V is the potential (V);

I is the current (A).

The control amplifier (CA) is the main unit of the device and responsible to maintain the potential between WE and RE close to the input E_i adjusting the cell current satisfying in this way the equilibrium (Fig. 68).

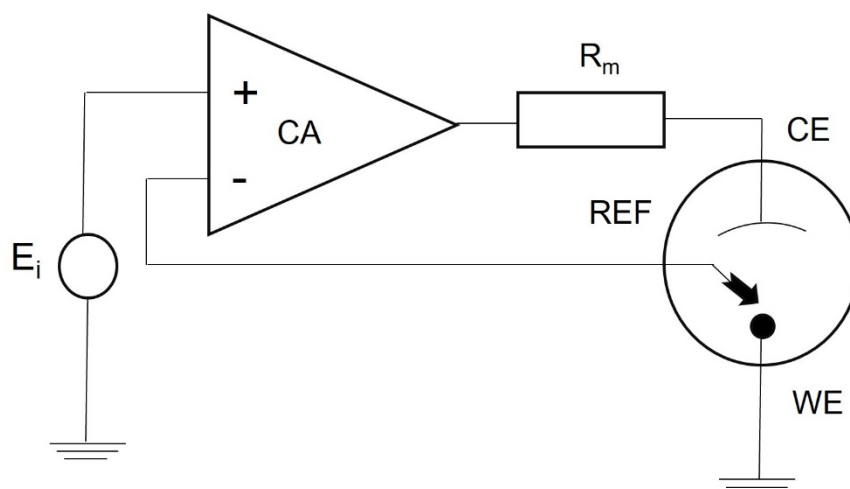


Figure 68: Schematic representation of the electric circuit regulating the potentiostat.

Through the dedicated software it is possible to set significant parameters for the generation of good results such as [194, 195]:

Electric potential range which is the potential window where it is possible to obtain the oxidation and reduction of the species involved.

Scan rate essential to regulate the speed of the reactions.

Sensitivity defines the range of currents in particular application of large currents for experiments which involve a large bulk electrolysis or smaller currents for experiments that involve the use of micro-electrodes.

Number of sweep scans defining the number of scans to run, normally 2 one for the oxidation reaction to happen and the other for the reduction.

The ECL workstation used for the tests reported in the results section, is composed of several devices all interconnected with the main instrument that is the potentiostat CHI 705E (Fig. 69).

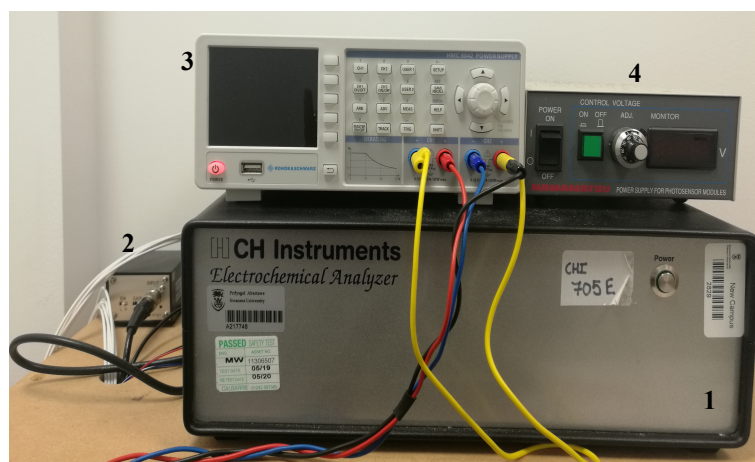


Figure 69: ECL workstation composed of the Potentiostat CHI 705E, DC power supply, photomultiplier amplifier and PMT power supplier.

The initial potential is applied to the WE by the potentiostat to trigger the cascade of reactions starting from the electro transfer reactions on the electrode surface and finishing with the emission of light. The potentiostat (1) establishes three different connections: one with the three-electrodes through “crocodile” cables, with the laptop where the dedicated software is installed to set the parameters and obtain the voltammogram and ECL plots, the last connection is via BNC-R connector with the PMT amplifier (2). The amplifier unit model C7319, has been purchased by Hamamatsu and it’s connected with a current source like the photomultiplier. This amplifier converts the PMT current output to a voltage so that the signal could be processed, in fact this device is composed of a current-to-voltage conversion circuit. It is also connected to the power supplier purchased from Rohde & Schwarz model HMC804

with two channels and an output voltage range from -15 to +15 V (3). The other essential instrument is the photomultiplier (PMT) also purchased from Hamamatsu model H10721-20 (Fig. 70). It is connected to a high-voltage power supply circuit, model C10709, with a 5 V input (4). This permits the adjustment of the voltage in a window range from 0.25 to 1.8 V. The PMT uses these volts to accelerate electrons in the chain of dynodes.

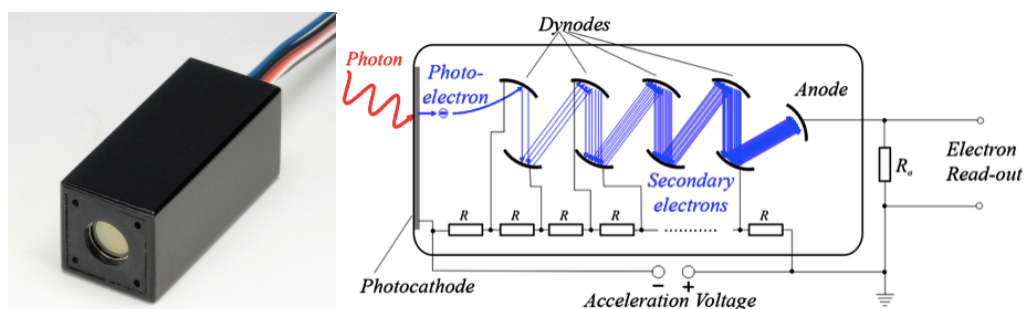


Figure 70: Photomultiplier tube used for the detection of photons during the ECL emission (left) and schematic representation of the working principle of the device (right) [196].

The PMT is a photo-emissive device that converts the absorption of a photon into an emission of electrons. It detects light through a quartz glass window that protects a photosensitive surface called photocathode. The photocathode can release electrons which are then multiplied and accelerated by a series of electrodes called dynodes. The chain of dynodes ends with a photo-anode which collects the electrons and sends a current flow which is directly proportional to the photoelectron flux coming from the photocathode [196] (Fig. 70). To detect the light produced on the WE electrode surface, the PMT is placed very close to the electrochemical cell where the WE surface is. Because of their sensitivity to light, all the system, electrochemical cell and PMT, is enclosed into a dark faraday cage to reduce the background noise. Fig. 71 shows the connections between all the instruments composing the ECL workstation.

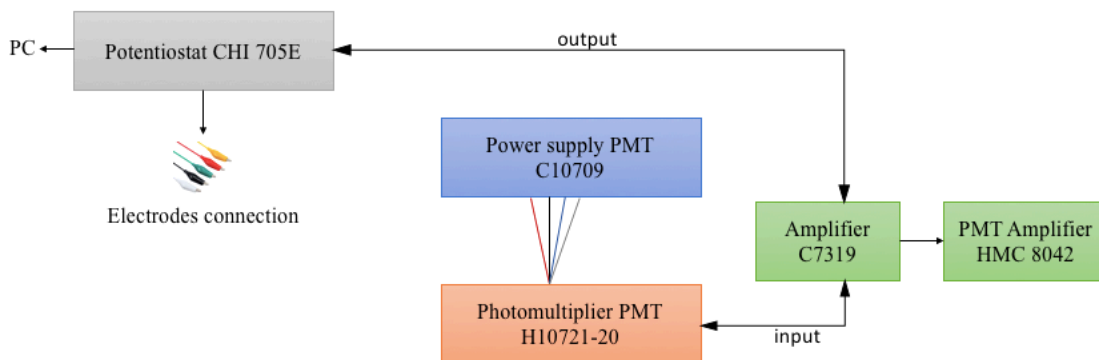


Figure 71: Schematic representation of the connections between the devices of the ECL workstation.

4.4.2. Measurements protocol

The ECL experiments reported in this thesis were performed in a 10 mL volume three-electrodes configuration electrochemical cell made out of glass and covered with a 3D printed lid. The ECL measurements were carried out into a dark chamber purchase from Cairn Research able to create a dark environment ideal for the detection of photons produced during the experiments.

The procedure followed for the ECL experiments was the following:

1. Cleaning of the electrochemical cell with DI water (18 MΩ cm) and dried with compressed air.
2. Preparation of the electrochemical solution.
3. Adjust the pH using pH meter and strong base like 10M NaOH.
4. Cleaning procedure of the GCE.
5. Modification of the GCE surface following the encapsulation technique above described.
6. Immersion of the three electrodes in the electrochemical cell containing the electrolytic solution and stirring for 15 seconds.
7. Connection of the electrodes to the potentiostat and setting the parameters for the CV and ECL tests.
8. Running a first experiments without the addition of the substrate to obtain a baseline measurement.

9. Add different concentrations of substrate and stir 15 second before each run.
10. At the end of the experiment, disconnect the electrodes and clean the electrochemical cell.
11. Collection and analysis of the data.

All the ECL experiments were repeated three times for the realisation of calibration curves characterised by mean and standard deviation of a triplicate data point.

All data analysis were performed using Origin software and Matlab.

4.5 Conclusions

Among all the natural polymers used in the biomedical field, alginate is the most studied due to its properties of biocompatibility, cytocompatibility, biodegradability, low cost, and mild gelation conditions. The combination of CaCO₃ microspheres, polyelectroactive microcapsule and modified alginate hydrogels *via* ionic cross-linking offers a good method for the enzyme encapsulation preserving their biological activity and sensitivity. Furthermore, the selectivity of the enzymes is coupled with the high sensitivity of the ECL detection of photons making the biosensor here proposed a powerful candidate among all the analytical techniques.

In this chapter the encapsulation procedure and the ECL-workstation are described showing the simple architecture of the biosensor characterised by a low number of fabrication steps and low-cost of the materials.

Chapter 5: Luminol – H₂O₂ system

The detection of the enzyme's activity is an effective tool for the prediction and prevention of developing diseases and downside risks. In literature, several biosensors differ in terms of the analytical technique employed. Particularly, amperometric biosensors own the advantages of high sensitivity, easy reproducibility, rapidity, low costs, and disposable.

In this chapter, the system based on electrochemiluminescence (ECL) for the detection of low concentrations of hydrogen peroxide (H₂O₂) is described in detail. The method involves the presence of luminol as luminophore and encapsulated enzymes belonging to the class of oxidase which catalyse an oxidation and reduction involving di-oxygen (O₂) as electron acceptor.

Firstly, a review of the main research related to different kinds of biosensors for the detection of hydrogen peroxide is offered. Following, a deep description and analysis of the method and the instrumentation is conducted concluding then with the results related to the enzymes analysed.

5.1 Luminol- H₂O₂ system: introduction

The proposed ECL-based biosensor relies on the detection of hydrogen peroxide because of the enzyme's activity. H₂O₂ plays important roles in several physiological processes [197] like the regulation of the cell growth [198], immune activation [199] and apoptosis [200]. On the other hand, when H₂O₂ reaches very high levels, it can be very harmful as it is responsible of cell damage [201], inflammatory diseases [202] and even cancer [203]. For these reasons, researchers are studying different methods for the development of biosensors to detect hydrogen peroxide under different conditions. During the years, a variety of procedures have been developed to quantify the H₂O₂ and they can be summarised in the following different approaches in particular electrochemical sensors for the measurement of the chemical energy using an electrical detector.

Considerable attention is given also to the chemiluminescent techniques involving a chemical compound able to be excited and produce an emission of light allowing the measurements of the concentration of hydrogen peroxide. For this type of detection, a

luminophore such as luminol and a catalyst like enzymes, reacting with H_2O_2 , produce a light emission which correspond to the peroxide concentration [204] (Fig. 72).

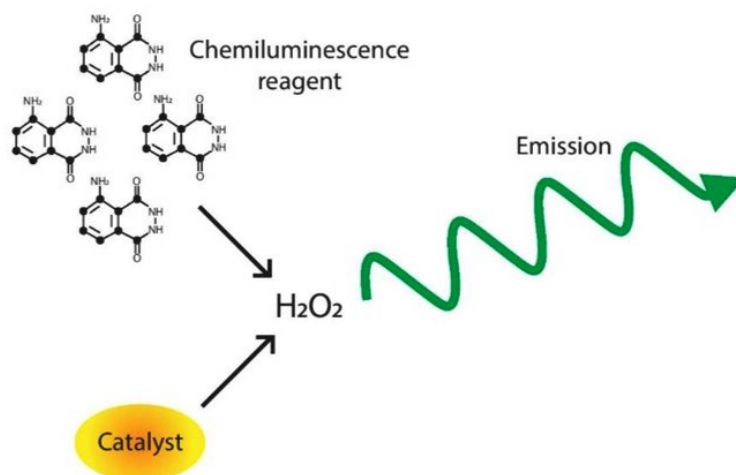


Figure 72: Schematic description of the chemiluminescent reaction between the catalyst and the reagent to generate hydrogen peroxide. Adapted from [205].

In 1989 Igarashi's group proposed an enzymatic assay using the luminol chemiluminescence for the determination of the L-phenylalanine in micellar systems and to determine the concentration of glucose in human serum [206]. In 2007, Lee et al.'s developed instead a chemiluminescent biosensor for the analysis and the detection of the hydrogen peroxide produced in the peritoneal cavity during an induced-stress activity and the intramuscular exogenous H_2O_2 representing one of the first study in vivo [207].

In 2011, the luminol- H_2O_2 system has been used for the analysis the detection of hydrogen peroxide in rainwater proposing a methodology that could be generalised in a protocol for the determination of H_2O_2 produced by oxidase enzymes reaction [208].

Following in 2015, Yu et al. proposed a cheaper method to catalyse the luminol reaction instead of Horseradish Peroxide assay (HRP) using iodophenol blue. This method has been applied for the detection of the hydrogen peroxide and glucose [209]. In 2016 a luminol-chemiluminescent biosensor has been developed to detect the glycated-hemoglobin (HbA1c) using a modified gold electrode. The chemiluminescent reaction of luminol in the presence on hydrogen peroxide resulted to be linearly proportional to the amount of the HbA1c trapped on the biosensor area. This method has been used for the analysis in human blood [210]. In the same year, Koren's group presented a quasi-reversible fibre-optic sensor for the

measure of H_2O_2 at very low linear range into biological samples using a Prussian-blue redox cycles obtaining a very high spatial and temporal control [211]. Afterward, in 2017, Sheng et al. used the bovine serum (BSA) as catalyst for the luminol- H_2O_2 reaction for the detection of uric acid in human serum obtaining a sensor with high sensitivity and selectivity [212]. Gradually, the system based of luminol-hydrogen peroxide started to involve the utilisation of enzymes able to produce H_2O_2 like the work of Moßhammer's group where adopting a micro dialysis probe was possible to detect the H_2O_2 concentration produced by the glucose oxidase and a corresponding catalyst in PBS glucose solution [151].

Considering the electrochemical approaches for the determination of hydrogen peroxide it is possible to discriminate between the potentiometric and amperometric sensors which use respectively the potential and the current to quantify the levels of H_2O_2 [213, 214]. Potentiometric sensors specifically grant the measurement of the potential between the working and the reference electrodes when any current flows in the system (Fig. 73).

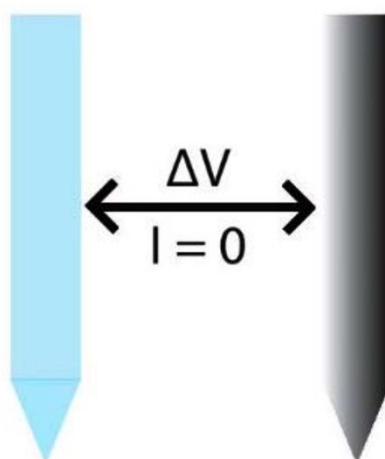


Figure 73: Schematic representation of a potentiometric sensors with the potential running between the WE and the RE when a constant current is applied. Adapted from [205]

In 2012 Wang et al. proposed a sensor for the potentiometric detection of H_2O_2 and glucose used as indicator for glucose levels in blood sample, offering a valid probe for the biomedical research in particular related to the DNA hybridisation detection and glucose oxidase assay [215]. Another example in 2017 by Cànovas' group with a low cost potentiometric cell hosting paper-based We and RE for a quick determination of glucose in a drop of blood using the enzyme entrapped into a Nafion membrane [216].

On the other hand, the amperometric sensors are composed of two-three electrodes to measure the current produce in an electrochemical cell after the application of an appropriate voltage (Fig. 74).

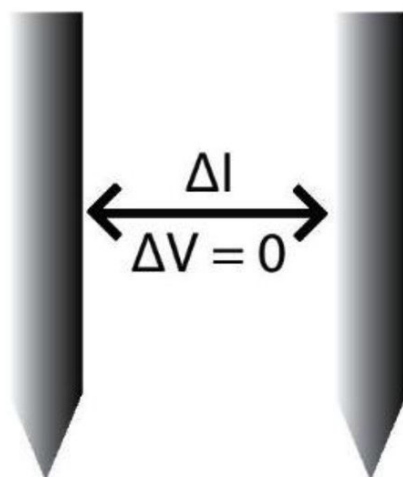


Figure 74: Schematic representation of an amperometric sensor with the current running between the WE and the RE when a constant potential is applied. Adapted from [205].

ECL amperometric biosensors have been widely studied due to their rapidity, accuracy, and sensitivity in the determination of the H_2O_2 and used in the physiological, pathological, and environmental fields. These devices convert a biological reaction into an electronic signal measured using various techniques like cyclic voltammetry and electrochemiluminescence [217].

In 2000 a modified carbon paste electrode was employed for the development of an amperometric biosensor for the quantitative and qualitative detection of drugs combining hydrogen peroxide and the corresponding biocatalyst HRP [218]. In the same year, a luminol-based ECL biosensor has been developed for the measurement of cholesterol in different natural samples detecting H_2O_2 produced by the cholesterol oxidase immobilised on immunodyne membrane [219]. In 2001, Marquette et al. proposed, an ECL-based fibre-optic biosensor to study the activity of glucose, lactate, cholesterol and choline systems for the detection of hydrogen peroxide with luminol [220]. Afterward in 2003, Marquette's group proposed a novel ECL biosensor base on multiple enzymes and luminol in solution to measure glutamate, lysine and uric acid, glucose, choline and lactate [221].

In 2005, an electrochemical biosensor based on sol-gel immobilised cholesterol oxidase has been developed to measure cholesterol in human serum applying cyclic voltammetry [222]. An ECL glucose biosensor has been proposed in 2008 using gold nanoparticles to immobilise the enzyme. The performances of this device depended on different factors such as the scan rate, luminol concentration and in particular by the size of the nanoparticles [223]. Luminol-H₂O₂ system has been utilised also for the monitoring on protein using the hydrogen peroxide generated by the glucose oxidase for the development of a promising ECL-based immunosensor for clinical applications [224]. Recently, in 2019, an hydrogel-composed ECL biosensor for the detection of hydrogen peroxide produced by cardiomyocytes has been proposed [225]. Through the years these electrochemical biosensors have been widely studied and improved reaching good stability, high selectivity, and detection sensitivity. The ECL-based biosensor described in this chapter, can be placed in this area since allows the detection of hydrogen peroxide enzymatically produced during the chemical reaction between the substrate and the enzyme encapsulated into alginate hydrogels. The biosensor uses the combination of cyclic voltammetry and electrochemiluminescence techniques to study the oxidation process of the species involved and the light emission after the reaction of luminol and H₂O₂. This device has been tested for different enzymes like glucose oxidase, horseradish peroxidase, lactose oxidase and cholesterol oxidase.

5.2 Description of the system

The enzymes have been previously encapsulated in alginate hydrogels following the procedure described in the chapter 4 and then immobilised on the WE ready to be analysed (Fig. 75).

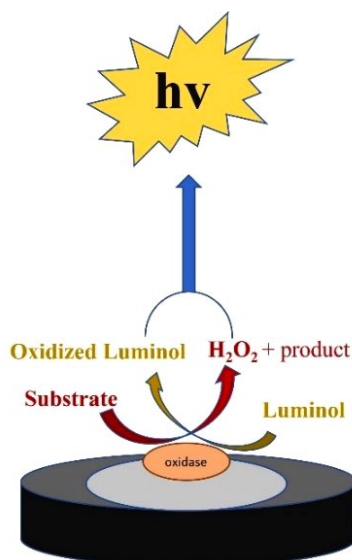


Figure 75: Schematic representation of the luminol-oxidase-H₂O₂ system with immobilised enzyme on the glassy carbon electrode surface.

Once the electrodes are immersed in the electrolytic solution, a suitable potential can be applied to the WE to start the ECL reaction. The species involved undergo an electron transfer reaction happening at the electrode surface. Luminol after multiple steps reaches its oxidised form, meanwhile the substrate reacting with the immobilised enzyme, produce hydrogen peroxide and other products of the reaction. H₂O₂ itself does not contribute to the emission of light, but its OH radicals reacting with the negative ions of luminol generate luminol negative ion radicals which in turn reacting with O₂⁻ radicals generate hydroperoxide intermediate. This new intermediate forms an excited energy level, 3-aminophtalate, which decays into the ground state emitting photons at 425 nm of wavelength [226] (Fig. 76).

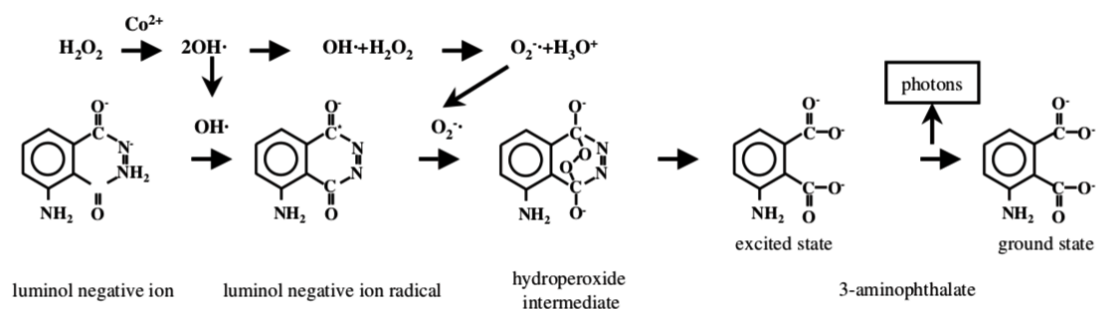


Figure 76: Intermediates of luminol formed during the reaction with the H_2O_2 . After the emission of photons, the excited form of luminol decay to the ground state [226].

The concentration of the luminophore plays an important role during the ECL experiments. In 2007, Chen et al. studied the effects of the luminol concentration maintaining constant the concentration of hydrogen peroxide and silver nanoparticles in solution. The range that has been analysed covered the concentrations from 0.3 to 0.01 mmol/L to 1 mmol/L finding that the maximum CL intensity was for 0.3 mmol/L of luminol in solution. Further investigations suggested that the CL signal of luminol increases linearly with the increase of the luminol concentration [227]. Prior to performing the ECL experiments reported in this thesis, different concentrations of luminol have been studied concluding that the best performance have been achieved adding to the electrolytic solution 0.2 mM of luminophore. In fact, the ECL emission of luminol has been studied in the presence of 22 μM of H_2O_2 in 0.01 M PBS at pH 12 discovering that the emission of light increases in the concentration range from 0.005 mM to 0.3 mM as anticipated by Chen. After reaching the highest emission for 0.3 mM of concentration, the signal gradually reduced intensity (Fig. 77).

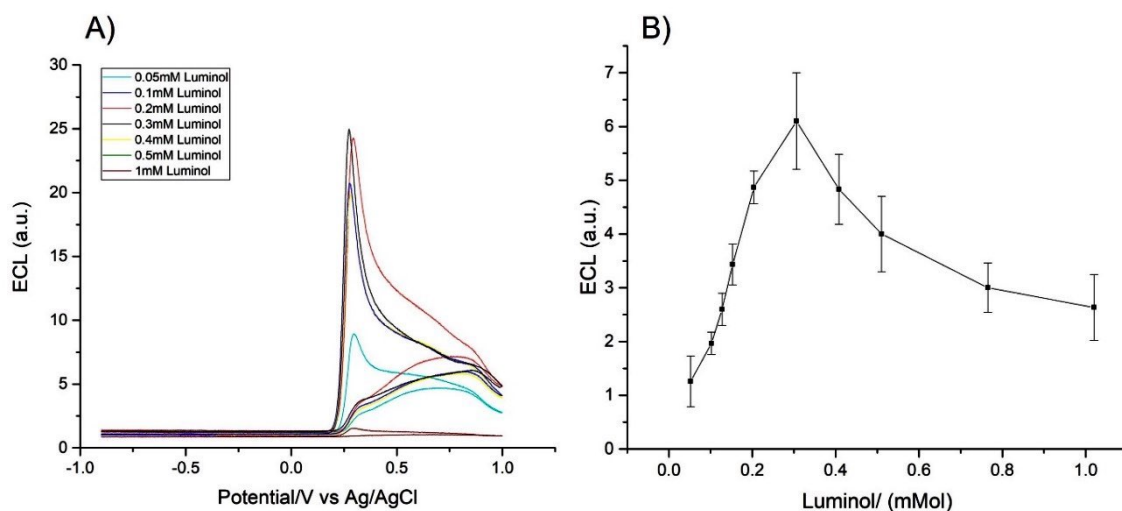


Figure 77: Study of the ECL signal for different concentrations of luminol obtaining the calibration curve showing an initial increase of the signal reaching the highest signal at 0.3 mM in the presence of 22 μ M of hydrogen peroxide in 0.01 M pH 12. Error bars represent triplicate data points.

From the calibration curve obtained by analysing three repetitions of ECL experiments under the same conditions, it is possible to conclude that the best ECL performance has been obtained for the concentrations of 0.2 mM and 0.3 mM. However, considering that for 0.3 mM the standard deviation is higher than 0.2 mM, the latter has been chosen as the luminol concentration for the ECL experiments with the encapsulated enzyme into alginate hydrogels and cryogels.

5.3 Role of pH in electrochemical measurements

All ECL tests were performed in PBS buffer solution that is one of the most common supporting electrolyte utilised in the electrochemistry experiments. The use of buffers is essential for biological system as they are able to maintain a constant pH upon addition of an acid or a base. The pH of the buffer can influence the ECL signal as it could affect the generation of precursors.

0.01 M PBS solution prepared in 1 L of DI water (18 M Ω cm) has a pH = 7.4 and a pK_a = 7.21 at 25 °C. The buffer pH was then adjusted to meet the needs of alkaline conditions of the luminol and optimal pH for the encapsulated enzyme.

In fact, one of the factors which plays an essential role for the CL of luminol is the pH of the solution. In fact, at acidic pH, the activity of luminol is drastically reduced with no emission of light, while moving at more alkaline pH solutions, also the luminescence sees a significant increase in the intensity (Fig. 78).

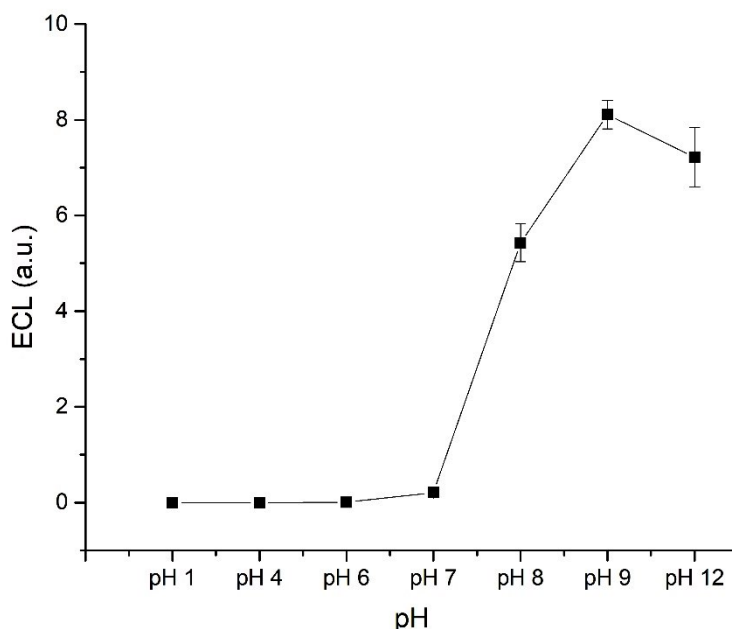


Figure 78: Study of the behaviour of luminol at different pH. Error bars represent triplicate data points.

The maximum chemiluminescent intensity is measured for pH in the range of 9.0 and 10.0, but good results can be achieved also for pH 8.0. The pH represents the most significant variable parameter for the oxidase-luminol-H₂O₂ (Fig. 78). In fact, it is necessary to find a good compromise between the optimal pH for the enzyme reaction to occur and the right pH to obtain a noticeable intensity of light from luminol.

The second contribute comes from the optimum pH of the enzymes. The enzyme activity is at its maximum value when the environment of solution is set at the optimum pH. Increasing the pH value above or below the optimum pH could cause a decrease of the enzyme activity. In fact, if the pH is set at very acidic or alkaline values, the morphology of the enzyme can be altered, therefore it is no longer complementary to the specific substrate causing the so-called denaturation [228]. Thus, each enzyme has an optimum pH but also a working range of pH values around the optimal one at which the enzyme is still able to

efficiently work bonding with the corresponding substrate. Most of the enzymes have a working pH range of 5-9 with the neutral pH 7 being as their optimum [229].

Another important aspect is the coreactant produced as a byproduct of the enzymatic reaction. Hydrogen peroxide produced from the reaction substrate-enzyme is the molecule which plays the important role of oxidising agent able to increase the luminescence intensity of luminol [230]. During the redox reaction involving the oxidase enzyme, the substrate undergoes to an oxidation meanwhile O_2 is reduced to H_2O_2 . The most stable form of H_2O_2 is the undissociated peracid (HO_2H) with $pK_a = 11.6$. To produce hydrogen peroxide and the other products of the reaction, the substrate must interact with the active site of the corresponding enzyme [231]. Alteration of the pH could affect the binding site of the enzyme as the acidic and basic chains in the active site [232]. As described in Fig. 77, hydrogen peroxide does not contribute to the emission of light until it is converted to $HO_2\cdot$ which in turn rapidly deprotonates to form the superoxide ($O_2^{\cdot-}$) at high pH with a $pK_a = 4.8$, therefore the ECL of luminol is more efficient in alkaline pH because at high pH the anion HO_2^- is generated and can react with the oxidised and unprotonated form of luminol also known as diazaquinone.

Therefore, the three main contributions for the pH choice are:

1. the optimum pH of the enzyme and their working pH range
2. alkaline pH for the luminescence of luminol
3. high pH for the H_2O_2 de-protonation to $O_2^{\cdot-}$ and form in this way the excited state of luminol.

5.4 Characterisation of the biosensor: Randless-Sevcik equation

The CV and ECL characterisation of the luminol-oxidase-H₂O₂ biosensor is based on different aspects related in particular to the study of the diffusive processes with the Randless-Sevcik equation, the analysis of the performances of the system at different pH and the luminol concentration [233].

The Randless-Sevcik (R-S) equation describes how the scan rate affects the peak current i_p depending on the diffusive properties of the material. In this case, with the R-S equation it is possible to understand if the luminol can diffuse into the alginate hydrogel hosting the enzyme to react with the produced H₂O₂. This aspect is essential as everything that happens on the WE surface is recorded by the PMT. If luminol does not diffuse into the hydrogel matrix, no signal will occur as there will not be any interaction with the hydrogen peroxide [11].

For this characterisation, two different conditions have been considered:

1. the diffusion of luminol on a bare GCE
2. the diffusion of luminol on the modified GCE.

In both cases, 0.2 mMol luminol were added to 10 mL of 0.01 M PBS at pH 9.0. Different cycles of cyclic voltammetry have been performed at different scan rate starting from the slowest 0.001 Vs⁻¹ to the fastest 0.15 Vs⁻¹. At higher scan rate, the size of the diffusion layer decreases leading to the observation of higher currents. The Radles-Sevcik equation linearly relate the increase of the current peak with the square root of the scan rate considering the number of electrons transferred during the redox reaction ($n = 1$ in the considered case).

$$i_p = 0.446nFAC^0 \left(\frac{nFvD_0}{RT} \right)^{\frac{1}{2}} \quad (54)$$

Where:

i_p is the studied peak current (A)

n is the number of electrons transferred during the reactions

F is the Faraday constant (96,4853 C mol⁻¹)

A is the area of the electrode where the reaction occurs (cm²)

C is the concentration of the analyte (mol cm⁻³)

ν is the scan rate (V s⁻¹)

D is the diffusion coefficient (cm² s⁻¹)

R is the gas constant (8,314 J K⁻¹ mol⁻¹)

T is the temperature (K).

Considering the first condition cited above, 0.2 mM luminol has been added to 10 mL 0.01 M PBS at pH 9.0 and after 15 seconds of stirring the CV tests. The current peak i_p increases linearly with the scan rate showing a linear relationship with the square root of the scan rates. This demonstrates that luminol freely diffuses on the bare surface of the GCE (Fig. 79).

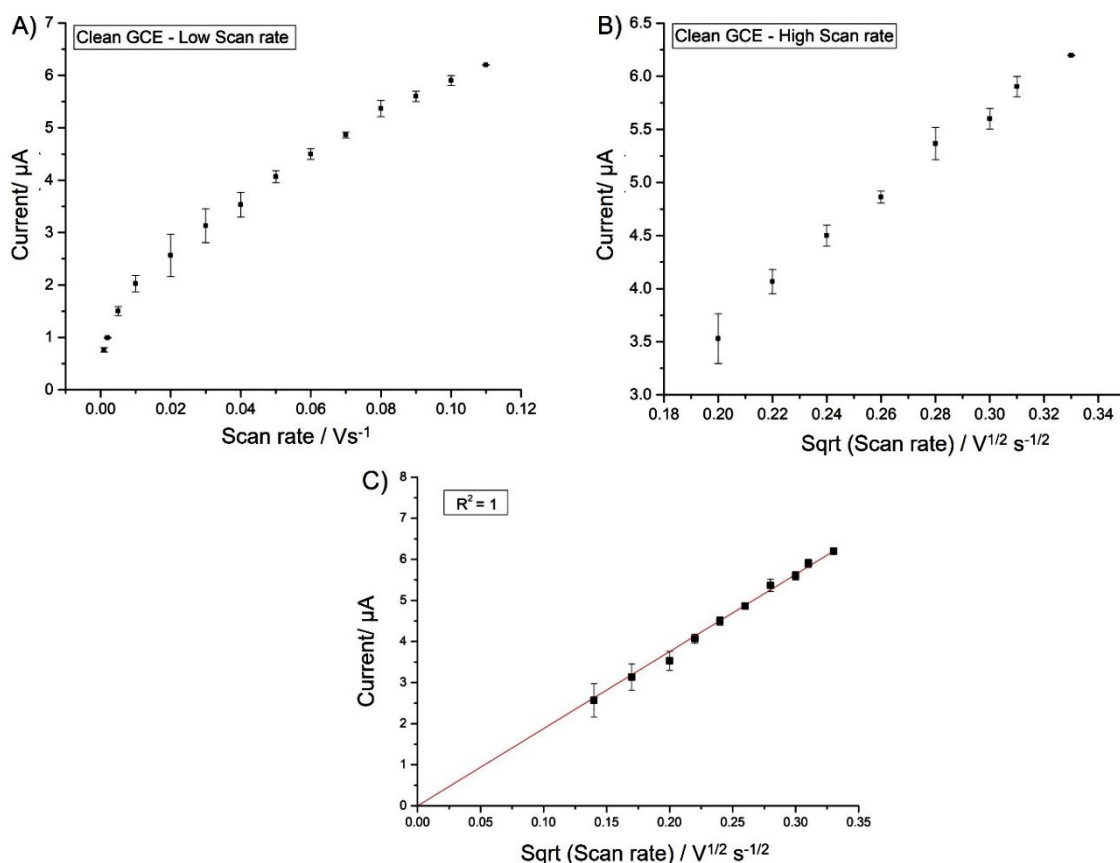


Figure 79: Description of the dependence of the current peak from the scan rate (low rates) A) and from the square root of the scan rates (high rates) B) applied during the cycles of cyclic voltammetry. The linear range of the square root of the scan rates has also been plotted C). Error bars represent triplicate data points.

Considering now the second condition, 3 μL of alginate hydrogel has been used to modify the surface of the GCE to study the diffusive process of the luminol into its matrix obtaining a diffusion coefficient $D = 5.63 \times 10^{-6} \text{ cm}^2 \text{ s}^{-1}$ obtained at 0.05 Vs^{-1} with peak current $i_p = 2.029 \mu\text{A}$ at $\sim 0.6 \text{ V}$. In Fig. 80 a linear relationship between the current peak and the square root is still in place even if the standard error is higher compared to Fig.79 indicating that the signal is less stable due to the presence of a 3D matrix on the electrode surface, but the luminol diffusion close to the GCE surface is not inhibited.

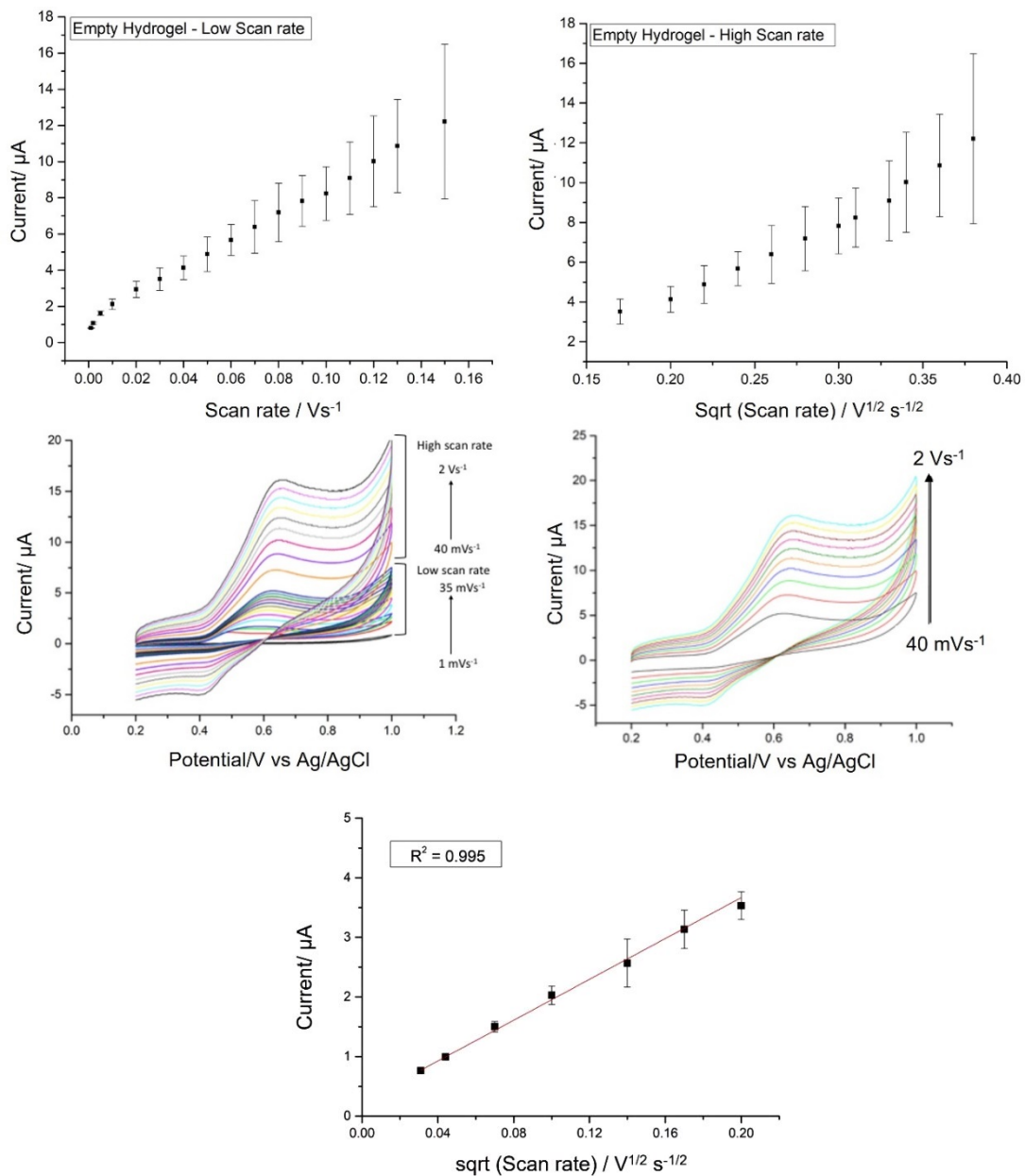


Figure 80: Dependence of the current peak from the different scan rates applied to the working electrode hosting an empty alginate hydrogel. Higher values of standard error have been recorded in this case. Error bars represent triplicate data points.

5.5 Result and discussion

5.4.1. HRP-luminol- H_2O_2 system

Horseradish peroxidase/luminol/ H_2O_2 represents one of the most studied systems in the field of the ECL and CL, HRP (Fig. 81) is an enzyme widely used in biochemistry due to the ability to catalyse various organic substrates by using hydrogen peroxide. This enzyme was first studied in 1997 by X-ray crystallography and it is composed of a large alpha-helical glycoprotein which binds a heme group that acts as a redox cofactor.



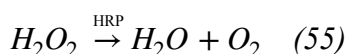
Figure 81: Structure of horseradish peroxidase (HRP) obtained by PDB database (Berglund, G.I., Carlsson, G.H., Hajdu, J., Smith, A.T., Szoke, H., Henriksen, A. (2002), 10.2210/pdb1HCH/pdb).

This enzyme was essential in the development of the sensitive CLEIA method (chemiluminescent enzyme immunoassay) based on enzyme-antibody conjugates with the utilisation of substrates with chemiluminescent properties and a luminometer for the light detection. CLEIA, ELISA (enzyme-linked immunosorbent assay) and ECLIA (electrochemiluminescence immunoassay) are the three most used methods for the detection and analysis. HRP can catalyse the reaction between a hydrogen acceptor (such as hydrogen peroxide) and a hydrogen donor like luminol [234].

Horseradish peroxidase can be used for chemiluminescent and fluorescent detection when conjugated with a fluorogen substrate [235-238], but HRP received great attention for the electrochemical detection in particular for measurements based on electron transfer

reactions in the electrolytic solution [239]. In 2003, Wilson et al. proposed an ECL enzyme immunoassay based on magnetic beads and peroxidase-labelled antibodies. The determination of the analyte was achieved measuring the light emitted when the generated H_2O_2 reacted with the luminol in solution [28]. In the same year, HRP-luminol- H_2O_2 system was used for the chemiluminescent detection of DNA and antigen-antibody interactions in the presence of rotating magnetic particles [240]. In 2009 a rapid and sensitive magnet chemiluminescent was developed for the measurement of luteinising hormone in human serum involving HRP-luminol- H_2O_2 system with a detection limit of 0.2 mIU/mL showing a good correlation with already approved radioimmunoassay (RIA) [241]. In 2017, two step-enzyme reactions were used for the development of a new chemiluminescent cloth-based biosensor for the determination of glucose. The first reaction involves the enzymatic oxidation of glucose to gluconic-acid and H_2O_2 followed by the second reaction between the generated hydrogen peroxide and HRP which reacting with luminol generate the final chemiluminescent light emission detected by a CCD camera [242].

Luminol to exhibit its luminescence needs to be activated with an oxidant. In the case of this system, hydrogen peroxide reacting with the enzyme HRP produce water and O_2 . The oxygen in solution, oxidises part of the luminol producing an unstable peroxide leading to the generation of the excited state which decaying to the ground state emits light.



A pH study of the HRP/ H_2O_2 system has been done to define the best conditions considering the optimum pH for the enzyme and the need for luminol to work in alkaline conditions. From Fig. 82, the best ECL results are achieved for the electrolytic solution at pH 9.0.

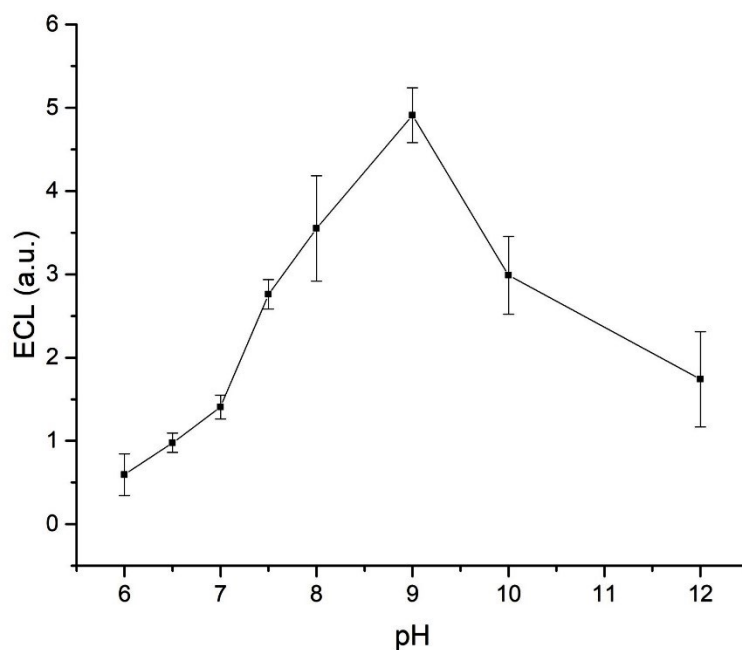


Figure 82: ECL performances of the HRP/H₂O₂ system at different pH showing that the best results are obtained at 0.01 M PBS pH 9.0. Scan rate 0.05 V s⁻¹. Error bars represent triplicate data points.

The working principle of the HRP-luminol-H₂O₂ is slightly different from the other enzyme analysed where the hydrogen peroxide is generated by the chemical reaction between the corresponding substrate and the encapsulated enzyme. In this case the hydrogen peroxide is added to the solution to be degraded by the enzyme HRP in water and oxygen. By increasing the concentration of H₂O₂ increases the amount of oxygen as well produced with the consequent generation of peroxide reacting with luminol (Fig.83).

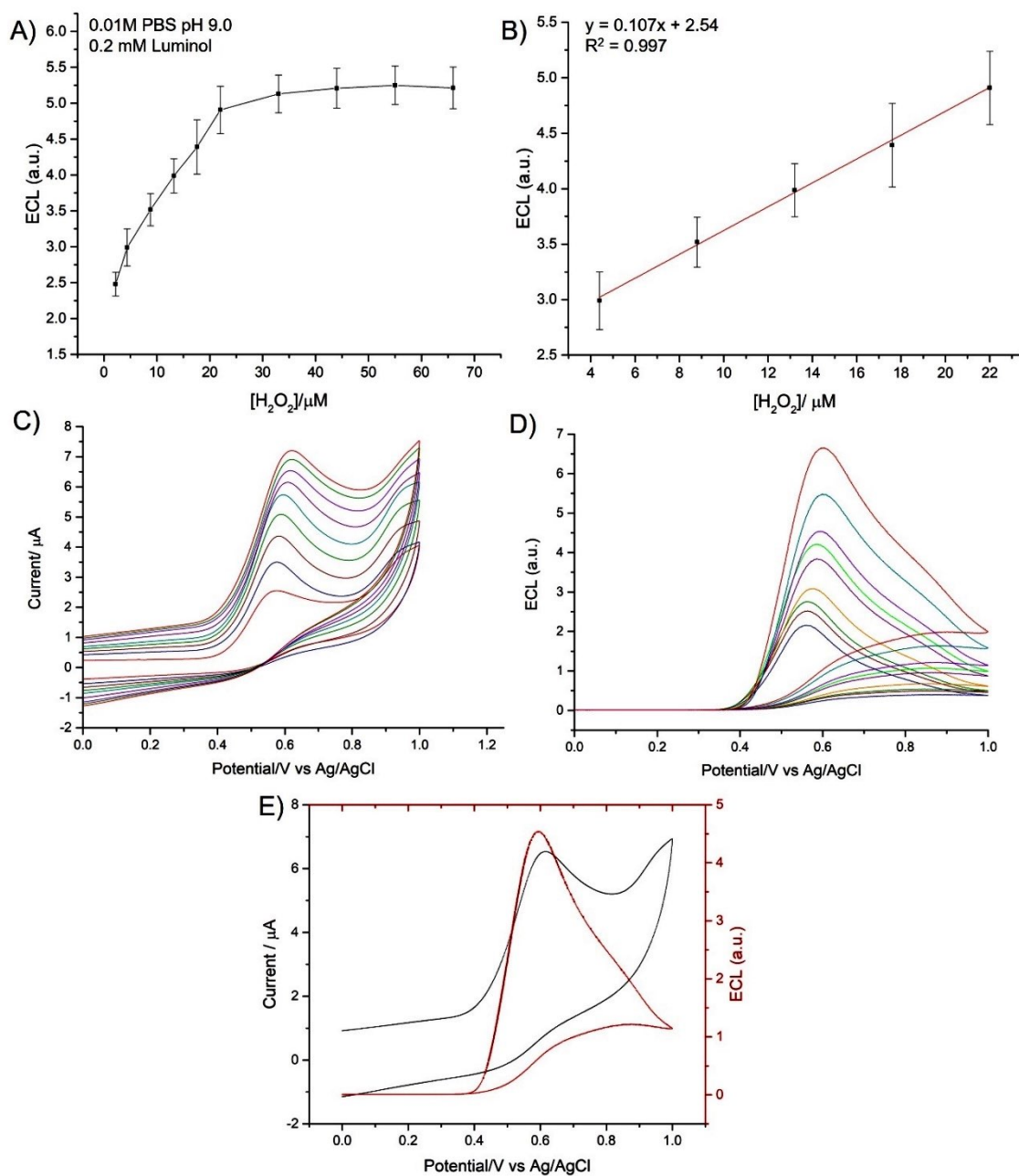


Figure 83: Calibration curve of the HRP-luminol-H₂O₂ system A). Error bars represent triplicate data points. Study of the linear range B). CV and ECL plots showing the increasing of the oxidation peak C) and the ECL emission D). E) CV and ECL scans at 44 μM H₂O₂ in 0.01 M PBS pH 9.0 with 0.2 mMol of luminol in solution. Scan rate 0.05 V s⁻¹.

5.4.2 GOx -luminol-glucose system

The monitoring of glucose in blood is essential for the control of the diabetes and for this reason the study of glucose biosensors exponentially increased in the last 50 years [243]. In general, the measurement of glucose is based on the reaction of one of three kind of enzymes: hexokinase, glucose oxidase or glucose-1-dehydrogenase. GOx (Fig. 84) and GDH are mainly used for electrochemical biosensors, and they have been used for the development of the ECL-based described in this work [244, 245]. Glucose oxidase has been widely used for glucose biosensors thanks to its high selectivity for glucose, low cost, ionic strength, stability at different temperatures [48, 246]. The ECL-based system relies on the catalysis action of the immobilised GOX to oxidised glucose in the presence of O₂ producing Gluconolactone and hydrogen peroxide as stated by equation (54) [247]:



Glucose oxidase is an oxidoreductase enzyme with a dimeric structure, extracts from *Aspergillus Niger* and discovered for the first time in 1928 by Detlev Muller.

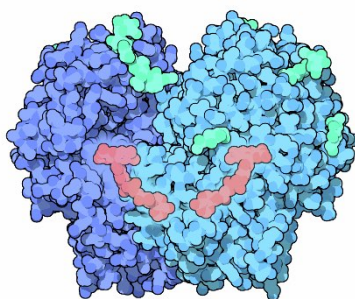


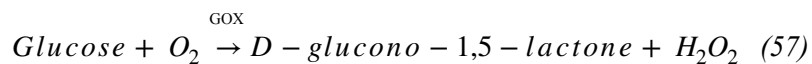
Figure 84: Structure of Glucose Oxidase (GOx) obtained by PDB database. (PDB: 1gpe; Goodsell D. (May 2006). “Molecule of the Month: Glucose Oxidase”. RCSB Protein Data Bank. doi: 10.2210/rcsb_pdb/mom_2006_5).

In the literature, three different generations of glucose biosensors can be identified. The first one consists of biosensors based of natural oxygen as substrate and the detection of hydrogen peroxide produced during the chemical reaction. The first biosensor for the detection of glucose appears in 1962 with Clarke and Lyons proposing a device whit an

oxygen electrode, a thin layer of glucose oxidase, an inner oxygen membrane and an outer dialysis membrane. They discovered that the concentration of oxygen measured decreased proportionally with the glucose concentration [248]. Instead, in 1975 Clark's produce the first glucose biosensor for the direct measurement of glucose with an amperometric sensor for clinical laboratories uses. Different problems characterised the first generation, such as the interferences of species like ascorbic acid, drugs and uric acid affected the selectivity of the device. Furthermore, the oxygen was not always easy to solubilise in biological fluids representing a big obstacle for the sensitivity and repeatability of biosensors [249]. The second generation employed for the first-time redox mediators as electron acceptor instead of the oxygen reducing the problem related to the "oxygen deficit" of the first generation. These mediators were able to transport electrons from the enzyme to the WE surface. Example of mediators were ferrocene, methylene blue, ferricyanide, quinines which when reduced replace the previous hydrogen peroxide. The first system was proposed in 1970 with the publication of a device for the detection of glucose in blood using the redox couple-mediator reaction [250]. In 1987, the first biosensor for the self-monitoring of blood glucose for diabetic patients was proposed leading to a big revolution in the diabetes monitoring and to the development of a variety of self-monitoring diabetes sensors based on ferrocene/ferrocyanide [251].

Finally, with the third generation, the direct transfer of electrons between the enzyme and the electrode was introduced. The mediators used for the second-generation sensors were discovered to be very toxic. The third-generation of glucose biosensors allow the direct charge-transfer involving organic conducting materials increasing in this way also the selectivity [252]. This invention consented the development of implantable devices for the continuous in-vivo monitoring of the glucose level in blood [253]. Nowadays, this systems is still the object of study for most of the research for the development of a no-invasive way to monitor the levels of glucose in human blood [254].

The glucose biosensor proposed, uses glucose oxidase encapsulated into Alginate Hydrogels as reagent for the determination of glucose thanks to its high selectivity for the substrate. GOx produces H_2O_2 reacting with the glucose after the stimulation with the application of the potential to the WE.



The hydrogen peroxide gradually degrades producing oxygen and water to react with the oxidised form on luminol presents in solution forming the excited state. The ECL tests have been performed using 0.01 M PBS at pH 9.0. Different tests have been carried out to determine the right pH for the ECL tests considering that the optimum pH for the GOx activity is 9.0 and that luminol is highly sensitive to pH achieving the best performances for alkaline pH (Fig. 85).

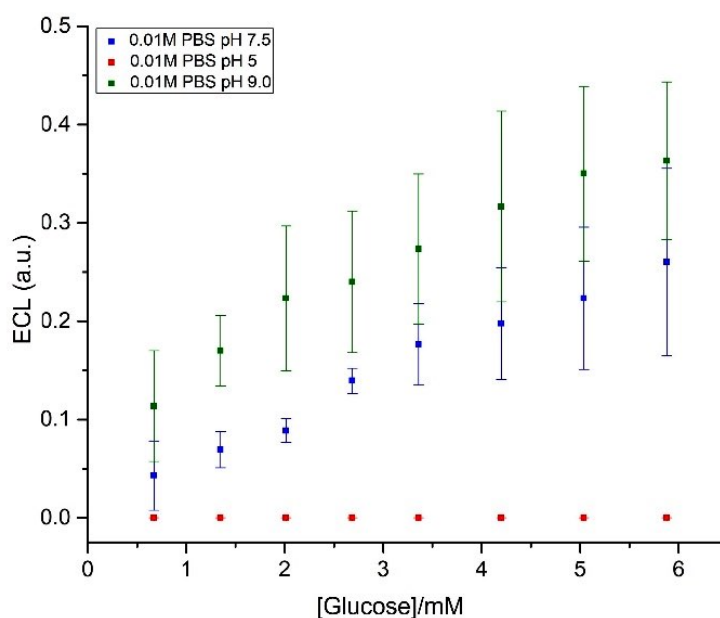


Figure 85: ECL performances of the GOx-glucose system at different pH. Scan rate 0.05 V s⁻¹. Error bars represent triplicate data points.

Using luminol, it is possible to monitor in an indirect way the concentration of glucose and the enzyme activity using the detection of hydrogen peroxide produced during the enzyme-substrate reaction. In fact, the intensity of the light emission proportionally increases with the increment of the glucose concentration in solution leading to the growth of the generation of hydrogen peroxide to be detected (Fig. 86).

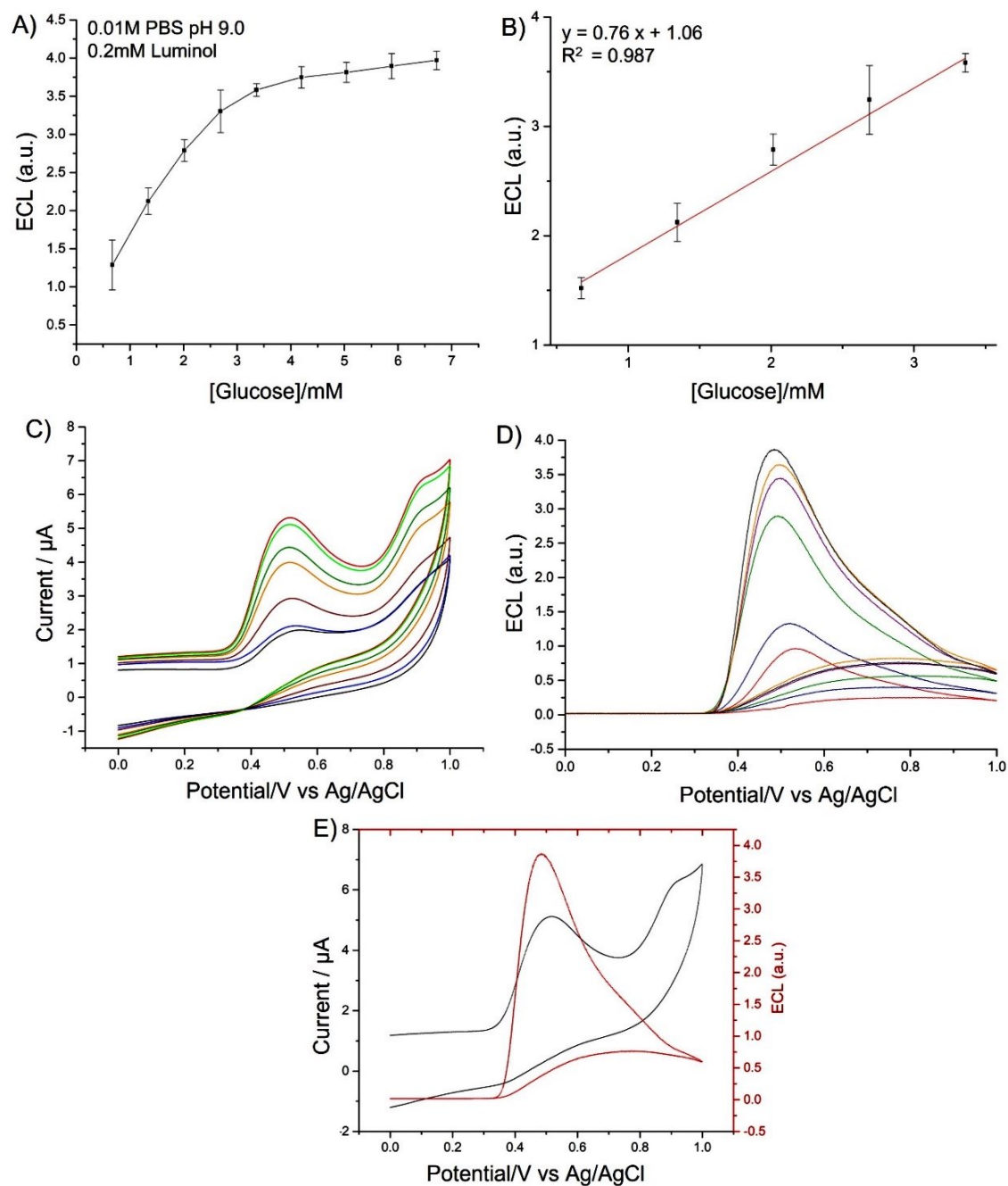


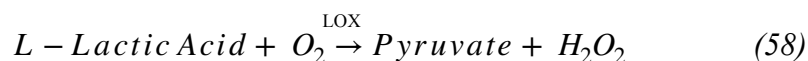
Figure 86: A) Calibration curve for the GOx-glucose system in 0.01 M PBS at pH 9, and study of linear range and regression equation B). Error bars represent triplicate data points. C) CVs of the glucose-GOx-luminol system, D) ECL for different concentrations of glucose. E) CV and ECL scans at 5 mM glucose in 0.01 M PBS pH 9.0 with 0.2 mM of luminol in solution. Scan rate 0.05 V s⁻¹.

The CV and ECL characterisation were performed in 0.01 M PBS at pH 9 with different concentrations of glucose added after a stirring of 10 seconds. The results show how the oxidation peak in the voltammograms linearly grows with the amount of glucose in solution

and as consequence also the intensity of the current peak of the ECL increases as result of the reaction between luminol and hydrogen peroxide produced.

5.4.3 LOx-lumino-L-lactic acid system

Lactate detection is a significant tool for the control of haemorrhage, sepsis, hypoxia, respiratory problems, and hepatic diseases. Furthermore, lactate plays an important role in sport medicine and shock or trauma situations. For these reasons, multiple sensors for the monitoring of the concentrations of lactate in human blood have been proposed during the years [255, 256]. In the literature, different electrochemical sensors have been proposed based on two types of enzymes, lactate oxidase (LOx) (Fig. 87) [257] and lactate dehydrogenase (LDH) [26]. As for the glucose, these two enzymes react with the same substrate but in different conditions and with different luminophores [258]. In human blood the concentration of lactate must be in the range from 0.5 mmol/l to 1.5 mmol/l in rest conditions, increasing to 25 mmol/L under fatigue so it is essential the development of a biosensor highly sensitive and with appropriate limits of detection. Lactate is a metabolite of the anaerobic metabolism and becomes essential when the energy required by tissues is not satisfied by the aerobic respiration, therefore an increase of lactate concentration from the anaerobic pathway will occur. Simultaneously, liver and kidneys work for the removal of the accumulated lactic acid to avoid the lactic acidosis caused by a decreased tissues oxygenation and/or by certain drugs or toxins and systemic diseases like diabetes or cancer. For these reasons a fast and non-invasive way for the blood lactate level monitoring can represent an important way to improve the diagnosis and the consequent treatment of a wide number of diseases [259]. Different methods have been used for the lactate detection like high performance liquid chromatography (HPLC), chemiluminescence, magnetic resonance spectroscopy, electrochemical techniques to provide a sensor with a good time and spatial response, high sensitivity, low limits of detection, stability, and linearity. As anticipated, two enzymes are involved in the lactate determination and so used for the development of biosensor. In this chapter, the Lactate oxidase from *Aerococcus Viridians* is analysed in the luminol-H₂O₂ ECL biosensor. LOx is a flavoprotein that catalyses in the presence of oxygen the oxidation of lactic acid to pyruvate with the generation of hydrogen peroxide [260, 261].



LOx is also known as lactate 2-monooxygenase and belongs to the oxidoreductase's enzymes playing the essential role in the pyruvate metabolism. The enzyme used for this research is obtained from *Aerococcus Viridians* with the molecular structure shown in Fig. 86.

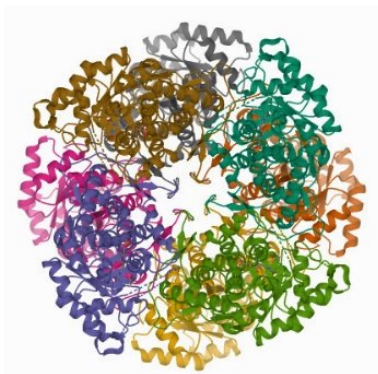


Figure 87: Structure of Lactate 2-monooxygenase or lactate oxidase (LOx) obtained from PDB database. (H.M. Berman, J. Westbrook, Z. Feng, G. Gilliland, T.N. Bhat, H. Weissig, I.N. Shindyalov, P.E. Bourne. (2000) The Protein Data Bank *Nucleic Acids Research*, 28: 235-242.)

A variety of methods have been used for the lactate monitoring like amperometry [258], potentiometry [262], chemiluminescence [263], high-performance liquid chromatography [264], fluorometry [265] and magnetic resonance spectroscopy [266].

The first biosensor for the detection of lactate was developed in 1964 by Broder and Weil proposing an optical sensor based on the photo-spectrometric method where an incident light was sent to the region of interest and the transmitted light was detected changing intensity with the analyte concentrations [267]. Following in 1999, Yang and al. proposed a needle-type lactate biosensor to monitor continuously the intravascular lactate concentration using lactate oxidase as immobilised enzyme. This sensor showed a long-term stability and was evaluated in blood in vitro and afterwards also in vivo [268]. An amperometric sensor based on the H₂O₂ monitoring has been proposed in 1993 using the immobilisation of the enzyme in polycarbonate and polytetrafluoroethylene membranes used for the measure of lactate in sweat samples in normal conditions and after physical exercise [269]. In 1999,

Marquette et al., proposed an ECL-based fiber-optic for the analysis of glucose and lactate using luminol. The two enzymes were immobilised in collagen and polyamide membranes reaching very low detection limits[270]. Marquette developed another fiber-optic biosensor in 2000 with flow injection analysis for the determination of the presence of H₂O₂ produced by lactate oxidase entrapped in the same polyamide membranes [271]. In 2001 an amperometric biosensor based on Prussian-blue was used for the determination of lactic acid building a flow injection system with the enzyme LOx immobilised in Nafion films [272]. Claver and his group instead, developed an ECL-based disposable biosensor for the determination of lactate in saliva using luminol and Lox restrained in Methocel membranes. This work is one of the examples of the research of non-invasive methods for the monitoring of metabolites in fluids like saliva or sweat [273]. In fact, saliva is the most interesting sample for the non-invasive lactate analysis due to its high correlation to the lactate in blood, 1:4 saliva/blood ration in human saliva reaching concentrations in the range of 2 x 10⁻⁴ M. Another example of determination of lactate in a non-invasive way was offered by Lamas-Ardisana et al. in 2014. They used a scree-printed carbon electrodes (SPCE) modified by a dispersion of platinum nanoparticles to obtain a sensitive, low cost, disposable, and reliable hydrogen peroxide sensor tested in real sample of saliva compared then with the results obtained using blood samples [274]. Recently in 2017, a scree-printed carbon electrode and a single hydrophilic cloth have been used to obtain ECL signals for the non-invasive monitoring of lactate in human saliva. Thanks to its acceptable stability and selectivity, this device connected to a smartphone could detect a wide range of analytes of medical interest [275]. Although, it can be an expensive tool and not simple to be used for the self-monitoring. In 2019, an ECL platform was incorporated in a flexible and wearable device for the non-invasive monitoring of lactate and urea contained into sweat. Wearable ECL devices represent a promising non-invasive tool for monitoring metabolites in bio-fluids like tears, saliva and sweat [276].

The results below are obtained after the encapsulation of the LOx into the alginate hydrogels cores and the cross-linking process. Differently from the glucose oxidase, one unit of this enzyme can oxidise 1 µM of L-lactic acid to pyruvate and H₂O₂ at pH 7.4. The ECL tests have been performed in 0.01 M PBS at 7.4 pH with 0.2 mM of luminol. From the statistical analysis, it is possible to appreciate how the sensor is stable in the range of

concentrations analysed. In fact, by increasing the concentration of lactic acid in PBS also the production of hydrogen peroxide raises and so the consequent emission of light. The following figure shows the electrochemical behaviour of the enzyme (Fig. 88) underlying the dependence of the ECL emission from the generation of hydrogen peroxide. Particularly, in Fig. 88D, the ECL plots shows how the peak shifts with the increase of the L-lactic acid in solution. This behaviour is probably caused by a slight change of pH which goes from the initial 7.4 to 7.2.

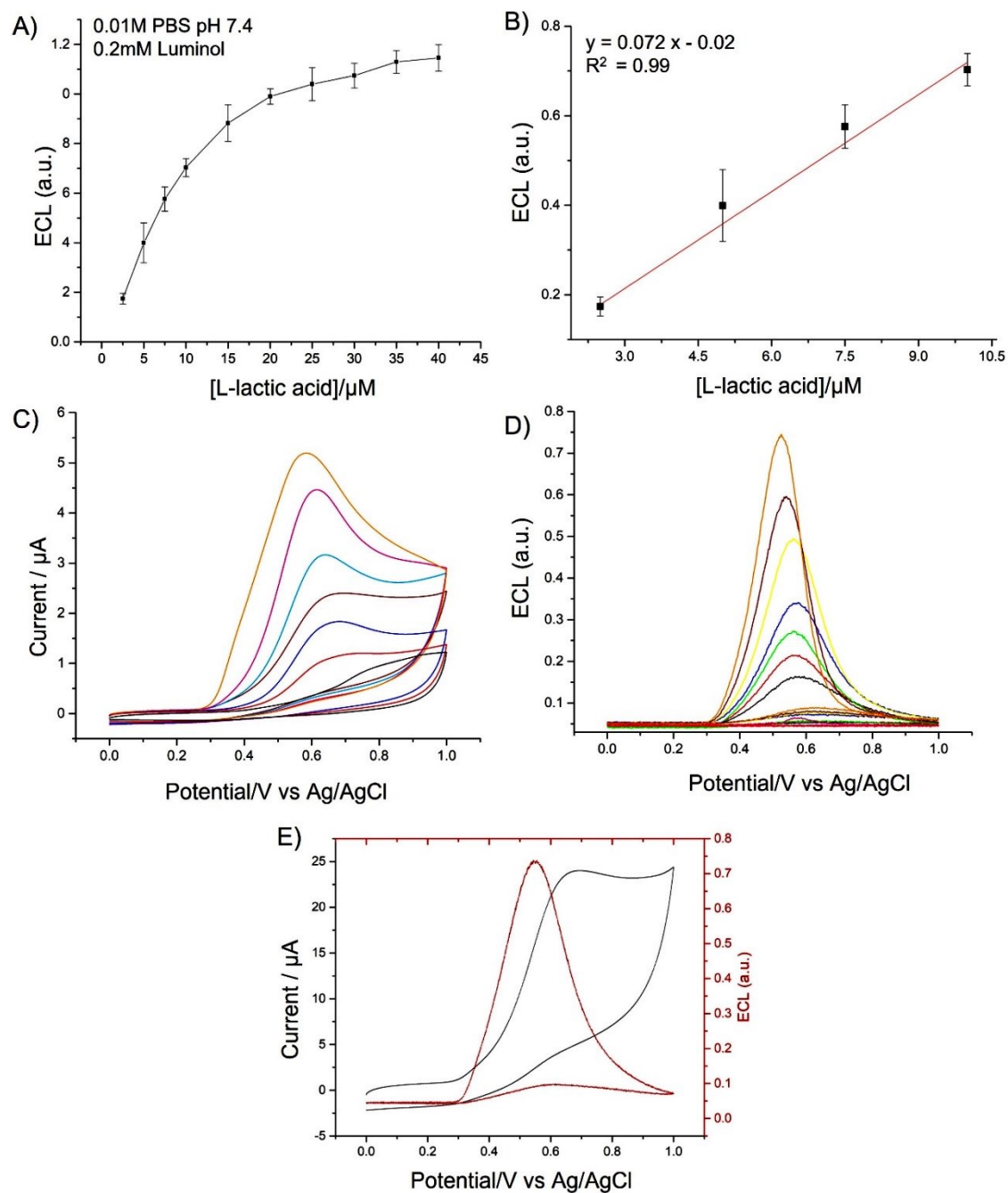


Figure 88: A) Calibration curve of the L-Lactate-LOx system and study of the linear range B). Error bars represent triplicate data points. C) CVs showing the oxidation peak increasing with the increase of the substrate in solution. ECL curves B). E) CV and ECL scans at 30 μM L-lactic acid in 0.01 M PBS pH 7.4 with 0.2 mMol of luminol in solution. Scan rate 0.05 V s^{-1} .

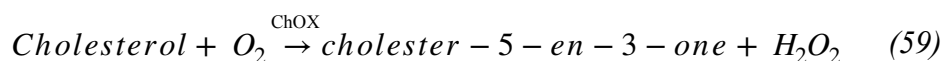
5.4.4 ChOx-luminol-cholesterol system

Cholesterol is a lipid biosynthesised by the mammalian cells for biosynthesis of vitamin D, bile acid and steroid hormones. The control of cholesterol's level is essential for the prevention of clinical disorders such as hypercholesterolemia and hypocholesterolemia which could lead to heart attack, stroke, peripheral artery disease, cancer, and cerebral haemorrhage. In 1987, the National Cholesterol Education Program [277] proposed the total blood cholesterol levels range as show in the Table 7:

Table 7: Values of the cholesterol range obtained from the National Cholesterol Education Program.

<i>mg/dL</i>	<i>mmol/L</i>	<i>Interpretation</i>
< 200	< 5.2	Desirable level
200-240	5.2 – 6.2	Borderline high risk
>240	>6.2	High risk

Three enzymes are involved in the cholesterol monitoring, cholesterol oxidase, cholesterol esterase and cholesterol dehydrogenase. In particular, cholesterol oxidase (ChOX) is a monomeric flavoprotein containing FAD that catalyses the first step in the cholesterol catabolism by oxidising cholesterol to cholester-5-en-3-one with the concomitant release of hydrogen peroxide at the optimum pH 7 [278](Fig.89).



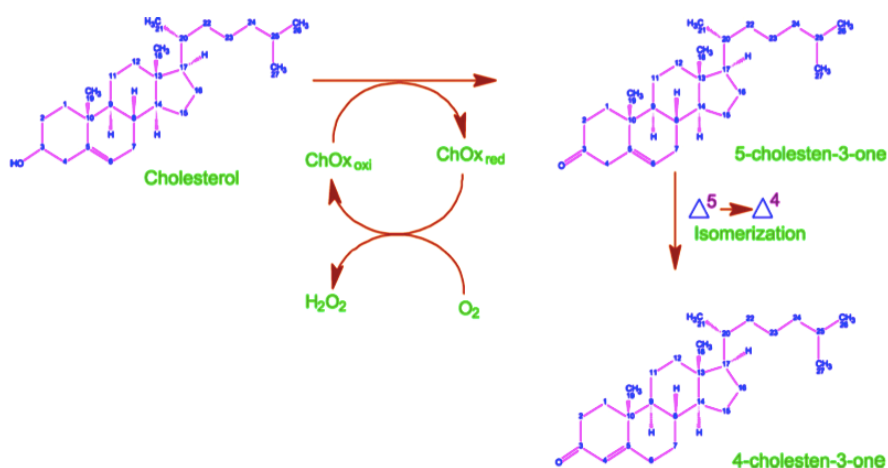


Figure 89: Representation of the pathway for the cholesterol-cholesterol oxidase system [278].

Cholesterol oxidase is an oxidoreductase enzyme playing an important role in the bile acid biosynthesis. In 2007, 14 different structures of this enzyme have been discovered and all of them have been stored in the PDB database. The enzyme used for this study has been obtained from *Streptomyces* with the molecular structure shown in Fig. 90.

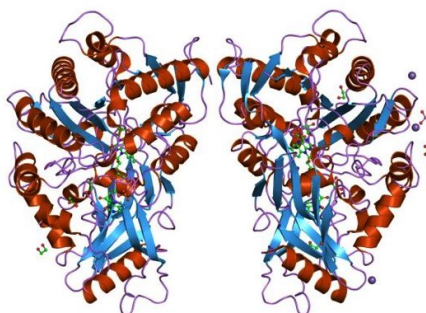


Figure 90: Structure of cholesterol oxidase (ChOx). (Jawahar Swaminathan and MSD staff at the European Bioinformatics Institute <http://www.ebi.ac.uk/>).

Several techniques have been adopted to develop a biosensor for the cholesterol monitoring. However, few references of amperometric methods have been reported in the literature [279]. The concentration of cholesterol has been measured studying the decrease in the dioxygen electroreduction current or the most frequently used oxidation current and H₂O₂ generation. Furthermore, in literature a wide range of non-enzymatic studied for the cholesterol monitoring are reported showing some advantages compare the enzymatic route. In fact, the enzymatic approach has to deal with the low stability of the enzymes involved and

the effect of factors like the temperature and the pH [280]. In 1994, Markas et al. proposed a disposable screen-printed biosensor for the monitoring of the cholesterol using the ChOx absorbed on a screen-printed carbon electrode with an H₂O₂-sensing cobalt surface [281]. The year after, an amperometric biosensor has been proposed for the direct determination of cholesterol in serum using a sensitive modified carbon paste electrode. Cyclic voltammetry and chronoamperometry were performed obtaining linear current signals with the cholesterol concentrations in solution [282]. In 1998 instead the enzyme was immobilised into sol-gel improving the sensibility by using an electrochemically generated poly(1,2-diaminobenzene) film [283]. Following in 1999, ChOx has been entrapped in poly-pyrrole film electro-deposited in a flow system for the detection of cholesterol in serum. The poly-pyrrole film has been over-oxidised in order to reduce the interference of electroactive species like ascorbic acid and uric acid which can be found in the serum [103]. Instead, an amperometric method has been used in 2001 for the determination of cholesterol using a two-steps process involving cholesterol oxidase entrapped in poly-pyrrole hydrogels membrane obtaining a detection limit of 120 μ M toward cholesterol [284]. Cholesterol oxidase and cholesterol esterase have been both employed for the fabrication of an amperometric-biosensor for the estimation of cholesterol. Both the enzymes were co-immobilised onto conductive poly-pyrrole films using an electrochemical entrapment technique [285]. One of the few works involving the use of luminol and ECL technique was proposed in 2008 with a flow injection analysis biosensor based on luminol/H₂O₂ ECL process using ChOx immobilised on UltraBind and Immunodyne membranes. With the use of 2 M NaCl in solution, Marquette et al. achieved very low detection limits of 0.6 nmol. In fact, a very high salt concentration, like 3 M NaCl, can reduce the enzyme activity. Decreasing the concentration of salts in solution, the generation of H₂O₂ in solution increased improving the performances of the biosensor [270]. In 2010, a highly sensitive amperometric biosensor for the detection of hydrogen peroxide and cholesterol was proposed using nano-sized Pt particles modified electrode with cholesterol oxidase and cholesterol esterase immobilised on the surface of graphene-nanoparticle electrode obtaining a sensitive and selective bi-enzyme platform [286]. Luminol ECL was used for the cholesterol biosensor based on gold nanoparticles self-assembled on the surface of the GCE with absorbed the cholesterol oxidase for the CV and atomic force microscopy characterisation. With this biosensor, a detection limit of 1.1 μ M was achieved

obtaining good reproducibility, stability and selectivity but it is not a good choice in term of costs [287]. More recently, in 2015 Stewart et al., proposed a near infra-red ECL biosensor using a modified quantum dot-chitosan-ChOx modified GCE tested with clinical samples [288].

For the biosensor proposed in this research, an amperometric approach for the luminol/cholesterol oxidase/H₂O₂ system is proposed. As for the previous enzymes analysed, also cholesterol oxidase has been encapsulated into alginate hydrogels and then drop-casted on the sensitive area of the GCE. For the ECL tests, a cholesterol bulk solution has been prepared to use as substrate for the redox reaction with the enzyme. 0.2 g of cholesterol have been dissolved in 5 mL Triton-X 100 and 5 mL isopropanol solution by heating at 50 °C. The solution obtained has been then slowly diluted in 0.01 M PBS at pH 7.4 obtaining a stock solution of 2 mM stored then in the fridge when not in use. The ECL tests have been performed using 0.01 M PBS and 0.1 M NaCl at pH 9.0 and electrolytic solution to increase the enzyme activity and obtaining a higher generation of the hydrogen peroxide. Different tests have been performed to determine the right pH for the ECL tests considering that the optimum pH for the ChOx activity is 7.5 retaining more than 80% activity for the pH range 6.5-9.0. Considering that luminol is highly sensitive to pH achieving the best performances for alkaline pH, different tests have been run to determine the best pH for the biosensor in question. The pH ranges from 6.0 to 9.0 have been analysed obtaining the ECL response in Fig.91.

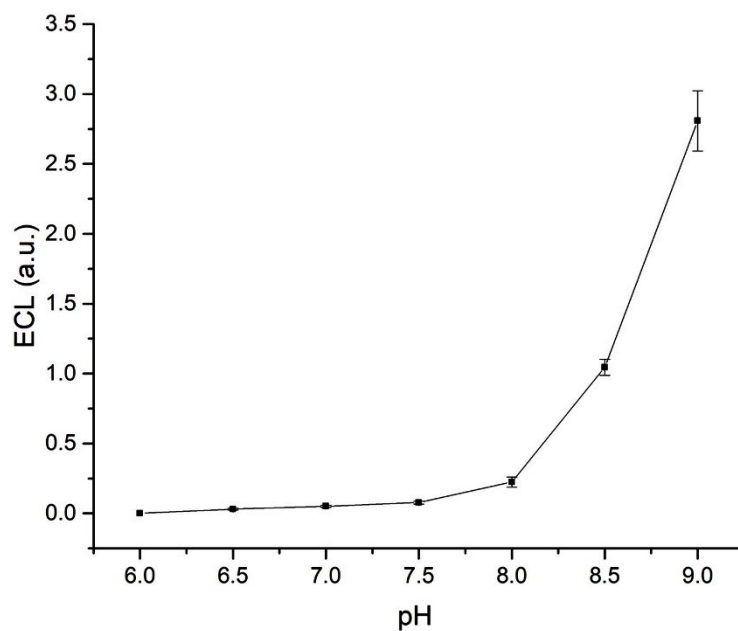


Figure 91: pH study for the cholesterol/ChOx system. Increasing the alkalinity of the pH of the electrolytic solution also the ECL intensity increases. Scan rate 0.05 V s^{-1} . Error bars represent triplicate data points.

Under these conditions, the ECL characterisation has been accomplished using different concentrations of cholesterol in 0.01 M PBS at pH 9.0 (Fig. 92).

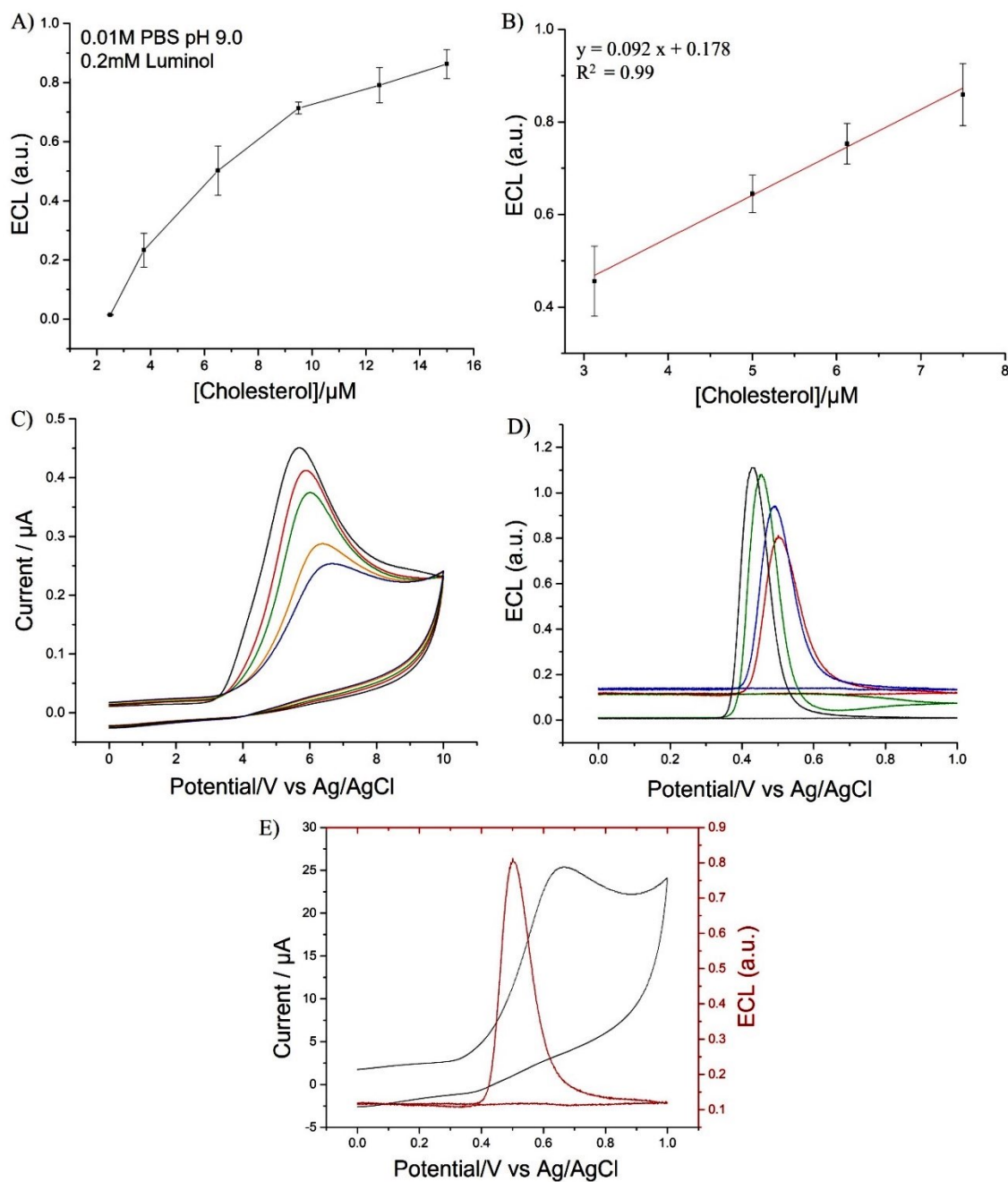


Figure 92: A) Calibration curve of ECL results. Error bars represent triplicate data points. B) Linear range and regression equation study for the luminol-ChOx-cholesterol system. C) Cyclic voltammetry and ECL for different concentrations of cholesterol in solution D). E) CV and ECL scans at 15 μM of cholesterol in 0.01 M PBS pH 9.0 with 0.2 mM of luminol. Scan rate 0.05 V s^{-1} .

From the statistical analysis, it is possible to notice that with the increase of the cholesterol concentrations in solution also the ECL signal rises showing a proportional relation with the H_2O_2 generated during the chemical reaction between the substrate (cholesterol) and the encapsulated enzyme.

5.5 Michaelis-Menten kinetics study

Michaelis-Menten kinetics represents one of the most used models for the study of enzyme kinetics in biochemistry. The equation (58) describes the enzymatic reaction rate v relating the rate of formation of product $[P]$, with the concentration of the substrate $[S]$. V_{max} is the maximum velocity of the system at the highest substrate concentrations [147].

$$v = \frac{d[P]}{dt} V_{max} \frac{[S]}{K_M + [S]} \quad (60)$$

The Michaelis-Menten constant K_M is numerically equal to the substrate concentration at which the reaction velocity is 50% of the V_{max} . The plot in Fig. 93 describes the Michaelis-Menten prediction of the reaction rate as function of the substrate concentration; with the increase of the concentration of the substrate also the velocity proportionally heightens with a factor K_M corresponding, as said, to the half of the V_{max} . Once the substrate concentration is saturated the system reaches a maximum velocity corresponding to a plateau in the plot.

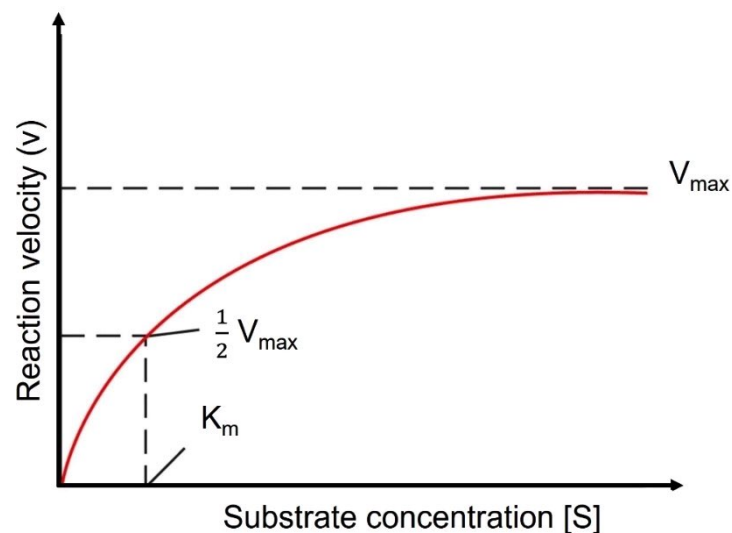


Figure 93: Michaelis-Menten prediction of the reaction rate as a function of the substrate concentration.

This model can be applied when the enzyme is free in solution and can interact with the substrates. Enzyme immobilisation is advantageous for the improvement of the enzyme

stability, activity, and selectivity towards the corresponding substrate, but on the other side it can introduce some new conditions for the determination of the enzyme's activity and kinetics. For this reason, when the system involves an immobilised enzyme, the Michaelis-Menten constant is called “apparent” due to the limitation of the substrate diffusion from the solution to the matrix containing the enzyme. Especially for the electrochemical measurement, the enzyme activity is related to the enzyme as catalyst of an oxidation/reduction reaction, so instead to define the Michaelis-Menten model as the reaction rate versus the substrate concentration [7], it is possible to relate the model with the current peak measured during the reaction versus the substrate concentration where I_{max} is the maximum obtainable current:

$$I = \frac{I_{max} S}{S + K_{Mapp}} \quad (61)$$

Alternatively, the reaction rate for these systems can be related to the Faraday's constant and the moles of electrons released during the oxidation process.

$$v = \frac{I}{n F A} \quad (62)$$

Another important element interesting to estimate in the case of immobilised enzymes is the diffusion effects of the substrate into the matrix containing the enzyme. The flux through the immobilisation matrix, in this case the alginate hydrogel or the cryogel, can be estimated by studying the peak current versus the square root of the scan rate and so following the Randles-Sevcik equation [289]. The flux can also be calculated considering the peak current:

$$Flux = \frac{I_p}{n F A} \quad (63)$$

Considering the systems proposed in this chapter, it is possible to notice that all the enzymes activity can be related with the Michaelis-Menten. For each enzyme, the K_{Mapp} has been calculated considering the maximum current that each enzyme can achieve and the substrate

concentration at which the current corresponds to the 50% of the I_{max} obtaining the values shown in the Table 8 and in Fig. 94.

Table 8 Values of the Michaelis-Menten apparent for the systems studied.

<i>Enzyme</i>	I_{max} (μA)	K_{Mapp}
<i>HRP</i>	5.89	7.71 μM
<i>GOX</i>	4.26	1.30 mM
<i>LOX</i>	1.15	8.41 μM
<i>ChOX</i>	0.98	6.31 μM

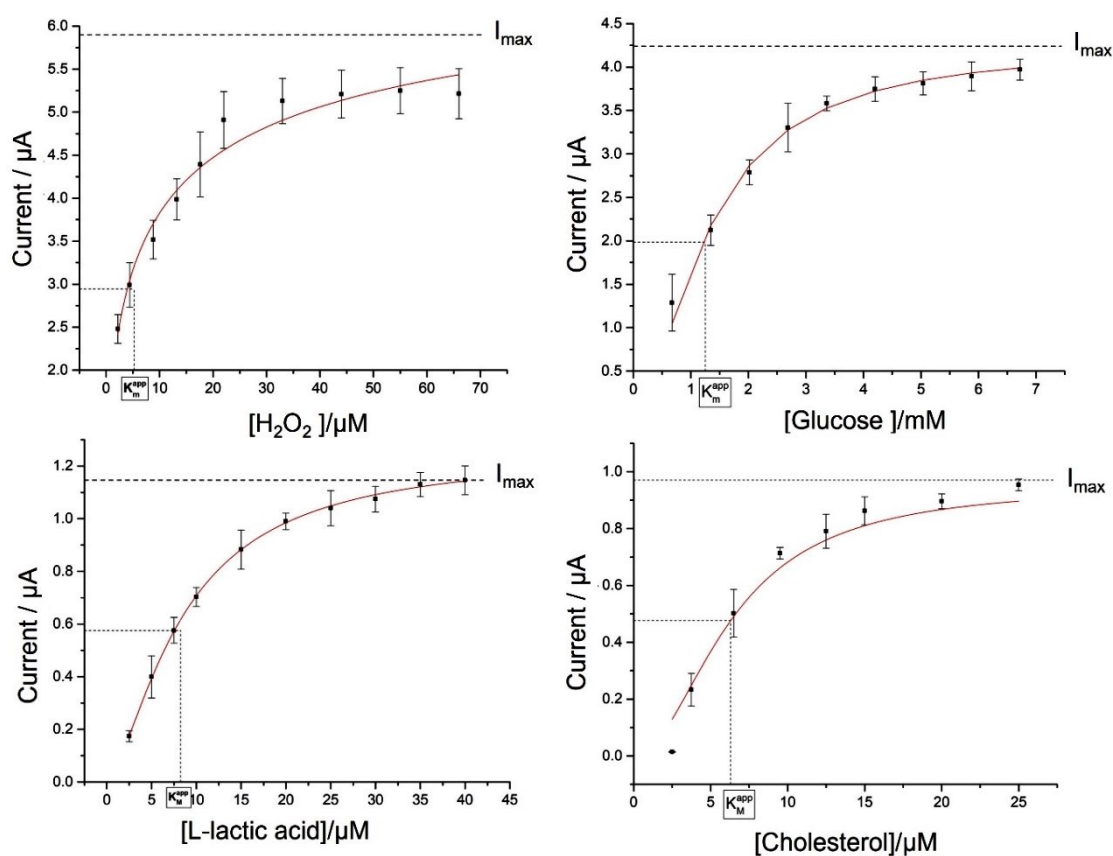


Figure 94: Michaelis-Menten behaviours of the enzymes analysed in this chapter. Error bars represent triplicate data points.

5.6 Limit of detection and limit of quantification study

The detection limit (LOD) represents the lowest quantity of substance that can be detected with a given analytical method. For the systems considered, the LOD corresponds to the lowest concentration of substrate that can be discriminated from the measurement of a blank sample also called baseline. It is calculated considering the mean, the standard deviation and the slope of the calibration curve and a confidence factor as described in the equation (62):

$$LOD = 3,3 \frac{SD}{Slope} \quad (64)$$

From the calibration plot it is necessary to extrapolate the model $y = a + b(x)$ where:

y represents the ECL signal obtained from the experiments performed.

A is the value where the equation intercepts the ordinates axis.

B is the slope of the plot also known as the sensitivity of the system.

The LOD is the x value where y is close to the average values of the baseline plus a confidence factor which is a confidence of 95%. The limit of quantification instead (LOQ) derives from the concept of LOD and can be defined as the probability density function representing the difference between two distinct values and is 10 times the standard deviation of the blank (Fig. 95):

$$LOQ = 10 \frac{SD}{slope} \quad (65)$$

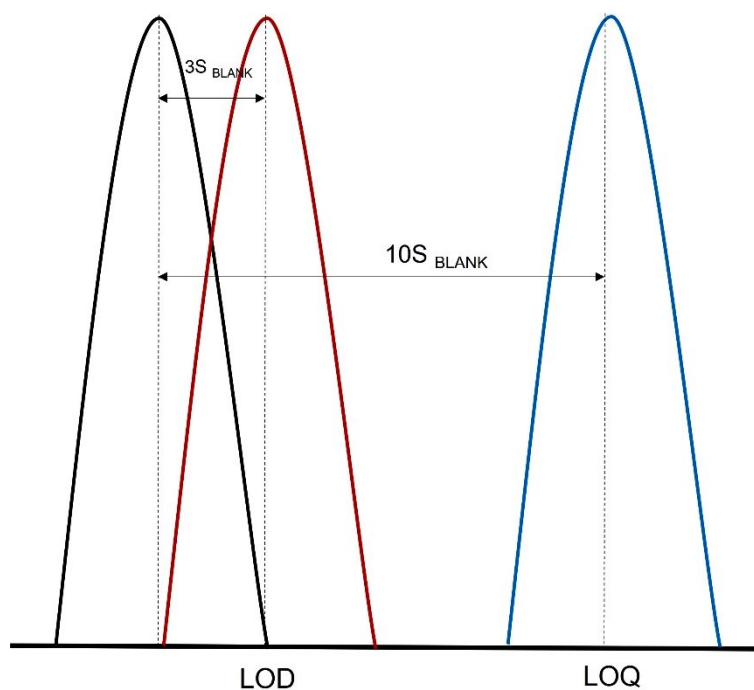


Figure 95: Scheme representing the theoretical normal distribution respect the blank of the LOD and the LOQ.

In table 9 are defined the theoretical LOD and LOQ of the systems studied with the enzymes encapsulated into alginate hydrogels:

Table 9 Theoretical values of LOD and LOQ of the four systems analysed using the oxidase enzymes encapsulated into alginate hydrogels.

<i>Enzyme</i>	<i>LOD</i>	<i>LOQ</i>
<i>HRP</i>	0.38 μ Mol	1.17 μ Mol
<i>GOX</i>	5.05 mMol	15.33 mMol
<i>LOX</i>	0.35 μ Mol	1.072 μ Mol
<i>ChOX</i>	0.42 μ Mol	1.093 μ Mol

5.7 Interference's study

These biosensors have been tested again to determine the cross-reactivity in the presence of substance that are commonly found in samples such as saliva, blood and sweat. The interferents tested are ascorbic acid and dopamine for all the biosensors, furthermore glucose have been added to the solutions for the cholesterol and lactate biosensors. 0.1 mM of AA and DA have been added to the electrolytic solutions and none of them had any effect on the ECL response of the biosensors indicating a positive specificity for all the enzymes to the corresponding substrate. In Fig. 96 the voltammograms obtained for the glucose biosensor is shown, indicating two peaks for the anodic currents due to the oxidation of luminol in the presence of the generated hydrogen peroxide (ca. 0.4 V) and the AA added to the solution (ca. 0.6 V).

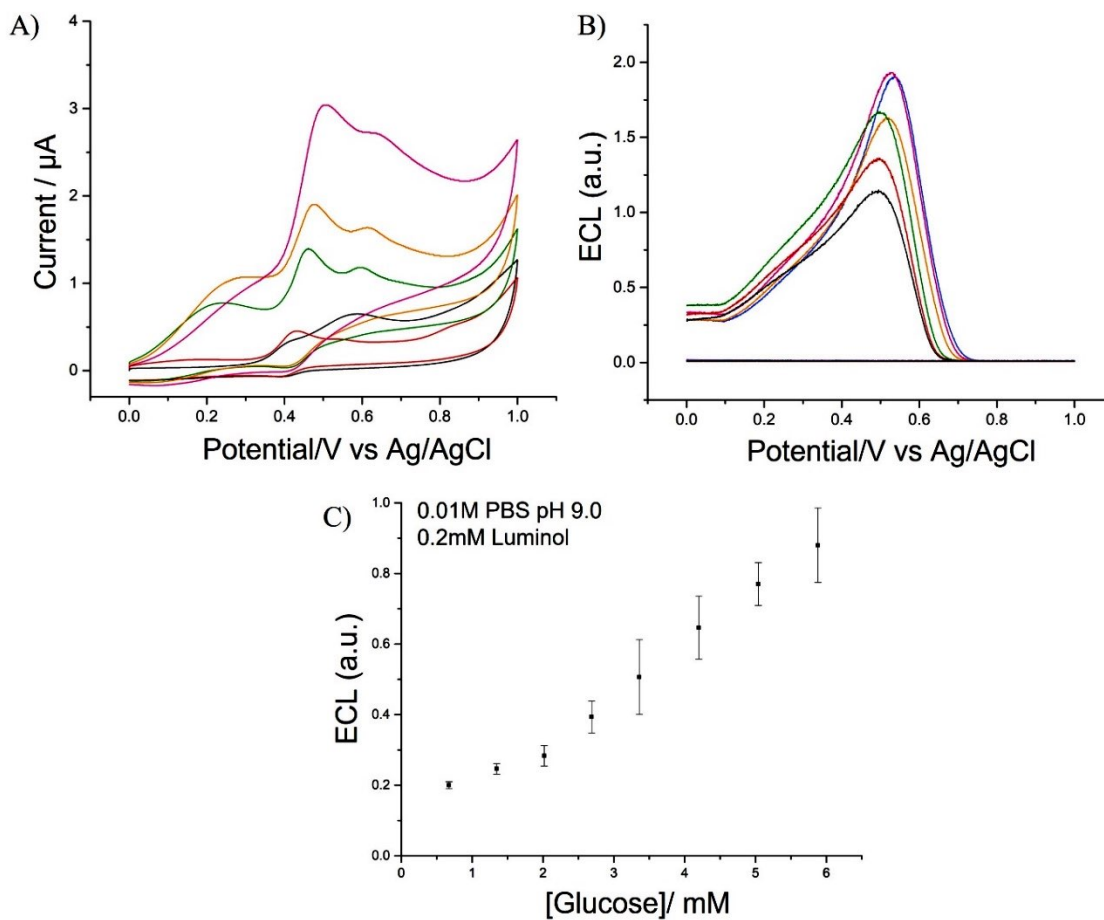


Figure 96: A) Voltammograms and B) ECL of glucose biosensors with the addition of 0.1 mM of AA to test the specificity of GOx for the substrate. C) Calibration curve showing the relation between the ECL intensity and the different concentrations of glucose in solution in presence of 0.1 mM of AA. Scan rate 0.05 V s⁻¹. Error bars represent triplicate data points.

In Fig. 97, the results of each biosensor are summarised showing the no-effect of the interferents on the ECL signal.

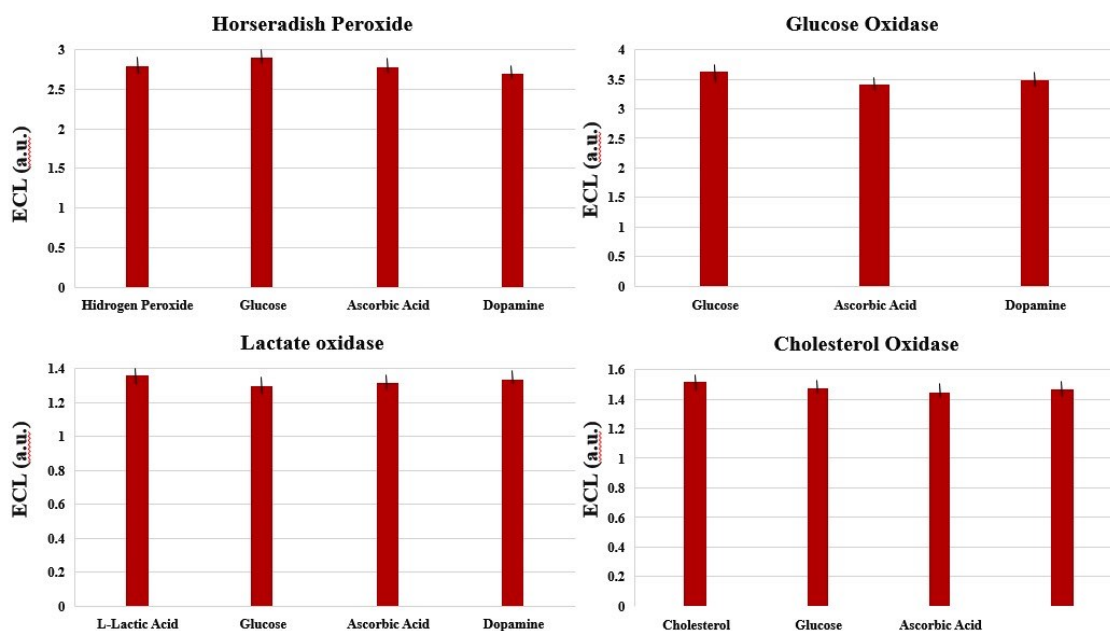


Figure 97: Histograms showing the ECL signals obtained for each biosensor in the presence of different interferents added in 0.01 M PBS electrolytic solution. Error bars represent triplicate data points.

5.8 Real sample tests

Finally, the biosensors have been tested adding at the electrolytic solution a real sample such as the contact lenses liquid for HRP/H₂O₂/luminol system and artificial sweat for GOx/glucose/luminol and LOx/L-lactic acid/luminol systems.

A commercial contact lenses liquid has been used for the ECL tests of the HRP-H₂O₂-luminol biosensor adding small aliquots. The sample has been diluted in 0.01 M PBS obtaining a stock solution of 20 mM added in different concentrations in the electrolytic solution prepared with 0.01 M PBS at pH 9.0 and 0.2 mM luminol (Fig. 98).

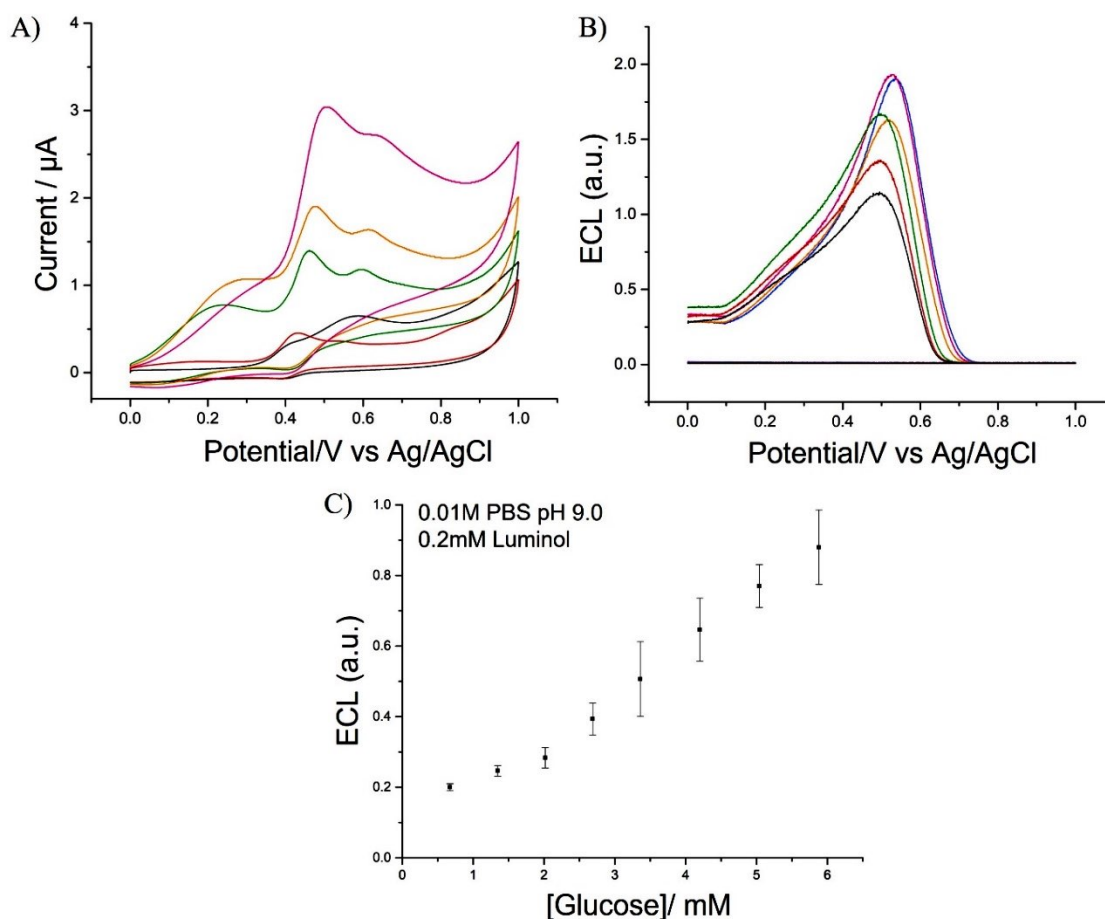


Figure 98: CV and ECL of HRP-H₂O₂-luminol system for different concentrations of contact lenses liquid added to the 0.01 M PBS electrolytic solution. Scan rate 0.05 V s⁻¹. Error bars represent triplicate data points.

The artificial sweat solution has been prepared mixing 300 mM NaCl, 40 mM of Urea, 100 mM L-lactic acid, 100 mM D-(+) glucose and 100 mL of distilled water. The ECL tests have been performed in 0.01 M PBS pH 9.0 with the addition of different aliquots of the real samples. No substrate has been added to the solution as both glucose and the lactic acid are included into the preparation of the artificial sample.

The results reported in Fig. 99 demonstrate again the selectivity of each biosensor for the corresponding substrate and that other substrates do not interfere with the ECL signal.

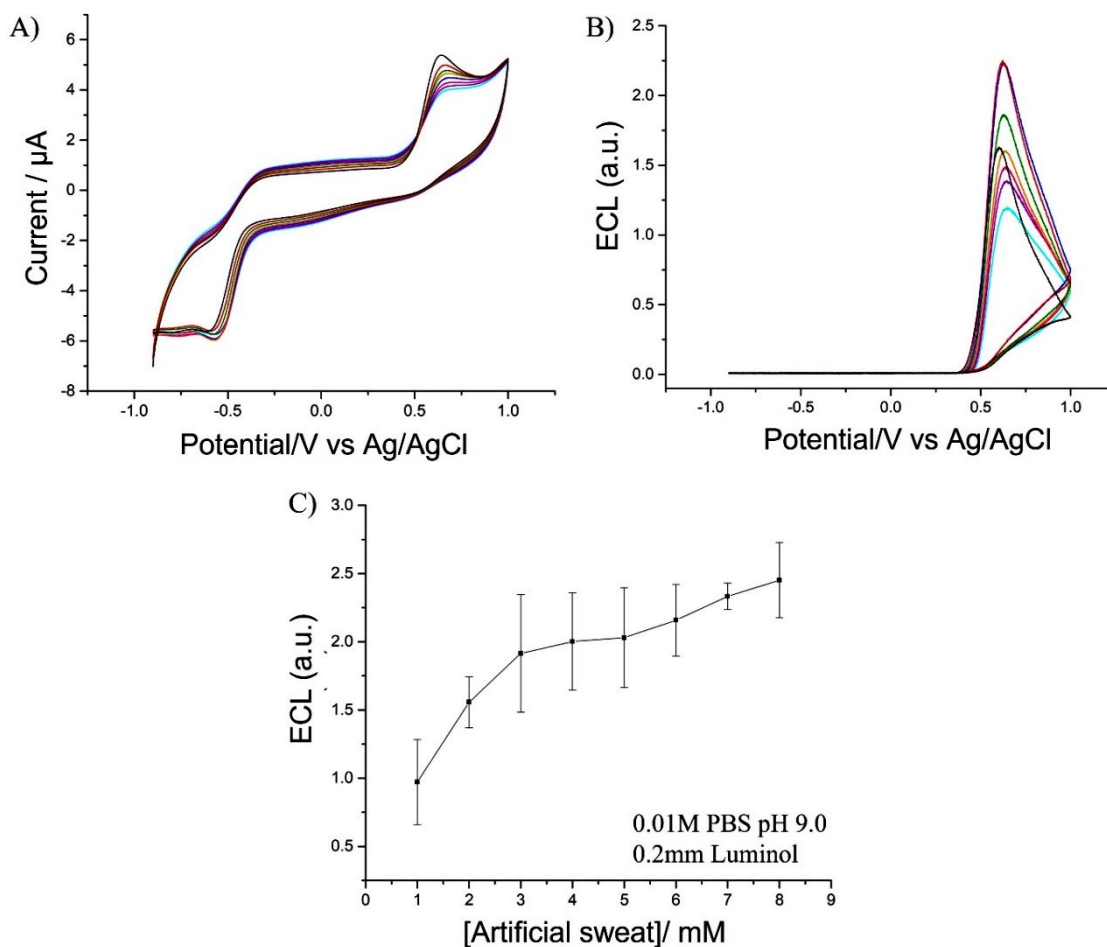


Figure 99: Electrochemical study of the GOx-glucose-luminol biosensors with artificial sweat solution. A) Voltammograms showing the oxidation peak of luminol and B) ECL results showing an increase of the intensity with the addition of different aliquots of sample. Scan rate 0.05 V s⁻¹. Error bars represent triplicate data points.

The artificial sweat has been used also for the analysis of the LOx-luminol biosensor performances. As for the GOx system, the encapsulated enzymes show a high selectivity for the corresponding biosensor allowing the generation of an ECL signal that increases with the augmentation of the aliquots in solution. The calibration curve describes the increasing behaviour of the ECL in relation to the artificial sweat concentration; for higher concentrations the signal starts decreasing revealing a saturation of the active sites of the enzyme and so a decrease in the production of hydrogen peroxide (Fig. 100).

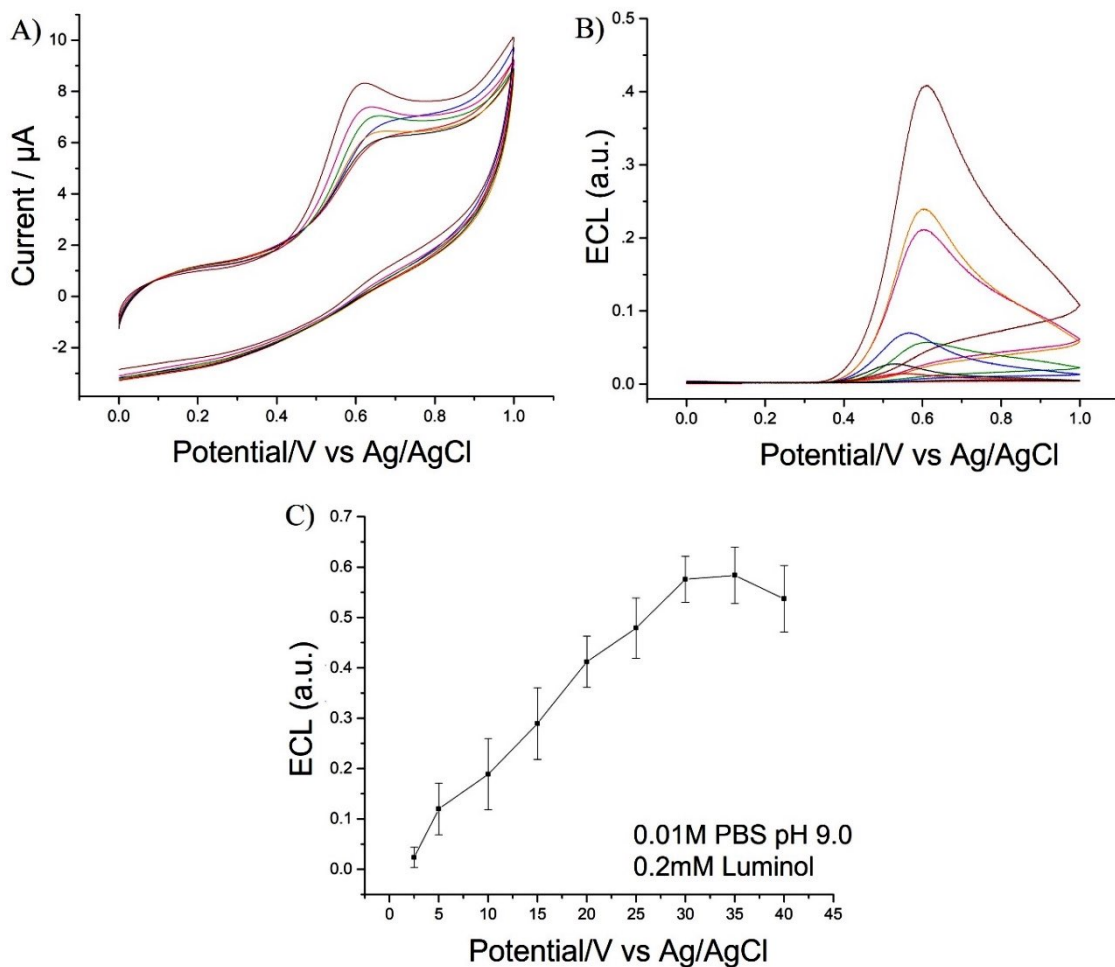


Figure 100: Electrochemical study of the LOx-luminol biosensors with artificial sweat solution. A) Voltammograms showing the oxidation peak of luminol and B) ECL results showing an increase of the intensity with the addition of different aliquots of sample. Scan rate 0.05 V s^{-1} . Error bars represent triplicate data points.

From the test with the real sample, the selectivity of the encapsulated enzymes for the substrate is proved by the obtainment of the calibration curves that relate the ECL signal with the concentration of the samples added to the PBS. For these experiments, the electrolytic solution was composed of 0.01 M PBS set at the optimum pH for the enzyme and 0.2 mM of luminol. Furthermore, to prove the reliability of the systems three repetitions of the measurements have been performed for each enzyme, encapsulating, and depositing a new hydrogel on the GCE and using a new electrolytic solution.

5.9 Conclusions

The first biosensor based on luminol-H₂O₂-oxidase has been described in this chapter for four enzymes encapsulated into alginate hydrogels. The working principle is based on the ECL detection of the co-reactant hydrogen peroxide generated during the redox reaction between the encapsulated enzyme and the corresponding substrate.

A diffusion study has been carried out to study the effective diffusion of luminol into the hydrogel matrix. Different scan rates have been applied to a modified GCE showing a linear relation between the peak current and the scan rate demonstrating that the luminol is able to diffuse in the hydrogel. With the Randles-Sevcik equation the diffusion coefficient was found to be $D = 5.63 \times 10^{-6} \text{ cm}^2 \text{ s}^{-1}$ at scan rate $v = 0.05 \text{ V s}^{-1}$ and peak current $i_p = 2.029 \text{ } \mu\text{A}$.

The electrochemiluminescence experiments performed of the four enzymes show an increase of the ECL signal due to higher generation of hydrogen peroxide after the addition of different concentrations of substrate. The calibration curves obtained from the analysis of mean and standard deviation of a triplicate data point, show a typical Michaelis-Menten behaviour, for these reasons the apparent Michaelis-Menten constant has been calculated for each of the enzyme analysed. This represents an innovative aspect in the analytical experiments as it gives a graphical understanding of the kinetics of the enzyme activity and of its saturation level.

The aim of this work was to develop an ECL-based biosensor for the detection of clinically relevant parameters using non-invasive human fluids such as saliva and sweat. For these reasons, the sensor has been investigated also in the presence of interferent species which exist in human biological samples demonstrating the selectivity of the enzyme towards the corresponding substrate and giving as output an undisturbed ECL signal.

Chapter 6: Luminol and oxidase encapsulated into cryogels

In this chapter a novel matrix for the encapsulation of the enzymes has been developed and studied in collaboration with the university of Cardiff. The previous study of the encapsulation into alginate hydrogels presents some drawbacks due to architecture of the workstation. Once the alginate hydrogel was deposited on the GCE and then immersed into the solution, it detached easily if the stirring was too strong. Also, alginate hydrogels have the tendency to dehydrate very quickly [290, 291]. Furthermore, regarding their mechanical stability, studies demonstrated that hydrogels can only tolerate 20% strain compared to the 70% of cryogels without causing any rupture [292, 293]. Finally, hydrogels needs to be constantly dehydrated in order to maintain their consistency whereas cryogels are able to stay dry retaining their properties [294]. For these reasons, this new kind of material has been used to improve the performances of the system by encapsulating the enzymes into cryogels. As for the hydrogels, the enzyme is immobilised so it is less active as it cannot freely mix with the substrate in solution, but the substrate is able to diffuse into the material through the pores of the cryogels and reacting then with the enzyme. The use of hydrogels as encapsulating material is due to the closely chemical properties of the extracellular matrix which naturally enfolds biological tissues and cells. Cryogels are characterised by an interconnected macro-porous structure ideal for cell scaffolds and drug delivery in the biomedical field [295].

6.1 Cryogels: introduction

Cryogels is a new biosynthetic material belonging to the hydrogel group and are composed of a 3D hydrophilic, hydrophobic or amphipathic structure with a highly interconnected macro-porous matrix [296]. This material can be used for several different applications compared to the conventional hydrogels thanks to microporous structure which is essential for an effective mass transport of substrate and the high biocompatibility [297]. In literature, cryogels are widely used as 3D scaffolds for different kind of cells growing like chondrocytes implanted on chitosan-agarose-gelatine cryogels [298], cardiomyocytes and skeletal cells proliferated on poly-hydroxyethyl methacrylate-gelatine cryogels [299] and

fibroblasts adherent to thermoresponsive poly(N-vinyl caprolactam) based cryogels [300]. These materials obtained with both natural and/or synthetic polymers have the relevant characteristic of microporous system reminding a sponge which allows a quicker swelling when immersed in solution improving in this way the mass transport of the solutes into the cryogel including the facilitation of the cellular filtration as described by Bencherif in 2012 [301]. This represents the main difference between this novel material and the conventional nano-porous hydrogels and making cryogels a promising material for bioengineering studies of tissue engineering [302].

Gelatine-based cryogels have been widely studied to develop bio-scaffolds for cells based on the biopolymer derived from collagen [303]. Koshy et al. in 2014 proposed a new protocol for the development of bio scaffolds-characterised by a very highly porous surface using a modified gelatine with methacrylate groups (GelMA). This protocol allows the obtainment of a highly interconnected pore structure where the pores diameter increases in depth going from the surface to the interior of the scaffold [304]. Fassina et al. instead used the gelatine-based cryogels to seed human bone marrow stromal cells as a bio scaffolding-guided approach for the building of extracellular matrices [305]. Cryogels have been prepared also with collagen representing the primary constituent of the extracellular matrix of mammalian tissues. Due to its properties of biocompatibility, non-toxicity, easily absorbable into the body and non-mutagenic making this material suitable for a wide range of tissue engineering applications [106]. Different groups used cryogelation to obtain collagen-based cryogels like the collagen-nano-hydroxyapatite produced by Rodrigues et al. in 2013 [306]. These materials were highly porous and acted like a sponge allowing a great mass transport. The collage based cryogels have been also used as scaffolds for osteoblasts and stem cell therapy [307]. Cryogels have been utilised also for neurogenic applications through the cryogelation based on laminin representing the main component of the brain ECM. Jurga et al. in 2011 observed the ability of laminin-based scaffolds to allow infiltration of neuroblasts, neuro-regeneration owing to the highly porous matrix [308]. Kathuria et al. improved the use of cryogels as wound dressing by using chitosan that as result of its ability to promote wound healing [309]. The chitosan-cryogels show a porosity greater than 90% compared the other types of cryogels above described allowing this material to have a greater resistance to breakage. Furthermore, chitosan-cryogels have been used as scaffolds for cartilage

regeneration upon their microporosity and elastic properties. Better elasticity has been achieved with the fibroin-based cryogels which allow the material to resist a complete compression without any rupture [310]. Silk fibroin is a fibrous protein with high biocompatibility, biodegradability, high strength, and toughness and under these properties can be used for cell culture, drug delivery, wound dressing, enzyme immobilisation and scaffolds for bone tissue engineering [311, 312]. For the soft-tissues instead, agarose-alginate based cryogels have been developed based on the durable mechanical strength property and flexibility. These kind of cryogels have been employed for applications like bio scaffolding for culturing insulinoma cells [313] and bio scaffolding for fibroblasts enabling adherence and proliferation of these cells [314]. Finally, poly (ethylene glycol)-based cryogels have been developed in 2010 by Hwang et al. who proposed the potential use of these materials for the cartilage tissue engineering due to the microporous network and the high interconnections between the pores. The PEG-cryogels supported the attachment, viability, proliferation and activity of chondrocytes [315]. Cryogels used for immobilised the enzymes and the following ECL study are based on Poly (ethylene glycol) diacrylate (PEGDA) that is a water soluble photopolymerisable polymer. These microporous hydrogels have been used for the first time as a tool for lysophosphatidylcholine (LPC) delivery to create an *ex vivo* model of the demyelination for the multiple sclerosis research [316]. Newland et al. in 2019 proposed a PEGDA-based cryogels used as micro-carrier for the delivery of the doxorubicin, an anticancer drug, for the treatment of glioblastoma multiform. This method provided a controlled transfer through the brain parenchyma [317]. The idea of encapsulating the enzymes into the cryogels matrices came from the ability of PEGDA-based cryogels to steadily retain molecules and drugs into the network.

6.2 Description of the system

For the synthesis of the PEGD-cryogels the standard protocol has been followed using polystyrene templates with different sizes with a photochemical cross-linking method. The templates were obtained by drilling the polystyrene sheet purchased by Evergreen Scale Models (USA) at different diameter pores (0.5 mm, 1 mm) and different thickness (0.5 mm

and 1 mm). From the preliminary ECL characterisation emerged that the best template for stable results is 0.5 mm x 1 mm dimension (Fig. 101).



Figure 101: Empty template (left) and filled (right) with cryogels for the realisation of 1 mm diameter and 0.5 mm thickness cryogels.

To create a cavity in the template where the cryogels can be synthesised, one side of the template has been covered by tape. An aqueous PEGDA solution has been prepared by mixing Poly (ethylene glycol) dyacrilate 700 (PEGDA $M_w = 700$ g/mol) in 1% HMPP that is a photo initiator. The enzyme stock solution 0.1875 mg/mL has been added to the polymer obtaining a total volume of 4 μ L. The cavities of template have been filled with 4 μ L of the polymer solution and then placed in the freezer for 20 mins at the temperature of -20 °C. Afterwards, the templates were exposed to UV light (365 nm) whilst still in freezer at -20 °C for 1 minute; then the templates have been placed at room temperature and again exposed to the same intensity of UV light for another minute to complete the cross-linking process. Once the cryogels were completely dry, they were washed with ethanol and Milli-Q water to remove the remains of polymer and photo initiator still on the template. After removing the tape, each cylindrical cryogel was pulled out from the template by pressing the cavity with a tip and then stored at room temperature ready to be drop-casted on the GCE surface for the ECL tests [316] (Fig. 102).

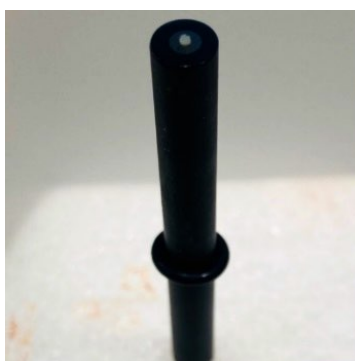


Figure 102: Cryogels deposited on the GCE sensitive area.

To improve the immobilisation of the cryogels on the electrode surface, a drop of 1 μL empty alginate gel has been deposited on the GCE to seal completely the cryogels to the electrode. By doing so, it was possible to repeat several ECL tests with the same cryogels in a three-electrodes configuration electrochemical cell (Fig. 103).

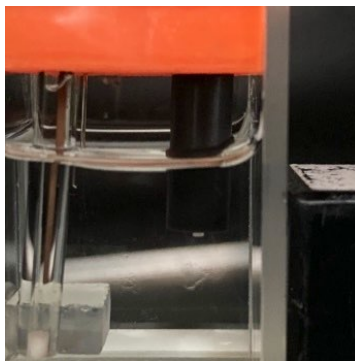


Figure 103: Three-electrodes configuration electrochemical cell with the modified-GCE immersed into the supporting electrolyte and the photomultiplier positioned to detect photons resulting for the chemical reaction.

6.3 Characterisation of the material

The morphological properties of this novel material have been studied through microscopic imaging after the coupling of the cryogels with BSA-Rhodamine and with the SEM (Fig. 104).

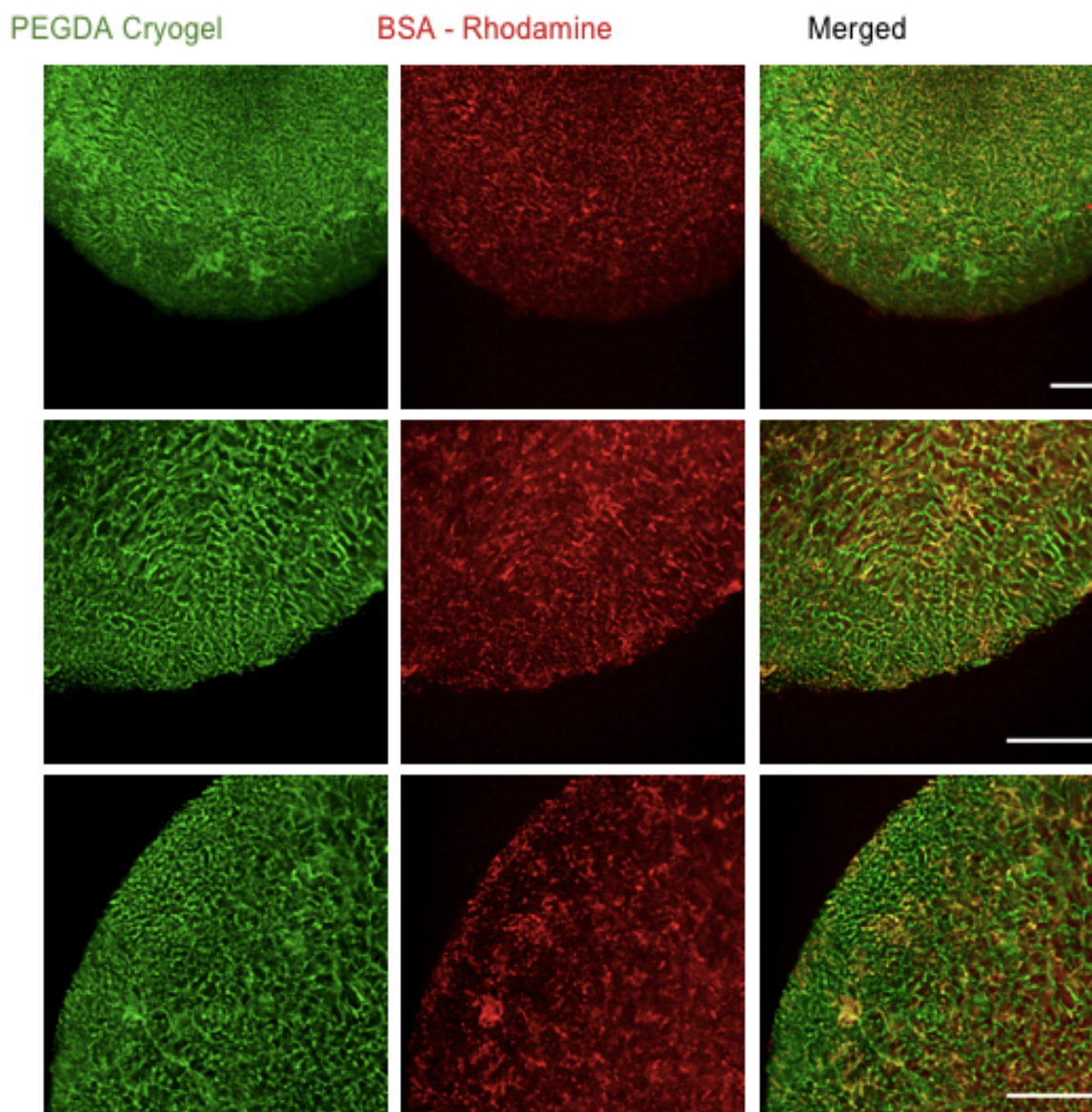


Figure 104: Microscopic imaging obtained in Cardiff University of the cryogels. Scale bar represents 300 μm .

The PEGDA cryogels images (green) show the porosity of this material (Fig. 105). The pores are interconnected with an index of 92% [301] of connectivity providing the flow of fluids into the matrix and so the diffusion of the species such as the substrate and luminol to be in direct contact with the immobilised enzyme [318]. This aspect was crucial for the ECL experiment and in general for tissue engineering applications where the diffusion needs to be guaranteed. The demonstration of a success encapsulation has been demonstrated with the use of the BSA coupled with the Rhodamine (as done previously with the alginate hydrogels). The images (red and green) show how the BSA is contained into the matrix. It is possible to

notice the porosity surface of the cryogels which is an advantageous aspect for the use of this network as drug or cell delivery system or also for the proliferation and infiltration of cells [295, 319].

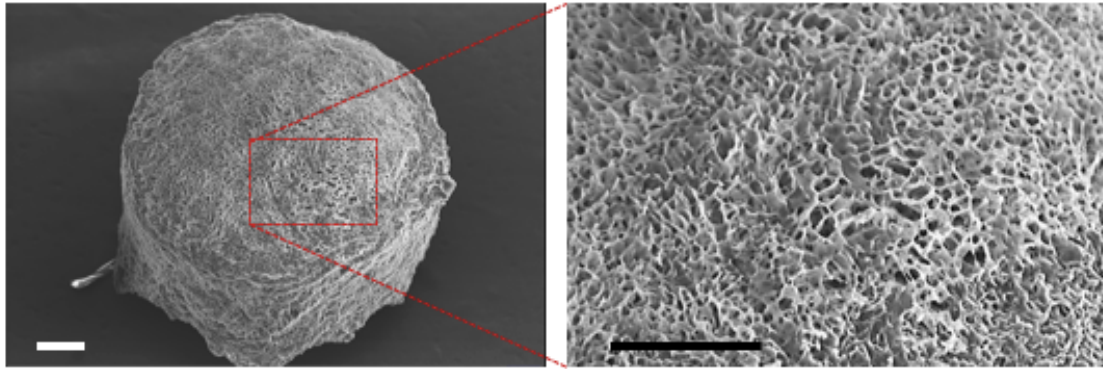


Figure 105: SEM imaging. 100x mag, WD = 32.36 mm EHT = 15 kV, I Probe = 250 pA. Scale bars = 100 μ m.

6.4 Characterisation of the biosensor: Randles-Sevcik equation

As for the alginate hydrogels, also for these materials it is crucial to learn if the luminophore and so the substrate freely diffuse into the matrix to be in direct contact with the encapsulated enzyme to start the reaction. Three empty cryogels have been used to study the diffusion of luminol using the Randles-Sevcik approach. In particular, the dependence of the current peak from different scan rates has been investigated following the equation (64):

$$i_p = 0.4463 n F A C \left(\frac{n F \nu D}{R T} \right)^{1/2} \quad (66)$$

i_p is the studied peak current (A)

n is the number of electrons transferred during the reactions

F is the Faraday constant (96,4853 C mol⁻¹)

A is the area of the electrode where the reaction occurs (cm²)

C is the concentration of the analyte (mol cm⁻³)

ν is the scan rate (V s⁻¹)

D is the diffusion coefficient (cm² s⁻¹)

R is the gas constant (8,314 J K⁻¹ mol⁻¹)

T is the temperature (K).

From Fig.106, the diffusion into alginate hydrogels and cryogels has been compared. The peak current rises with the increase of the scan rate showing an increment of luminol into the matrices of the two materials. Furthermore, the signal and the error bars are significantly higher for the hydrogels and cryogels compared to the bare electrode indicating that the luminophore not only diffuse into the matrices but also it remains partly entrapped in the networks. According to (64), the diffusion coefficient for the cryogels system is $D = 5.67 \times 10^{-6} \text{ cm}^2 \text{ s}^{-1}$ for a scan rate $\nu = 0.05 \text{ V s}^{-1}$ and a peak current $i_p = 2.040 \text{ } \mu\text{A}$.

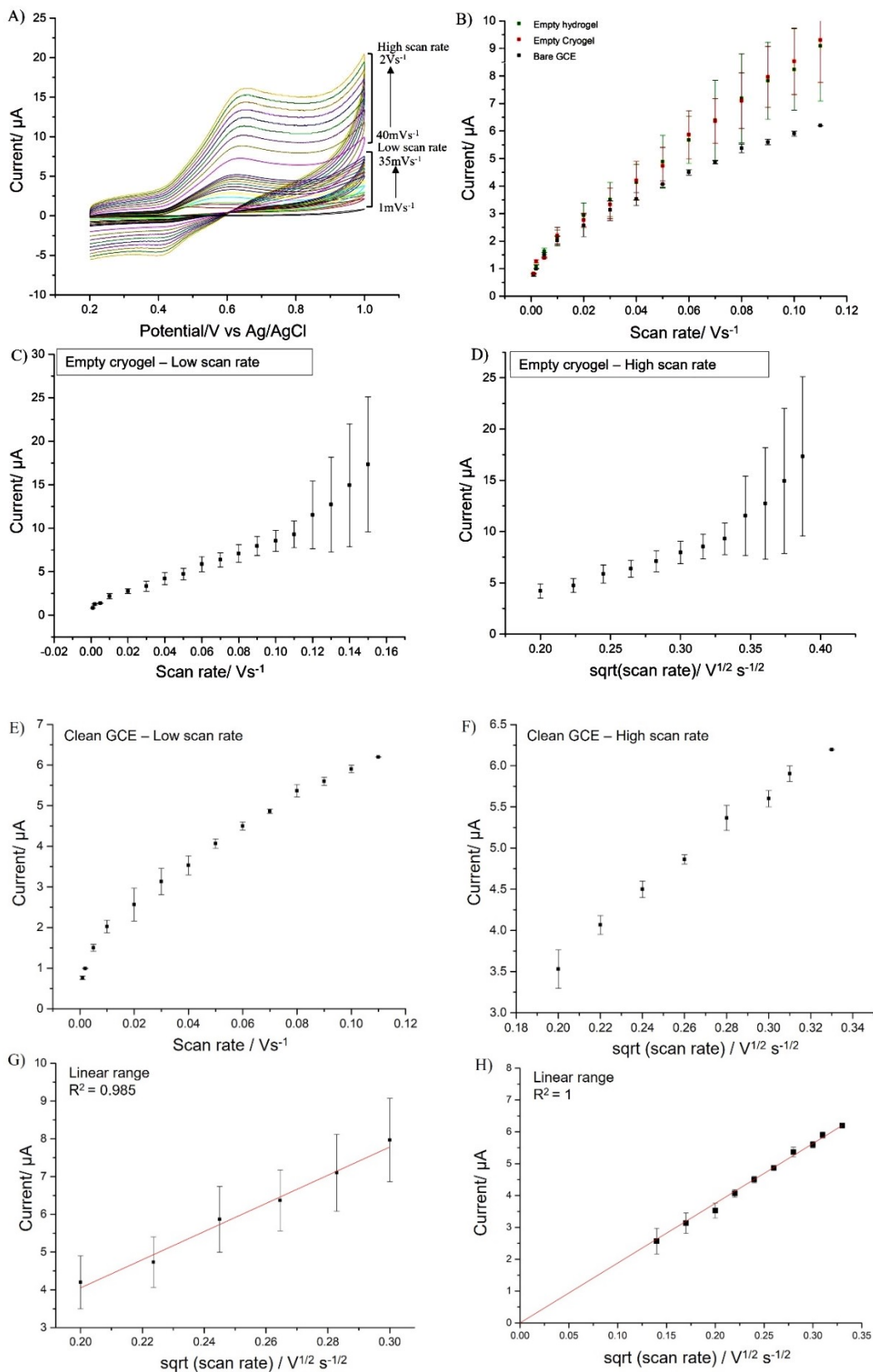


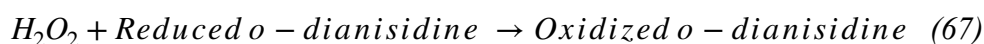
Figure 106: A) Dependence of the current peak from different scan rates. B) Comparison between alginate hydrogels, cryogels and bare GCE. Scan rate in an empty cryogels C), square root of the scan rate D) into an empty cryogels, bare GCE E) and F) Linear range the cryogel matrix G) and on the bare GCE H). Error bars represent triplicate data points.

6.5 Results and discussion

In this section, the ECL results obtained with the different enzymes encapsulated into the cryogels have been reported. All the systems work following the same principle described in chapter 5 “*Luminol and oxidase system*”. For each system different repetitions for each enzyme have been performed to build the calibration curves relating the ECL Intensity with the different concentrations of the substrate in solution. The ECL tests have been performed in 0.01 M PBS with the addition of 0.2 mM luminol; each electrolytic solution has been set at the right pH for the corresponding enzyme to be analysed.

6.5.1 HRP-luminol- H_2O_2 cryogel system

The ECL and CVs have been recorded into 0.01 M PBS at pH 9.0 with 0.2 mM of luminol in solution.



By adding different concentrations of hydrogen peroxide in PBS, the encapsulated HRP catalyses the degradation of the substrate obtaining water and oxygen. The amount of oxygen produced increases with the increment of the substrate in solution producing peroxide that consequently reacts with luminol leading to the emission of light. In Fig. 107A) it is shown the increase of the enzyme activity with the substrate concentration reaching a plateau corresponding at its saturation level.

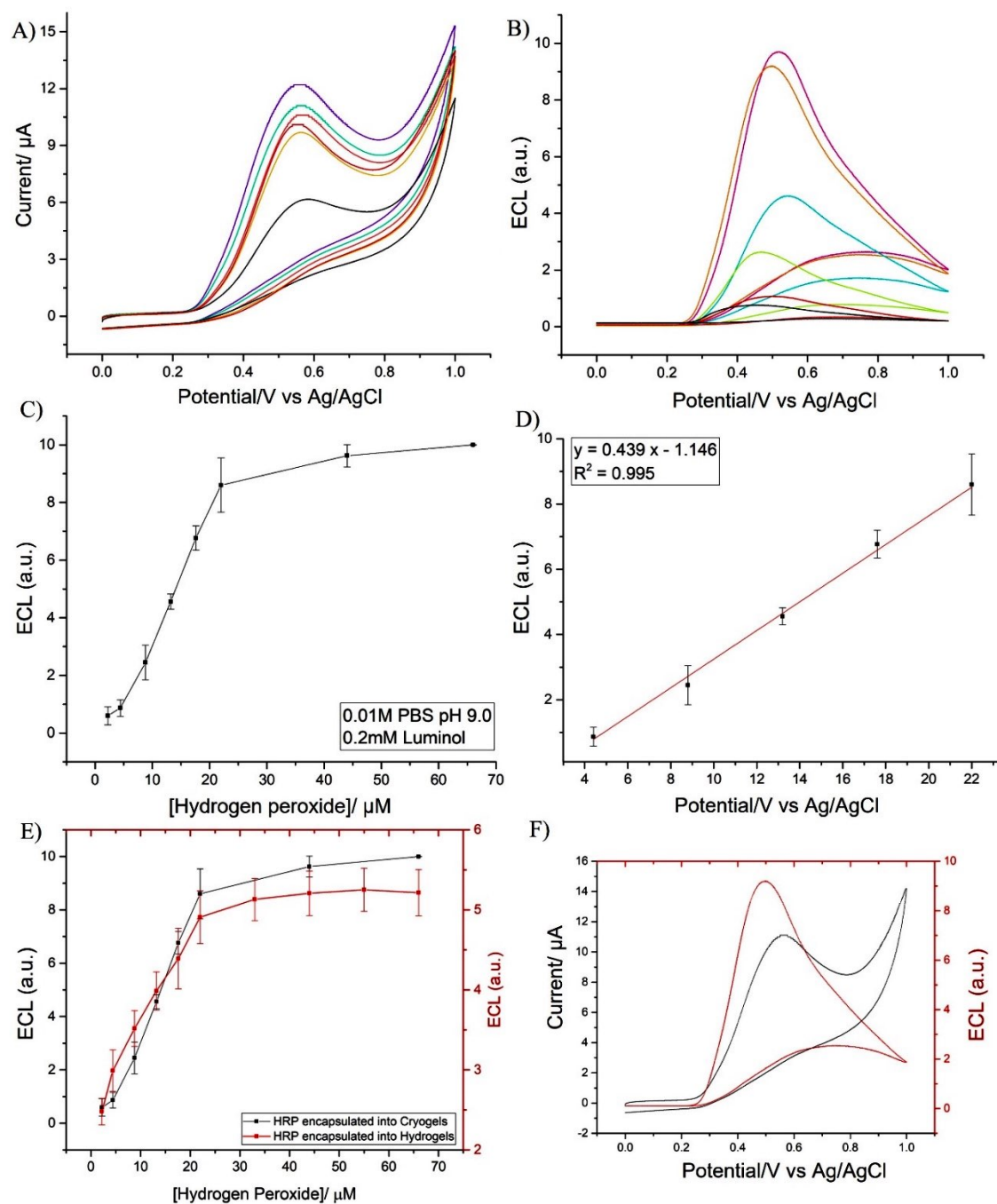


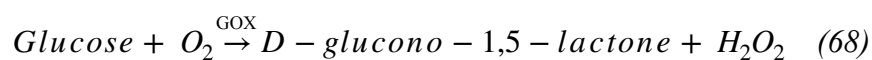
Figure 107: A) CVs and B) ECL of HRP-cryogel-luminol system in 0.01 M PBS at pH 9.0 with 0.2 mM C) Calibration curve obtained with different concentrations of H_2O_2 . Linear Range of the curve showing a R^2 value of 0.99 D). E) Comparison between the calibration curves of the HRP into cryogels and alginate hydrogels. F) ECL and CV scans for $44 \mu\text{M}$ of H_2O_2 . Scan rate 0.05 V s^{-1} . Error bars represent triplicate data points.

In Fig. 107 C) the statistical analysis is reported through the calibration curve obtained studying the mean and standard deviation of the three repetitions of ECL tests. The ECL emission raises with the growth of the substrate in solution reaching a plateau as result of the saturation of the enzyme. Fig. 107 E) represents the comparison between the calibration

curves obtained under the same experimental conditions by encapsulating the HRP into cryogels (green) [320] and into alginate hydrogels (red). The plot underlines how the cryogel encapsulation permits the obtainment of higher ECL emission due to the higher porosity of the matrix and so better diffusion of the substrate and luminol into the cores.

6.5.2 GOx -luminol-glucose cryogel system

Glucose oxidase incapsulated into cryogels produces hydrogen peroxide when reacts with the glucose. The reaction starts after the application of a suitable potential to the WE modified with the cryogel leading to the electron transfer reaction and so the formation of the oxidised form of luminol. This reacting with the produced H₂O₂ emits the consequent light detected by the PMT.



The statistical analysis reported in Fig. 108 shows that increasing the glucose concentration in solution, the ECL signal raises showing a linear behaviour in the range between 2.6 mM and 5.88 mM. In the case of the enzyme encapsulated into alginate hydrogels instead, the linear range was situated in the between 0.67 mM and 3.36 with a correlation factor R² of 0.98 compared to the R² = 0.99 of the cryogel. Also, in this case as for the HRP, the signal obtained with the GOx-cryogel system is higher than the GOx-hydrogel showing a better diffusion of the species into the matrix and so becoming in direct contact with the enzyme itself.

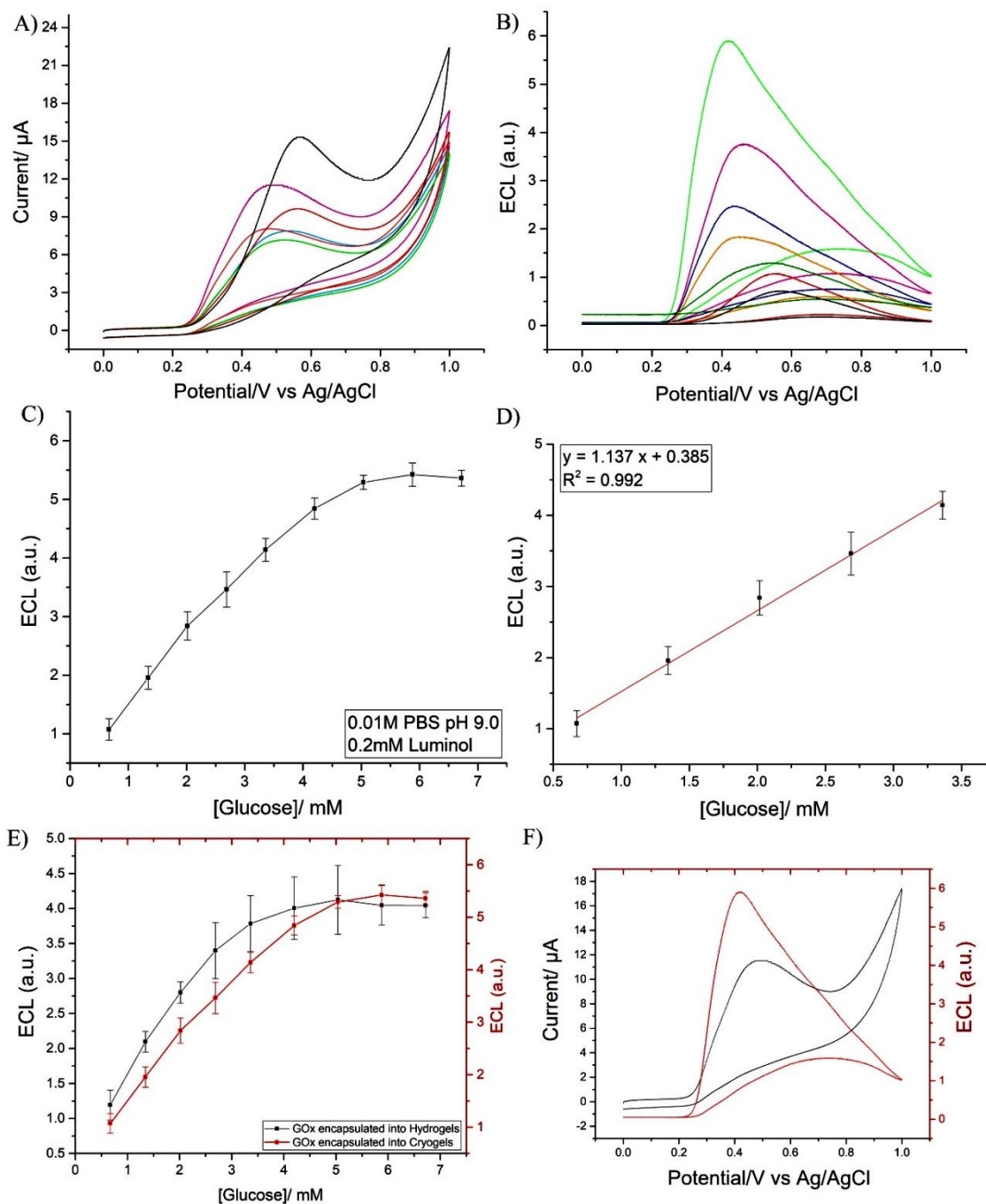
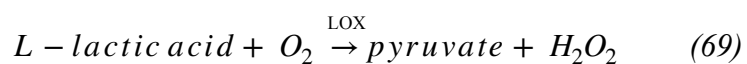


Figure 108: A) CVs and B) ECL of GOx-cryogel-luminol system in 0.01 M PBS at pH 9.0 with 0.2 mM luminol. C) Calibration at different concentrations of glucose added in the solution containing 0.2 mM luminol. D) Linear range of the curve showing a R^2 value of 0.99. E) comparison of the calibration curves of GOx in alginate hydrogel and cryogels. F) ECL and CV scans for 6,72 mM of glucose. Scan rate 0.05 V s⁻¹. Error bars represent triplicate data points.

6.5.3 LOx-luminol-lactic acid cryogel system

The results reported below are obtained after the encapsulation of the lactate oxidase into the cryogel matrices and the following UV cross-linking process. One unit of LOx can oxidise 1 μM of L-lactic acid to pyruvate and hydrogen peroxide at pH 7.4 in the presence of 0.2 mM of luminol (Fig 108).



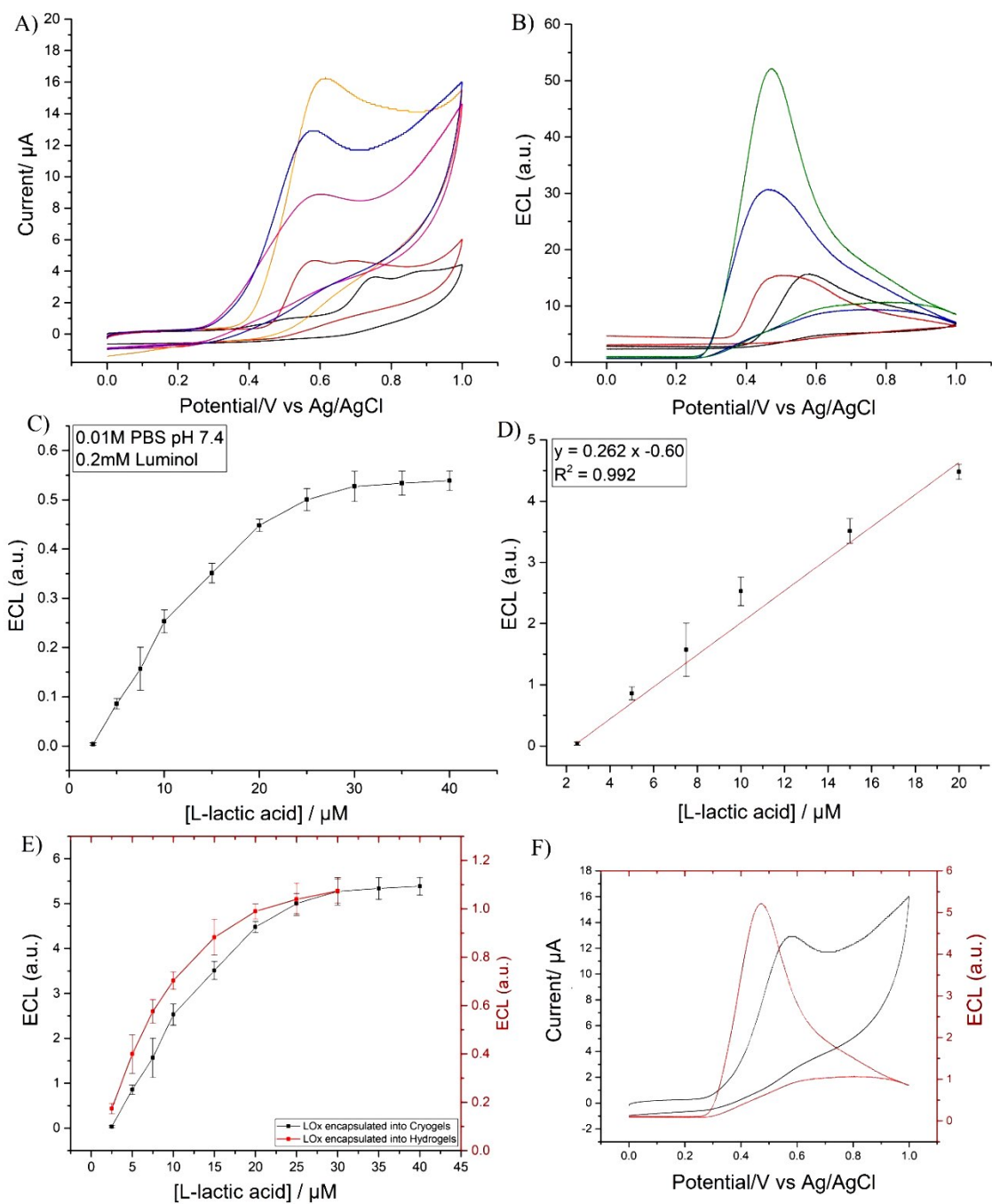
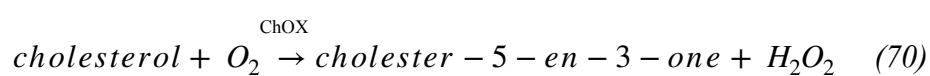


Figure 109: A) CVs and B) ECL of LOx-cryogel-luminol system in 0.01 M PBS at pH 7.4 with 0.2 mM luminol. C) Calibration curve of three repetitions of ECL tests at different concentrations of L-lactic acid added. D) Linear range and R^2 value of 0.97. E) ECL and CV scans for 30 μM of L-lactic acid. Scan rate 0.05 V s^{-1} . Error bars represent triplicate data points.

6.5.4 ChOX-luminol-cholesterol cryogel system

For the ECL tests of the cholesterol oxidase-cryogel-luminol system, a bulk solution of the substrate has been prepared. Cholesterol has been dissolved in a 2% surfactant solution of Triton-X 1000 by heating to 50°C. The solution obtained has been then slowly diluted in PBS 0.01 M at pH 7.4 obtaining a final concentration of 2 mM. The ECL tests have been performed using 0.01 M PBS and NaCl 0.1 M at pH 9.0 to increase the enzyme activity and obtaining a higher generation of the hydrogen peroxide (Fig. 110).



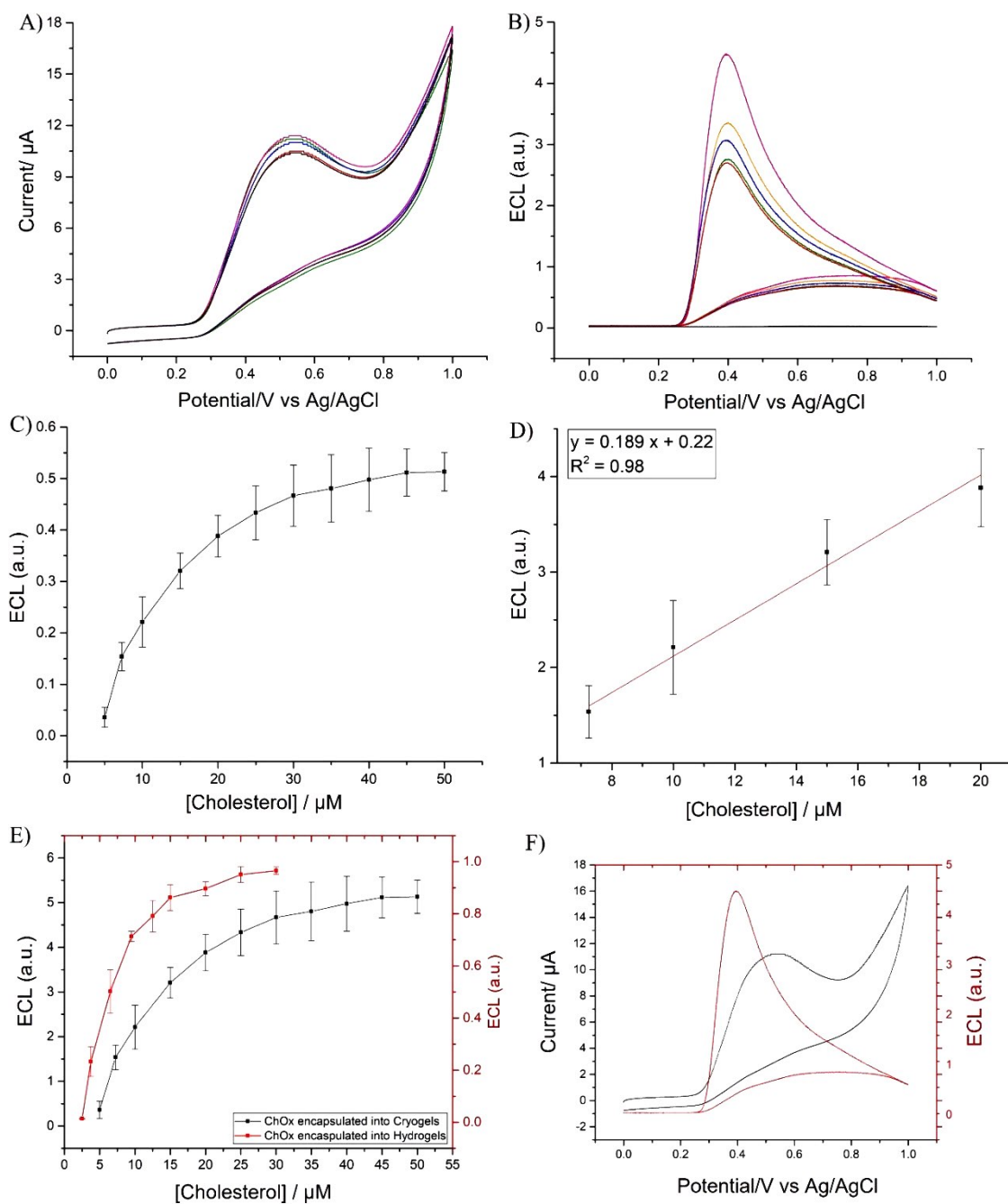


Figure 110: A) CVs and B) ECL of ChOx-cryogel-luminol system in 0.01 M PBS at pH 9.0 with 0.2 mM luminol. C) Calibration curve obtained from three repetitions at different concentrations of cholesterol. D) Linear range and R^2 value. E) ECL and CV scans for 15 μM of cholesterol. Scan rate 0.05 V s⁻¹. Error bars represent triplicate data points.

6.6 Michaelis-Menten kinetics study

As for the system involving the alginate hydrogels as encapsulation matrices, the enzymes immobilised into cryogels have a behaviour that could be related with the Michaelis-Menten curve. By using the Origin software for the calculation of the two parameters K_m^{app} and I_{max} and, the oxidase calibration curves have been fitted with the Michaelis-Menten curve (Fig. 111).

The Michaelis-Menten constant K_m represents the substrate concentration when the reaction rate is the 50% of the maximum rate and it is also an inverse measure of the substrate's affinity with the specific enzyme, so small values of the K_m indicate a high affinity of the enzyme for the corresponding substrate. The Michaelis-Menten constant is dependent on the enzyme and the substrate but also on experimental parameters such as the pH and the temperature.

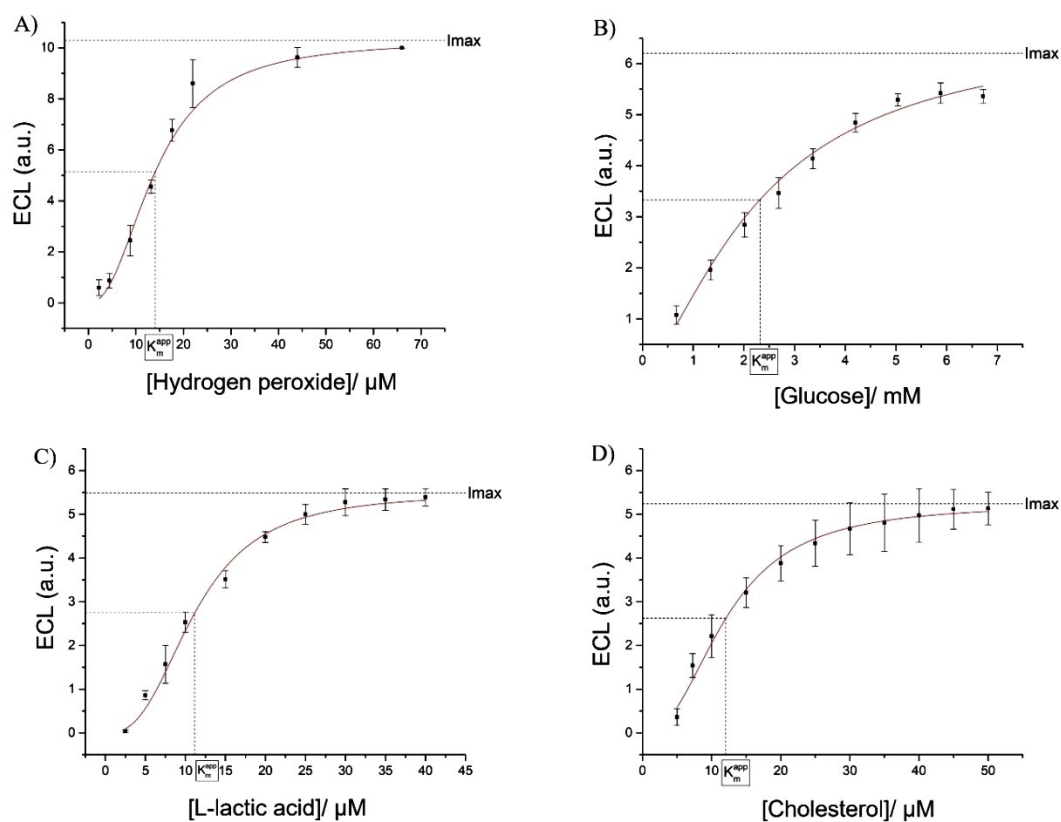


Figure 111: Michaelis-Menten study for the oxidase enzymes encapsulated into cryogels. A) HRP-H₂O₂ -luminol system, B) GOx-glucose-luminol system, C) LOx-L-lactic acid-luminol system, D) ChOx-cholesterol-luminol system. Error bars represent triplicate data points.

6.7 Limit of detection and limit of quantification study

Considering the analysis obtained from the study of mean and standard deviation of three repetitions data points, it is possible to calculate the theoretical limit of detection (LOD) and theoretical limit of quantification (LOQ) of each enzyme. The LOD is the x value where y is close to the average values of the baseline plus a confidence factor which is a confidence of 95%. The limit of quantification instead (LOQ) derives from the concept of LOD and can be defined as the probability density function representing the difference between two distinct values and is 10 times the standard deviation of the blank.

$$LOD = 3,3 \frac{SD}{Slope} \qquad LOQ = 10 \frac{SD}{slope} \qquad (71)$$

Table 10 Theoretical values for the LOQ and LOD for each enzyme encapsulated into cryogels matrices.

<i>Enzyme</i>	<i>LOQ</i>	<i>LOD</i>
<i>HRP</i>	10.8 μ M	9.88 μ M
<i>GOX</i>	2.7 mM	8.10 mM
<i>LOX</i>	11.8 μ M	35.8 μ M
<i>ChOX</i>	25.7 μ M	77.9 μ M

6.8 Study of the duration

Differently from the encapsulation in alginate hydrogels, cryogels can be reused after the ECL experiments. A study for the determination of the duration of the cryogel has been carried out to establish if the same cryogel could be used for the multiple experiments. Particularly, HRP encapsulated into cryogel has been used as a sample for the 15 days tests performing ECL measurements at day 0,1,3,5,7 and 15 adding to the solution 44 μM of H_2O_2 . From the curve shown in Fig. 112 it is shown how drastically decreases the ECL signal due to a possible leakage of the enzyme from the cryogel matrix even if the signal is still increasing with the addition of substrate in solution. As for the alginate hydrogels, the encapsulation is successful for the real time measurement of the enzymatic activity hence for the development of a disposable biosensor able to detect the level of vital parameters such as glucose, cholesterol and lactic acid in a non-invasive way and real time. However, due to the loss of almost 80% of enzymes in one, the system is not suitable for multiple experiments as the performances are drastically reduced.

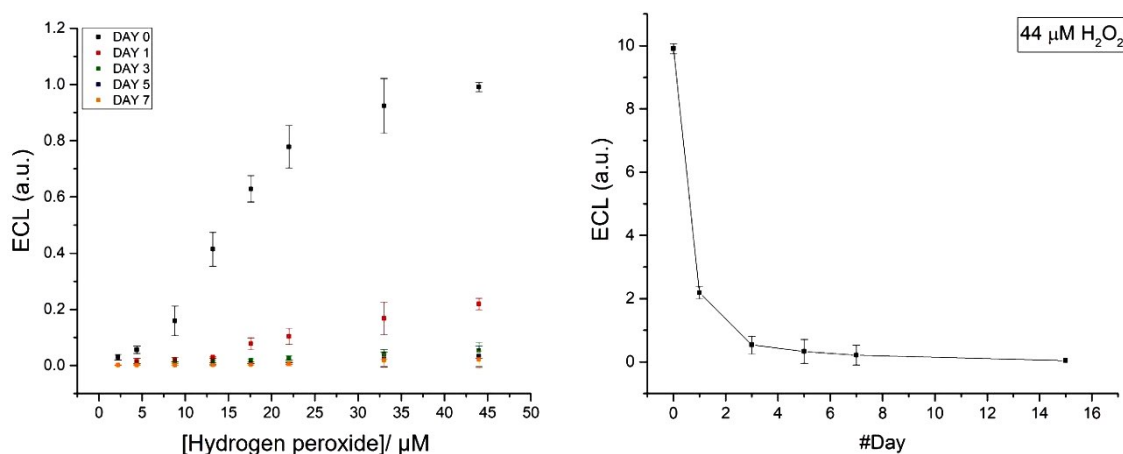


Figure 112: Calibration curves obtained with the addition of different concentrations of hydrogen peroxide for HRP encapsulated into cryogels. Three repetitions have been performed to study the statistical analysis. Error bars represent triplicate data points.

6.9 Real sample study

As for the enzymes encapsulated into alginate hydrogels, the biosensors based on the cryogel have been tested using real samples like contact lenses and artificial sweat. The results show the high specificity of the entrapped enzyme for the corresponding substrates that for these measurements is not added to the solution but is included into the aliquots of real sample analysed. In fact, the ECL signal increases linearly with the sample concentration demonstrating an increment in the production of hydrogen peroxide from the redox reaction between the enzyme and the sample.

The HRP cryogels have been tested with a commercial contact lenses liquid diluted in 0.01 M PBS obtaining a stock solution of 20 mM. different concentrations have been added in the electrolytic solution of 0.01 M PBS set at pH 9.0 and in the presence of 0.2 mM luminol (Fig. 113).

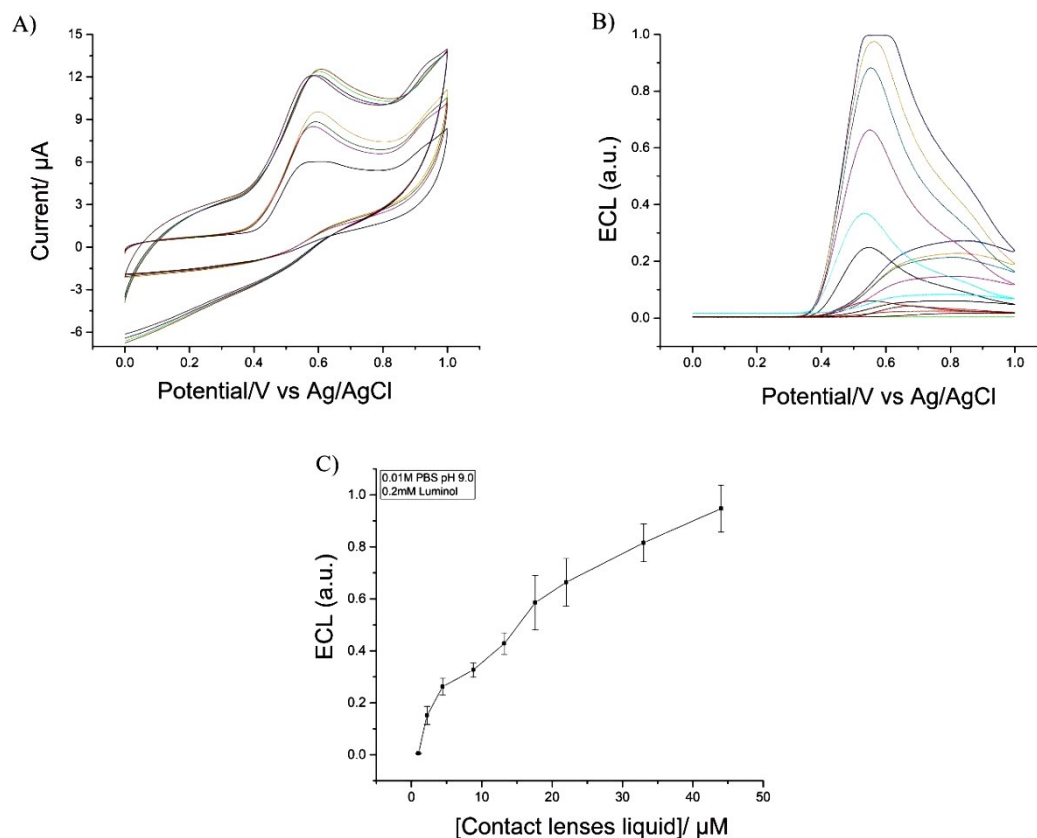


Figure 113: Real sample analysis of the HRP encapsulated into cryogels. A) CV at different concentrations of contact lenses liquid added to 0.01 M PBS pH 9.0 B) ECL signal increases with the increment of the aliquots of real sample in solution. C) calibration curve obtained from the statistical analysis of three repetitions of measurements. Scan rate 0.05 V s^{-1} . Error bars represent triplicate data points.

Following the same recipe proposed in chapter 5.8, an artificial sweat solution has been used to test the GOx and LOx enzymes into cryogels (Fig. 114).

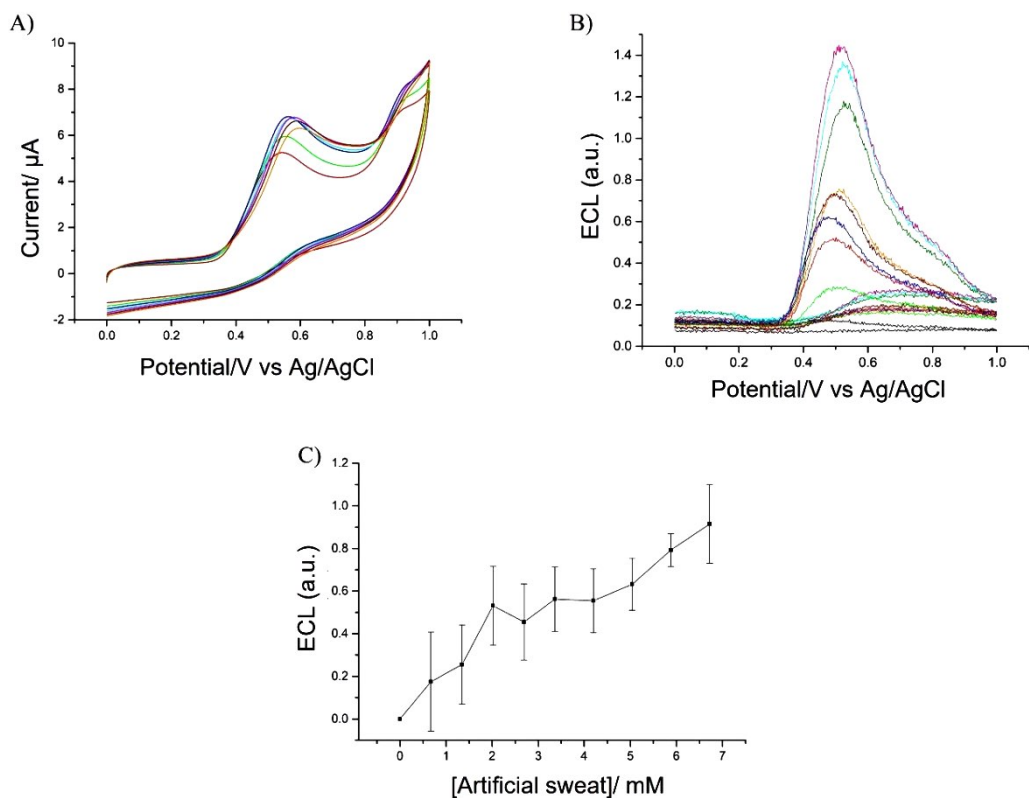


Figure 114: Real sample analysis of the GOx encapsulated into cryogels. A) CV at different aliquots of artificial sweat added to 0.01 M PBS pH 9.0 B) ECL signal C) Calibration curve obtained from the statistical analysis of three repetitions of measurements. Scan rate 0.05 V s⁻¹. Error bars represent triplicate data points.

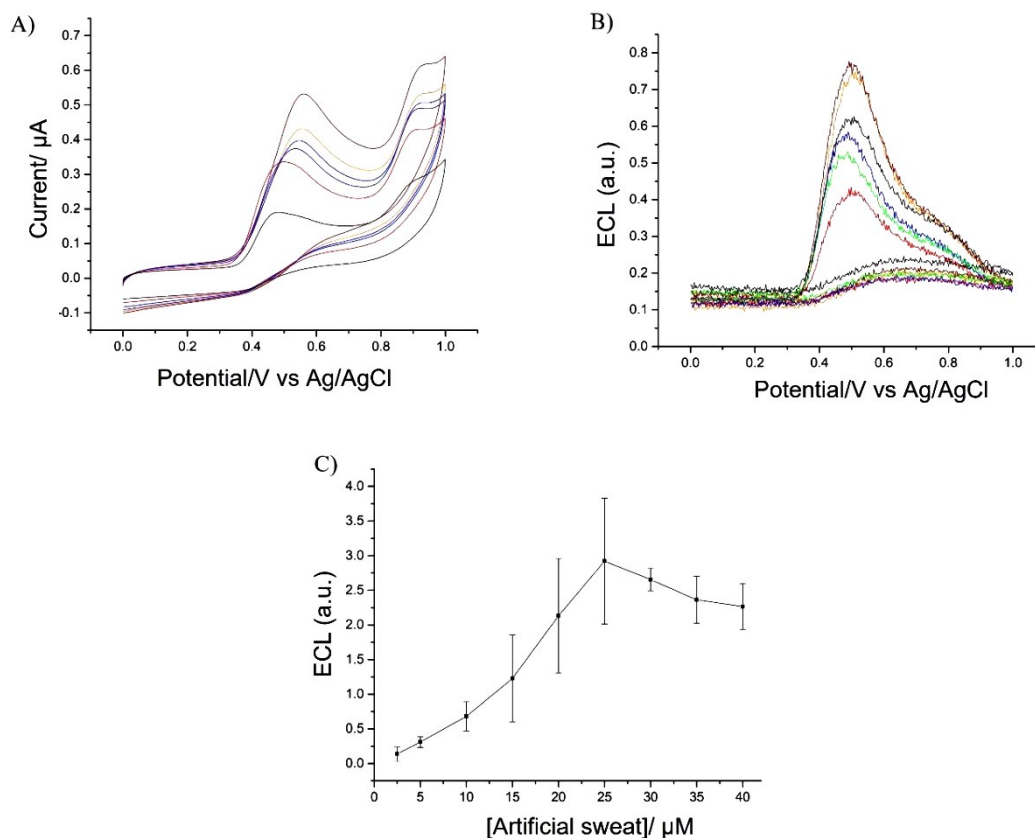


Figure 115: Real sample analysis of the LOx encapsulated into cryogels. A) CV at different aliquots of artificial sweat added to 0.01 M PBS pH 7.4 B) ECL signal C) Calibration curve obtained from the statistical analysis of three repetitions of measurements. Scan rate 0.05 V s⁻¹. Error bars represent triplicate data points.

With real sample analysis, it has been demonstrated the crucial property of the selectivity of the biosensors for the corresponding substrate. For all the tests, the substrate has not been added to the electrolytic solution as it was already contained into the aliquots of the sample analysed. These results also show how the systems are indifferent to the presence of interferences which do not affect the ECL signal. However, the ECL curves are more disturbed compare the ECL tests performed in 0.01 M PBS with the addition of prepared substrate solutions showing a higher standard deviation. Furthermore, the signal after an initial increase corresponding to the addition of samples in solution, reaches a plateau or starts to decrease as for the LOx case representing a saturation of the active binding site of the enzyme (Fig. 115).

6.10 Conclusions

In this chapter the co-reactant ECL was investigated for the HRP, Gox, Lox and ChOx enzymes encapsulated into cryogel matrices. This enzyme encapsulation and immobilisation is a novel technique developed in collaboration with Cardiff university. The ECL signal obtained after the generation of the co-reactant H_2O_2 and the reaction with the luminol display strong signal which is considerably more intense if the signal achieved with the alginate hydrogels materials. This aspect confirms the improved diffusion of the substrate and luminol into the cryogel structure as demonstrated by the Randless-Sevckic study. The diffusion coefficient was found to be $D = 5.67 \times 10^{-6} \text{ cm}^2 \text{ s}^{-1}$.

The effectiveness of the enzyme encapsulation was tested with the ECL experiments performed following the same procedure used for the enzymes encapsulated into alginate hydrogels and described in chapter 4. The addition of different concentrations of substrate allows the production of hydrogen peroxide which increases for high quantities of substrate. This also shows the capacity of the cryogels to retain the enzyme into their matrices and at the same time to allow the diffusion of species through their pores. However, as for the alginate hydrogels, the cryogels can be successfully used for the development of a disposable biosensor for real time measurements of vital parameters such as glucose, cholesterol and lactic acid in a non-invasive way. In fact, the duration study shows that the intensity of the ECL signal drastically decreases from day 0 to day 1 due to a possible leakage of the enzyme from the cryogel matrix.

Overall, this represents the first ECL biosensor with encapsulated enzymes into cryogels for the indirect non-invasive detection of glucose, cholesterol, and lactic acid. The data has demonstrated the diffusivity, sensitivity, selectivity, and versatility of the sensor which provide an option for the future development of an innovative biosensor focused on the real time self-monitoring.

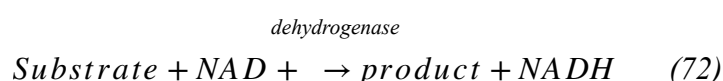
Chapter 7: [Ru(bpy)₃]²⁺ and dehydrogenase system

In this chapter, the ECL of systems involving dehydrogenase enzymes and [Ru(bpy)₃]²⁺ as luminophore is studied. The main difference between the oxidase and the dehydrogenase enzymes is related to the charges involved during the reaction. Oxidases use only the molecular oxygen O₂ as the acceptor of electrons, whereas dehydrogenases are enzymes that can oxidase the corresponding substrate by transferring a hydrogen to an H⁺ acceptor like NAD⁺/NADP⁺.

Dehydrogenase enzymes use NAD⁺ as cofactor for the redox reaction allowing the production of NADH detected via the ECL obtained by the reaction with the [Ru(bpy)₃]²⁺ [321]. Also, for these systems, the enzymes have been encapsulated following the procedure described in the chapter 5 and then drop-casted on the GCE.

7.1 [Ru(bpy)₃]²⁺-NADH system: introduction

Dehydrogenase enzymes are intracellular enzymes that catalyse oxidation-reduction reactions necessary for the respiration of organic compounds; furthermore these enzymes are not active outside the cell so they are the characteristic of the microbial activity [322]. They belong to the oxidoreductase family, and they need nicotinamide adenine dinucleotide (NAD⁺) as cofactor following the general reaction



The analytical systems use the dehydrogenase as catalysts to produce NADH related to the substrate concentration added to the reaction and then detected throughout the ECL of [Ru(bpy)₃]²⁺. Tris(2,2'-bipyridyl) ruthenium (II) has been widely studied in different branches of chemistry, like such as photochemistry, electrochemistry, photo-electrochemistry, chemiluminescence and electrochemiluminescence, for its chemical stability, redox properties and luminescence emission. The chemiluminescence of [Ru(bpy)₃]²⁺ was first studied in 1966 by Hercules and Lytle and following studies revealed a wide range of oxidants and reductants which can produce the CL of the luminophore [323] (Fig. 116).

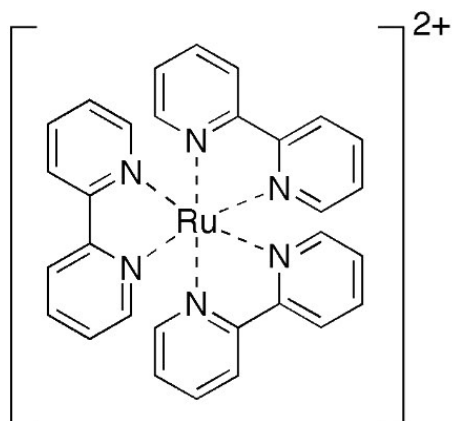


Figure 116: Structure of the Tris(2-2'-bipyridyl) ruthenium (II) [174].

In literature, it is possible to find several studies related to different co-reactants such as oxalate [172], tripropyl-amine [36] and amino acids [324] that working with $[\text{Ru}(\text{bpy})_3]^{2+}$ are able to produce intermediate ion radicals. The mechanism of TPrA- $[\text{Ru}(\text{bpy})_3]^{2+}$ can be used to explain the process of NADH- $[\text{Ru}(\text{bpy})_3]^{2+}$ as both the of them contain a tertiary amine as shown in Fig.117:

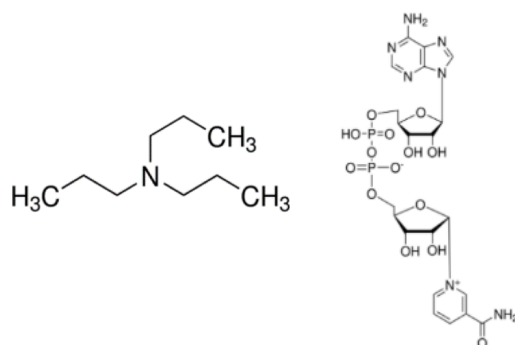
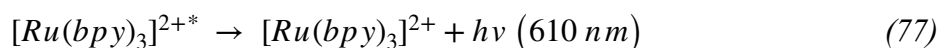
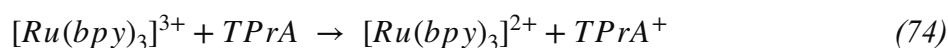
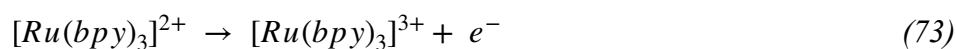


Figure 117: Structures of Tripropylamine (left) and Nicotinamide adenine nucleotide (right) showing the tertiary amine in both the structures. (edited by Robert E. Lenga. The Sigma-Aldrich Library of Chemical Safety Data. [Milwaukee, Wis., USA]: Sigma-Aldrich Corp., 1988).

Considering TPrA-[Ru(bpy)₃]²⁺ the reactions responsible of the emission of light are shown in the following cascade of equations [179]:



The chemiluminescence of NADH and [Ru(bpy)₃]²⁺ was first reported in 1989 by Ruppert and Steckhan [179]. They proposed the regeneration of NAD⁺ and NADH using bipyridyl metal complexes associated with enzymatic reactions [325-327]. In 1992, the ECL of [Ru(bpy)₃]²⁺ was studied for the detection of the NADH obtaining an ECL signal proportional to the NADH concentrations with immobilisation of the luminophore in Nafion film on the electrode surface [326]. In 1997, Martin and Nieman proposed an ECL biosensor based on Tris(2,2-bipyridyl)ruthenium(II) and dehydrogenase enzymes immobilised in cation exchange polymer films like Nafion for flow injection analysis [321]. Other studies used the same principle with different immobilisation techniques. [Ru(bpy)₃]²⁺ and the enzymes were immobilised also in sol-gel material for the development of an ECL-based biosensor for the detection of NADH [328] (Fig. 118).

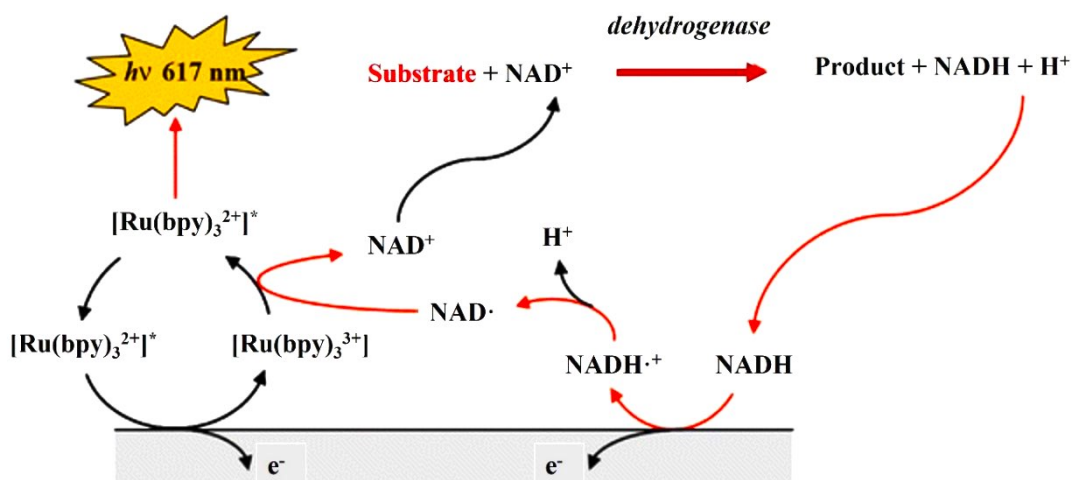


Figure 118: Electrochemiluminescence mechanism of $[\text{Ru}(\text{bpy})_3]^{2+}$ with NAD^+ and dehydrogenase enzymes [329].

7.2 Description of the system

To understand the dehydrogenase/ $[\text{Ru}(\text{bpy})_3]^{2+}$ /NADH working principle, it is necessary to start from the $\text{NAD}^+ / \text{NADH}$ couple (Fig. 119). As anticipated, NADH is a pyridine nucleotide oxidative cofactor essential for the eukaryotic cells playing the essential role of energy production through redox reactions. On the other side, NAD is the cofactor of dehydrogenases, reductases and hydroxylases and it is the H^+ and e^- carrier in the main metabolic pathways like glycolysis, fatty acids synthesis and steroid synthesis [330]. Because of the positive charge on the nitrogen atom in the nicotinamide ring, the oxidised form of the redox agent is also known as NAD^+ .

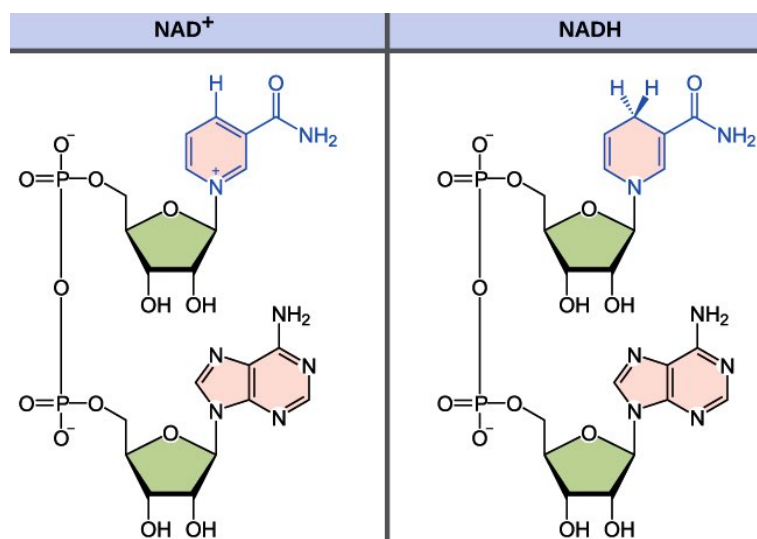
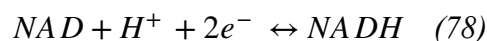
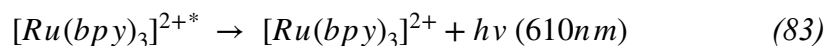
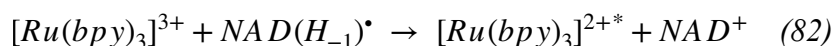
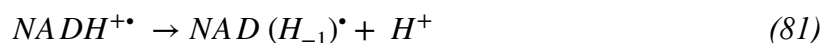
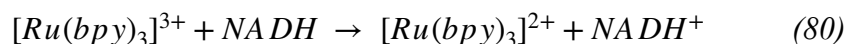
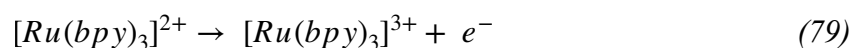


Figure 119: Chemical structure of NAD⁺ and NADH. (N. R. Gough, Anti-Aging Supplements: The Basis for *Basis. BioSerendipity* (11 June 2018) <https://www.bioserendipity.com/anti-aging-supplements-the-basis-for-basis/>).

The reaction leading to the formation of NADH is the following:



NADH presents in its structure a tertiary amine like the typical co-reactant of the [Ru(bpy)₃]²⁺, TPrA. [Ru(bpy)₃]²⁺ and NADH are both oxidised on the WE surface after the application of the suitable potential [331]. The one-electrode-oxidised cation radical NAD⁺ losing a proton become a strong reducing radical which subsequently, reacting with [Ru(bpy)₃]³⁺, produces the excited state in situ on the WE. [Ru(bpy)₃]^{2+*} emits photons decaying to the ground state [Ru(bpy)₃]²⁺ ready for the next reaction [331].



From Fig.119 it is possible to notice that NAD⁺ is formed by an aromatic amine, the pyridine ring, which do not generate ECL when react with [Ru(bpy)₃]²⁺, instead in the NADH

structure the aromaticity of the pyridine group has been destroyed during the reaction forming an aliphatic tertiary amine which reacting with the $[\text{Ru}(\text{bpy})_3]^{2+}$ emits light. Hence, when the NAD^+ is added to the solution, the ECL signal is not generated until the substrate of the dehydrogenase enzyme is added to the same electrolytic solution.

In Fig.120 the calibration curves of $[\text{Ru}(\text{bpy})_3]^{2+}$ at different concentrations of NADH and TPrA have been reported. For both the reactants, the ECL intensity increases with the concentration of the two co-reactants enhancing the signal-to-noise ratio as well. Furthermore, after the reaching of the highest intensity current value, the curve starts decreasing showing a saturation of the luminophore.

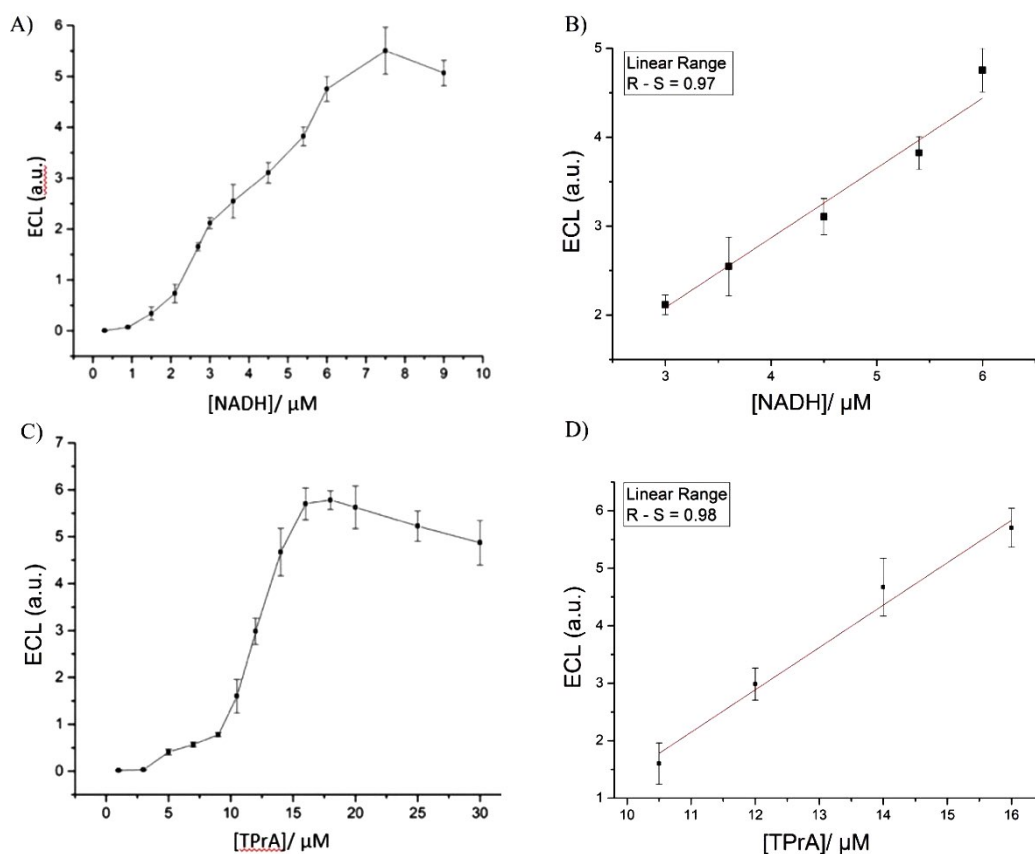


Figure 120: Calibration curve of $[\text{Ru}(\text{bpy})_3]^{2+}$ at different concentration of NADH 3 mMOL in solution (A) and study of the linear range and R^2 value (B). Calibration curve for $[\text{Ru}(\text{bpy})_3]^{2+}$ at different concentrations of TPrA 0.1 Mol in solution (C) and study of the linear range and R value (D). Scan rate 0.05 V s^{-1} . Error bars represent triplicate data points.

For these systems, the enzyme encapsulated and entrapped on the working electrode surface, allows the oxidation of the corresponding substrate while the NAD^+ undergoes a reduction process forming NADH completing in this way the redox reaction (Fig. 121).

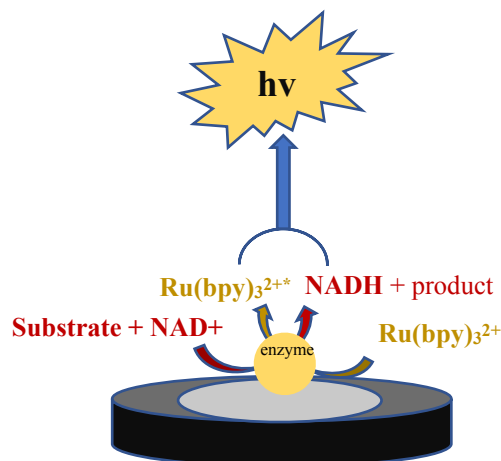


Figure 121: Schematic representation of the dehydrogenase/ $[\text{Ru}(\text{bpy})_3]^{2+}/\text{NADH}$ system.

As for the oxidase system, it is important to set the electrolytic solution at the right pH to create the right conditions for the reaction to occur. Following, the behaviour of $[\text{Ru}(\text{bpy})_3]^{2+}$ has been studied at different pH of 0.01 M PBS with 1.5 μMol of NADH in solution. To obtain the curve in Fig. 122, three repetitions for each pH have been done to perform a statistical analysis. It is possible to notice that $[\text{Ru}(\text{bpy})_3]^{2+}$ shows an ECL response from pH 6.5 enhancing the intensity with the increase of the alkalinity of the solution. This behaviour makes the luminophore suitable for the ECL study of dehydrogenase activities.

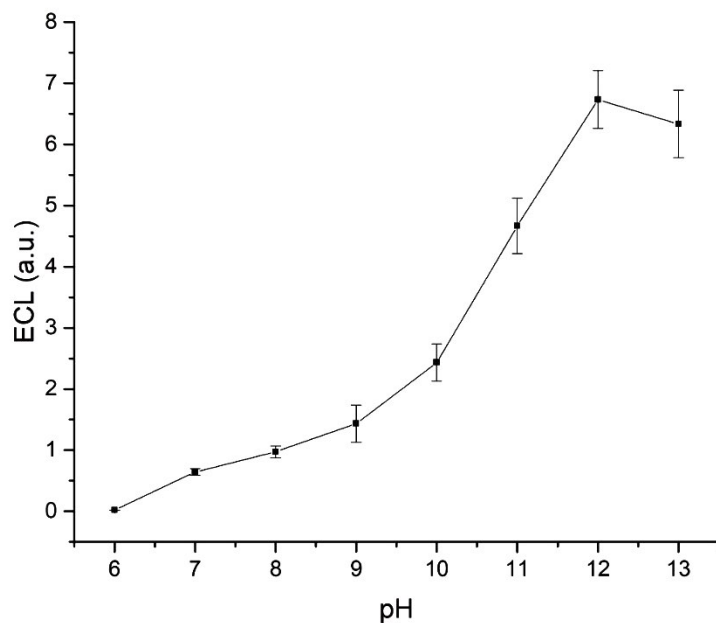


Figure 122: Study of the behaviour of $[\text{Ru}(\text{bpy})_3]^{2+}$ at different pH levels with $1.5 \mu\text{M}$ of NADH in solution. Scan rate 0.05 V s^{-1} . Error bars represent triplicate data points.

7.3 Characterisation of the biosensor: Randles-Sevcik equation

As for the previous system, also the diffusion of $[\text{Ru}(\text{bpy})_3]^{2+}$ into the alginate hydrogel has been investigated with the Randles-Sevcik equation. Different scan rates have been tested starting from 0.001 Vs^{-1} (Fig. 123). The current peak increases linearly with the square root of the scan rate demonstrating that $[\text{Ru}(\text{bpy})_3]^{2+}$ diffuses into the hydrogel with a $D = 0.125 \times 10^{-6} \text{ cm}^2 \text{ s}^{-1}$ obtained using the peak current $i_p = 4.098 \mu\text{A}$ at the scan rate $v = 0.05 \text{ Vs}^{-1}$. Based on the D value, it is possible to predict the regeneration time of $\text{Ru}^{3+}/\text{Ru}^{2+}$ that is $\sim 12 \text{ s}$.

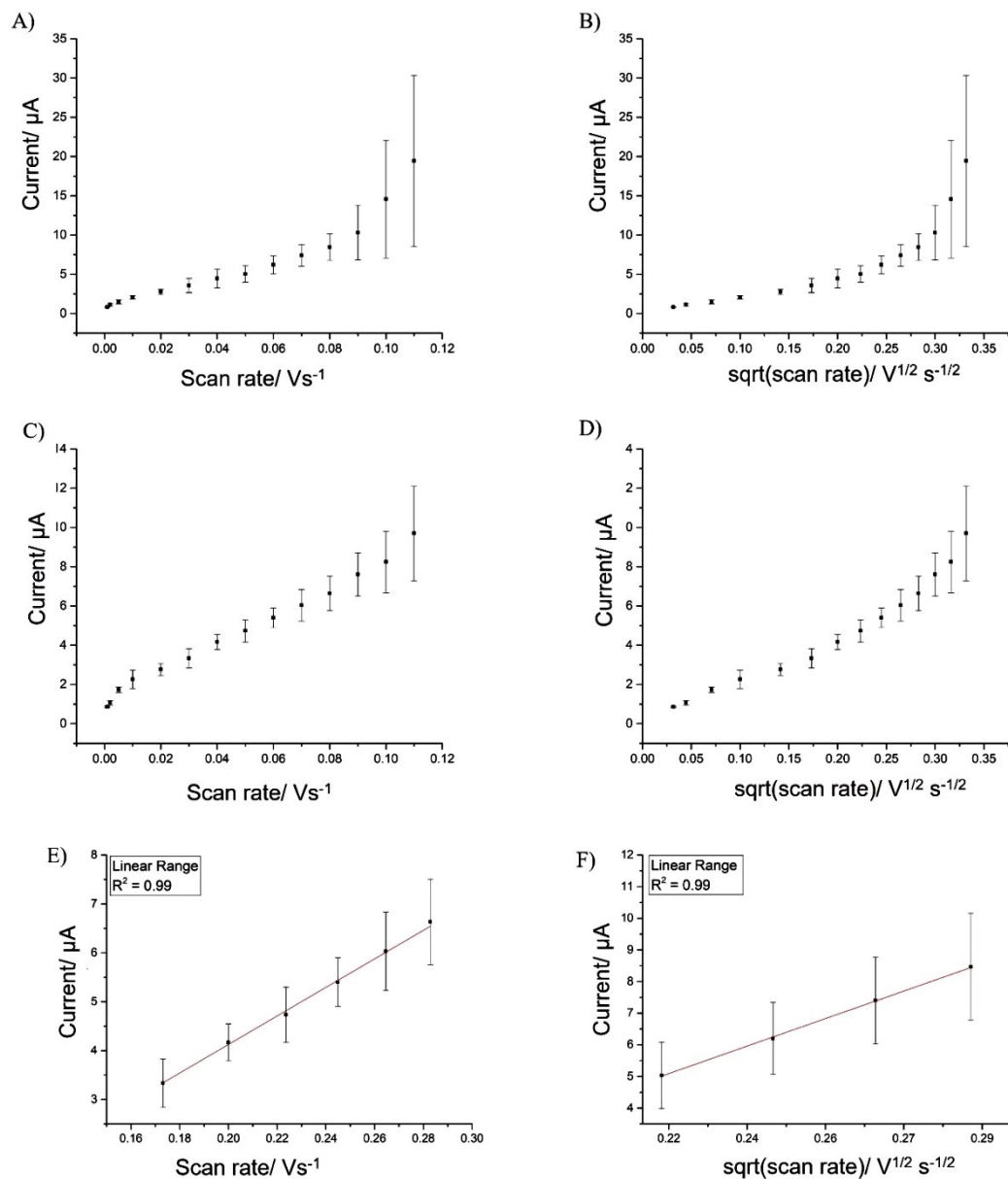


Figure 123: Dependence of the current peak from the different scan rates A) and square root of the scan rate B) into an empty alginate hydrogel and the same study has been done for a bare GCE C), D). Study of the linear range and R² value for the [Ru(bpy)₃]²⁺ diffused into the alginate hydrogel matrix E) and on the bare GCE F). Error bars represent triplicate data points.

7.4 Results and discussion

7.4.1 ADH-[Ru(bpy)₃]²⁺-NADH system

The first enzyme analysed with the [Ru(bpy)₃]²⁺ is the alcohol dehydrogenase (ADH) (Fig. 124) belonging to the dehydrogenase family. This enzyme facilitates the conversion of alcohols into aldehydes and/or ketones with the concomitant reduction of NAD⁺ to NADH. In human body, these enzymes are essential to decompose alcohols that could be otherwise toxic by forming effective organic compounds during the biosynthesis of metabolites. ADH was first isolated in 1927 from *Saccharomyces cerevisia* and was investigated by Hugo Theorell [332]

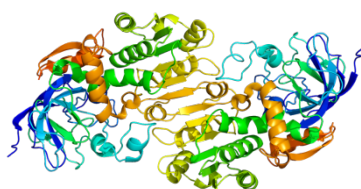


Figure 124: Structure of ADH [333].

ADH incorporates different isoenzymes able to catalyse the oxidation of alcohols to aldehydes and ketones in a redox reaction which involves the coenzyme NADH⁺. In human body the hepatic form of ADH is used to oxidise the ethanol to acetaldehyde following the reaction:

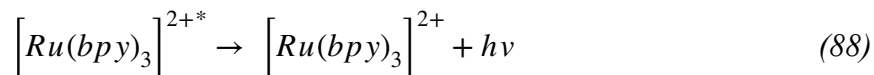
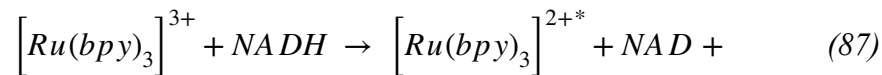
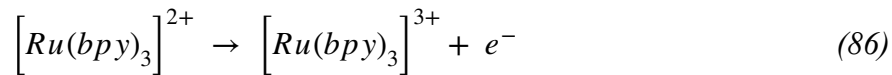
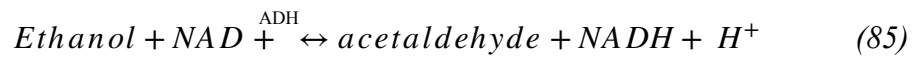


Through the action of ADH it is possible to consume alcoholic beverages and to disrupt the alcohols naturally included the one into foods [334].

During the years, different biosensors have been developed for the detection of breath alcohol and reduce problems related to the alcoholism and driving. One of the first ECL biosensors involving ADH/NAD⁺/[Ru(bpy)₃]²⁺ system appeared in 1997 with Martin's group. They proposed the immobilisation of the luminophore and enzyme in cation exchange polymers

like Eastman AQ and Nafion covering a platinum electrode. With this biosensor, a detection range from 0.1 to 100 μM was achieved [321]. In 1999, Park et al. proposed an amperometric biosensor based on alcohol dehydrogenase and the cofactor NAD^+ . The biosensor was composed of two electrodes, an active containing the ADH and an inactive with only BSA to minimise the several oxidisable species in human's breath. The NADH generation on the active electrode during the enzymatic reaction allowed the measure of the breath alcohol for a range of concentrations of 20-800 ppm [335]. Alcohol dehydrogenase has been immobilised also in sol-gel hybrid material to be investigated with the ECL of tri(2,2'-bipyridyl) ruthenium (II) in 2005. With this biosensor was possible to achieve a detection limit of 1.0×10^{-5} M [166]. More recently, an ethanol ECL biosensor based on $[\text{Ru}(\text{bpy})_3]^{2+}$ -doped silica nanoparticles were studied by Jia et al. The enzyme was cross-linked with the RuSiNPs and then immobilised on the GCE using chitosan obtaining very low limit of detection (5.0×10^{-8} M) and a good stability but expensive and not easy to obtain [166].

The biosensor here proposed, observes the following process:



After the initial electron transfer reaction occurring on the GCE surface triggered by the application of a suitable potential (83), the chemical reaction between the cofactor NAD^+ , the substrate and the enzyme starts generating NADH (84) which in turn reacting with the $[\text{Ru}(\text{bpy})_3]^{3+}$ produces the excited state $[\text{Ru}(\text{bpy})_3]^{2+*}$ and the following emission of light at 620 nm of wavelength (86). To optimise the ECL experimental conditions and to achieve good stability and reliability of the biosensor, the effect of pH and NAD^+ concentrations have been investigated. The pH influence was studied in the range from 6.0 to 9.0 and from Fig. 125 it is noticeable how important is setting the solution at the right pH. In fact, the response of the enzymatic reaction is linearly dependent from the alkalinity of the solution, in

particular good stability and high ECL intensity were obtained for pH from 7.5, to 9.0 and the maximum response was obtained for pH 8.5. It is significant to remember that NAD^+ becomes unstable for alkaline pH as Park et al. showed in 1999 [335], so for the ECL experiments involving ADH and ethanol was used a 0.01 M PBS solution at pH 7.5 (Fig. 125).

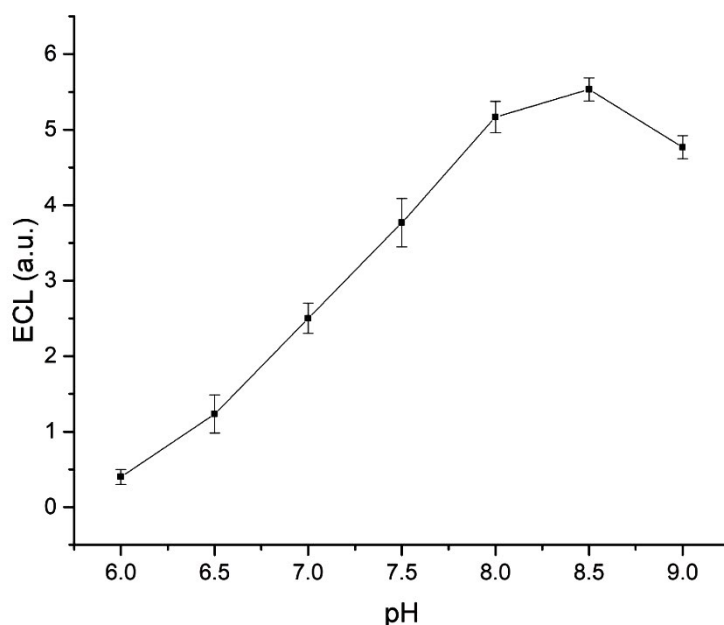


Figure 125: Effect of different pH values for the ADH- $[\text{Ru}(\text{bpy})_3]^{2+}$ -NADH system in 0.01 M PBS. Scan rate 0.05 V s^{-1} . Error bars represent triplicate data points.

The effect of different concentrations of NAD^+ in the range from 0.25 mM to 3.0 mM were investigated 0.01 M PBS at pH 7.5. The ECL intensity increases significantly with the cofactor concentration showing a higher conversion to NADH during the enzymatic reaction. The highest response is obtained for a concentration around 2.5 mM and then the signal starts to decrease showing probably a saturation of the enzyme encapsulated into the alginate hydrogel. Since the cofactor is expensive, the concentration used for the all the ECL tests was 1 mM giving a good stability and reproducibility of the biosensor (Fig. 126).

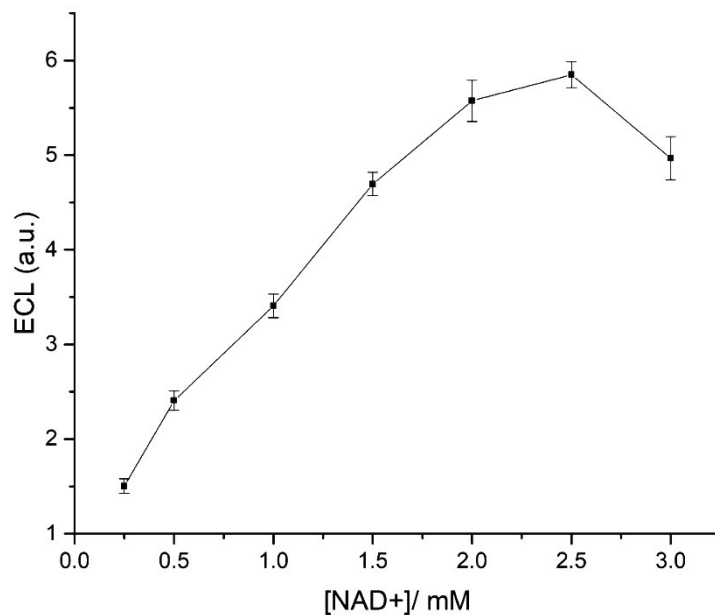


Figure 126: Effect of different concentrations of NAD⁺ for the ADH-[Ru(bpy)₃]²⁺-NADH system in 0.01 M PBS at pH 7.5. Scan rate 0.05 V s⁻¹. Error bars represent triplicate data points.

Considering the results obtained for the pH and the NAD⁺ concentrations, the following ECL tests have been performed in 0.01 M PBS at pH 7.5 with 1 mM NAD⁺ and 2.5 mM [Ru(bpy)₃]²⁺ in solution. Different concentrations of Ethanol have been added to study the ECL response of the biosensor. The ECL signal raises linearly with the increase of the Ethanol in solution due to the conversion of NAD⁺ to NADH catalysed by the ADH encapsulated and immobilised on the GCE surface. The tests have been carried out on three different GCE studying the mean and standard deviation and obtain the curve in Fig. 127A). After the addition of different ethanol concentration, a stirring of 15 seconds was run to allow the diffusion of the cofactor and luminophore into the hydrogel matrix). The increase of the oxidation peaks is shown in the CVs obtained for different concentrations of ethanol added in the solution. The CVs show two peaks at the two different potentials 0.7 V and 1.1 V, regarding the conversion of NAD⁺/NADH and the [Ru(bpy)₃]²⁺, respectively (Fig.127 C)).

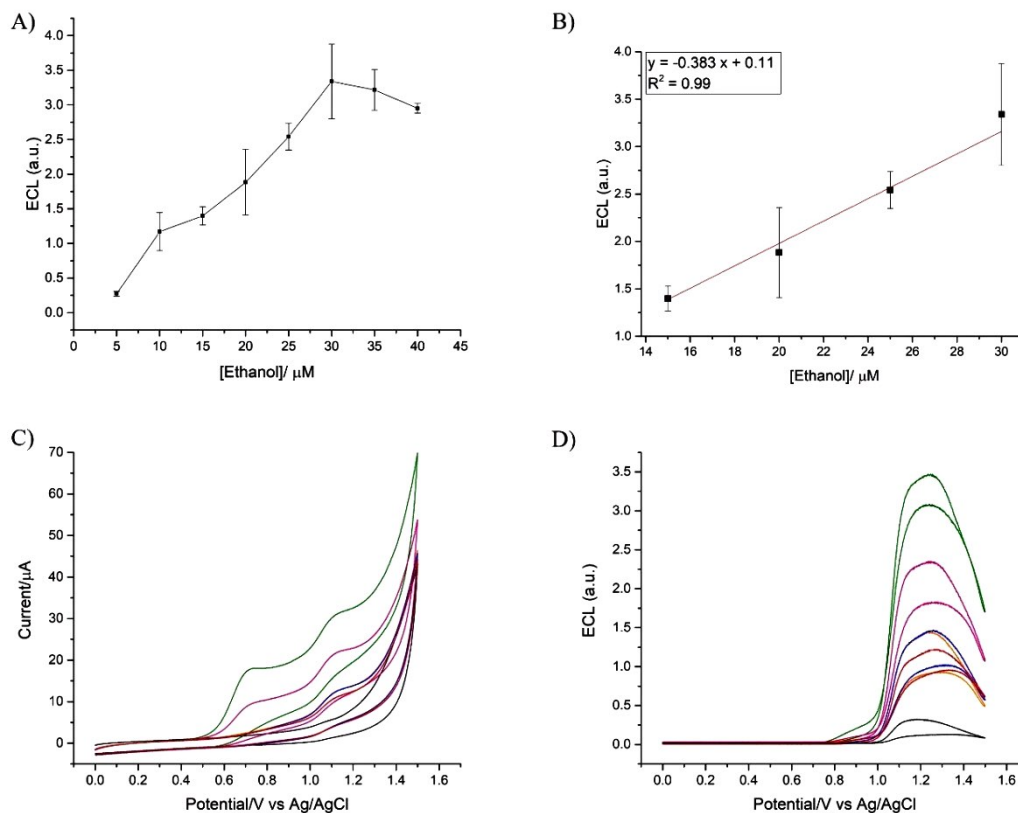


Figure 127: A) Calibration curve of the ADH-ethanol-[Ru(bpy)₃]²⁺ system in 0.01 M PBS with 1 mM NAD⁺ at pH 7.5. Error bars represent triplicate data points. B) and study of the regression equation in the linear range between 15-30 μM of Ethanol. Electrochemical results: CVs and ECL (D) obtained by adding Ethanol in 0.01 M PBS at pH 7.5 in the presence of 1 mM NAD⁺ and 2.5 mM [Ru(bpy)₃]²⁺. Scan rate 0.05 V s⁻¹.

7.4.2 GDH-[Ru(bpy)₃]²⁺-NADH system

Glucose dehydrogenase (GDH) (Fig. 128) is an oxidoreductase enzyme that catalyses the following reaction:

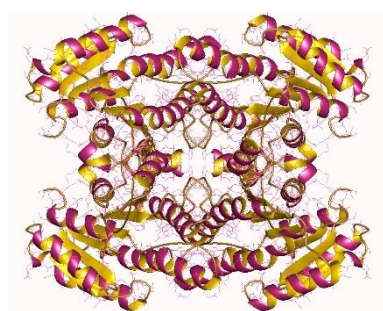
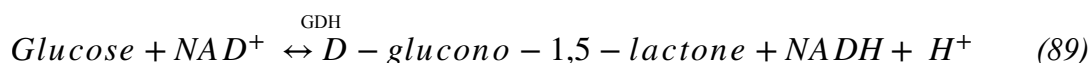


Figure 128: Structure of glucose dehydrogenase obtained by PDB database [336].

GDH is dependent from the cofactor nicotinamide adenine dinucleotide (NAD) and it is one of the enzymes used for the determination of glucose. Different ECL-based glucose sensors have been proposed throughout the years. In 1993 Martin et al. proposed a flow injection analysis for the determination of glucose using an immobilised GDH and [Ru(bpy)₃]²⁺. In particular, the enzyme was immobilised via glutaraldehyde cross-linking and the luminophore instead in a Nafion film on platinum WE to obtain a chemiluminescent biosensor [337]. Glucose dehydrogenase has been immobilised also into an electro-deposited redox hydrogel and used for the generation of NADH by the enzymatic reaction of the enzyme with the co-reactant and the substrate [160]. Another glucose sensor was proposed using Ru(bpy)₃Cl₂-doped silica nanoparticles to study the enzymatic activity of the glucose dehydrogenase on GCE. The NADH generated after the reduction reaction between NAD⁺ and glucose was detected by the ECL emission of [Ru(bpy)₃]²⁺ [338].

To obtain the right parameters for the ECL tests GDH-[Ru(bpy)₃]²⁺-NAD⁺ system, a calibration curve at different pH has been studied. Solutions with 0.01 M. PBS, 1 mM NAD⁺, 2.5 mM [Ru(bpy)₃]²⁺ and 3,4 mM glucose at pH in the range from 6.0 to 9.0 have been prepared. Considering the stability of the plateau between pH 8.0 and 8.5, for the ECL tests at

different glucose concentrations have been performed at pH 8.3. The optimum pH for the enzyme GDH is 9.0 but due to a high instability and deactivation of the cofactor NAD^+ at very alkaline pH, the signal starts to decrease after pH 8.0 (Fig. 129).

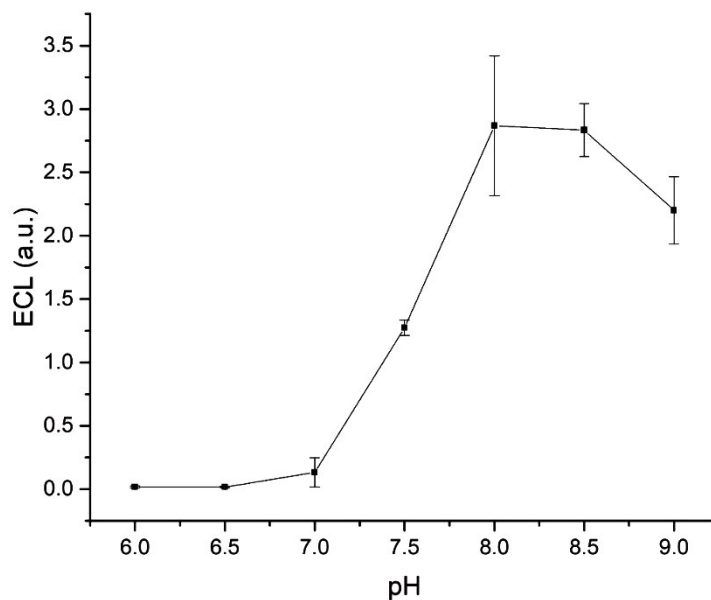


Figure 129: Effect of pH for 1 mM NAD^+ , 2.5 mM $[\text{Ru}(\text{bpy})_3]^{2+}$ and 3.36 mM glucose in 0.01 M. PBS. Scan rate 0.05 V s^{-1} . Error bars represent triplicate data points.

For the ECL characterisation of the biosensor, different glucose concentrations have been studied obtaining the calibration curve in Fig. 130A). The ECL signal increases due to the increment of the generation of NADH from the enzymatic reaction of GDH with different concentrations of the substrate and the presence of the cofactor NAD^+ in solution. In Fig. 129C), the voltammograms show two anodic peaks related respectively to the NAD^+/NADH conversion obtained via enzymatic reaction at $\sim 0.8 \text{ V}$ and the characteristic oxidation peak of the ruthenium complex for higher potentials ($\sim 1.1 \text{ V}$). With the increases of the glucose concentration in solution the amount of NADH consequently generated raises allowing in this way a higher intensity for the ECL signal (Fig. 130D).

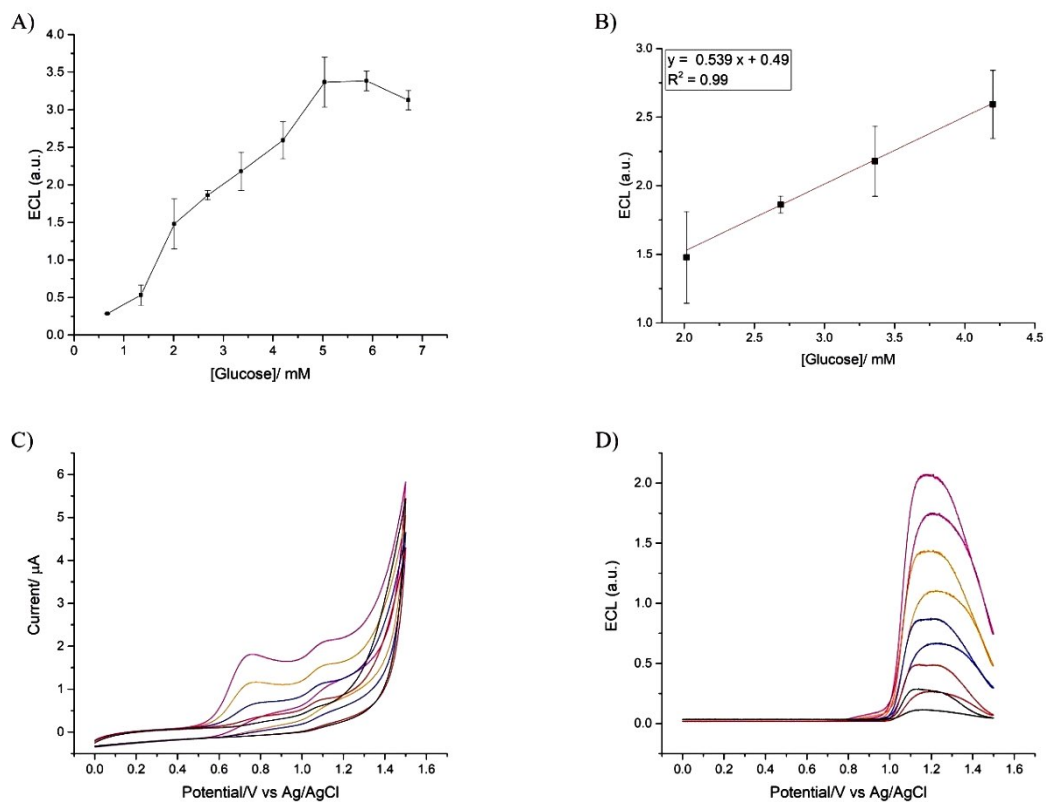


Figure 130: Calibration curve of the GDH-glucose-[Ru(bpy)₃]²⁺ system showing the ECL-emission at different concentrations of glucose added to 0.01 M PBS with 1 mM NAD⁺ at pH 8.3 A) and study of the regression equation in the linear range between 2-4.2 mM of glucose B). Error bars represent triplicate data points. Electrochemical results: CVs C) and ECL D) obtained by adding glucose. Scan rate 0.05 V s⁻¹.

7.4.3 LDH-[Ru(bpy)₃]²⁺-NADH system

Lactate dehydrogenase LDH (Fig. 131), is one of the essential enzymes that our body uses to convert sugars into form of energy such as ATP. It catalyses the reversible conversion of L-lactic acid into pyruvate with the concomitant interconversion NAD⁺ into NADH. This reaction occurs during the Cori cycle in the liver when there is a high concentration of lactate, the enzyme starts its catalytic action. Lactate dehydrogenase intervenes also in the reverse reaction that starts at the end of the glycolysis process when pyruvate is produced to convert NADH to NAD⁺ and pyruvate in lactic acid.

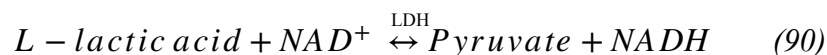


Figure 131: Lactate dehydrogenase molecular structure (Biologydictionary.net Editors. "Lactate Dehydrogenase." *Biology Dictionary*, Biologydictionary.net, 08 Apr. 2018, <https://biologydictionary.net/lactate-dehydrogenase/>).

Monitoring the levels of LDH is essential for the prevention of important diseases and conditions such as cancer, hemolysis, HIV, meningitis and encephalitis, liver and lung diseases [339]. Low and normal level of LDH don does not indicate any condition, but when the concentration of lactate dehydrogenase reaches high levels in blood tests it indicates a potential tissue damage [163, 339]. The most used analytical technique for the determination of lactate concentration is the high-performance liquid chromatography (HPLC) [340] but it requires quite some times for the pretreatment procedures. For these reasons an amperometric approach is more suitable to obtain higher sensitivity and accuracy of the results. In literature several works have been published proposing different ways for the immobilisation of the enzyme on the sensing layer like adsorption [257], conducting polymer entrapment using ITO as electrode [341, 342], cross-linking [343], entrapment in sol-gel matrix [344] and covalent

attachment [345]. The biosensor here proposed, includes the enzyme encapsulated into alginate hydrogels matrix and immobilised on the GCE surface.

The reaction which describes the behaviour of the biosensor is the following:



For the optimisation of the experimental conditions, the pH behaviour of the enzyme has been studied for a range of pH from 6.0 to 9.0. Knowing that the optimum pH for LDH to obtain pyruvate and NADH is 7.5, different 0.01 M PBS solutions have been studied with the addition of 1 mM NAD⁺, 2.5 mM [Ru(bpy)₃]²⁺ and 10 μM of L-lactic acid. The results in Fig. 132 show an ECL intensity signal that increases with the alkalinity of the solution from pH 6.0 to 7.5 then the signal starts to decrease for pH above 7.5 due to the poor enzyme activity. For these reasons, a 7.4 pH has been chosen for all the ECL experiments involving LDH as enzyme.

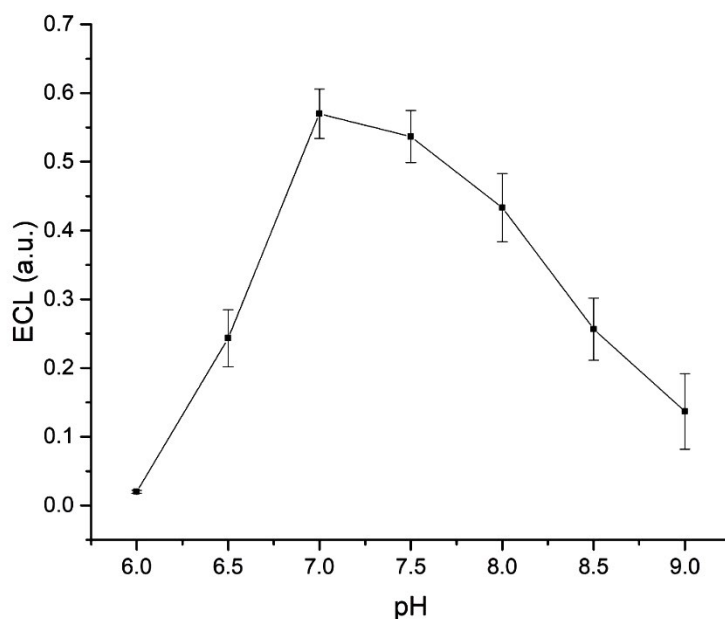


Figure 132: Effect of the pH on the LDH activity in the presence of 2.5 mM [Ru(bpy)₃]²⁺, 1 mM NAD⁺ and 10 μM L-lactic acid. Scan rate 0.05 V s⁻¹. Error bars represent triplicate data points.

The amperometric response of the system has been studied using different concentrations of L-lactic acid in the electrolytic solution composed of 0.01 M PBS, 1 mM NAD⁺ and 2.5 mM

$[\text{Ru}(\text{bpy})_3]^{2+}$. From the calibration curve plot, the current increases linearly with the addition of different concentrations of the substrate in solution showing an increment of the generation of NADH from NAD^+ already present in the solution. The ECL response then shows a plateau that can be related to the Michaelis-Menten behaviour of the enzyme kinetics, in fact the enzymes reached the saturation level. The currents show a linear relationship with the lactate concentration in the range from 5 to 20 μM obtaining the correlation coefficient $R^2 = 0.989$ (Fig. 133B)).

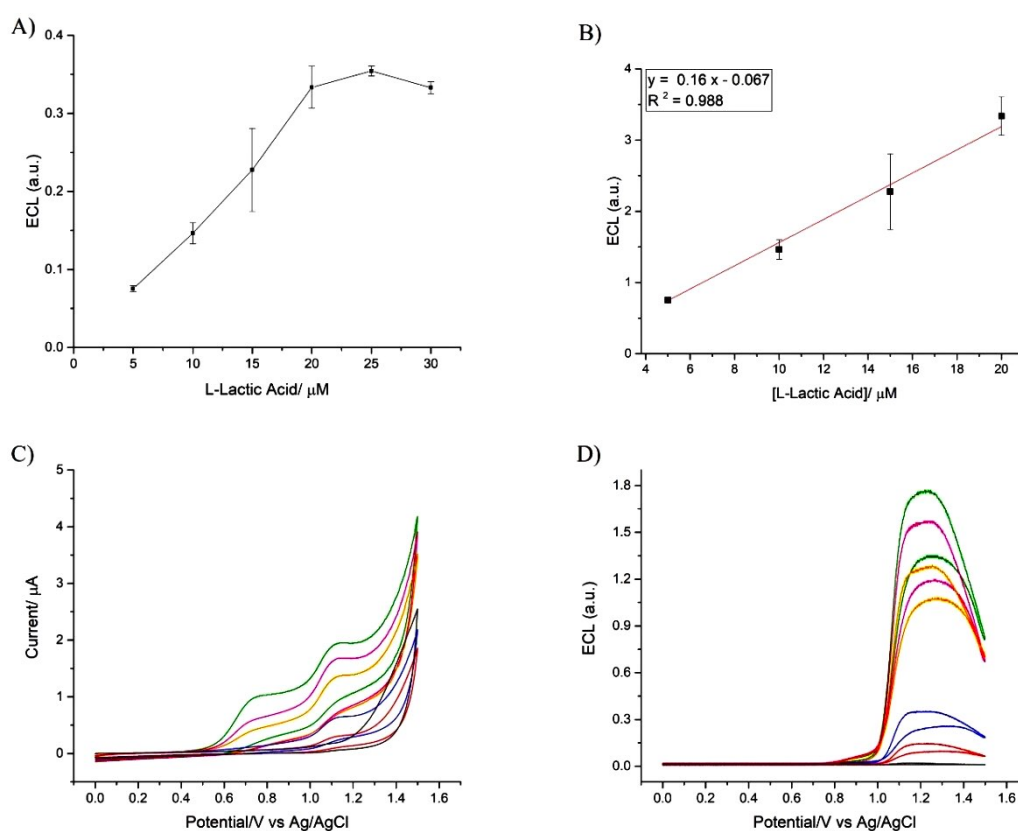


Figure 133: Calibration curve of the LDH-L-Lactic Acid- $[\text{Ru}(\text{bpy})_3]^{2+}$ system with the ECL-emission at different concentrations of L-lactic acid added to 0.01 M PBS with 1mM NAD^+ at pH 7.4 (A) and study of the regression equation in the linear range between 5-20 μM of L-lactic acid (B). Electrochemical results: CVs (C) and ECL (D) obtained by adding the substrate in solution. Scan rate 0.05 V s^{-1} . Error bars represent triplicate data points.

7.4.4 ChDH-[Ru(bpy)₃]²⁺-NADH system

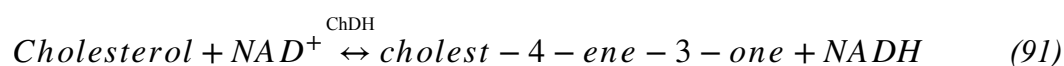
The last enzyme analysed with the ECL-based biosensor is the cholesterol dehydrogenase (ChDH) (Fig. 134).



Figure 134: Crystal structure of cholesterol dehydrogenase [346].

As all the other dehydrogenases, ChDH is NAD-dependent, and it can oxidise the 3- β -hydroxyl group of cholesterol to obtain cholest-4-en-3-one. When ChDH is coupled with cholesterol esterase it can determine the cholesterol in plasma.

The system is described by the equation (91):



Cholesterol is one of the essential components of cells, however when it reaches very high concentrations in human blood it can trigger several diseases as already anticipated in the chapter 4 related to the cholesterol oxidase. ChDH can be used as an alternative enzyme for the monitoring of cholesterol instead of the commonly used cholesterol oxidase. In fact, cholesterol dehydrogenase does not use the O₂ as the electron acceptor, therefore, the catalytic reaction takes place in the absence of O₂ and H₂O₂. Nowadays, the monitoring of the cholesterol corresponds with the collection of blood samples from a patient and the following clinical laboratory analysis that normally uses a very expensive equipment and takes hours before to obtain the results. With this electrochemical biosensor tested for different enzymes and ultimately also for the cholesterol dehydrogenase, the idea is to obtain a disposable biosensor that each patient could use for the daily monitoring. Different cholesterol biosensors have been developed and commercialised for example using tests strips [347-349].

Once the blood touches the strips, they change colour thanks to the chemical reaction happening between the analyte in the sample and the chemicals contained on the strips showing the different cholesterol levels. This kind of sensor could present problems and limitation due to the difficulties of some people to read the different colours or to match the colour obtained on the strip with the one on the chart scaled. To overcome this limit, during the years these tests have become more accurate using digital readout. Another approach for the rapid monitoring of cholesterol involves electrochemical biosensors. Several of these biosensors include cholesterol esterase, cholesterol oxidase and peroxidase immobilised onto different matrix and/or polymers [156, 284, 350, 351]. The goal of these amperometric biosensors was the detection of hydrogen peroxide produced during the chemical reaction involving O_2 as natural substrate but several interferences of electroactive species such as ascorbic acid and uric acid were found. Furthermore, the limited solubility of oxygen in the biological fluids caused the so called “oxygen deficit”. These problems can be overcome with the use of dehydrogenase enzymes which do not use oxygen as substrate and can similarly detect the analyte of interest, in this case cholesterol. In the literature, the works related to the use of cholesterol dehydrogenase is very limited. In 2011, Fang proposed a disposable amperometric biosensor based on the use of an integrated reagent layer coated by a working ink containing cholesterol esterase and cholesterol dehydrogenase for the detection of total cholesterol in human blood. The biosensor presents a high sensitivity and a range of linearity and has the great advantage that could be used by the patient at home [349].

For the proposed ECL-based biosensor, cholesterol dehydrogenase has been encapsulated in alginate hydrogels and then immobilised on the GCE to perform different ECL tests at different concentrations. To run the experiments at the right conditions, the enzyme activity has been studied for different pH solutions. Different pH in the range from 6.0 to 9.0 have been tested showing that the best pH for the obtainment of good ECL signal is pH 8.5. From Fig.135 it is possible to notice how the signal drastically decrease for alkaline solutions due to the high instability of the cofactor NAD^+ at high pH. Also, the standard deviation studied for the three electrodes used for the pH-calibration curve, increases with the pH alkalinity showing how the system becomes unstable at high pH values.

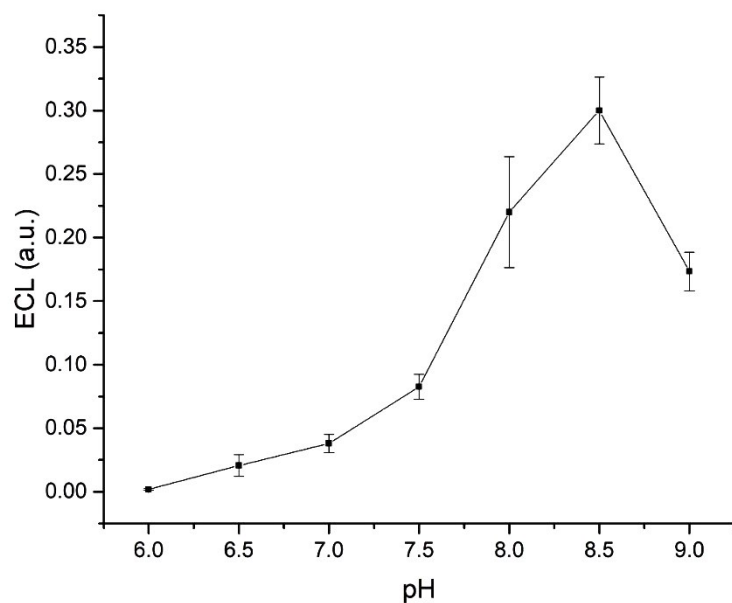


Figure 135: pH study for the cholesterol dehydrogenase in the presence of 2.5 mM $[\text{Ru}(\text{bpy})_3]^{2+}$, 1 mM NAD^+ and 15 μM of Cholesterol in 0.01 M PBS. Scan rate 0.05 V s⁻¹. Error bars represent triplicate data points.

For the ECL tests, cholesterol and cholesterol dehydrogenase have been dissolved in 0.01 M PBS with 2.5% surfactant Triton-X 100 by heating till 50°C. By adding different concentrations of cholesterol in solution, the oxidation peak showed in the voltammograms increases producing NADH which in turn reacting with the $[\text{Ru}(\text{bpy})_3]^{2+}$ generates the excited state and the following emission of light described in the ECL vs. potential graph (Fig. 136C and D).

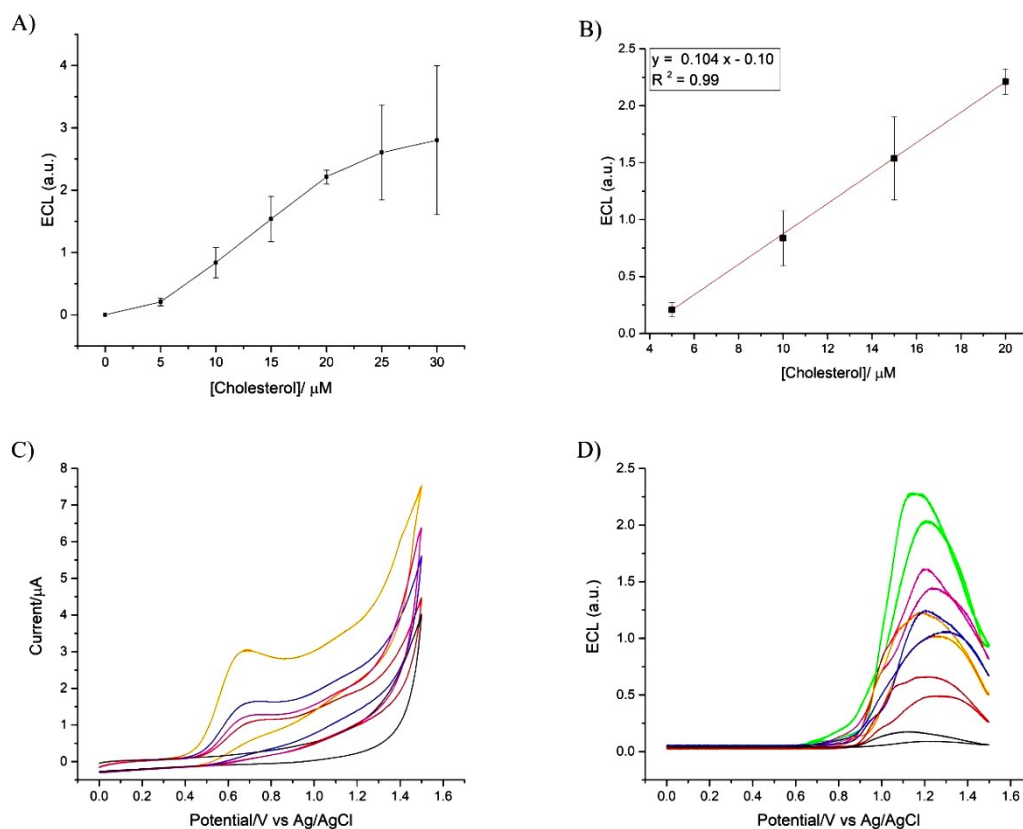


Figure 136: Calibration curve of the ChDH-cholesterol-[Ru(bpy)₃]²⁺ system the ECL-emission at different concentrations of cholesterol added to 0.01 M PBS with 1 mM NAD⁺ at pH 8.5 (A) and study of the regression equation in the linear range between 5-20 μM of cholesterol (B). Electrochemical results: CVs (C) and ECL (D) obtained by adding the substrate in solution. Scan rate 0.05 V s⁻¹. Error bars represent triplicate data points.

From the statistical analysis showed in Fig. 136A) and B), it is noticeable that the ECL signal increases with the concentration of the substrate in solution, but there is also an increment of the standard deviation due to the high instability of the NAD⁺ for high pH. Despite this, the system follows the Michaelis-Menten model with the current peak growing till the saturation level indicating the saturation of the enzyme. The linear range is found in the range from 5 μM to 20 μM of cholesterol and indicates a correlation value of $R^2 = 0.997$.

7.5 Michaelis-Menten kinetics study

As anticipated in the chapter 5 “Luminol and oxidase system”, the enzymes kinetics can be determined by using the Michaelis Menten model which relates the rate of the reaction with the concentration of the substrate. In electrochemistry most of the systems present an immobilised enzyme on the electrode so the Michaelis-Menten model in these cases will consider the different currents peak related to the concentrations of substrate in solution obtaining in this way a Michaelis-Menten apparent value $K_{m^{app}}$.

Considering the equation (90):

$$I = \frac{I_{max} S}{S + K_{Mapp}} \quad (92)$$

The apparent Michaelis-Menten values for the dehydrogenase enzymes have been reported in the following Table 11. $K_{m^{app}}$ values for all the enzymes indicates the substrate’s affinity with the related enzyme, in particular lower is the constant and higher is the affinity (Fig. 137).

Table 11 Michaelis-Menten model studied for the dehydrogenase enzymes system

<i>Enzyme</i>	<i>I_{max}</i> (μA)	<i>K_{Mapp}</i>
<i>ADH</i>	3.4	19.21 μM
<i>GDH</i>	3.3	2.19 mM
<i>LDH</i>	3.5	11.2 μM
<i>ChDH</i>	2.8	12.34 μM

Compared to oxidase systems, the K_m^{app} are higher showing that the substrates are more selective for the oxidase enzyme rather than the dehydrogenase.

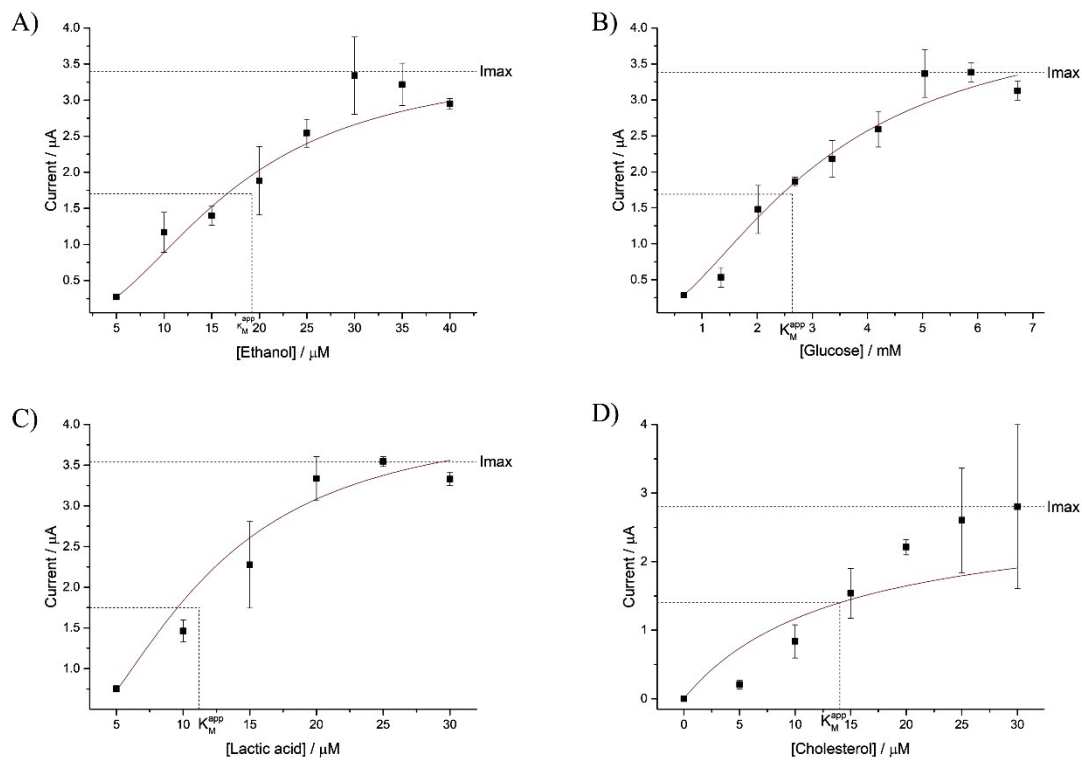


Figure 137: Graphical representation of apparent Michaelis-Menten behaviour of the encapsulated dehydrogenase enzymes. The plots show the maximum current and the apparent Michaelis-Menten constant at the 50% of the I_{max} . Error bars represent a triplicate data point.

7.6 Limit of detection and limit of quantification study

To complete the characterisation of the biosensor based on encapsulated dehydrogenase enzyme into alginate hydrogels, the theoretical limit of detection and limit of quantification have been studied for the systems described in this chapter.

Considering the following equations:

$$LOD = 3.3 \frac{SD}{Slope} \quad (93) \quad LOQ = 10 \frac{SD}{slope} \quad (94)$$

The results are reported in Table 12 below.

Table 12 Theoretical limit of detection and limit of quantification study for the dehydrogenase systems studied.

<i>Enzyme</i>	<i>LOD</i>	<i>LOQ</i>	<i>SE</i>
<i>ADH</i>	6.75 μ Mol	20.5 μ Mol	± 0.12
<i>GDH</i>	0.68 mMol	2.05 mMol	± 0.05
<i>LDH</i>	2.52 μ Mol	7.6 μ Mol	± 0.06
<i>ChDH</i>	0.50 μ Mol	1.5 μ Mol	± 0.01

In general, the limits of detection for the dehydrogenase enzymes are lower than the limits related to the oxidase systems. This can be due to the stability of the enzyme encapsulated into alginate matrices or to the ability of $[\text{Ru}(\text{bpy})_3]^{2+}$ to work for a bigger range of pH compared to luminol.

7.7 Conclusions

An ECL-based sensor was developed in this chapter involving the dehydrogenase enzymes and $[\text{Ru}(\text{bpy})_3]^{2+}$ as luminophore. This biosensor based on the co-reactant approach for the generation of the ECL signal, demonstrated the possibility to detect clinically relevant parameters such as glucose, lactic acid, and cholesterol with a stable response for both the substrate added to the electrolytic solution, and for the real sample.

The addition of the cofactor NAD^+ in the electrolytic solution was essential for the redox reaction to happen as the enzymes are coreactant dependent. In fact, after the application of the potential to the WE, the electron transfer reaction starts leading to the oxidation of the substrate and the concomitant reduction of the NAD^+ to NADH that is the co-reactant for this novel ECL biosensor. The electrochemical experiments show how the ECL signal increases with the addition of substrate concentrations. As for the other systems, monitoring of the coreactant levels produced during the enzyme-catalysed redox reaction was used to derive the glucose, lactic acid, ethanol, and cholesterol concentrations in solution.

The diffusion of $[\text{Ru}(\text{bpy})_3]^{2+}$ in alginate hydrogels was investigated running different cyclic voltammetry at different scan rate. For the 0.05 Vs^{-1} scan rate the diffusion coefficient was found to be $D = 0.125 \times 10^{-6} \text{ cm}^2 \text{ s}^{-1}$ for the peak current $i_p = 3.781 \text{ } \mu\text{A}$ and the scan rate $v = 0.05 \text{ Vs}^{-1}$ demonstrating an efficient diffusion of the luminophore in the hydrogels matrix with a predicted regeneration time of $\sim 12 \text{ s}$.

The ECL results obtained have been related to the Michaelis-Menten kinetic behaviour showing how the current signal initially increases with the addition of substrate in solution and then reaches a plateau for higher concentrations due to a saturation of the active sites of the enzyme.

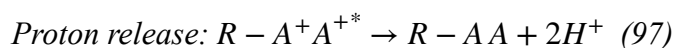
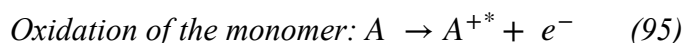
These experiments highlighted the versatility of the ECL biosensor here developed that could be applied to different categories of enzymes and luminophores. Furthermore, also it has been demonstrated that the alginate hydrogels are suitable for the diffusion of both the luminophore analysed for different scan rates.

Chapter 8: Electro-polymerisation

The need to improve the performance of the proposed biosensors, particularly to increase the sensitivity and stability of the electrochemical detection, induced the employment of a novel approach related to the formation of an electroactive layer of polymer on the electrode surface by using the electrochemical polymerisation technique [352]. This approach is widely used for the implementation of conducting films due to the easy realisation and reproducibility by using potentiostatic, galvanostatic and voltametric techniques [353].

8.1 General principles

In general, the electro-polymerisation is based on the application of a suitable potential to the WE immersed into an electrochemical cell containing the electrolyte solution and the monomer to create a polymer on the electrode surface. Through the oxidation of the monomer, the positively charged radicals are generated leading to the formation of the polymer.



This technique can be divided into two groups, anodic and cathodic electro-polymerisation. The *anodic* process is the most used for the generation of conducting polymers through the oxidation of the monomer by forming an oxidative radical cation[354]. A classic example of this method of polymerisation is the polyaniline shown in Fig.138 showing the beginning of the process after the application of a potential to the working electrode with the consequent formation of the radical due to the electron transfer reaction at the surface[355].

The *cathodic* procedure instead is not often used for the synthesis of polymers as involves the use of reductive electro-polymerisation reaction. With this method the poly(p-phenylenevinylenes)(PPVs) has been polymerised (Fig.139) [356].

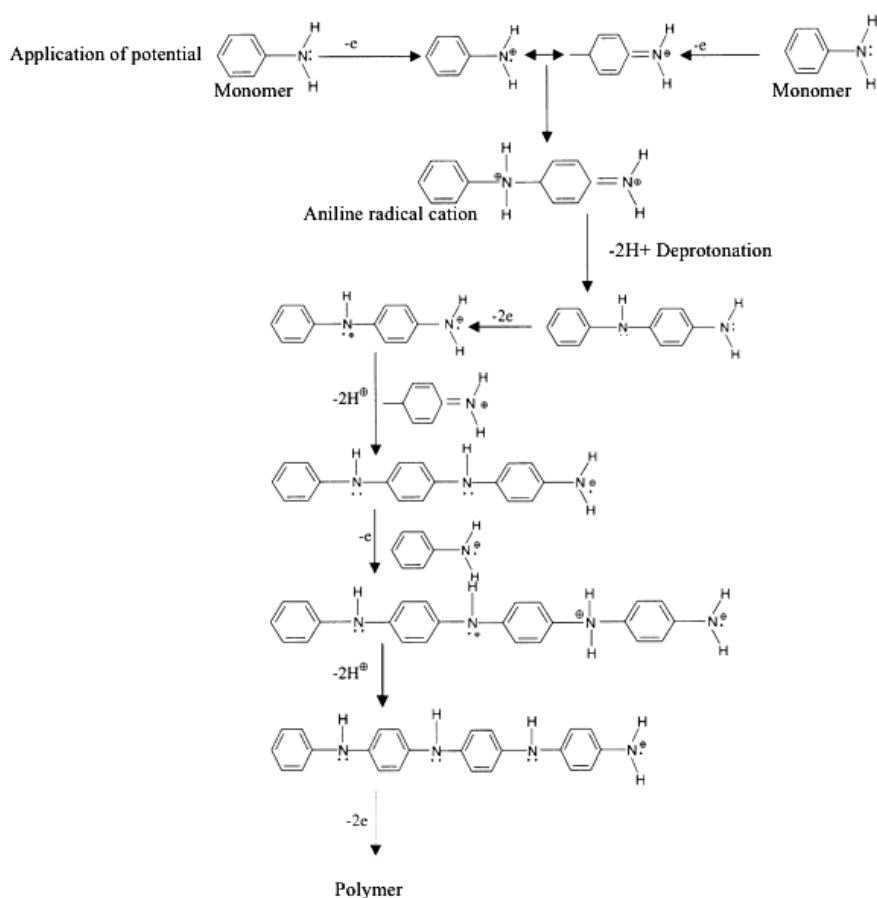


Figure 138: Oxidative electro-polymerisation of aniline mechanism [357].

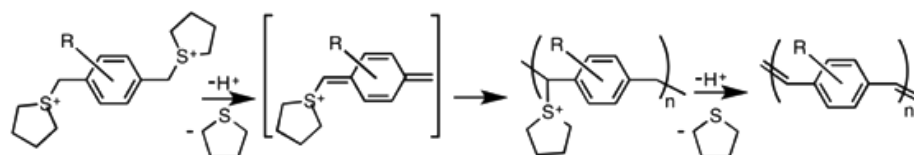


Figure 139: Cathodic electro-polymerisation method to produce poly(p-phenylenevinylenes) (PPVs) [357].

The electro-polymerisation is carried out by using the potentiostat connected to a three-electrodes electrochemical cell as for the ECL tests described in the previous chapters. The surface of the WE is the region where the monomer is polymerised obtaining the conducting polymer. The type of material of the WE can influence the oxidation of the monomer and so the growth of the polymer on its surface. The most used materials for the WE are inert metal such as gold, platinum and titanium [358-360], carbon materials for

example the glassy carbon electrode used for the electro-polymerisation of luminol and $[\text{Ru}(\text{bpy})_3]^{2+}$ or other carbon types like boron-doped diamond, pyrolytic graphite [361-363]. Also conducting glass materials have been used to perform electro-polymerisation like ITO and alloy but the latter have not been used very often due to the high oxidation potentials of the monomers [364-366]. In literature most of the research are based on polymerisation on metal, carbon, and ITO as WE electrodes due to the properties discussed in chapter 1. The other two electrodes used to close the current circuit into the electrochemical cell are the Ag/AgCl as the RE and platinum wire as the CE. The characteristics of the polymer are influenced by different factors such as the scan rate, the nature of the supporting electrolyte chosen and, as said, the material of the WE. The supporting electrolyte is an essential factor for the polymerisation of the monomer in both aqueous and inorganic solutions (Table 13).

Table 13 Combination of some supporting electrolyte with mediums polymerisation.

<i>Medium</i>	<i>Supporting Electrolyte</i>	<i>Polymer</i>	<i>References</i>
<i>Aqueous solution</i>	H ₂ SO ₄ , HCL, HNO ₃ , copper (II) nitrate, sodium sulfate, sodium sulfate/sodium perchlorate, lithium perchlorate, sodium benzoate, propylene carbonate/lithium perchlorate, phosphoric acid, trifluoroacetic acid	Polyaniline (PANI)	[354, 367-369]
	Aqueous sulfuric acid, boron trifluoride diethyl etherate	Polyindole	[370, 371]
<i>Organic solution</i>	HClO ₄ /acetonitrile, tetramethylammonium trifluoromethane-sulfonate/acetonitrile, periodic acid/tetraethylammonium tetrafluoroborate/acetonitrile, tetrabutylammonium tetrafluoroborate/trifluoroacetic acid, tetrabutylammonium perchlorate/acetonitrile, perchloric acid/benzenesulfonic acids	Polyaniline (PANI)	[362, 372-374]
	Acetonitrile, dichloromethane	Polyindole Polypyrrole	[377]
	Acetonitrile, dichloromethane, nitrobenzene, propylene carbonate	Polypyrrole, Polyaniline,	[378, 379]
	Ionic liquids	Polypyrrole	

In the literature, most of the work identify aqueous solutions as the optimum medium for the electro-polymerisation due to their adequacy for several applications, but there are also some drawbacks like the low solubility of some of the monomers. To solve the solubility issue, many works proposed the use of microemulsions as supporting electrolyte. In fact, these microemulsions are composed of water and surfactant forming a micellar solution able to

solubilise monomers such as benzene, thiophenes and pyrrole that are otherwise insoluble in water[380-382].

Another important aspect of the electro-polymerisation is the solvent contained into the electrochemical cell in addition to the supporting electrolyte[383]. The choice of the solvent is decisive for the solubility of the monomer in particular it has to be pure in order to avoid any kind of reaction of oxygen with the radicals formed after the applications of the initial potential to the WE[384]. These reactions could generate hydroxide ions on the WE surface interfering in this way with the formation of the polymer[356].

Finally, the monomer is the last ingredient for the electro-polymerisation. Most of the monomers described in the literature are aromatic compounds which are electro-polymerised by electrophilic aromatic substitution corresponding to the attachment of an electrophile atom to the aromatic ring substituting an atom that normally is hydrogen [354]. Different techniques have been proposed during the years in the literature for the generation of conductive polymers and the polymers' features depend on the technique used. The most used techniques are potentiodynamic and / or potentiostatic (1) and galvanostatic (2)[385].

The galvanostatic electro-polymerisation is based on the use of a constant current producing a doped polymer. This method presents different advantages like the possibility to control the thickness of the polymer by defining the time of the polymerisation[385, 386]. The potentiostatic methods instead, allow the electro-polymerisation by applying a constant potential to the WE which lead to the oxidation of the monomer initiating in this way the polymerisation.

Finally, the potentiodynamic methods include the cyclic voltammetry and represents the approach chose for the electro-polymerisation of the luminol and $[\text{Ru}(\text{bpy})_3]^{2+}$ on the GCE surface. With this procedure there is a continue switch from the oxidative scan and the reductive one due to the change of the potential applied to the electrode. The monomer in the electrolytic solution is exposed to the different scans undergoing to continue oxidation and reduction resulting in the generation of the polymer on the electrode surface. Depending on the direction of the scan, the polymer shifts between the non-conducting form and the conductive [387]. The number of scans of the cyclic voltammetry is an essential parameter for the determination of the thickness of the polymer, increasing the number of scans also the

thickness linearly increases. The resulting voltammograms are characterised by different peaks describing the oxidation and reduction reactions.

An example of voltametric polymerisation by using LSV technique was proposed by Fomo et al. who described the polymerisation of anyline on a pyrolytic graphite WE (PGE) using as electrolytic solution composed of perchloric acid and acetonitrile[362] (Fig. 140).

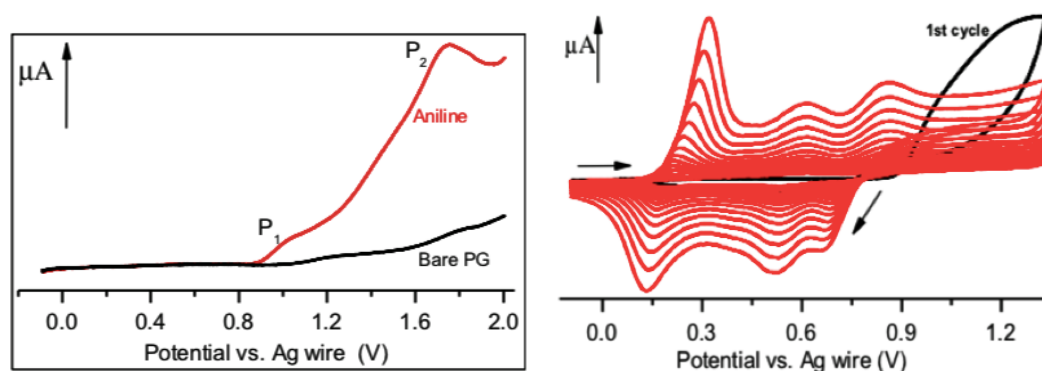


Figure 140: LSV of aniline in HClO₄/CH₃CN on PGE (left). Formation of the polyaniline film in acetonitrile performing 15 scans at 50 mV s⁻¹ (right) [362].

In Fig. 140 is showed the polymerisation of aniline in acetonitrile presenting two oxidation peaks. The first P₁ at ~1.0 V is related to the oxidation of the monomer, instead P₂ is proper of the polymer showing how the polyaniline film grows on the PG electrode surface performing different scans in 0.1M HClO₄/CH₃CN [362].

The first cycle (black line) represents the oxidation peak of aniline that starts from 0.9 V to 1.4 V and it is not present in the next cycles (red lines) indicating the formation of the cation radicals. This first oxidation peak indicates the beginning of the polymerisation of the aniline. The electropolymerisation of the aniline is characterised by the redox couple in the window from 0.2-0.3 V representing the transition from the reduced leucoemeraldine form to the partially oxidised emeraldine; with the increase of the potential another redox couple appears in the range 0.65-0.9 V showing the final conversion from the reduced leucoemeraldine to the final fully oxidised pernigraniline state (Fig.141).

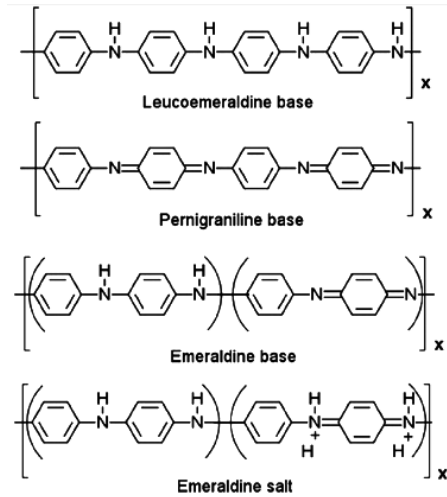


Figure 141: Oxidation states of the aniline formed during the electro-polymerisation process [388].

An important aspect for the electro-polymerisation is the concentration of the monomer added to the electrolytic solution. Yong et al. demonstrated the current density linearly increases with the increment of the monomer concentration [389]. This relation is described in the following equations:

$$i_{ox} = i_0 e^{\frac{(1-\alpha)nF(E - E_{OCV})}{RT}} \quad (98)$$

$$i_0 = nFA C_R^{bulk(1-\alpha)} C_{ox}^{bulk(\alpha)} k_{\alpha} \quad (99)$$

Where:

i_{ox} is the current oxidation (A).

i_0 is the exchange current (A).

k_{α} is the oxidation rate.

R is gas constant ($J \text{ mol}^{-1} \text{ K}^{-1}$).

T is the temperature (K).

C_R and C_{ox} represent the concentrations of the reduced and oxidised monomer.

F is the Faraday constant ($s \text{ A mol}^{-1}$).

n is the number of electrons that are exchanged during the initial electron transfer reaction.

E and E_{OCV} are respectively the potential of oxidation and the open circuit voltage.

The electro-polymerisation has been widely used for the synthesis of polymers achieved through the oxidation of the desired monomer and the formation of radicals absorbed on the electrode surface. A great advantage of this technique is the possibility to control the thickness of the polymer by defining the number of scans. Furthermore, the formation of the polymer is straightforward and it can be directly characterised without any additional treatment as for the chemical synthesis where polymers requires a purification and characterisation steps before the use of the film[390].

The polymers electrochemically obtained have been used for different applications like materials for solar cells, sensors[391, 392], electronic and electrochromic devices and batteries[393-397]. These polymers have been also used for biomedical applications such as for the development of probes and biological sensor as result of their biocompatibility and the simple realisation[398]. Moreover, the electrochemically polymerised materials are widely used also for biosensing, food manufacturing, health-care products, wastewater treatment and biotechnology due to their highly selective sensing layer[399].

8.2 Modified GCE with polyluminol

Luminol has been used in several research based on its high ECL efficiency in aqueous solutions [400, 401]. In chapter 5, the ECL results regarding the detection of hydrogen peroxide produced by the redox reactions between the encapsulated oxidase enzyme and the corresponding substrate are reported. The detection of H₂O₂ was achieved by its interaction with the oxidised form of the luminol in the electrolyte solution.

The need to improve the sensor, reducing the quantity of compounds into the electrolytic solution, increasing the sensitivity of the sensor by forming a luminescent layer on the electrode, leads to the last chapter of this work related to the modification of the electrode surface with the polyluminol film. In this section the electro-polymerisation of luminol is reported with all the different attempts performed to obtain a polymer with the luminescent properties of its monomer.

This polymer has been characterised with ECL tests by detecting hydrogen peroxide produced after the redox reaction between the enzyme encapsulated into alginate hydrogel

and cryogels and the corresponding substrate. The polymer has also been characterised with FTIR and UV to describe its molecular properties.

8.2.1 Luminol electro-polymerisation

The first work reported in literature regarding luminol polymerisation was proposed by Zhang and Chen in 2000 showing the formation of the polymer using potentiodynamic and potentiostatic techniques in acidic solution[402]. The procedure proposed was obtained by applying the constant potential ($E=1.2$ V) in the case of potentiostatic method and by using the cyclic voltammetry in a potential range 0.2-1.2 V for the potentiodynamic case. In both cases, the polymerisation was registered versus the saturated calomel electrode (SCE) as reference electrode in 0.5M H_2SO_4 (Fig. 142).

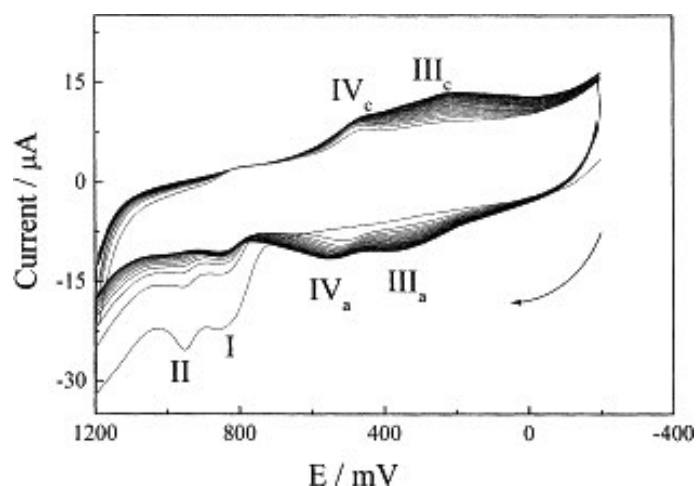


Figure 142: Zhang and Chen electro-polymerisation of luminol in H_2SO_4 , 50 scans with 100 $mV s^{-1}$ scan rate showing the growth of the polymer (black peaks) and the decrease of the monomer (red peaks) [402].

In Zhang and Chen work (Fig.142) different peaks are shown referring to different phases of the process. Peaks I and II identify the oxidation of the luminol as monomer in the solution. The redox couples III_a/III_c and IV_a/IV_c in the cathodic and anodic scans respectively show the formation of the polyluminol on the surface of the electrode. The evidence of the growth of the polymer can be found in the increase of the cathodic peaks IV_c/III_c and anodic III_a/IV_a and the consequent gradual decrease of the peaks I and II related to the monomer.

The electro-polymerisation of luminol can be defined as a method for the luminophore immobilisation on the electrode surface since the polymer is formed on the WE electrode surface as anticipated in the section 7.1. Luminol molecular structure can be partially compared to the structure of the aniline (Fig.143), the presence of the amino group in both the structures makes the polymerisation of luminol comparable to the formation of the polyaniline.

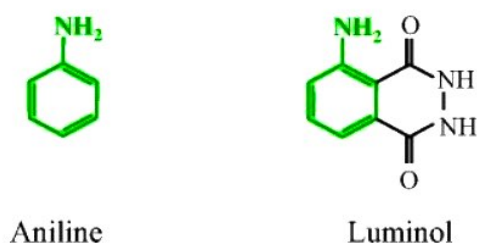


Figure 143: Molecular structures of the aniline and luminol [403].

The amino-group is involved in the electro-polymerisation of luminol, due to the fact that the -NH₂ group is not implicated in the ECL emission, the resulting polymer has the same luminescent properties of the monomer and it results to be ECL-active [402] (Fig. 144).

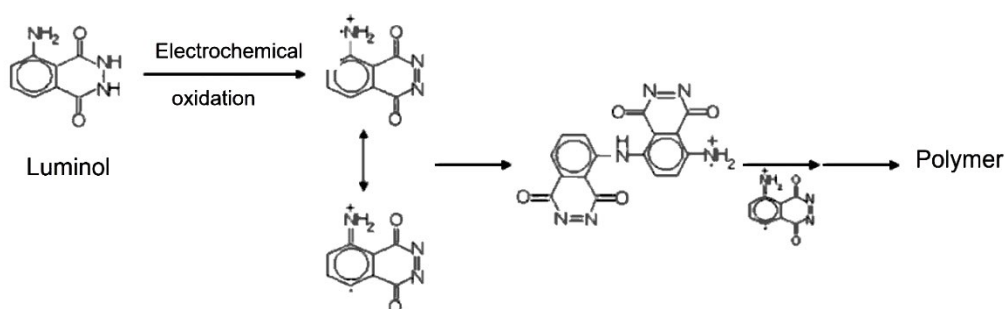


Figure 144: Schematic reaction for the electro-polymerisation of luminol with the implication of the amino-group [403].

In 2002 Wang et al. proposed the anodic polymerisation of luminol in acidic solution on ITO working electrodes. The process has been performed in 1 mM and 1 M sulfuric acid in the potential range 0-1.0 V versus SCE reference electrode at 10 mV s⁻¹ of scan rate[404]. The

anodic polymerisation shown in Fig. 145 in acidic solutions grants the detection of high concentrations of H_2O_2 in the range between 10^{-5} - 10^{-3} M.

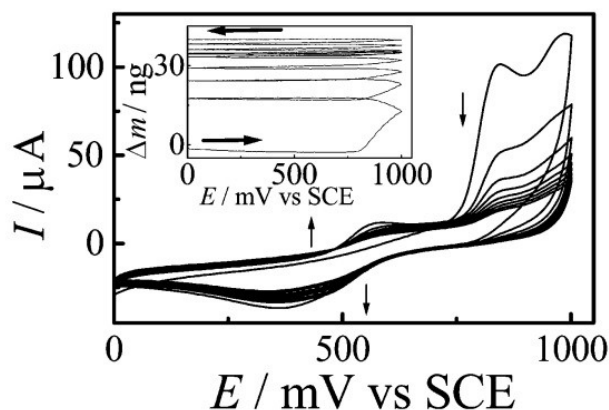


Figure 145: Voltammograms of 1 mM luminol performed in 1 M H_2SO_4 [404].

The luminol polymerisation in near-neutral medium has been proposed by Sassola's group obtaining a different polymer respect to the acidic one. They use a buffered medium that is essential for this process as during the formation of the polymer, the monomer is integrated into the chain releasing protons. Sassola's methods has been performed on a screen-printed electrode in a buffered solution at pH 6.0 by chronocoulometry and cyclic voltammetry. The cyclic voltammetry was performed in the potential range 0-0.6 V with a 0.1 V s^{-1} scan rate versus Ag/AgCl reference electrode. The chronocoulometry instead, was performed applying a fixed potential (0.4-0.5 V) to the SPE. The ECL properties of the polyluminol have been tested in veronal-HCl buffer at pH 9.0 with the injection of different concentrations of hydrogen peroxide[403]. In 2009, Sassolas et al. proposed a new biosensor with the polyluminol deposited by CV on a SPE combined with the choline oxidase for the detection of hydrogen peroxide produced by the enzymatic reaction with the choline (Fig. 146).

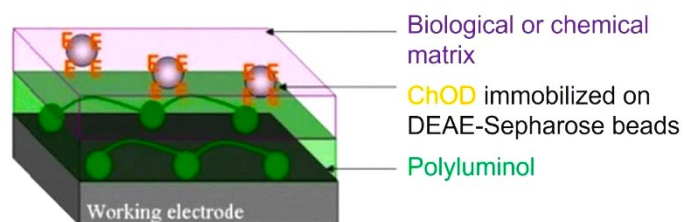


Figure 146: Schematic representation of the choline biosensor proposed by Sassolas' group [405].

For this biosensor the luminol has been formed in 0.1 M phosphate/0.1 M KCl at pH 6.0 in the presence of 1 mM of luminol by applying 10 scans in the potential range 0-0.6 V at 0.1 Vs⁻¹ of scan rate. The system has been tested to study the ECL properties of the film by detection of the hydrogen peroxide produced by the choline oxidase activity[405] (Fig. 147).

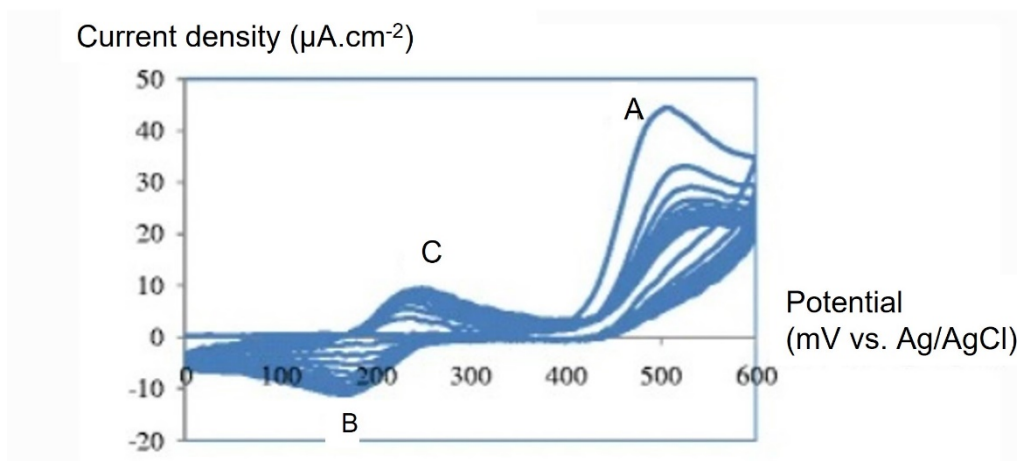


Figure 147: Sassolas' polymerisation of luminol in 0.1 M phosphate/0.1 M KCl at pH 6.0 for 10 scans at 100 mV s⁻¹ scan rate [405].

Leca-Bouvier et al. in 2014 proposed a biosensor based on a polyluminol/hydrogel sensing layer for the detection of H₂O₂ produced as result of the redox reaction between immobilised choline oxidase and the substrate choline. This biosensor is close to the one proposed in this work except for the type of WE used, the immobilisation technique and the electro-polymerisation technique. The group proposed a polymerisation on a modified screen-printed electrode by applying different number of scans at variable potential sweep and at different scan rate. The polymerisation in Fig.148 shows a voltammogram composed of three different

peaks, in particular peak A representing luminol oxidation which decreases with the number of scans showing the consumption of the monomer, however peaks B and C are related respectively to the reduced form of polyluminol and the oxidised form the polymer increase gradually underlying the redox couple of polyluminol and so the growth of the polymer on the electrode surface [405].

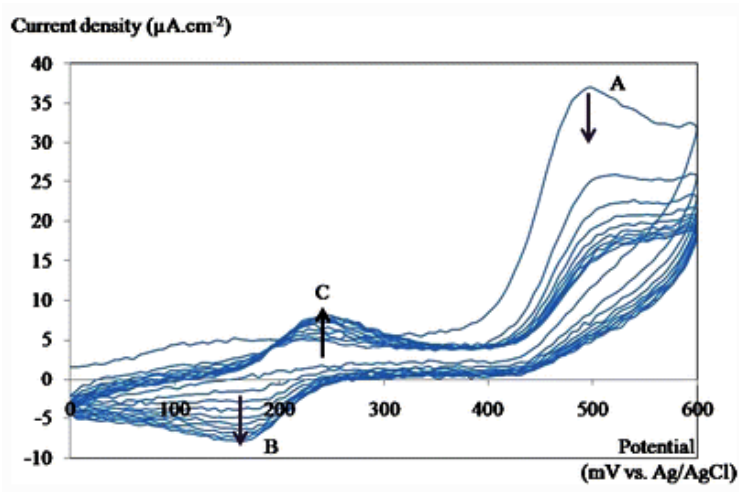


Figure 148: CVs showing the polymerisation of luminol on modified screen printed graphite working electrode proposed by Leca-Bouvier et al. the polymerisation has been performed in 0.1 M phosphate/0.1 M KCl at pH 6.0 in the presence of 1 mM luminol with 20 scans and at 100 mV s⁻¹ scan rate [403].

In this work, an electro-polymerisation in buffered alkaline solution of luminol is proposed to obtain an ECL-active polymer on the surface of the GCE working electrode. Two approaches have been tested to achieve the best performances of the biosensor for the detection of hydrogen peroxide:

1. The monolayer system based on the diffusion and polymerisation process forming a polymer into the alginate hydrogel. In this way the polyluminol is in direct contact with the enzyme encapsulated into the hydrogels.
2. The bilayer system composed of two layers deposited on the GCE. The first is obtained by the electropolymerisation of luminol directly of the electrode surface and the second consists in the drop-casting of the hydrogel containing the encapsulated enzyme.

For both the systems, different number of CV scans have been studied finding that the best film formed was for 20 scans. The CV scans have been applied in the voltage range between 0-1 V versus Ag/AgCl reference electrode at 0.05 V s⁻¹ scan rate anticipated by 5 mins of magnetic stirring. The electrolytic solution is composed of 0.1 M PBS/0.1 M KCl at pH 8.0 and 0.2 mM luminol from the luminol/KOH stock solution.

As for Sassolas' group, it is possible to observe the three peaks related to the behaviour of the monomer and polymer during the electro-polymerisation. A) indicates the consumption of the monomer decreasing with the number of scans; B) and C) are instead related to the growth of the film of the GCE surface. B indicates the reduced form of the poly(luminol) and C the oxidised with an increasing current density with the number of scans. Differently from Sassolas' et al. this procedure has been performed in alkaline buffered solution at lower scan rate and with a lower concentration of luminol in solution.

For both the systems, the ECL properties of the polymer have been tested by adding different concentrations of hydrogen peroxide building in this way a calibration curve. The ECL responses shown in Fig.149 show a completely different behaviour of the poly(luminol) formed in monolayer case into the Alginate hydrogel matrix and in the case of a bilayer system on the GCE surface. For the monolayer system, the calibration curve is not linear with the increase of the H₂O₂ concentrations added to the PBS solution. Furthermore, the repetitions with different GCEs were not consistent as the Hydrogel deposited onto the electrode surfaces detached during the ECL experiments interrupting thereby the measurements. This behaviour is due to the high weight of the hydrogel containing the poly(luminol) inside the matrix.

In the case of the bilayer system instead, the hydrogel is deposited on the polymer film creating two layers on the GCE surface. The calibration curve obtained shows a growth in the ECL intensity which raises with the addition of the hydrogen peroxide concentrations in solution.

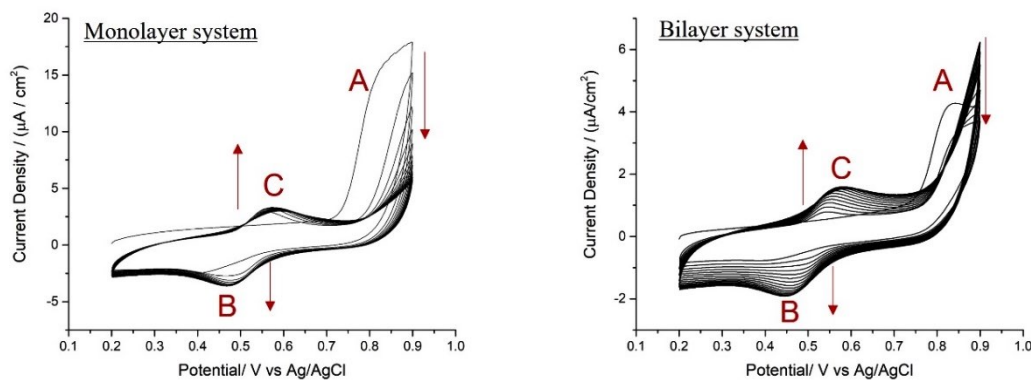


Figure 149: Electro-polymerisation of 1 mM luminol in 0.1 M PBS/KCl at pH 8.0. 20 scans at 50 mV s^{-1} of scan rate showing the three peaks related to the consumption of the monomer (A) and the redox couple of the growing polymer film.

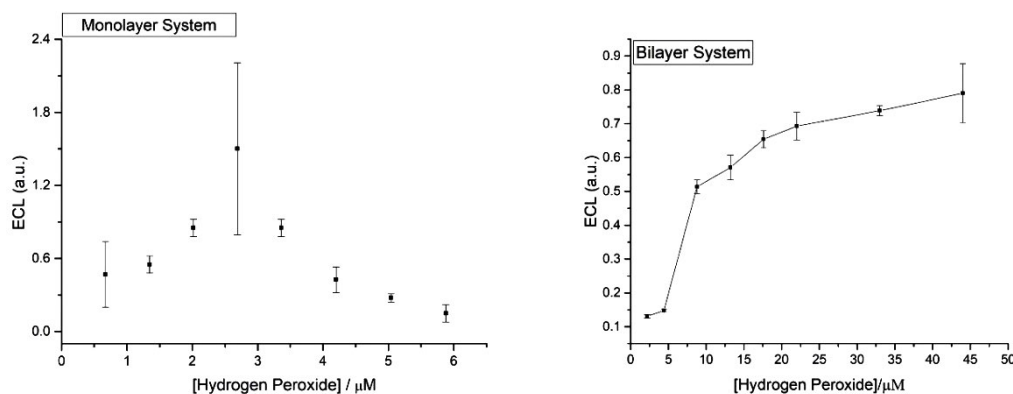


Figure 150: ECL response of the monolayer system (top) and bilayer system (bottom) showing a completely different behaviour of the polyluminol. The two calibrations curves have been obtained for different concentrations of hydrogen peroxide added to the 0.1 M PBS at pH 9.0. Scan rate 0.05 V s^{-1} . Error bars represent triplicate data points.

Thanks to these preliminary results, the bilayer system configuration has been chosen for the development of the ECL-biosensor based on polyluminol for the detection of enzymatic activity. In Fig.151 the calibration curves obtained for different number of scans are reported. The polyluminol has been formed on the GCE surface applying potentials in the range between 0-1 V versus Ag/AgCl reference electrode at 0.05 V s^{-1} scan rate. The electrolytic solution is composed of 0.1 M PBS/0.1 M KCl at pH 7.4 and 0.2 mM luminol from the luminol/KOH stock solution. Prior the electro-polymerisation process, the electrolytic solution is mixed for 5 minutes by magnetic stirring. By studying the calibration curves, it is possible to find that the best ECL-behaviour is observed for the polyluminol formed with 20

and 30 number of scans. In these cases, the signal rinses with the increase of different concentrations of hydrogen peroxide added to the solution of 0.1 M PBS at pH 9.0. For the development of the ECL-biosensor, 20 scans have been used to polymerise luminol on the electrode surface due to the low standard deviation. Furthermore, the ECL-signal shows a continuous increase with the H₂O₂ concentrations instead in the case of the 30 scans the signal reaches a plateau starting then to drop. In this case the signal is also defined by a higher standard deviation compared the case of 20 scans.

For the other cases instead the relation between the ECL-intensity and the H₂O₂ concentrations is not linear showing high standard deviations.

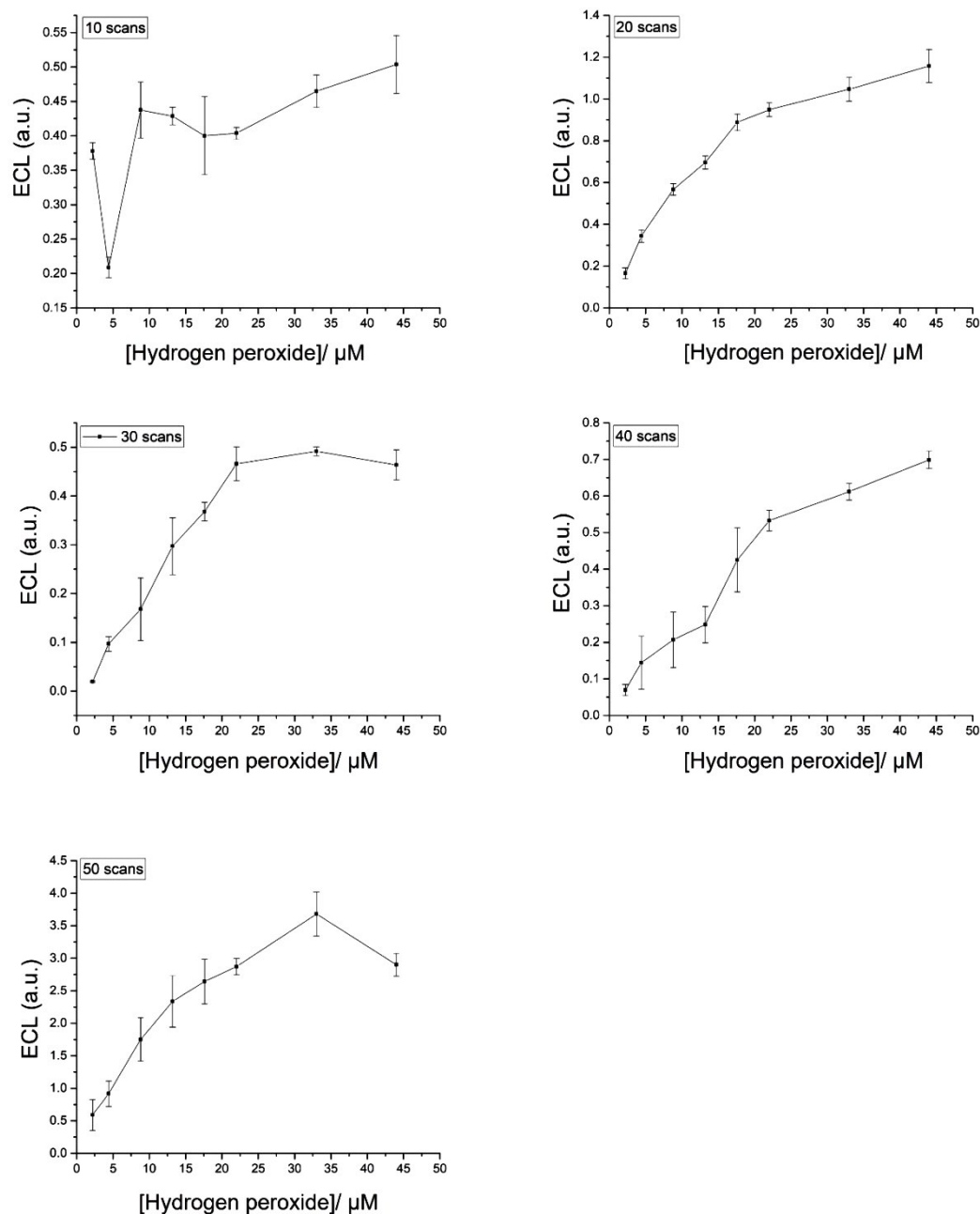


Figure 151: Calibration curves of bilayer systems obtained for different number of scans. Different concentrations of hydrogen peroxide have been added to test the ECL-properties of the polyluminal. Scan rate 0.05 V s^{-1} . Error bars represent triplicate data points.

Different pH tests have been performed to select the best conditions for the polymerisation of luminol on the GCE. Sassolas' group obtained an ECL-active film by electro-polymerisation in acidic solutions and near-neutral conditions as shown above. The procedures have been performed at different pH from 1.5 to 9.0 by adjusting the pH level adding NaOH and HCl to establish the best conditions to generate an ECL-active polymer. After the polymerisation

using 20 CV scans in the potential range between 0-1 V, the ECL properties have been studied by adding different concentrations of hydrogen peroxide in the 0.1 M PBS at pH 9.0. For polymerisation at low pH values an ECL signal can be observed characterised by an initial increase of the ECL intensity followed by a decrease of signal for higher H₂O₂ concentrations. For more alkaline pHs instead, the ECL signal linearly increases with the hydrogen peroxide concentrations showing a more stable polymer with the same ECL properties of its monomer (Fig. 152).

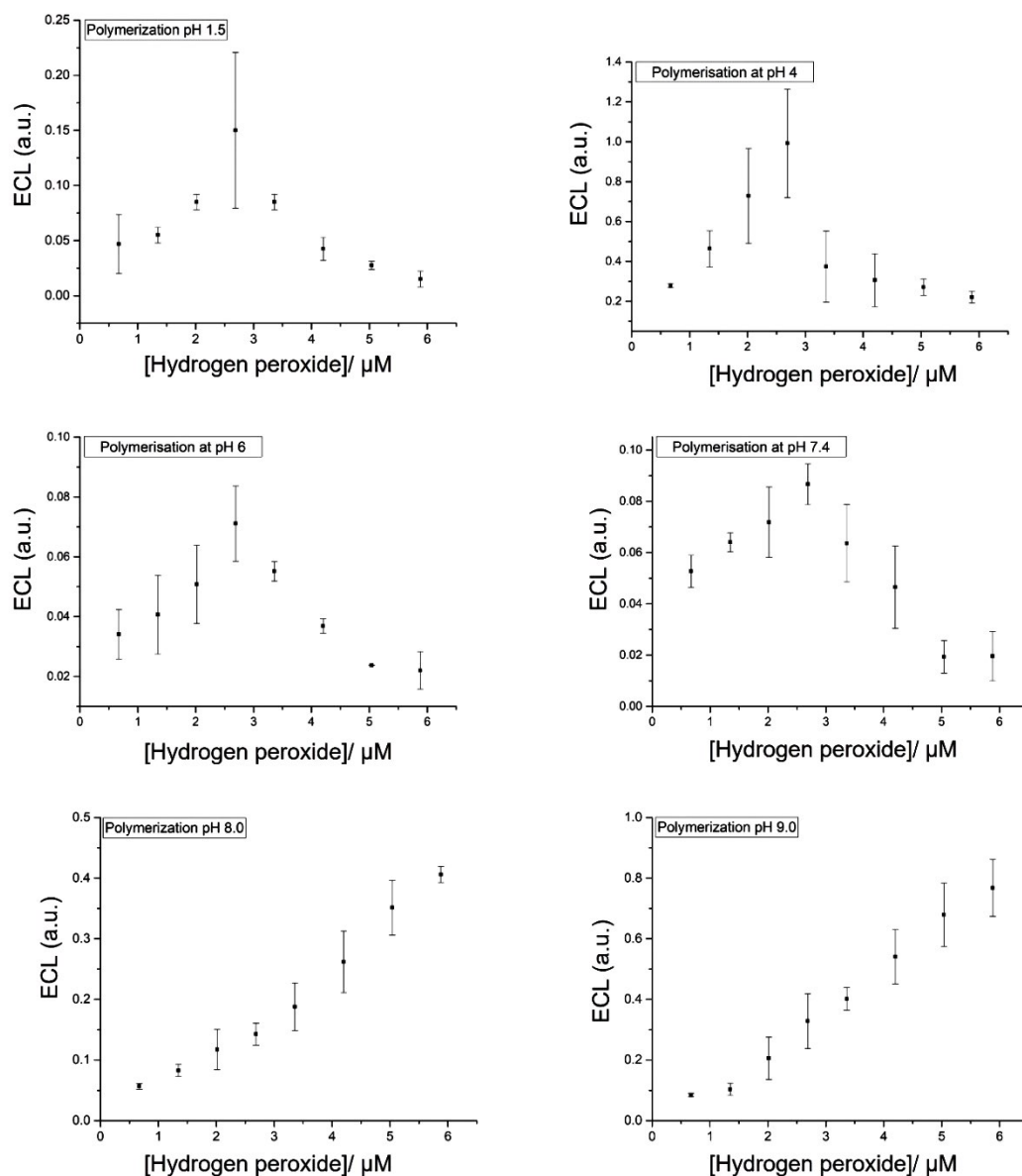


Figure 152: Calibration curves for the different polymerisation performed at different pHs of 0.1 M PBS/0.1 M KCl. The curves have been obtained by studying the ECL signal at different concentrations of hydrogen peroxide added to the electrolyte solution. Scan rate 0.05 V s⁻¹. Error bars represent triplicate data points.

The results in Fig.152 show that the electro-polymerisation performed at more alkaline pHs allows the formation of more stable films able to produce a linear ECL signal in response to the addition of different concentrations of hydrogen peroxide in the electrolytic solution. The ECL tests have been performed in 0.1 M PBS at pH 8.0 with 10 seconds of magnetic stirring between each H₂O₂ concentration.

For the development of the biosensor based on polyluminol, a film has been formed on the GCE surface by applying a voltage in the range between 0-1 V and 20 scans at 0.05 Vs⁻¹ of scan rate. The electrolytic solution was composed of 0.1 M PBS/0.1 M KCl pH 8.0 with the addition of 0.2 mM of luminol from the luminol/KOH stock solution. After the polymerisation, the GCE has been washed with deionised water removing the excess remained after the polymerisation and then left to dry at room temperature. 3 µL of Alginate Hydrogel containing the immobilised enzyme have been drop-casted on the polyluminol layer allowing then a first dry at room temperature followed by the cross-linking process by depositing the D-Glucono-1,5-lactone [117] and waiting for the second dry overnight. The modified GCE with a bilayer system was ready for the ECL tests in 0.1 M PBS by adding the corresponding substrate for the entrapped enzyme.

8.3 Polyluminol: Results and Discussion

For each enzyme encapsulated into alginate hydrogels, a double-layer system has been built on GCEs surface to be tested. In this section, the results for each enzyme are reported studying the limit of detection and quantification and comparing the results with the biosensor based on luminol in solution.

8.3.1 HRP-polyuminol- H_2O_2 hydrogel bilayer system

Considering the same conditions described in chapter 5, the modified GCE with peroxidase enzyme has been studied in 0.1 M PBS at pH 9.0. The hydrogen peroxide added to the electrolytic solution is degraded by the encapsulated HRP to obtain water and oxygen. By increasing the concentration of H_2O_2 the amount of oxygen produced raises generating the peroxide that reacts with the polyuminol on the electrode surface. The calibration curve in Fig. 153C shows the increment of the ECL intensity with the increment of the amount of hydrogen peroxide added to the solution as expected.

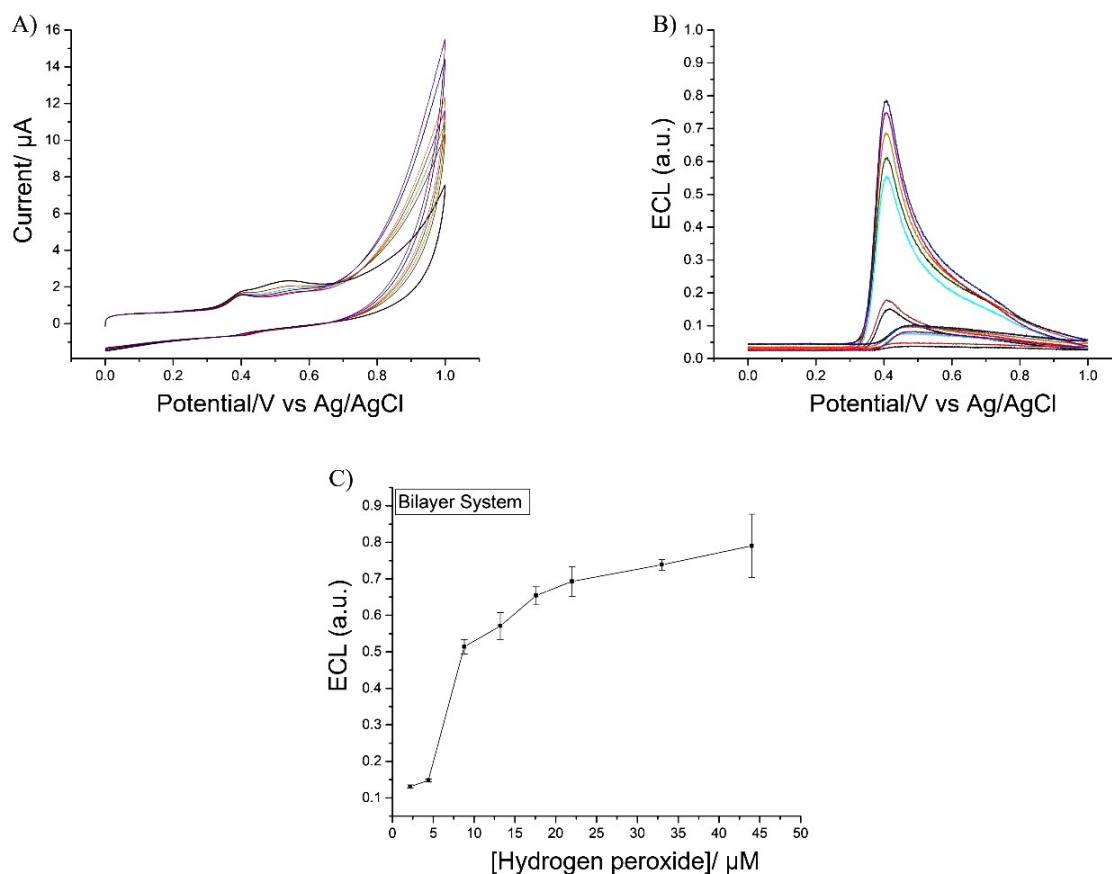
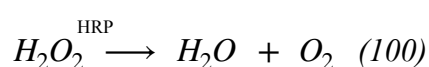


Figure 153: HRP bilayer system. A) CV at different concentrations of H_2O_2 . B) ECL of the polyuminol deposited on the GCE. C) Calibration curve of the increment of ECL signal corresponding to the increase of H_2O_2 produced. Scan rate 0.05 V s^{-1} . Error bars represent triplicate data points.

8.3.2 GOx-polyluminalol-glucose hydrogel bilayer system

After the deposition of the polyluminalol film and the deposition of the glucose oxidase hydrogels, the ECL and CV tests have been performed in PBS 0.01 M at pH 9 with the addition of different concentrations of glucose after a magnetic stirring of 10 seconds. As for the experiments reported in Chapter 5, the ECL signal linearly rises with the increment of the substrate in solution due to a growth of hydrogen peroxide at the electrode surface. The calibration curve in Fig.154C shows this behaviour obtained by the statistical analysis of three repetitions with different GCEs.

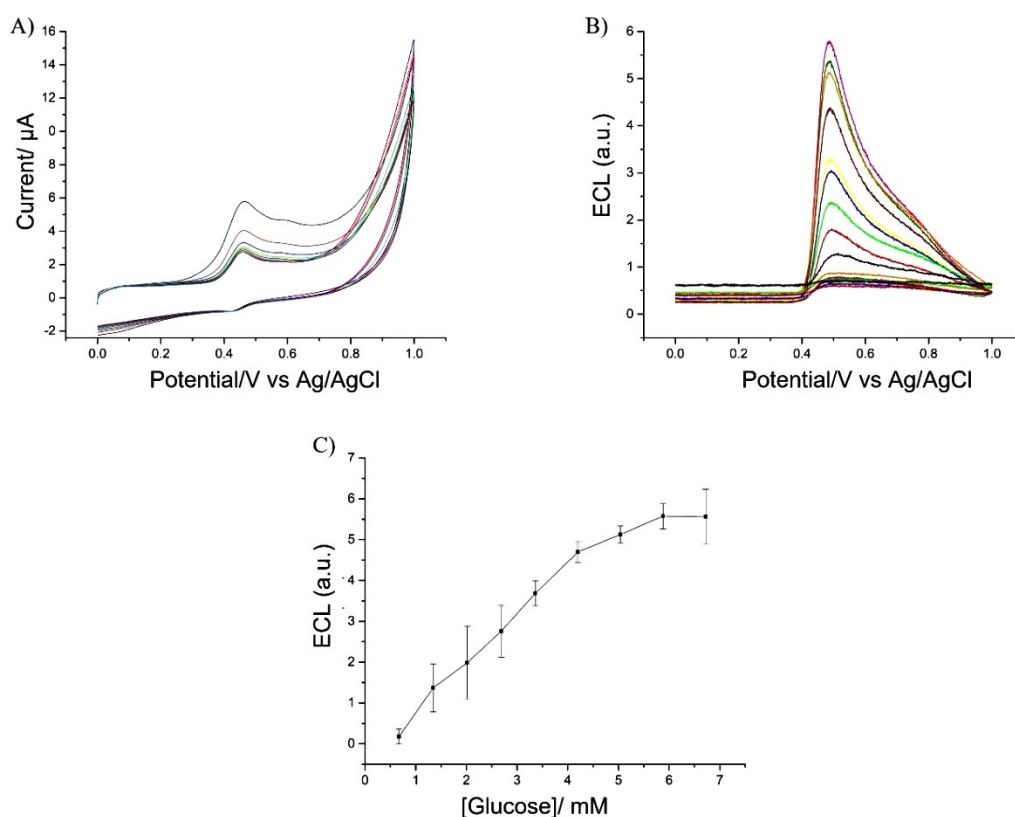
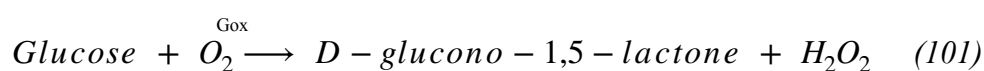


Figure 154: GOx bilayer system. A) CV at different concentrations of glucose in 0.01 M PBS pH 9.0. B) ECL signal of polyluminalol on the GCE. C) Calibration curve of the increment of ECL signal corresponding to the increase of the glucose in solution. Scan rate 0.05 V s⁻¹. Error bars represent triplicate data points.

8.3.3 LOx-polyluminal-lactic acidhydrogel bilayer system

The immobilised lactate oxidase enables the oxidation of 1 μM of L-lactic acid to pyruvate and H_2O_2 in PBS at pH 7.4. The addition of different concentrations of lactic acid in the electrolytic solution allows an increase of the ECL signal as reported in Fig.155.

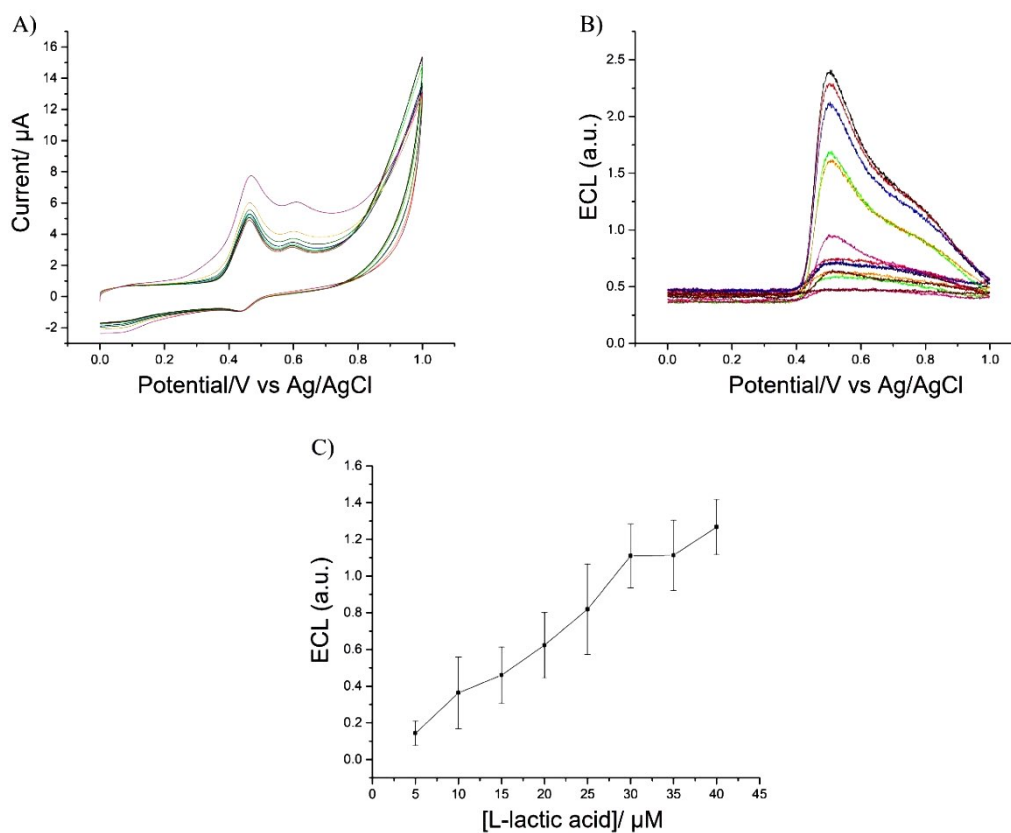
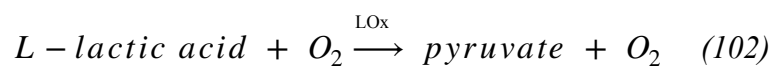


Figure 155: LOx bilayer system. A) CVs curves obtained at different concentrations of L-lactic acid added in 0.1 M PBS at pH 7.4. B) ECL signal obtained from the reaction of the hydrogen peroxide and the polyluminal film deposited on the GCE surface. C) Calibration curve of the ECL signal showing an increase in the ECL signal corresponding to the increase of the corresponding substrate added to the electrolytic solution. Scan rate 0.05 V s^{-1} . Error bars represent triplicate data points.

8.3.4 ChOx-polyluminal-cholesterol hydrogel bilayer system

The ECL tests for the encapsulated cholesterol oxidase have been performed in 0.01 M PBS/0.01 M NaCl at pH 9.0 with the addition of different concentrations of cholesterol. The substrate has been dissolved in a 2% surfactant solution of Triton-X 100 by heating till 50°C. The solution obtained has been then slowly diluted in PBS 0.01 M at pH 7.4 obtaining a final concentration of 2 mM. With the addition of different concentrations of cholesterol in solution, the ECL signal increases due to a production of hydrogen peroxide from the redox. The statistical analysis has been calculated on the results of different GCEs to build the calibration curve in Fig.156C) showing the behaviour of the bilayer system based on polyluminal film electro-polymerised on the electrode surface.

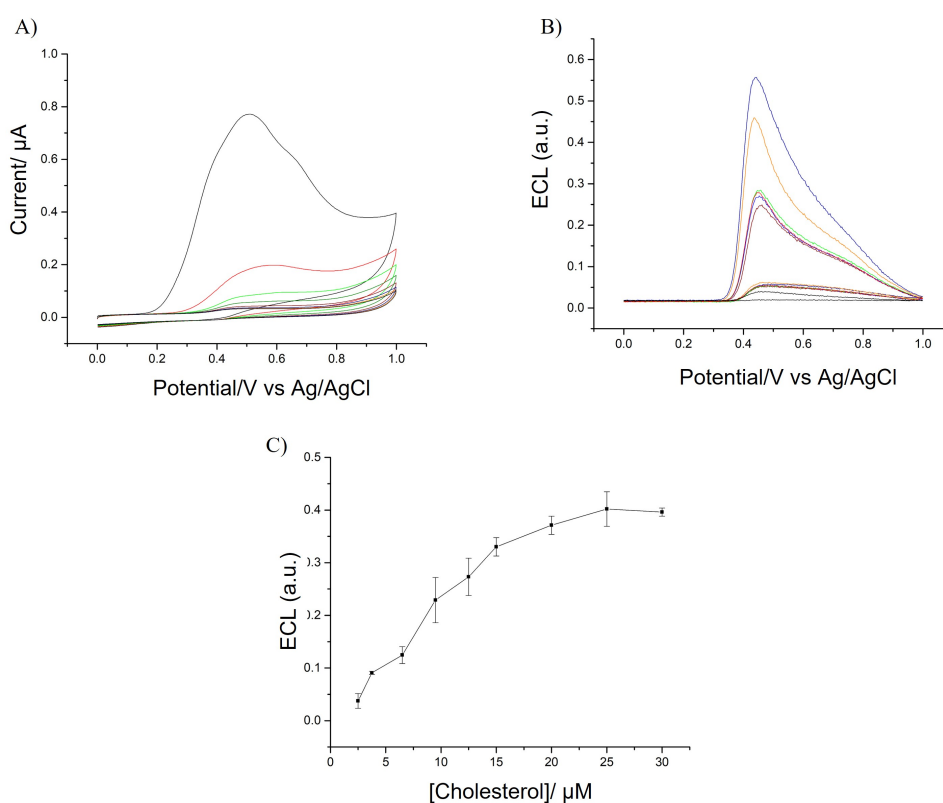


Figure 156: ChOx bilayer system. A) Voltammograms obtained at different concentrations of cholesterol in 0.1 M PBS at pH 8.0. B) ECL signal obtained from the reaction of the H_2O_2 produced by the redox reaction and the polyluminal film deposited on the GCE surface. C) Calibration curve of the ECL signal showing an increase in the ECL signal corresponding to the increase of the cholesterol. Scan rate 0.05 V s^{-1} . Error bars represent triplicate data points.

8.3.5 Comparison luminol-polyluminol

The results obtained with the use of polyluminol formed on the electrode surface have been compared with the results obtained using luminol in solution. The ECL tests with 0.2 mM of luminol in solution reported in chapter 5, show a linear behaviour of the biosensor with an ECL curve that rise with the increase of the amount of substrate added to the solution. For the polyluminol tests instead, the luminophore is not in the electrolytic solution but deposited on the electrode surface and in direct contact with the hydrogel containing the enzyme. The polymerisation of luminol, as described above, have been performed by applying continuous CV cycles to 0.2 mM of luminol from the stock solution of luminol/KOH. After this process, the concentration of luminol in the polymer is lower than the one adopted for the luminol in solution tests. Furthermore, the hydrogen peroxide produced must encounter the polyluminol to generate the emission of light. For each enzyme the ECL calibration curve raises with the augment of the corresponding substrate added to the solution, showing the successful production of hydrogen peroxide hence the following interaction with the polyluminol.

In all the cases, the polyluminol systems have a lower ECL intensity compared to the ECL signal achieved with the luminol in solution. This aspect could be the result of different factors such as the luminol concentration involved in the two different biosensors, the interaction between the produced hydrogen peroxide and the oxidised form of the luminophore. These aspects interfere also with the standard deviation that is higher in the polyluminol systems than luminol. In fact, once the hydrogen peroxide is produced, it ought to interact with the oxidised form of the luminol to produce light and so the ECL emission. In the case of the luminol dissolved in solution, the interaction occurs more easily than the case of polyluminol, as both the species are in the electrolytic solution. In the polyluminol case instead, the hydrogen peroxide must reach the polyluminol film on the electrode surface, enter the polymer chain and then interacts with it (Fig.157).

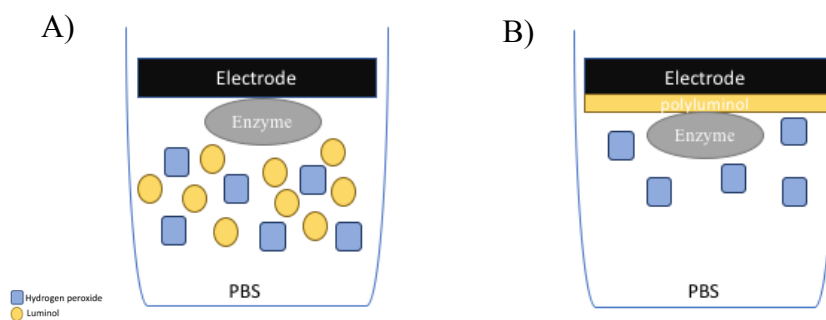


Figure 157: Schematic representation of the two systems developed in this research. A) Representation of the ECL-based biosensor with the use of luminol in solution (yellow parts); B) representation of the ECL-based system with the use of poly(luminol) electro-deposited on the GCE surface.

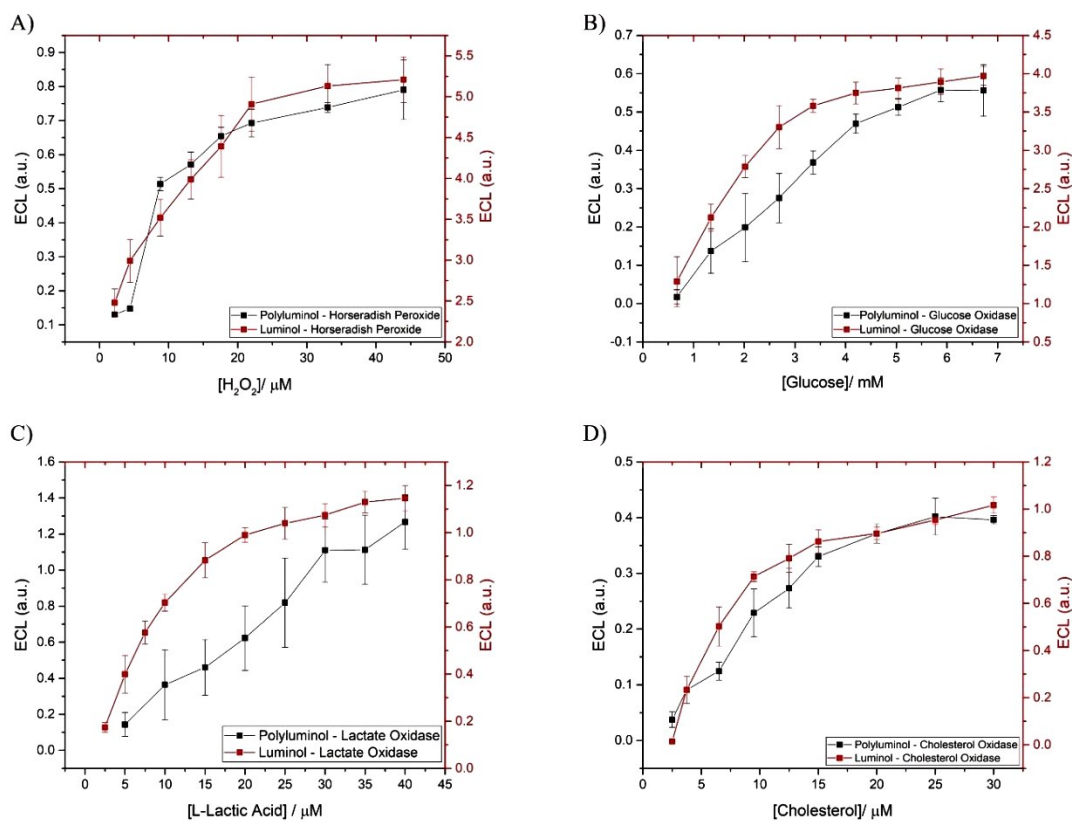


Figure 158: Comparison between the calibration curves of the results obtained from the luminol in solution and poly(luminol) tests. Scan rate 0.05 V s^{-1} . Error bars represent triplicate data points.

8.3.6 HRP-polyuminol- H_2O_2 cryogel bilayer system

The electro-polymerisation of luminol on the GCE surface has been used also to study the activity of enzymes encapsulated into cryogel matrices.

With the addition of different concentrations of hydrogen peroxide at the electrolytic solution (0.01 M PBS at pH 9.0) also the ECL signal increases. This behaviour has been studied on different repetitions applying the same conditions of encapsulation, polymerisation, and electrochemical measurements. The statistical analysis shows that the encapsulated enzyme responds to the variation of substrate concentrations as the study of luminol in solution (Fig. 159).

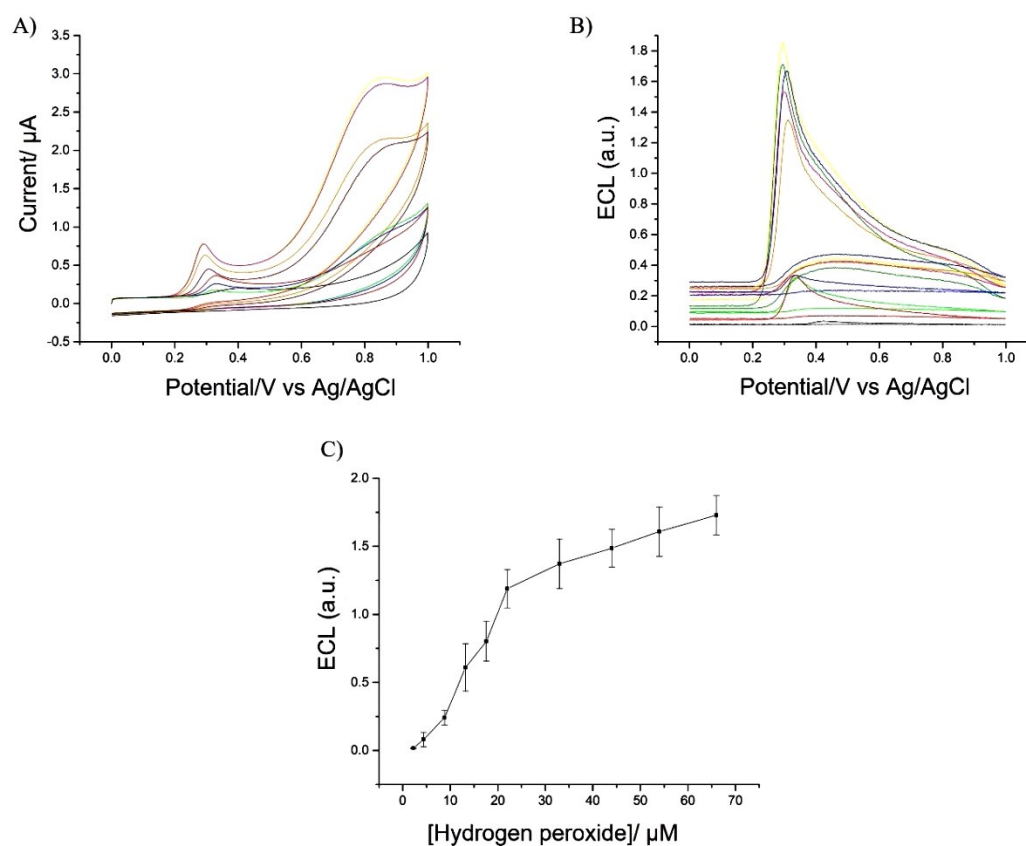


Figure 159: CV and ECL plots of the HRP-cryogel-polyuminol bilayer system at different concentrations of hydrogen peroxide in solution. C) Calibration curve studying the dependence of the ECL intensity from the substrate concentrations. Scan rate 0.05 V s^{-1} . Error bars represent triplicate data points.

8.3.7 GOx-polyuminol-glucose cryogel bilayer system

In this section, the results obtained for the GOx encapsulated into cryogels system and immobilised on the GCE forming a bilayer system with the polyuminol film are reported. The CV and ECL tests have been performed observing the same conditions of the luminol in solution tests using the same range of concentrations of glucose added to 0.01 M PBS pH 9.0. The ECL signal increases with the addition of glucose in solution showing a sigmoidal behaviour reported in the calibration curve in Fig.160C.

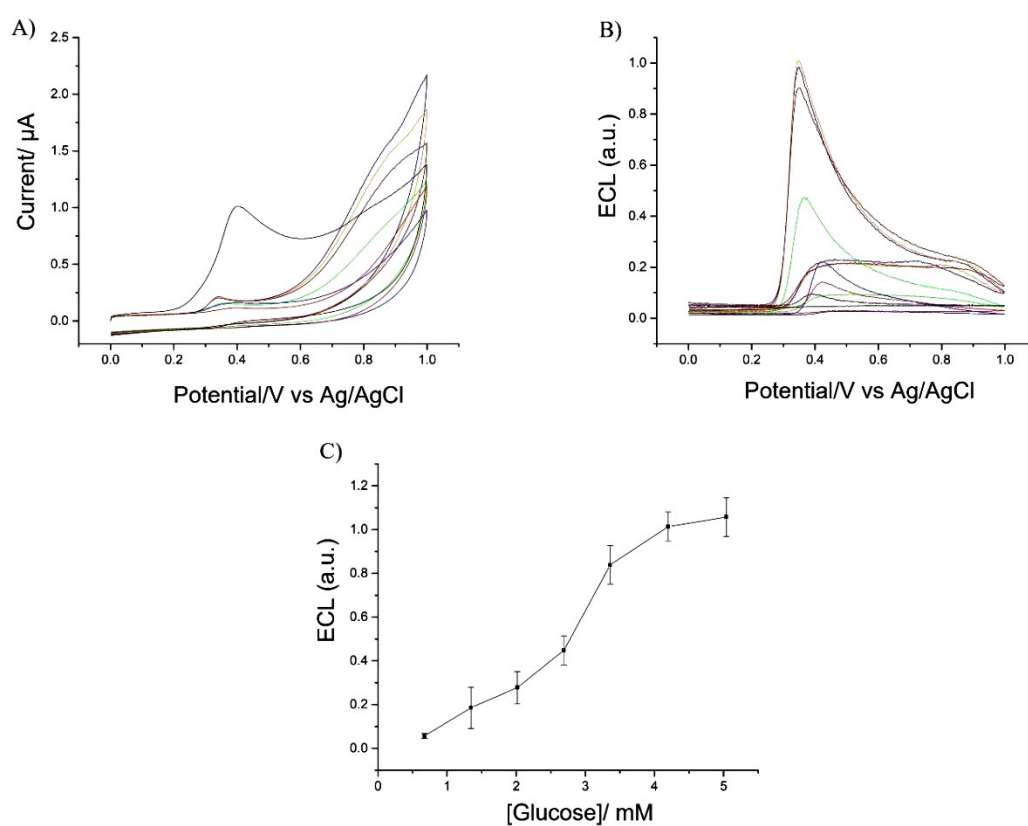


Figure 160: CV and ECL results of the GOx-cryogels-polyuminol bilayer system in 0.01 M PBS at pH 9.0 (A, B); calibration curve of the system showing the dependence of the ECL signal from the different concentrations of glucose in solution. Scan rate 0.05 V s⁻¹. Error bars represent triplicate data points.

8.3.8 LOx-polyuminol- L-lactic acid cryogel bilayer system

The LOx-cryogel-polyuminol system has been studied in 0.01 M PBS at the optimum pH (pH 7.4) for the enzyme to produce hydrogen peroxide by reacting with the substrate L-lactic acid. In Fig. 161B the ECL results are reported for different concentrations of L-lactic acid. It is possible to notice that a shift in the potential axis occurs with the increase of the substrate amount added. This is also noticeable in the results obtained for the LOx encapsulated into hydrogels and cryogels with luminol in solution. This behaviour could be due to a slight change of the pH during the tests as result of the increase of L-lactic acid in solution. In fact, at the end of each electrochemical tests the final pH of the electrolytic solution is decreased from the initial pH pf 7.4 to the final value of 7.1-7.2.

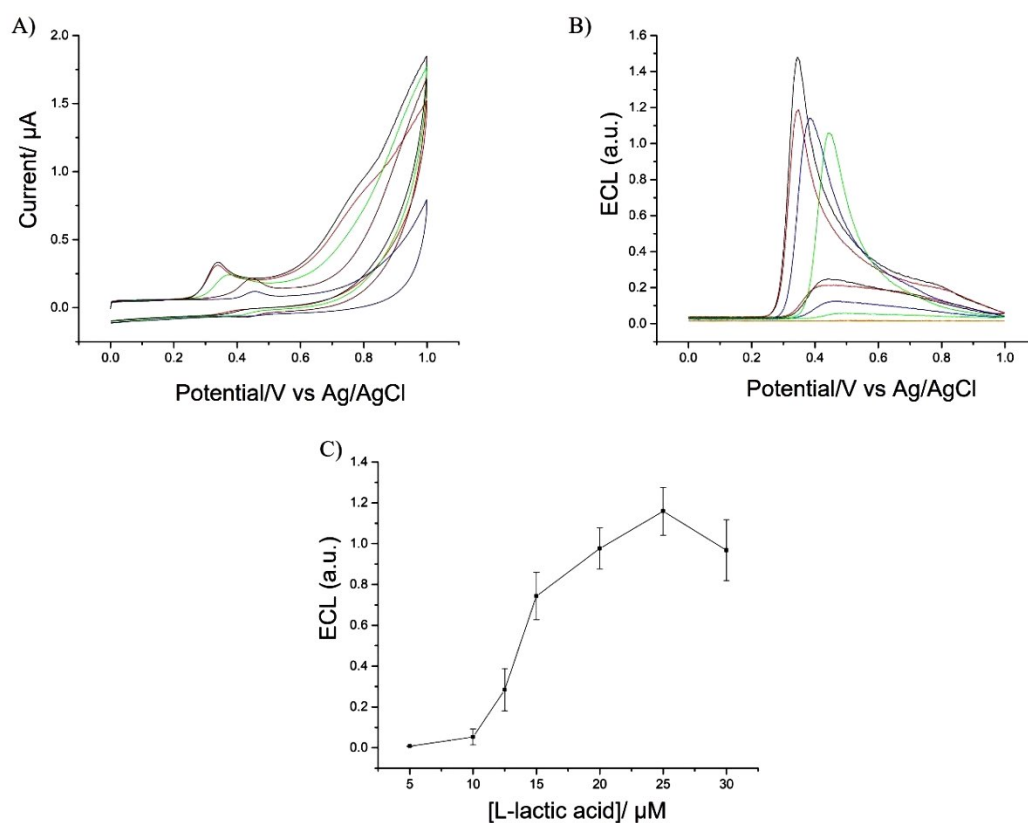


Figure 161: CV and ECL plots of the study of the enzymatic activity of LOx encapsulated into cryogel with the presence of polyuminol film on the GCE surface (A, B); calibration curve obtained from the statistical analysis of three repetitions of the ECL tests. Scan rate 0.05 V s⁻¹. Error bars represent triplicate data points.

8.3.9 ChOx-polyuminol- cholesterol cryogel bilayer system

The ChOx-cryogel-cholesterol bilayer system was studied following the same conditions for luminol in solution, *e.g.*, 0.01 M PBS and pH 9.0, which has been confirmed to be the optimal pH for the cholesterol oxidase to produce hydrogen peroxide in the presence of cholesterol. Also, in this case, by increasing the cholesterol concentration in solution, the ECL signal rises (Fig. 162).

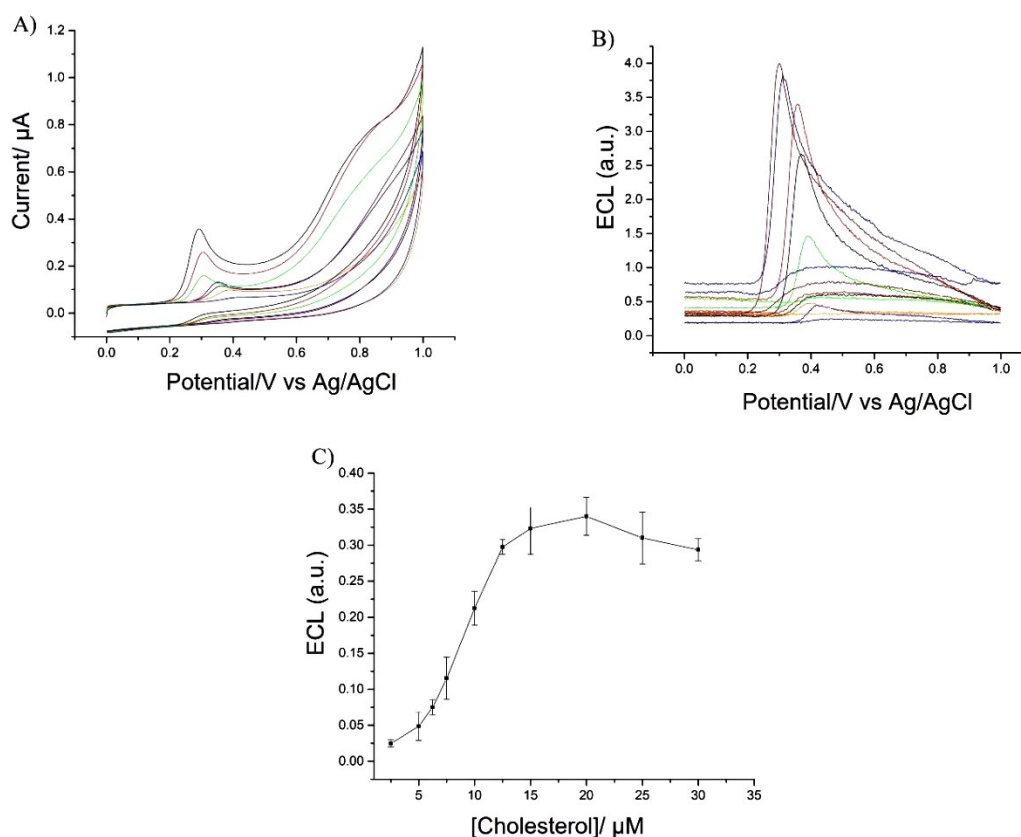


Figure 162: CV and ECL results for the ChOx-cryogels-polyuminol bilayer system in 0.01 M PBS at pH 9.0 (A,B). C) Calibration curve obtained for different concentrations of cholesterol added to the solution. Scan rate 0.05 V s⁻¹. Error bars represent triplicate data points.

8.3.10 Comparison luminol-polyluminol cryogel bilayer system

The results obtained with the bilayer system composed of a first layer of polyluminol and a second layer of cryogel containing the enzyme, generally show how the enzymatic activity allows the production of hydrogen peroxide during the redox reactions with the corresponding substrate and so the generation of an ECL signal. These results have been compared in this section with the ones reported in chapter 6 where the cryogels system was analysed with the 0.2 mM of luminol in dissolved into the electrolytic solution. For all the systems the ECL signal increases with the increment of the corresponding substrate concentrations in solution even if the calibration curves show that the ECL intensity is lower than the systems analysed with the luminophore in solution This aspect could be the result of the fact that to react with the luminophore, the generated H_2O_2 must enter the polymeric matrix, instead of freely interact with the luminol dissolved in solution.

Furthermore, it is known that the PMT, positioned close to the GCE surface, can capture all the photons emitted exclusively at the electrode surface. In the case of the bilayer system, the electrode of the GCE is composed of two layers (polyluminol + cryogels) with a final thickness higher than the luminol in solution system.

It is noticeable in all the systems, that after a linear increase of the ECL signal with the substrate concentrations, the curves start to decrease for higher concentrations. This behaviour is not shown in the case of the luminophore in solution probably because the luminol is present in the electrolytic solution with a concentration of 0.2 mM instead the polyluminol has a lower concentration. In some cases, the tests have been interrupted also because the bilayer system detached from the electrode surface due the high weight after the swelling of the cryogels (Fig. 163).

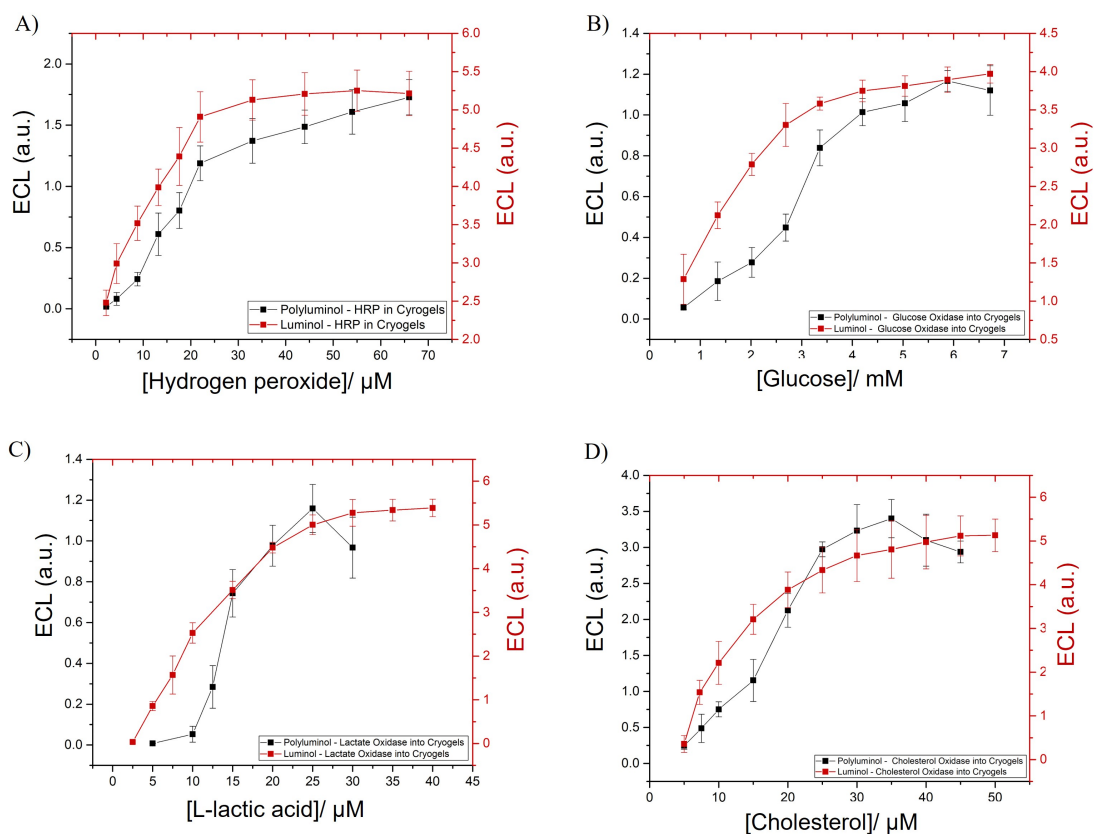


Figure 163: Comparisons of the calibration curves obtained from the statistical analysis of the cryogel-luminol systems and cryogel-polyluminol bilayer systems. A) HRP-cryogel-hydrogen peroxide systems, B) GOx-cryogel-glucose systems, C) LOx-cryogel-L-lactic acid, D) ChOx-cryogel-cholesterol systems. Scan rate 0.05 V s^{-1} . Error bars represent triplicate data point.

8.4 Modified GCE with Poly- $[\text{Ru}(\text{bpy})_3]^{2+}$

The electro-polymerisation technique has been applied also to the dehydrogenase- $[\text{Ru}(\text{bpy})_3]^{2+}$ system obtaining a compound whose properties are still subject of study. In this section, the electro-polymerisation of the luminophore is described and its characterisation by UV, FTIR, mass spectroscopy is proposed to establish if the material formed on the GCE surface is a polymer or oligomer. Furthermore, also the electrochemical properties are studied by detection of NADH produced during the redox reaction between the encapsulated enzyme and its corresponding substrate.

8.4.1 $[Ru(bpy)_3]^{2+}$ electro-polymerisation

The same principles seen for the poly(luminol) have been applied for the polymerisation of the $[Ru(bpy)_3]^{2+}$. In literature, there is no trace of reports regarding the possibility to polymerise such a luminophore, therefore all the results here reported are preliminary and need to be explored further.

Two electrolytic solutions have been tested to achieve the best conditions for the electro-polymerisation of $[Ru(bpy)_3]^{2+}$ and obtain an ECL-active material on the GCE surface: 0.1 M NaCl and 0.1 M acetonitrile.

The electro-polymerisation in 0.1 M acetonitrile has been performed with the addition of 2.5 mM of $[Ru(bpy)_3]^{2+}$ and 0.25 M of tetrabutylammonium hexafluorophosphate (TBAPF₆) used as supporting electrolyte to boost the conductivity in the electrochemical experiments in non-aqueous solutions. Different number of scans have been tested to determine the best conditions to obtain an ECL-active film. Considering that with the increase of the number of scans also the thickness of the film expands hence the distance from the GCE surface, scans from 10 to 100 have been tested obtaining that the best in terms of ECL properties was for 20 scans. In Fig. 164 the best ECL signal was obtained for 20, 30 and 40 scans of the 2.5 M $[Ru(bpy)_3]^{2+}$ in acetonitrile/TBAPF₆ solution. For higher number of scans the signal drastically decreases obtaining a very low and noisy ECL signal.

From this preliminary investigation, it has been noticed that each film electro-deposited on the GCE surface can emit only for one time after the addition of the substrate like TPrA or in this case NADH. After the emission, no more ECL signal can be detected for the film making the Poly- $[Ru(bpy)_3]^{2+}$ suitable for disposable biosensor performing only one test at the time. This property significantly distinguishes the two polymers obtained with the electro-polymerisation technique described in this thesis: poly(luminol) suitable for multiple tests on the same film and poly- $[Ru(bpy)_3]^{2+}$ for disposable biosensor.

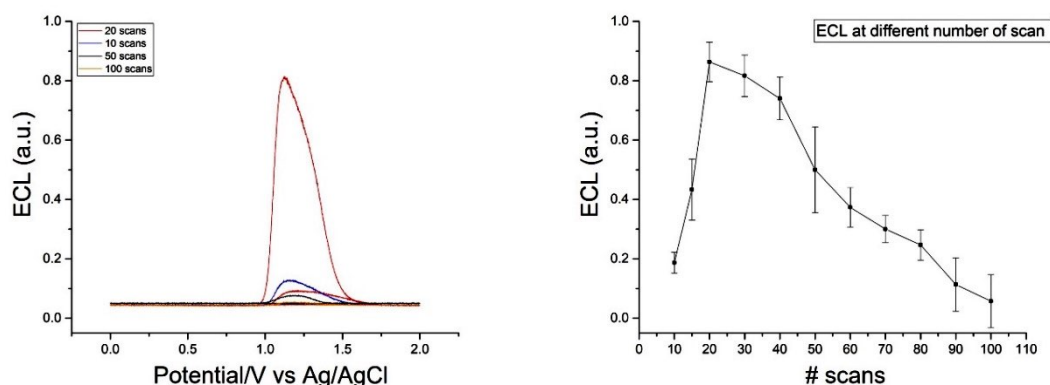


Figure 164: ECL results of the poly-[Ru(bpy)₃]²⁺ obtained for different number of scans (left). Calibration curve of ECL results obtained for three repetitions of each number of scans showing that the best signal is obtained for 20, 30 and 40 scans. Scan rate 0.05 V s⁻¹. Error bars represent triplicate data points.

Once defined the best number of scans to generate the film, different scan rate has been studied to identify which one can improve the ECL signal.

Scan rates in the range from 0.05 to 0.4 Vs⁻¹ have been tested for 2.5 mM [Ru(bpy)₃]²⁺ in 0.1 M acetonitrile/0.25 M TBAPF₆ solution in the potential range from -2 to 2 V for 20 scans. In all the cases reported in Fig.165, the peaks at 0.9 V and 1.5 V increase during the electro-polymerisation showing the possible formation of the film on the GCE electrode. Once the film was prepared and after a washing with DI water to remove the excess from the electrolytic solution, the GCE has been transferred in 0.01 M PBS to study the ECL with the addition of 5 μM TPrA. All the films generate only one ECL signal with a very high intensity with the best performances obtained at scan rate of 0.1 and 0.2 Vs⁻¹. In the case of electro-polymerisation at 0.4 mVs⁻¹ the signal was too high to be recorded with the PMT voltage settings obtained the underlined overflow of the channel.

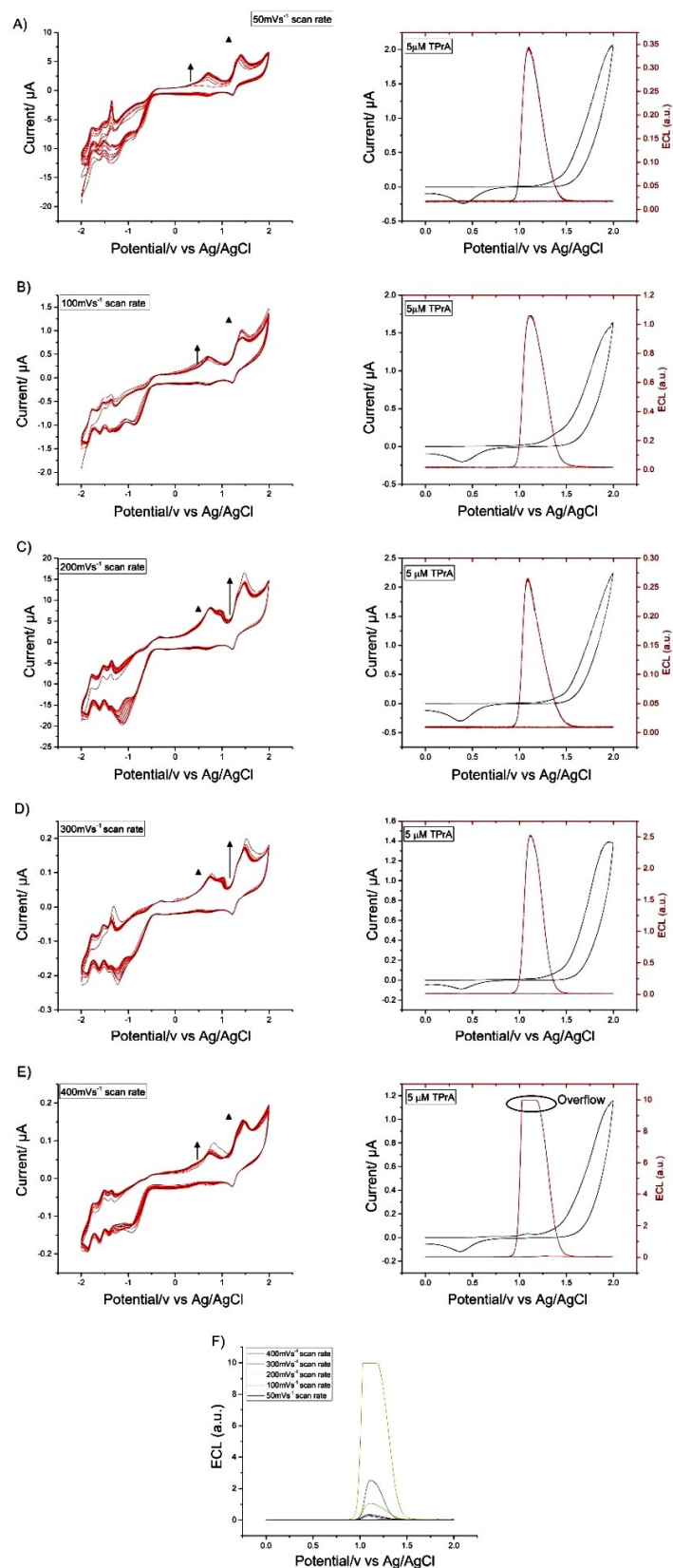


Figure 165: Electro-polymersation scans for the different scan rate from 50 to 400 mVs⁻¹ are reported with the corresponding ECL signal. (D) Comparison of the ECL signals for the different scan rate showing the best performance for 100 mVs⁻¹.

For these preliminary results the best conditions to form an ECL-active film of the GCE surface are 20 scans of 2.5 mM $[\text{Ru}(\text{bpy})_3]^{2+}$ in 0.1 M acetonitrile/0.25 M TBAPF6 solution in the potential range from -2 to 2 V.

8.4.2 Characterisation of the material: polymer or oligomer?

To understand the nature of the film formed with the electro-polymerisation of 2.5 mM of $[\text{Ru}(\text{bpy})_3]^{2+}$, the samples have been analysed with the UV and FTIR.

The UV tests have been performed using the film diluted in methanol. Firstly, the background of the solvent was scanned, then the monomer also diluted in methanol and finally the polymer solution (Fig. 166).

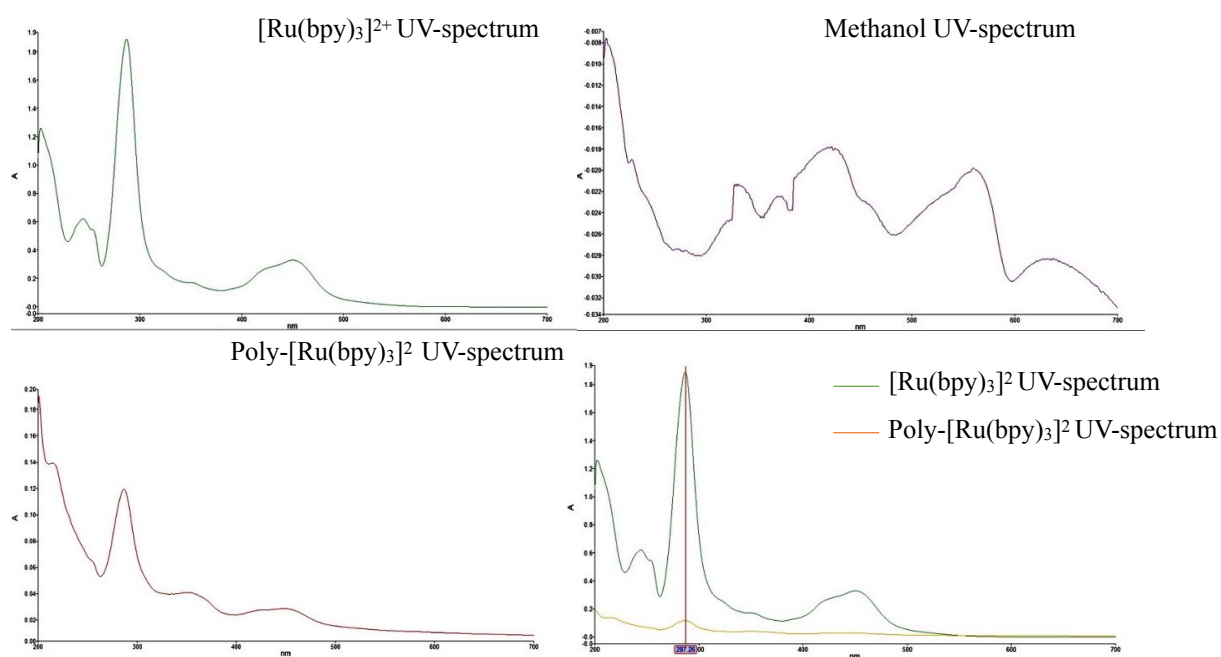


Figure 166: UVV results of the monomer and film diluted in methanol also scanned as background.

From the comparison of the monomer and the polymer, the characteristic peak appears at the same exact wavelength of 287 nm. This suggest that the film generated with the polymerisation is an oligomer with a small chain repeating the structure of the monomer and conserving its properties. This film in fact has the same ECL characteristics of the $[\text{Ru}(\text{bpy})_3]^{2+}$ with the emission at the same potential as demonstrated in the previous section.

One of the reasons responsible of the single emission of ECL could find a possible explanation in the small chain of the oligomer containing a small amount of aromatic group responsible of the chemiluminescent properties of the luminophore which instead has more aromatic groups in its molecular structure.

With the FTIR tests it was possible to identify the various functional groups composing the film. For this characterisation, the polymer has been dissolved in 1 mL MeOH which was then removed by evaporation first with compressed nitrogen and then leaving the sample under vacuum overnight (Fig. 167).

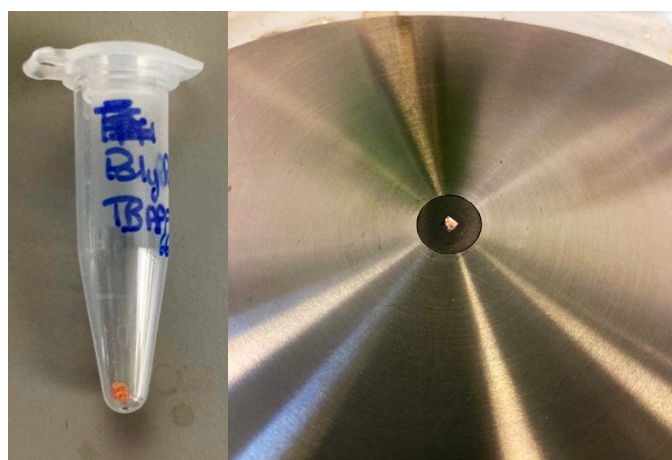


Figure 167: FTIR plate with the deposition of the film powder obtained after the evaporation overnight of the solvents. It is possible to notice that the film electro-polymerised conserved the red colour specific for the ruthenium compounds.

From the FTIR the peak related to the one present in the water scan is visible in both $[\text{Ru}(\text{bpy})_3]^{2+}$ and $\text{Poly-}[\text{Ru}(\text{bpy})_3]^{2+}$ (Fig. 168 red circle). In the monomer powder scan the characteristic three dentate pyridine's peaks are well visible, instead in the polymer this structure is wicker and slightly shifted but still present. All the other peaks of the polymer could be related with the one of the monomers, but with different intensity and in some cases shifted. Furthermore, in the polymer film a small peak related to acetonitrile and methanol is observable showing that probably the two solvents did not completely evaporate (Fig. 168 blue circle).

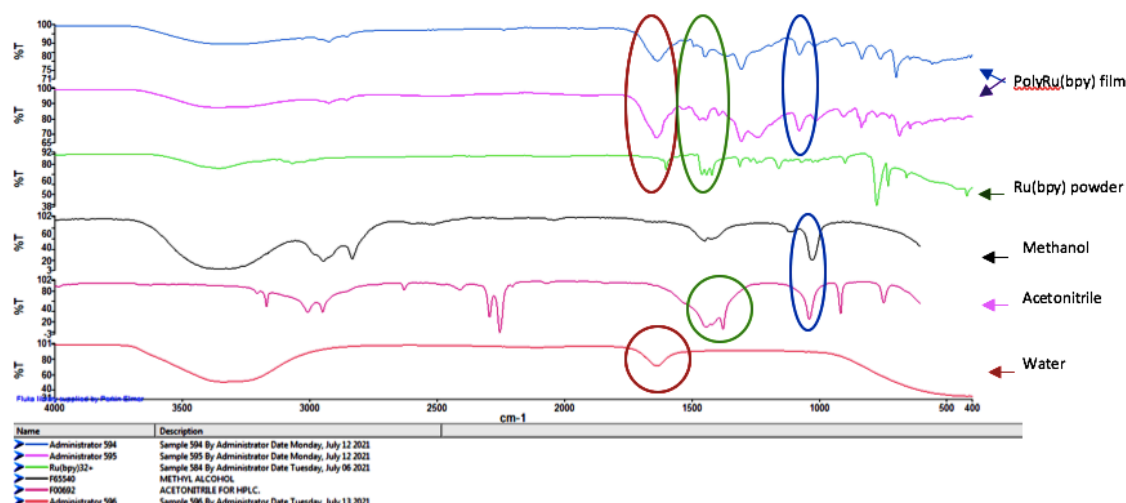


Figure 168: FTIR characterisation of different solvents and molecule which are involved in the generation of the Poly-Ru[(bpy)₃]²⁺ film on the GCE surface.

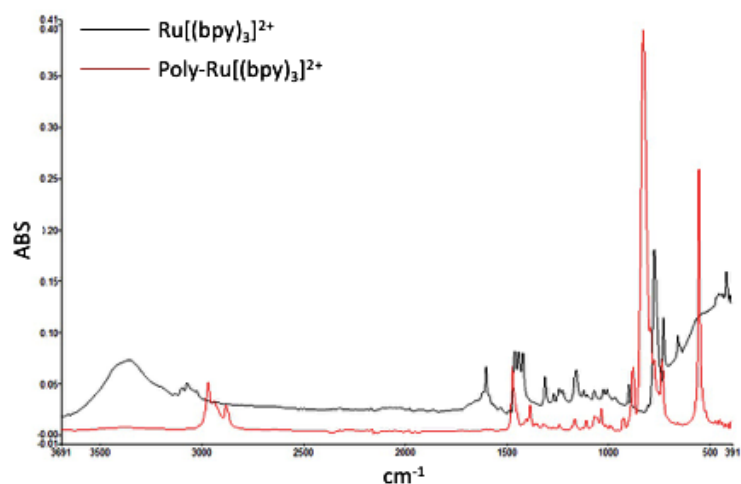


Figure 169: Comparison of the FTIR spectra of the monomer [Ru(bpy)₃]²⁺ and the oligomeric film electropolymerised.

8.5 Poly-[Ru(bpy)₃]²⁺-dehydrogenase system: Preliminary results

As for the polyluminal, the new material formed from the [Ru(bpy)₃]²⁺ electro-polymerisation has been tested with the dehydrogenase enzymes deposited on the GCE electrode surface forming a double layer system. The electro-polymerisation is first performed on a polished GCE following the conditions above described forming a first ECL-active layer and after the dry at room temperature, a second layer is built by depositing 3 μ L of Alginate hydrogels containing dehydrogenase enzyme encapsulated into the microsphere's cores.

As anticipated, the film can emit light just one time after been stimulated with the corresponding co-reactant that in the case of dehydrogenase system is produced after the redox reaction between enzyme and substrate in the presence of the co-factor NAD⁺ in solution. For this reason, to demonstrate the reliability of the proposed biosensor, three repetitions for each enzyme have been conducted by generating a new film each time on a clean GCE under the same conditions. Each enzyme is characterised by a specific pH at which can convert NAD⁺ into NADH and emitting so the ECL signal through the reaction with the luminophore. The results presented in Fig.170 show how the three repetitions give similar ECL emission for a specific amount of substrate added to the solution. From the plots representing the comparison between the ECL emission with [Ru(bpy)₃]²⁺ added to the electrolytic solution and the one generated by Poly-[Ru(bpy)₃]²⁺, the ECL-emission from the Poly-[Ru(bpy)₃]²⁺ shows higher intensity than the normal [Ru(bpy)₃]²⁺ for all the dehydrogenase systems herein analysed. These comparisons have been studied by confrontation of the same quantity of substrate added to the 0.01 M PBS containing 1 mM NAD⁺.

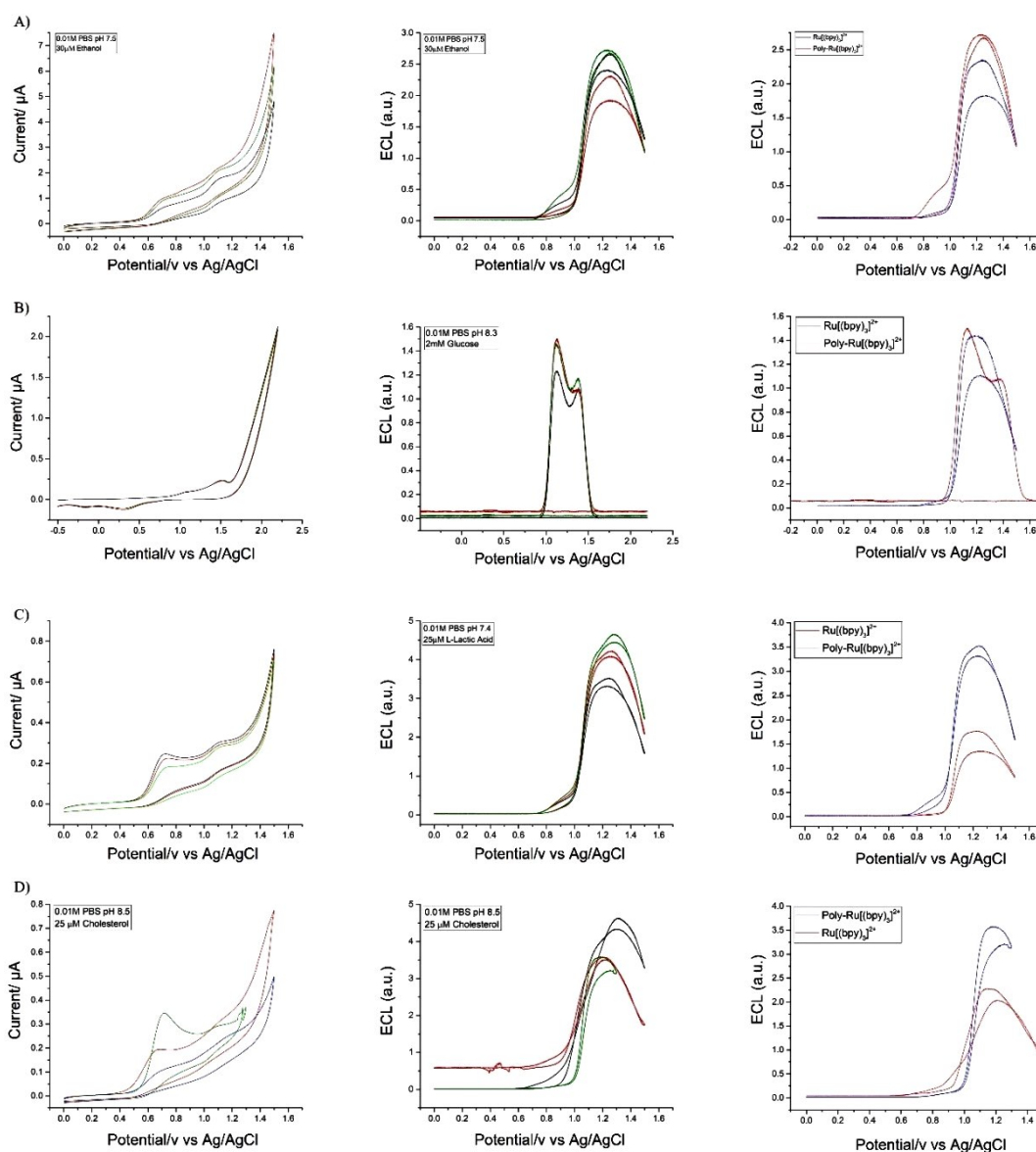


Figure 170: Results obtained for the four systems of dehydrogenase enzyme encapsulated into Alginate hydrogels and deposited on GCE in the presence of the Poly-[Ru(bpy)₃]²⁺ film forming a bilayer system. A) ADH-ethanol-poly-[Ru(bpy)₃]²⁺ system in the presence of 30 µM of ethanol; B) GDH-glucose-poly-[Ru(bpy)₃]²⁺ system with 20 mM of glucose; C) LDH-L-lactic acid-poly-[Ru(bpy)₃]²⁺ and 25 µM of substrate in solution and finally D) CDH-cholesterol-poly-[Ru(bpy)₃]²⁺ and 25 µM of cholesterol. Scan rate 0.05 V s⁻¹.

These preliminary results demonstrate the possibility of developing a disposable biosensor able to measure important parameters like cholesterol and glucose in a non-invasive way and real time by simply depositing on the sensitive area a small amount of sample.

8.6 Conclusions

In this chapter, the development of an ECL-active layer of luminophore on the WE surface permitted the detection of hydrogen peroxide and NADH reducing the number of analytes in the electrolytic solution. Further improvement of the electro-polymerisation technique will allow the development of a non-invasive probe composed of a bilayer system where the first layer is represented by the polyluminol or poly-[Ru(bpy)₃]²⁺ and the second by the encapsulated enzymes.

Two important parameters were investigated for the obtainment of the two materials: number of scans, and scan rate.

Polyluminol-based bilayer system was investigated with both the encapsulation materials, alginate hydrogels and cryogels, showing a slightly lower ECL signal compared to the ECL tests with luminol dissolved in the electrolytic solution. This aspect could have two explanations: limited diffusion of the generated hydrogen peroxide near the polyluminol film, and the concentration of the luminol into the polymeric chain. Despite these limitations, the ECL signal of each enzyme-system obtained for different concentrations of substrate introduced in solution still increases showing an efficient detection of hydrogen peroxide, therefore an indirect detection of glucose, lactic acid and cholesterol.

Poly-[Ru(bpy)₃]²⁺ systems are based on the same bilayer architecture. Despite the polyluminol sensor, the ECL-signal is limited to only one emission. The preliminary results show how the ECL-active film obtained after electropolymerisation in acetonitrile/TBAPF₆ solution allows the obtainment of a thin layer on the electrode surface able to emit light when reacted with NADH. UV-Vis and FTIR investigations suggest that the film could be related to an oligomer as it preserves the typical characteristic of the monomer. Further investigation needs to be done such as the study of mass spectrometry for the determination of the molecular weight of the formed material, and NMR spectrometry to define the atomic nucleus present in the structure of the material.

The aim of this work was the development of a non-invasive ECL-based biosensor for the detection of hydrogen peroxide and NADH. This last chapter offers an improvement of the already proved ECL-system offering an ECL-active probe composed of a first luminophore layer and an overlapping second layer hosting the enzymes encapsulated either in alginate

hydrogels or cryogels. The optimisation of this research can help for the development of a novel ECL biosensor for the self monitoring of clinically relevant parameters such as glucose, lactic acid and cholesterol.

Chapter 9: Conclusions and further investigations

Over the past decades, different studies have been carried out on the development of ECL biosensors and bioassays applicable in a variety of fields such as clinical diagnostics, environment, water treatment, food analysis, and chemical analysis. The main advantages of the electrochemiluminescence approach are the high specificity, sensitivity, simplicity of the architecture of the sensor, selectivity, fast response time, low detection limits and possibility of using very low amount of reagents when the luminophore is immobilised on the electrode surface. This aspect makes the ECL a potential low cost technique. The most used biological recognition element of the ECL-based sensor are enzymes, like oxidase and dehydrogenase, antibodies, aptamers, proteins able to selectively recognise their corresponding analyte and produce the coreactant which in turn, reacting with the luminophore, is able to generate the ECL emission upon the analyte concentration.

Nowadays, many diagnostic tests are performed in healthcare laboratories which necessitate qualified staff members, large volume amount of human samples for the analysis, expensive instruments and equipment leading to an overall increase of the costs. Furthermore, another relevant aspect is the time patients must wait in order to have an appointment and to receive the results, and of the qualified personnel who have to be trained for the use of the equipment. Therefore, to overcome the costs and time issues, there has been a significant demand for disposable sensors for the real-time and self monitoring of clinically relevant parameters such as glucose, cholesterol, and lactic acid. Overall, these biosensors are characterised by rapid diagnostics which reduce the waiting time and waiting lists, low amount of sample volumes to be analysed, high accuracy of the results due to the high selectivity and specificity of the ECL technique, and they do not require the presence of qualified professional figures to handle the device as result of a simple architecture of the device.

The aim of this thesis was to develop a novel, non-invasive ECL-based biosensor for the detection of the enzymatic activity for the self-monitoring of clinically relevant parameters like glucose, cholesterol, lactic acid. One of the main goals of the three years of PhD was the application of such a biosensor to encapsulate enzymes into biocompatible, cytocompatible, and biodegradable matrices. At the end of the work, it was demonstrated the

effective encapsulation of all the enzymes analysed and the efficient performances of the sensor.

As demonstrated, the enzymes were successfully encapsulated into two different matrices, alginate hydrogels and cryogels, following a low-cost, rapid and simple process. Both the systems represent novel approaches for the entrapment of biomolecules like enzymes. The encapsulation of the enzymes allowed the possibility to obtain repeatable measurements maintaining undamaged the catalytic activity and the specificity for the substrates. Furthermore, the sensitivity of the biosensor was investigated in the presence of different interferent species, present into human fluids such as ascorbic acid, dopamine and urea, discovering that the biosensors maintain the essential aspect of selectivity towards the substrate. The limit of detections of the corresponding substrate were calculated, showing the possibility to detect very low concentrations up to $\sim 9 \mu\text{M}$. These values make these biosensors very attracting for screening of parameters in human samples. Furthermore, the electro-polymerisation of luminophores were investigated as a tool for the improvement of performances of the biosensors achieving interesting results regarding the ECL-intensity and the sensitivity of the system. The polyluminoI-based approach was investigated in the literature from different research groups, but in this thesis, it was proved that ECL-active film deposited on the GCE surface represents an important tool for the *in-situ* investigation when coupled with encapsulated enzymes. In fact, the bilayer systems studied in chapter 8 could be applied for the development of biosensors, such as probes, for the real-time analysis of vital parameters. Moreover, the novel approach for the electro-polymerisation of $[\text{Ru}(\text{bpy})_3]^{2+}$ is proposed opening the possibility of developing a new ECL-active film for dehydrogenase enzymes investigations. The poly- $[\text{Ru}(\text{bpy})_3]^{2+}$ films were evaluated through UV and FTIR techniques and the results showed the nature of this specie as of an oligomer characterised by the same properties of the monomer. The results reported represent just preliminary results which need to be further investigated and explored.

The proposed prototype of ECL-based biosensors has several advantages including high selectivity and specificity of each enzyme for the corresponding substrate, reproducibility of the measurements, reliability demonstrated building the different calibration curves as result of three repetitions of the tests, low cost of the instrumentation and materials, simple and fast assembly of the system and measurement of the ECL signal.

All these aspects make this work very relevant in the research of device and methods for the non-invasive and real time monitoring of critical parameters. However, the set-up adopted for the ECL measurements represented a drawback of the system making sometimes challenging running the experiments. For example, the analysis of the enzymes into alginate hydrogels and/or cryogel on the GCE was several times interrupted as the material detached from the electrode surface during the experiment making the tests void. The set-up of the experiments represents one of the aspects that need to be revised and improved to achieve higher performances and stability.

This thesis represents the starting point for the development of further research for the advancement in the biosensing field. Different aspects need to be further investigated such as the test of the biosensor with human fluids, the development of an electronic platform to perform the ECL tests, the analysis of the ECL ruthenium-based polymer developed here for the first time. In addition, it is possible to widen the analysis of other enzymes encapsulated into the two systems here developed and to link two or more enzymes for the simultaneous study of different parameters in a single test.

In conclusion, the results in this thesis demonstrated that this encapsulation technique integrated with the ECL-technique is a versatile and very promising approach for the development of biosensors designated to the rapid self-monitoring in real time. This biosensor could be developed for example as a wearable device for the continuous real time monitoring of glucose and lactic acid in sweat in the case of luminophores in the monomer form, or as disposable device or probe for the analysis of the same parameters through saliva using the polymerised luminophore.

References

1. Sawyer, D.T., A. Sobkowiak, and J.L. Roberts, *Electrochemistry for chemists*. 1995: Wiley.
2. L. Galvani, A.V., *Philosophical Transactions of the Royal Society of London*, 1793. **83**: p. 10-44.
3. Volta, A., *The Philosophical Magazine* 1799. **4**(13): p. 59-68.
4. Nicholson W., A.C., *Journal of Natural Philosophy, Chemistry and the Arts*, 1800. **4**.
5. Faraday, M., *VI. Experimental researches in electricity.-Seventh Series*. *Philosophical Transactions of the Royal Society of London*, 1834(124): p. 77-122.
6. Laidler, K.J., *The world of physical chemistry*, ed. O.U. Press. 1995.
7. Hasanov, M., *Review of Components and Materials for Proton Exchange Membrane Unitized Reversible Fuel Cells*.
8. *The International Society of Electrochemistry*. Archived 20 June 2010 at the Wayback Machine.
9. Skoog, D.A.D.M.W.F.J.H., *Fundamentals of Analytical Chemistry (7th ed.)*. Harcourt Brace College Publishers. 1995.
10. Peter T. Kissinger, W.R.H., *Laboratory Techniques in Electroanalytical Chemistry*. 1996: CRC Press.
11. Bard, A.J., L.R. Faulkner, and H.S. White, *Electrochemical methods: fundamentals and applications*. 2022: John Wiley & Sons.
12. Zoski, C.G., *Handbook of electrochemistry*. 2006: Elsevier.
13. Wang, J., *Analytical electrochemistry*. New York, USA: Wiley, 2006. **10**: p. 0471790303.
14. Heineman, R.B. and D. Sawyer, *Chemistry experiments for instrumental methods*. 1984: New York: John Wiley & Sons.
15. Welty, J., G.L. Rorrer, and D.G. Foster, *Fundamentals of momentum, heat, and mass transfer*. 2014: John Wiley & Sons.
16. Perez, N., *Mass Transport by Diffusion and Migration*. 2016. 1-455.
17. Conway, B.E. and R. Greef, *Theory and principles of electrode processes*. *Journal of The Electrochemical Society*, 1966. **113**(12): p. 325C.
18. Bockris, J.M., M. Devanathan, and K. Müller, *On the structure of charged interfaces*, in *Electrochemistry*. 1965, Elsevier. p. 832-863.
19. Poggendorff, J.C., E. Wiedemann, and G.H. Wiedemann, *Annalen der Physik und Chemie*. Vol. 47. 1892: JA Barth.
20. Srinivasan, S., *Fuel cells: from fundamentals to applications*. 2006: Springer Science & Business media.

21. Stern, M., *Zur Theorie der Eulerschen Zahlen*. Journal für die reine und angewandte Mathematik (Crelles Journal), 1875. **1875**(79): p. 67-98.
22. Wang, Z.L. and A.C. Wang, *On the origin of contact-electrification*. Materials Today, 2019. **30**: p. 34-51.
23. Bard, A.J., *Electrogenerated Chemiluminescence*. 2004, New York. 213-271.
24. Smith, T., K. Stevenson, and C. Zoski, *Handbook of electrochemistry*. Elsevier, Amsterdam, 2007: p. 73-110.
25. Kulmala, S. and J. Suomi, *Current status of modern analytical luminescence methods*. Analytica Chimica Acta, 2003. **500**(1-2): p. 21-69.
26. Agbaria, R.A., et al., *Molecular fluorescence, phosphorescence, and chemiluminescence spectrometry*. Analytical chemistry, 2002. **74**(16): p. 3952-3962.
27. Miao, W., *Electrogenerated chemiluminescence and its biorelated applications*. Chemical reviews, 2008. **108**(7): p. 2506-2553.
28. Wilson, R., C. Clavering, and A. Hutchinson, *Electrochemiluminescence enzyme immunoassays for TNT and pentaerythritol tetranitrate*. Analytical Chemistry, 2003. **75**(16): p. 4244-4249.
29. Hercules, D.M., *Chemiluminescence resulting from electrochemically generated species*. Science, 1964. **145**(3634): p. 808-809.
30. Harvey, N., *Luminescence during electrolysis*. The Journal of Physical Chemistry, 2002. **33**(10): p. 1456-1459.
31. Dufford, R., D. Nightingale, and L. Gaddum, *Luminescence of Grignard compounds in electric and magnetic fields, and related electrical phenomena*. Journal of the American Chemical Society, 1927. **49**(8): p. 1858-1864.
32. Visco, R.E. and E.A. Chandross, *Electroluminescence in solutions of aromatic hydrocarbons*. Journal of the American Chemical Society, 1964. **86**(23): p. 5350-5351.
33. Santhanam, K. and A.J. Bard, *Chemiluminescence of electrogenerated 9, 10-Diphenylanthracene anion radical*. Journal of the American Chemical Society, 1965. **87**(1): p. 139-140.
34. Tokel, N.E. and A.J. Bard, *Electrogenerated chemiluminescence. IX. Electrochemistry and emission from systems containing tris (2, 2'-bipyridine) ruthenium (II) dichloride*. Journal of the American Chemical Society, 1972. **94**(8): p. 2862-2863.
35. Marcus, R.A., *On the theory of chemiluminescent electron-transfer reactions*. The Journal of Chemical Physics, 1965. **43**(8): p. 2654-2657.
36. Leland, J.K. and M.J. Powell, *Electrogenerated chemiluminescence: an oxidative-reduction type ECL reaction sequence using tripropyl amine*. Journal of the Electrochemical Society, 1990. **137**(10): p. 3127.
37. Blackburn, G.F., et al., *Electrochemiluminescence detection for development of immunoassays and DNA probe assays for clinical diagnostics*. Clinical Chemistry, 1991. **37**(9): p. 1534-1539.

38. Parveen, S., et al., *Electrogenerated chemiluminescence: protocols and applications*. 2013: Springer.
39. Dennany, L., *Electrochemiluminescence fundamentals and analytical applications*. Royal Society of Chemistry, 2018. **15**: p. 96-146.
40. Zheng, H. and Y. Zu, *Emission of Tris (2, 2 '-bipyridine) ruthenium (II) by Coreactant Electrogenerated Chemiluminescence: From O₂-Insensitive to Highly O₂-Sensitive*. The Journal of Physical Chemistry B, 2005. **109**(24): p. 12049-12053.
41. Hai-Juan, L., et al., *Progress in Ru (bpy) 3²⁺ electrogenerated chemiluminescence*. Chinese Journal of Analytical Chemistry, 2009. **37**(11): p. 1557-1565.
42. Chang, M.-M., T. Saji, and A.J. Bard, *Electrogenerated chemiluminescence. 30. Electrochemical oxidation of oxalate ion in the presence of luminescers in acetonitrile solutions*. Journal of the American Chemical Society, 1977. **99**(16): p. 5399-5403.
43. Richter, M.M., *Electrochemiluminescence (ecl)*. Chemical Reviews, 2004. **104**(6): p. 3003-3036.
44. Parveen, S., et al., *Generation Pathways of Electrogenerated Chemiluminescence*, in *Electrogenerated Chemiluminescence*. 2013, Springer. p. 15-31.
45. Fleet, B., G. Kirkbright, and C. Pickford, *The electrogenerated chemiluminescence of pyrene and some related compounds*. Journal of Electroanalytical Chemistry and Interfacial Electrochemistry, 1971. **30**(1): p. 115-121.
46. Forster, R.J., P. Bertoncello, and T.E. Keyes, *Electrogenerated chemiluminescence*. Annual Review of Analytical Chemistry, 2009. **2**: p. 359-385.
47. Bertoncello, P. and R.J. Forster, *Nanostructured materials for electrochemiluminescence (ECL)-based detection methods: Recent advances and future perspectives*. Biosensors and Bioelectronics, 2009. **24**(11): p. 3191-3200.
48. Hu, L. and G. Xu, *Applications and trends in electrochemiluminescence*. Chemical Society Reviews, 2010. **39**(8): p. 3275-3304.
49. Huang, R., M.-Y. Wei, and L.-H. Guo, *Enhanced electrogenerated chemiluminescence of Ru (bpy) 3²⁺/tripropylamine system on indium tin oxide nanoparticle modified transparent electrode*. Journal of electroanalytical chemistry, 2011. **656**(1-2): p. 136-139.
50. Roughton, S.M., *Electrogenerated Chemiluminescence Of Luminophores And Enhancement With Melatonin*. 2016.
51. JT, R., *Fluorescence and Phosphorescence*. Nature, 1939. **143**(3616): p. 267.
52. Liu, Z., W. Qi, and G. Xu, *Recent advances in electrochemiluminescence*. Chemical Society Reviews, 2015. **44**(10): p. 3117-3142.

53. Nicholson, R.S., *Theory and application of cyclic voltammetry for measurement of electrode reaction kinetics*. Analytical chemistry, 1965. **37**(11): p. 1351-1355.
54. Bertocello, P., A.J. Stewart, and L. Dennany, *Analytical applications of nanomaterials in electrogenerated chemiluminescence*. Analytical and bioanalytical chemistry, 2014. **406**(23): p. 5573-5587.
55. Mirasoli, M. and E. Michelini, *Analytical bioluminescence and chemiluminescence*. Analytical and Bioanalytical Chemistry, 2014. **406**(23): p. 5529-5531.
56. Bard, A.J., *Electrogenerated chemiluminescence*. 2004: CRC Press.
57. Dennany, L., *Electrochemiluminescence fundamentals and analytical applications*, in *Electrochemistry: Volume 15*. 2019, The Royal Society of Chemistry. p. 96-146.
58. Stewart, A.J., *An investigation into the electrogenerated chemiluminescence of near-infrared quantum dots for application in biomedical sensing*. 2014.
59. Zoski, C.G., *Handbook of Electrochemistry*, ed. Elsevier. 2007.
60. Kuhn, H., H.-D. Försterling, and D.H. Waldeck, *Principles of physical chemistry*. 2009: John Wiley & Sons.
61. Faulkner, L.R., H. Tachikawa, and A.J. Bard, *Electrogenerated chemiluminescence. VII. Influence of an external magnetic field on luminescence intensity*. Journal of the American Chemical Society, 1972. **94**(3): p. 691-699.
62. Abruña, H.D., *Electrogenerated chemiluminescence of bipyridine and phenanthroline complexes of osmium*. Journal of electroanalytical chemistry and interfacial electrochemistry, 1984. **175**(1-2): p. 321-326.
63. Elgrishi, N., et al., *A practical beginner's guide to cyclic voltammetry*. Journal of chemical education, 2018. **95**(2): p. 197-206.
64. Mabbott, G.A., *An introduction to cyclic voltammetry*. Journal of Chemical education, 1983. **60**(9): p. 697.
65. Sui, G., et al., *Solution-phase surface modification in intact poly (dimethylsiloxane) microfluidic channels*. Analytical chemistry, 2006. **78**(15): p. 5543-5551.
66. Kissinger, P.T. and W.R. Heineman, *Cyclic voltammetry*. Journal of Chemical Education, 1983. **60**(9): p. 702.
67. Savéant, J.-M., *Elements of molecular and biomolecular electrochemistry: an electrochemical approach to electron transfer chemistry*. 2006: John Wiley & Sons.
68. Turner, A., I. Karube, and G.S. Wilson, *Biosensors: fundamentals and applications*. 1987: Oxford university press.
69. Malhotra, B.D., *Biosensors: fundamentals and applications*. 2017: Smithers rapra.

70. Kaur, H.S., Munish *Nanomaterial based aptasensors for clinical and environmental diagnostic applications*. *Nanoscale Advances.*, 2019. **1**(6): p. 2123–2138.
71. Rocchitta, G., et al., *Enzyme biosensors for biomedical applications: Strategies for safeguarding analytical performances in biological fluids*. *Sensors*, 2016. **16**(6): p. 780.
72. Bertocello, P., *Nanomaterials for biosensing with electrochemiluminescence (ECL) detection*. *Front. Biosci*, 2011. **16**: p. 1084-1108.
73. Zanut, A., et al., *Insights into the mechanism of coreactant electrochemiluminescence facilitating enhanced bioanalytical performance*. *Nature communications*, 2020. **11**(1): p. 1-9.
74. Bartlett, P., V. Bradford, and R. Whitaker, *Enzyme electrode studies of glucose oxidase modified with a redox mediator*. *Talanta*, 1991. **38**(1): p. 57-63.
75. Valenti G, F.A., Li H, Sojic N, Paolucci F *Essential Role of Electrode Materials in Electrochemiluminescence Applications*. *ChemElectroChem*, 2016. **3**: p. 1990-1997.
76. Rosini, E., P. D'Antona, and L. Pollegioni, *Biosensors for D-Amino acids: Detection methods and applications*. *International Journal of Molecular Sciences*, 2020. **21**(13): p. 4574.
77. Chaubey, A. and B. Malhotra, *Mediated biosensors*. *Biosensors and bioelectronics*, 2002. **17**(6-7): p. 441-456.
78. Sánchez, F.G., A.N. Díaz, and J.G. García, *Study of the enhanced chemiluminescence from the luminol-horseradish peroxidase-hydrogen peroxide-p-coumaric acid system at very short times: stopped flow selective determination of p-coumaric acid in beers*. *Analytica chimica acta*, 1995. **310**(3): p. 399-406.
79. Díaz, A.N., F.G. Sanchez, and J.G. García, *Hydrogen peroxide assay by using enhanced chemiluminescence of the luminol-H₂O₂-horseradish peroxidase system: Comparative studies*. *Analytica Chimica Acta*, 1996. **327**(2): p. 161-165.
80. Homaei, A.A., et al., *Enzyme immobilization: an update*. *Journal of chemical biology*, 2013. **6**(4): p. 185-205.
81. Hartmeier, W., *Immobilized biocatalysts: an introduction*. 2012: Springer Science & Business Media.
82. Tosa, T., et al., *Studies on continuous enzyme reactions. I. Screening of carriers for preparation of water-insoluble aminoacylase*. *Enzymologia*, 1966. **31**(4): p. 214-224.
83. Brady, D. and J. Jordaan, *Advances in enzyme immobilisation*. *Biotechnology letters*, 2009. **31**(11): p. 1639-1650.
84. Nelson, J. and E.G. Griffin, *Adsorption of invertase*. *Journal of the American Chemical Society*, 1916. **38**(5): p. 1109-1115.
85. Hartmann, M., *Ordered mesoporous materials for bioadsorption and biocatalysis*. *Chemistry of materials*, 2005. **17**(18): p. 4577-4593.

86. Bai, Y., et al., *Identification of an acidic α -amylase from Alicyclobacillus sp. A4 and assessment of its application in the starch industry*. Food Chemistry, 2012. **131**(4): p. 1473-1478.
87. Gomes-Ruffi, C.R., et al., *Effect of the emulsifier sodium stearoyl lactylate and of the enzyme maltogenic amylase on the quality of pan bread during storage*. LWT, 2012. **49**(1): p. 96-101.
88. Groboillot, A., et al., *Immobilization of cells for application in the food industry*. critical reviews in biotechnology, 1994. **14**(2): p. 75-107.
89. Ismail, B. and S. Nielsen, *Invited review: Plasmin protease in milk: Current knowledge and relevance to dairy industry*. Journal of dairy science, 2010. **93**(11): p. 4999-5009.
90. Rao, C.S., et al., *Characterization of thermo-and detergent stable serine protease from isolated Bacillus circulans and evaluation of eco-friendly applications*. Process Biochemistry, 2009. **44**(3): p. 262-268.
91. Hakala, T.K., T. Liitiä, and A. Suurnäkki, *Enzyme-aided alkaline extraction of oligosaccharides and polymeric xylan from hardwood kraft pulp*. Carbohydrate polymers, 2013. **93**(1): p. 102-108.
92. Apetrei, I., et al., *Enzyme sensor based on carbon nanotubes/cobalt (II) phthalocyanine and tyrosinase used in pharmaceutical analysis*. Sensors and Actuators B: Chemical, 2013. **177**: p. 138-144.
93. Das, R., S. Ghosh, and C. Bhattacharjee, *Enzyme membrane reactor in isolation of antioxidative peptides from oil industry waste: a comparison with non-peptidic antioxidants*. LWT, 2012. **47**(2): p. 238-245.
94. Soldatkin, O., et al., *Novel conductometric biosensor based on three-enzyme system for selective determination of heavy metal ions*. Bioelectrochemistry, 2012. **83**: p. 25-30.
95. Dreifke, M.B., A.A. Jayasuriya, and A.C. Jayasuriya, *Current wound healing procedures and potential care*. Materials Science and Engineering: C, 2015. **48**: p. 651-662.
96. Mazaki, T., et al., *A novel, visible light-induced, rapidly cross-linkable gelatin scaffold for osteochondral tissue engineering*. Scientific reports, 2014. **4**(1): p. 1-10.
97. Iqbal, J., J. Gunn, and P.W. Serruys, *Coronary stents: historical development, current status and future directions*. Br Med Bull, 2013. **106**(1): p. 193-211.
98. Zurita, R., J. Puiggali, and A. Rodríguez-Galán, *Loading and release of ibuprofen in multi-and monofilament surgical sutures*. Macromolecular bioscience, 2006. **6**(9): p. 767-775.
99. Ma, P.X. and R. Zhang, *Microtubular architecture of biodegradable polymer scaffolds*. Journal of Biomedical Materials Research: An Official Journal of The Society for Biomaterials, The Japanese Society for Biomaterials, and The Australian Society for Biomaterials and the Korean Society for Biomaterials, 2001. **56**(4): p. 469-477.

100. Gombotz, W.R. and S. Wee, *Protein release from alginate matrices*. Advanced drug delivery reviews, 1998. **31**(3): p. 267-285.
101. Lee, K.Y. and D.J. Mooney, *Alginate: properties and biomedical applications*. Progress in polymer science, 2012. **37**(1): p. 106-126.
102. Sakiyama-Elbert, S. and J. Hubbell, *Functional biomaterials: design of novel biomaterials*. Annual Review of Materials Research, 2001. **31**(1): p. 183-201.
103. Talebian, S., et al., *Self-healing hydrogels: the next paradigm shift in tissue engineering?* Advanced Science, 2019. **6**(16): p. 1801664.
104. Agnihotri, S.A., N.N. Mallikarjuna, and T.M. Aminabhavi, *Recent advances on chitosan-based micro-and nanoparticles in drug delivery*. Journal of controlled release, 2004. **100**(1): p. 5-28.
105. Sandford, P.A. and A. Steinnes, *Biomedical Applications of High-Purity Chitosan: Physical, Chemical, and Bioactive Properties*. 1991, ACS Publications.
106. Lee, C.H., A. Singla, and Y. Lee, *Biomedical applications of collagen*. International journal of pharmaceutics, 2001. **221**(1-2): p. 1-22.
107. GUERIN, P., *Use of synthetic polymers for biomedical application*. Pacing and Clinical Electrophysiology, 1983. **6**(2): p. 449-453.
108. Gonçalves, A., et al., *Zeolites as supports for enzymatic hydrolysis reactions. Comparative study of several zeolites*. Journal of Molecular Catalysis B: Enzymatic, 1996. **1**(2): p. 53-60.
109. Sassolas, A., L.J. Blum, and B.D. Leca-Bouvier, *Immobilization strategies to develop enzymatic biosensors*. Biotechnology advances, 2012. **30**(3): p. 489-511.
110. Gupta, M. and B. Mattiasson, *Unique applications of immobilized proteins in bioanalytical systems*. Methods of biochemical analysis, 1992. **36**: p. 1-34.
111. Brena, B., P. González-Pombo, and F. Batista-Viera, *Immobilization of enzymes: a literature survey*. Immobilization of enzymes and cells, 2013: p. 15-31.
112. Lee, W.-F. and C.-T. Huang, *Immobilization of trypsin by thermo-responsive hydrogel for the affinity separation of trypsin inhibitor*. Desalination, 2008. **234**(1-3): p. 195-203.
113. Ber, S., G.T. Köse, and V. Hasırcı, *Bone tissue engineering on patterned collagen films: an in vitro study*. Biomaterials, 2005. **26**(14): p. 1977-1986.
114. Rowley, J.A., G. Madlambayan, and D.J. Mooney, *Alginate hydrogels as synthetic extracellular matrix materials*. Biomaterials, 1999. **20**(1): p. 45-53.
115. Lim, F. and A.M. Sun, *Microencapsulated islets as bioartificial endocrine pancreas*. Science, 1980. **210**(4472): p. 908-910.
116. Murua, A., et al., *Cell microencapsulation technology: towards clinical application*. Journal of controlled release, 2008. **132**(2): p. 76-83.
117. Kuo, C.K. and P.X. Ma, *Ionic crosslinked alginate hydrogels as scaffolds for tissue engineering: Part 1. Structure, gelation rate and mechanical properties*. Biomaterials, 2001. **22**(6): p. 511-521.

118. Šulek, F., et al., *Immobilization of horseradish peroxidase as crosslinked enzyme aggregates (CLEAs)*. *Process biochemistry*, 2011. **46**(3): p. 765-769.
119. Zelinski, T. and H. Waldmann, *Cross-linked enzyme crystals (CLECs): Efficient and stable biocatalysts for preparative organic chemistry*. *Angewandte Chemie International Edition in English*, 1997. **36**(7): p. 722-724.
120. Barredo, J.-L. and J.L. Barredo, *Microbial enzymes and biotransformations*. 2005: Springer.
121. Joshi, K.A., et al., *A disposable biosensor for organophosphorus nerve agents based on carbon nanotubes modified thick film strip electrode*. *Electroanalysis: An International Journal Devoted to Fundamental and Practical Aspects of Electroanalysis*, 2005. **17**(1): p. 54-58.
122. Bohner, M., et al., *Synthesis of spherical calcium phosphate particles for dental and orthopedic applications*. *Biomatter*, 2013. **3**(2): p. e25103.
123. Hong, S., et al., *Collagen microsphere production on a chip*. *Lab on a Chip*, 2012. **12**(18): p. 3277-3280.
124. Bergquist, N., et al., *The manufacture of protein microspheres by suspension polymerization*. *International Archives of Allergy and Immunology*, 1972. **43**(5): p. 791-799.
125. Freiberg, S. and X. Zhu, *Polymer microspheres for controlled drug release*. *International journal of pharmaceutics*, 2004. **282**(1-2): p. 1-18.
126. Athanasiou, K.A., et al., *Orthopaedic applications for PLA-PGA biodegradable polymers*. *Arthroscopy: The Journal of Arthroscopic & Related Surgery*, 1998. **14**(7): p. 726-737.
127. Martinelli, J., et al., *Synthesis and characterization of glass-ceramic microspheres for thermotherapy*. *Journal of non-crystalline solids*, 2010. **356**(44-49): p. 2683-2688.
128. Walsh, G., *Biopharmaceutical benchmarks 2018*. *Nature biotechnology*, 2018. **36**(12): p. 1136-1145.
129. Leader, B., Q.J. Baca, and D.E. Golan, *Protein therapeutics: a summary and pharmacological classification*. *Nature reviews Drug discovery*, 2008. **7**(1): p. 21-39.
130. Wang, W., *Lyophilization and development of solid protein pharmaceuticals*. *International journal of pharmaceutics*, 2000. **203**(1-2): p. 1-60.
131. Basu, S.K., et al., *Protein crystals for the delivery of biopharmaceuticals*. *Expert opinion on biological therapy*, 2004. **4**(3): p. 301-317.
132. Pechenov, S., et al., *Injectable controlled release formulations incorporating protein crystals*. *Journal of controlled release*, 2004. **96**(1): p. 149-158.
133. Volodkin, D., *CaCO₃ templated micro-beads and-capsules for bioapplications*. *Advances in colloid and interface science*, 2014. **207**: p. 306-324.
134. Volodkin, D.V., et al., *One-Step Formulation of Protein Microparticles with Tailored Properties: Hard Templating at Soft Conditions*. *Advanced Functional Materials*, 2012. **22**(9): p. 1914-1922.

135. Meldrum, F.C. and S.T. Hyde, *Morphological influence of magnesium and organic additives on the precipitation of calcite*. Journal of crystal growth, 2001. **231**(4): p. 544-558.
136. Kitamura, M., *Crystallization and transformation mechanism of calcium carbonate polymorphs and the effect of magnesium ion*. Journal of Colloid and Interface Science, 2001. **236**(2): p. 318-327.
137. Petrov, A.I., D.V. Volodkin, and G.B. Sukhorukov, *Protein—calcium carbonate coprecipitation: a tool for protein encapsulation*. Biotechnology progress, 2005. **21**(3): p. 918-925.
138. Blandino, A., M. Macías, and D. Cantero, *Glucose oxidase release from calcium alginate gel capsules*. Enzyme and microbial technology, 2000. **27**(3-5): p. 319-324.
139. Lamas, M., et al., *Calcium alginate microspheres of Bacillus subtilis*. Drug development and industrial pharmacy, 2001. **27**(8): p. 825-829.
140. Strand, B.L., Y.A. Morch, and G. Skjak-Braek, *Alginate as immobilization matrix for cells*. Minerva biotecnologica, 2000. **12**(4): p. 223.
141. Abasalizadeh, F., et al., *Alginate-based hydrogels as drug delivery vehicles in cancer treatment and their applications in wound dressing and 3D bioprinting*. Journal of biological engineering, 2020. **14**(1): p. 1-22.
142. Rinaudo, M., *Main properties and current applications of some polysaccharides as biomaterials*. Polymer International, 2008. **57**(3): p. 397-430.
143. Berg, J., *Biochemistry - Ninth Edition*, ed. N.W.F.a.C. New York. 2019.
144. Toone, E.J., *Advances in enzymology and related areas of molecular biology: Protein evolution*. 2010: John Wiley & Sons.
145. Bisswanger, H., *Enzyme kinetics: principles and methods*. 2017: John Wiley & Sons.
146. Michaelis, L., et al., *The original Michaelis constant: translation of the 1913 Michaelis-Menten paper*. Biochemistry, 2011. **50**(39): p. 8264-9.
147. Johnson, K.A. and R.S. Goody, *The original Michaelis constant: translation of the 1913 Michaelis–Menten paper*. Biochemistry, 2011. **50**(39): p. 8264-8269.
148. Fromm H.J., H.M.S., *Enzyme Kinetics*. Essentials of Biochemistry., ed. B. Springer, Heidelberg. 2012.
149. Schwuger, M.-J., K. Stickdorn, and R. Schomaecker, *Microemulsions in technical processes*. Chemical reviews, 1995. **95**(4): p. 849-864.
150. Bar-Even, A., et al., *The moderately efficient enzyme: evolutionary and physicochemical trends shaping enzyme parameters*. Biochemistry, 2011. **50**(21): p. 4402-4410.
151. Mosshammer, M., et al., *Extracellular hydrogen peroxide measurements using a flow injection system in combination with microdialysis probes - Potential and challenges*. Free Radic Biol Med, 2018. **128**: p. 111-123.
152. Canovas, R., et al., *A novel wireless paper-based potentiometric platform for monitoring glucose in blood*. Lab Chip, 2017. **17**(14): p. 2500-2507.

153. Ballesta Claver, J., M.C. Valencia Miron, and L.F. Capitan-Vallvey, *Disposable electrochemiluminescent biosensor for lactate determination in saliva*. *Analyst*, 2009. **134**(7): p. 1423-32.
154. Lamas-Ardisana, P.J., et al., *Disposable amperometric biosensor based on lactate oxidase immobilised on platinum nanoparticle-decorated carbon nanofiber and poly(diallyldimethylammonium chloride) films*. *Biosens Bioelectron*, 2014. **56**: p. 345-51.
155. Qiaocui, S., et al., *An Electrochemical Biosensor with Cholesterol Oxidase/Sol-Gel Film on a Nanoplatinum/Carbon Nanotube Electrode*. *Electroanalysis: An International Journal Devoted to Fundamental and Practical Aspects of Electroanalysis*, 2005. **17**(10): p. 857-861.
156. Suman and C.S. Pundir, *Co-immobilization of cholesterol esterase, cholesterol oxidase and peroxidase onto alkylamine glass beads for measurement of total cholesterol in serum*. *Current Applied Physics*, 2003. **3**(2-3): p. 129-133.
157. Voet, D., J.G. Voet, and C.W. Pratt, *Fundamentals of biochemistry: life at the molecular level*. 2016: John Wiley & Sons.
158. Alberts, B.J., A; et al. , *Molecular Biology of the Cell*, ed. N.Y.G. Science. 2002.
159. Ying, W., *NAD⁺/NADH and NADP⁺/NADPH in cellular functions and cell death: regulation and biological consequences*. *Antioxidants & redox signaling*, 2008. **10**(2): p. 179-206.
160. Milutinovic, M., et al., *Glucose sensing by electrogenerated chemiluminescence of glucose-dehydrogenase produced NADH on electrodeposited redox hydrogel*. *Bioelectrochemistry*, 2011. **82**(1): p. 63-68.
161. Guo, G., Q. Chen, and X. Chen, *Electrochemiluminescence glucose biosensor based on glucose dehydrogenase functionalized Ru(bpy)₃²⁺ doped silica nanoparticles*. *Science China Chemistry*, 2011. **54**(11): p. 1777-1781.
162. Farhana, A. and S.L. Lappin, *Biochemistry, lactate dehydrogenase*, in *StatPearls [Internet]*. 2021, StatPearls Publishing.
163. Ramanathan, R., et al., *Covalent binding of 4-hydroxy-2-nonenal to lactate dehydrogenase decreases NADH formation and metmyoglobin reducing activity*. *Journal of agricultural and food chemistry*, 2014. **62**(9): p. 2112-2117.
164. Kishi, K., et al., *The characteristics and applications of recombinant cholesterol dehydrogenase*. *Bioscience, biotechnology, and biochemistry*, 2000. **64**(7): p. 1352-1358.
165. So-Hyun Yoon, H.S.K., Ryong Nam Kim, So-Youn Jung, Bok Sil Hong, Eun Ji Kang, Han-Byoel Lee, Hyeong-Gon Moon, Dong-Young Noh & Wonshik Han *NAD(P)-dependent steroid dehydrogenase-like is involved in breast cancer cell growth and metastasis*. *BMC Cancer*, 2020. **20**.
166. Xu, Z., Z. Guo, and S. Dong, *Electrogenerated chemiluminescence biosensor with alcohol dehydrogenase and tris (2, 2'-bipyridyl) ruthenium (II) immobilized in sol-gel hybrid material*. *Biosensors and Bioelectronics*, 2005. **21**(3): p. 455-461.

167. Jia, T.-t., et al., *Electrogenerated chemiluminescence ethanol biosensor based on alcohol dehydrogenase functionalized Ru (bpy) 32+ doped silica nanoparticles*. *Biosensors and Bioelectronics*, 2009. **25**(1): p. 263-267.
168. Xue, B., et al., *Luminol: Extended hydrogen bond network in water solution*. *Computational and Theoretical Chemistry*, 2014. **1028**: p. 81-86.
169. Albrecht, D. and T. Jungi, *Luminol-enhanced chemiluminescence induced in peripheral blood-derived human phagocytes: obligatory requirement of myeloperoxidase exocytosis by monocytes*. *Journal of leukocyte biology*, 1993. **54**(4): p. 300-306.
170. Khan, P., et al., *Luminol-based chemiluminescent signals: clinical and non-clinical application and future uses*. *Applied biochemistry and biotechnology*, 2014. **173**(2): p. 333-355.
171. Merényi, G., J. Lind, and T.E. Eriksen, *Luminol chemiluminescence: chemistry, excitation, emitter*. *Journal of bioluminescence and chemiluminescence*, 1990. **5**(1): p. 53-56.
172. Rubinstein, I. and A.J. Bard, *Electrogenerated chemiluminescence. 37. Aqueous ecl systems based on tris (2, 2'-bipyridine) ruthenium (2+) and oxalate or organic acids*. *Journal of the American Chemical Society*, 1981. **103**(3): p. 512-516.
173. Yuan, Y., et al., *Coreactants of tris (2, 2'-bipyridyl) ruthenium (II) electrogenerated chemiluminescence*. *Electrochimica acta*, 2012. **82**: p. 484-492.
174. Broomhead, J.A., C.G. Young, and P. Hood, *Tris (2, 2 "-Bipyridine) Ruthenium (II) Dichloride Hexahydrate*. *Inorganic Syntheses: Reagents for transition metal complex and organometallic syntheses*, 1990. **28**: p. 338-340.
175. McCord, P. and A.J. Bard, *Electrogenerated chemiluminescence: Part 54. Electrogenerated chemiluminescence of ruthenium (II) 4, 4'-diphenyl-2, 2'-bipyridine and ruthenium (II) 4, 7-diphenyl-1, 10-phenanthroline systems in aqueous and acetonitrile solutions*. *Journal of electroanalytical chemistry and interfacial electrochemistry*, 1991. **318**(1-2): p. 91-99.
176. Wei, H. and E. Wang, *Electrochemiluminescence of tris (2, 2'-bipyridyl) ruthenium and its applications in bioanalysis: a review*. *Luminescence*, 2011. **26**(2): p. 77-85.
177. White, H.S. and A.J. Bard, *Electrogenerated chemiluminescence. 41. Electrogenerated chemiluminescence and chemiluminescence of the Ru (2, 21-bpy) 32+-S2O82-system in acetonitrile-water solutions*. *Journal of the American Chemical Society*, 1982. **104**(25): p. 6891-6895.
178. Raju, C.V., M. Sornambigai, and S.S. Kumar, *Ruthenium-Tris-Bipyridine Derivatives as a Divine Complex for Electrochemiluminescence Based Biosensor Applications*, in *Ruthenium-An Element Loved by Researchers*. 2021, IntechOpen.
179. Miao, W., J.-P. Choi, and A.J. Bard, *Electrogenerated chemiluminescence 69: The Tris (2, 2 '-bipyridine) ruthenium (II),(Ru (bpy) 32+)/Tri-n-propylamine*

- (TPrA) system revisited A new route involving TPrA•+ Cation Radicals. Journal of the American Chemical Society, 2002. **124**(48): p. 14478-14485.
180. N.E. Tokel, A.J.B., *Electrogenerated chemiluminescence. IX. Electrochemistry and emission from systems containing tris(2,2'-bipyridine)ruthenium(II) dichloride*. J. Am. Chem. Soc. , 1972. **94**: p. 2862-2863.
 181. Irkham; Watanabe, T.F., A.; Valenti, G.; Paolucci, F.; Einaga, Y., *Co-reactant-on-Demand ECL: Electrogenerated Chemiluminescence by the in Situ Production of S₂O₈²⁻ at Boron-Doped Diamond Electrodes*. Faraday Discussions, 2016. **138**: p. 15636-15641.
 182. Heard, D.M. and A.J. Lennox, *Electrode materials in modern organic electrochemistry*. Angewandte Chemie International Edition, 2020. **59**(43): p. 18866-18884.
 183. Kärkäs, M.D., *Electrochemical strategies for C–H functionalization and C–N bond formation*. Chemical Society Reviews, 2018. **47**(15): p. 5786-5865.
 184. Jörissen, J., *Practical aspects of preparative scale electrochemistry, encyclopedia of electrochemistry*. Organic electrochemistry. Wiley-VCH, Weinheim, 2004.
 185. Nichols, R. and A. Bewick, *Spectroscopic identification of the adsorbed intermediate in hydrogen evolution on platinum*. Journal of electroanalytical chemistry and interfacial electrochemistry, 1988. **243**(2): p. 445-453.
 186. Mandler, D. and S. Kraus-Ophir, *Self-assembled monolayers (SAMs) for electrochemical sensing*. Journal of Solid State Electrochemistry, 2011. **15**(7): p. 1535-1558.
 187. Gajdar, J., et al., *Recent applications of mercury electrodes for monitoring of pesticides: a critical review*. Electroanalysis, 2016. **28**(11): p. 2659-2671.
 188. Zittel, H. and F. Miller, *A Glassy-Carbon Electrode for Voltammetry*. Analytical Chemistry, 1965. **37**(2): p. 200-203.
 189. Ranganathan, S., T.-C. Kuo, and R.L. McCreery, *Facile preparation of active glassy carbon electrodes with activated carbon and organic solvents*. Analytical chemistry, 1999. **71**(16): p. 3574-3580.
 190. McCarthy, B.D., et al., *Electrochemical Reduction of Brønsted Acids by Glassy Carbon in Acetonitrile* [?] Implications for Electrocatalytic Hydrogen Evolution. Inorganic chemistry, 2014. **53**(16): p. 8350-8361.
 191. Srivastava, R., et al., *Stable encapsulation of active enzyme by application of multilayer nanofilm coatings to alginate microspheres*. Macromolecular bioscience, 2005. **5**(8): p. 717-727.
 192. Li, X., et al., *Synthesis of Size-Controlled Acid-Resistant Hybrid Calcium Carbonate Microparticles as Templates for Fabricating “Micelles-Enhanced” Polyelectrolyte Capsules by the LBL Technique*. Chemistry—A European Journal, 2006. **12**(22): p. 5770-5778.
 193. Boi, S., et al., *Alginate microbeads with internal microvoids for the sustained release of drugs*. International Journal of Biological Macromolecules, 2020. **156**: p. 454-461.

194. Kissinger, P. and W.R. Heineman, *Laboratory Techniques in Electroanalytical Chemistry, revised and expanded*. 2018: CRC press.
195. Skoog, D.A., F.J. Holler, and S.R. Crouch, *Principles of instrumental analysis*. 2017: Cengage learning.
196. Wright, A., *The photomultiplier handbook*. 2017: Oxford University Press.
197. Schreck, R., P. Rieber, and P.A. Baeuerle, *Reactive oxygen intermediates as apparently widely used messengers in the activation of the NF-kappa B transcription factor and HIV-1*. *The EMBO journal*, 1991. **10**(8): p. 2247-2258.
198. Abe, J.-i. and B.C. Berk, *Fyn and JAK2 mediate Ras activation by reactive oxygen species*. *Journal of Biological Chemistry*, 1999. **274**(30): p. 21003-21010.
199. Elias, H. and S. Vayssié, *Reactive peroxo compounds generated in situ from hydrogen peroxide: Kinetics and catalytic application in oxidation processes*. *Peroxide Chemistry: Mechanistic and Preparative Aspects of Oxygen Transfer*, 2000: p. 128-138.
200. WANG, X., et al., *The cellular response to oxidative stress: influences of mitogen-activated protein kinase signalling pathways on cell survival*. *Biochemical Journal*, 1998. **333**(2): p. 291-300.
201. Imlay, J.A. and S. Linn, *Mutagenesis and stress responses induced in Escherichia coli by hydrogen peroxide*. *Journal of Bacteriology*, 1987. **169**(7): p. 2967-2976.
202. Mittal, M., et al., *Reactive oxygen species in inflammation and tissue injury*. *Antioxidants & redox signaling*, 2014. **20**(7): p. 1126-1167.
203. LINN, S. and J.A. IMLAY, *Toxicity, mutagenesis and stress responses induced in Escherichia coli by hydrogen peroxide*. *Journal of Cell Science*, 1987. **1987**(Supplement_6): p. 289-301.
204. Tsaplev, Y., *Chemiluminescence determination of hydrogen peroxide*. *Journal of Analytical Chemistry*, 2012. **67**(6).
205. Meier, J., et al., *Hydrogen Peroxide Sensors for Biomedical Applications*. *Chemosensors*, 2019. **7**(4): p. 64.
206. Igarashi, S. and W.L. Hinze, *Enzymatic assay with detection by enhanced luminol chemiluminescence in a reversed micellar system: determination of L-amino acids and glucose*. *Analytica chimica acta*, 1989. **225**: p. 147-157.
207. Lee, D., et al., *In vivo imaging of hydrogen peroxide with chemiluminescent nanoparticles*. *Nature materials*, 2007. **6**(10): p. 765-769.
208. Wang, Z., et al., *Detection of hydrogen peroxide in rainwater based on Mg-Al-carbonate layered double hydroxides-catalyzed luminol chemiluminescence*. *Analyst*, 2011. **136**(23): p. 4986-4990.
209. Yu, D., et al., *Iodophenol blue-enhanced luminol chemiluminescence and its application to hydrogen peroxide and glucose detection*. *Talanta*, 2016. **146**: p. 655-661.

210. Ahn, K.-S., et al., *Luminol chemiluminescence biosensor for glycated hemoglobin (HbA1c) in human blood samples*. *Biosensors and Bioelectronics*, 2016. **75**: p. 82-87.
211. Koren, K., P.Ø. Jensen, and M. Kühl, *Development of a rechargeable optical hydrogen peroxide sensor–sensor design and biological application*. *Analyst*, 2016. **141**(14): p. 4332-4339.
212. Sheng, Y., et al., *Silver nanoclusters-catalyzed luminol chemiluminescence for hydrogen peroxide and uric acid detection*. *Talanta*, 2017. **166**: p. 268-274.
213. Ujjain, S.K., et al., *Nanoceria based electrochemical sensor for hydrogen peroxide detection*. *Biointerphases*, 2014. **9**(3): p. 031011.
214. Wang, X. and W. Qin, *Reactive intermediates-induced potential responses of a polymeric membrane electrode for ultrasensitive potentiometric biosensing*. *Chem Commun (Camb)*, 2012. **48**(34): p. 4073-5.
215. Wang, X. and W. Qin, *Reactive intermediates-induced potential responses of a polymeric membrane electrode for ultrasensitive potentiometric biosensing*. *Chemical Communications*, 2012. **48**(34): p. 4073-4075.
216. Cánovas, R., et al., *A novel wireless paper-based potentiometric platform for monitoring glucose in blood*. *Lab on a Chip*, 2017. **17**(14): p. 2500-2507.
217. Grieshaber, D., et al., *Electrochemical biosensors-sensor principles and architectures*. *Sensors*, 2008. **8**(3): p. 1400-1458.
218. ERDEM, A., et al., *Electrochemical biosensor based on horseradish peroxidase for the determination of oxidizable drugs*. *Turkish Journal of Medical Sciences*, 2000. **30**(4): p. 349-354.
219. Marquette, C.A., S. Ravaud, and L.J. Blum, *Luminol electrochemiluminescence-based biosensor for total cholesterol determination in natural samples*. 2000.
220. Marquette, C.A., B.D. Leca, and L.J. Blum, *Electrogenerated chemiluminescence of luminol for oxidase-based fibre-optic biosensors*. *Luminescence: The journal of biological and chemical luminescence*, 2001. **16**(2): p. 159-165.
221. Marquette, C., *Electrochemiluminescent biosensors array for the concomitant detection of choline, glucose, glutamate, lactate, lysine and urate*. *Biosensors and Bioelectronics*, 2003. **19**(5): p. 433-439.
222. Qiaocui, S., et al., *An Electrochemical Biosensor with Cholesterol Oxidase/Sol-Gel Film on a Nanoplatinum/Carbon Nanotube Electrode*. *Electroanalysis*, 2005. **17**(10): p. 857-861.
223. Liu, X., et al., *Glucose biosensor based on gold nanoparticle-catalyzed luminol electrochemiluminescence on a three-dimensional sol–gel network*. *Electrochemistry Communications*, 2008. **10**(9): p. 1250-1253.
224. Cao, Y., et al., *Ultrasensitive luminol electrochemiluminescence for protein detection based on in situ generated hydrogen peroxide as coreactant with glucose oxidase anchored AuNPs@ MWCNTs labeling*. *Biosensors and Bioelectronics*, 2012. **31**(1): p. 305-309.

225. Guo, X., et al., *An L012@PANI-PAAm hydrogel composite based-electrochemiluminescence biosensor for in situ detection of H₂O₂ released from cardiomyocytes*. *Electrochimica Acta*, 2020. **354**.
226. Yildiz, G., U. Tasdoven, and N. Menek, *Electrochemical characterization of luminol and its determination in real samples*. *Analytical Methods*, 2014. **6**(19): p. 7809-7813.
227. Ecol, M., *Luminol-Based Chemiluminescent Signals: Clinical and Non-clinical Application and Future Uses*. 2017. p. 1032-1057.
228. Enger, E., *Concepts in Biology'2007 Ed.* 2003: Rex Bookstore, Inc.
229. Bettelheim, F.A., et al., *General, Organic & Biochemistry*. 2009: Brooks/Cole Cengage Learning.
230. Barni, F., et al., *Forensic application of the luminol reaction as a presumptive test for latent blood detection*. *Talanta*, 2007. **72**(3): p. 896-913.
231. Seager, S.L. and M.R. Slabaugh, *Organic and biochemistry for today*. 2013: Cengage Learning.
232. Shan, D. and W.-R. Cai, *7. Biomaterials for electrochemiluminescence*, in *Bioelectrochemistry: Design and Applications of Biomaterials*, C. Serge, Editor. 2019, De Gruyter. p. 121-142.
233. Salah, N.N., A. Khelef, and T. Lanez, *Investigation of diffusion of ferrocene and ferricenium in aqueous and organic medium using voltammetry techniques*. 2010.
234. Yang, L., et al., *Study on enhancement principle and stabilization for the luminol-H₂O₂-HRP chemiluminescence system*. *PLoS One*, 2015. **10**(7): p. e0131193.
235. González-Martínez, M.Á., R. Puchades, and Á. Maquieira, *Comparison of multianalyte immunosensor formats for on-line determination of organic compounds*. *Analytical chemistry*, 2001. **73**(17): p. 4326-4332.
236. Ramanathan, K., et al., *Gold-coated capillary based 2, 4-dichlorophenoxyacetic acid chemi-luminescent assays: possibilities towards multianalysis*. *Biosensors and Bioelectronics*, 2002. **17**(4): p. 283-288.
237. Krämer, P. and R. Schmid, *Flow injection immunoanalysis (FIIA)—a new immunoassay format for the determination of pesticides in water*. *Biosensors and Bioelectronics*, 1991. **6**(3): p. 239-243.
238. González-Martínez, M.A., et al., *Monoclonal antibody-based flow-through immunosensor for analysis of carbaryl*. *Analytical Chemistry*, 1997. **69**(14): p. 2812-2818.
239. Alfonta, L., et al., *Chronopotentiometry and Faradaic impedance spectroscopy as signal transduction methods for the biocatalytic precipitation of an insoluble product on electrode supports: routes for enzyme sensors, immunosensors and DNA sensors*. *Biosensors and Bioelectronics*, 2001. **16**(9-12): p. 675-687.
240. Weizmann, Y., et al., *Amplified DNA sensing and immunosensing by the rotation of functional magnetic particles*. *Journal of the American Chemical Society*, 2003. **125**(12): p. 3452-3454.

241. Xiao, Q., et al., *Development of a rapid and sensitive magnetic chemiluminescent enzyme immunoassay for detection of luteinizing hormone in human serum*. *Clinical biochemistry*, 2009. **42**(13-14): p. 1461-1467.
242. Li, H., et al., *Chemiluminescence cloth-based glucose test sensors (CCGTSs): A new class of chemiluminescence glucose sensors*. *Biosensors and Bioelectronics*, 2017. **91**: p. 268-275.
243. Cowie, C.C., et al., *Prevalence of diabetes and high risk for diabetes using A1C criteria in the US population in 1988–2006*. *Diabetes care*, 2010. **33**(3): p. 562-568.
244. D'costa, E., I. Higgins, and A. Turner, *Quinoprotein glucose dehydrogenase and its application in an amperometric glucose sensor*. *Biosensors*, 1986. **2**(2): p. 71-87.
245. Bankar, S.B., et al., *Glucose oxidase—an overview*. *Biotechnology advances*, 2009. **27**(4): p. 489-501.
246. Guilbault, G. and G. Lubrano, *An enzyme electrode for the amperometric determination of glucose*. *Analytica chimica acta*, 1973. **64**(3): p. 439-455.
247. Weibel, M.K. and H.J. Bright, *The glucose oxidase mechanism: interpretation of the pH dependence*. *Journal of Biological Chemistry*, 1971. **246**(9): p. 2734-2744.
248. Clark Jr, L.C. and C. Lyons, *Electrode systems for continuous monitoring in cardiovascular surgery*. *Annals of the New York Academy of sciences*, 1962. **102**(1): p. 29-45.
249. Wang, J., *Electrochemical glucose biosensors*. *Chemical reviews*, 2008. **108**(2): p. 814-825.
250. Williams, D.L., A.R. Doig, and A. Korosi, *Electrochemical-enzymatic analysis of blood glucose and lactate*. *Analytical Chemistry*, 1970. **42**(1): p. 118-121.
251. Frew, J.E. and H.A.O. Hill, *Electrochemical biosensors*. *Analytical chemistry*, 1987. **59**(15): p. 933A-944A.
252. Khan, G.F., M. Ohwa, and W. Wernet, *Design of a stable charge transfer complex electrode for a third-generation amperometric glucose sensor*. *Analytical chemistry*, 1996. **68**(17): p. 2939-2945.
253. Palmisano, F., et al., *A disposable, reagentless, third-generation glucose biosensor based on overoxidized poly (pyrrole)/tetrathiafulvalene–tetracyanoquinodimethane composite*. *Analytical chemistry*, 2002. **74**(23): p. 5913-5918.
254. Yoo, E.-H. and S.-Y. Lee, *Glucose biosensors: an overview of use in clinical practice*. *Sensors*, 2010. **10**(5): p. 4558-4576.
255. Kost, G.J. and M. McQueen, *New whole blood analyzers and their impact on cardiac and critical care*. *Critical reviews in clinical laboratory sciences*, 1993. **30**(2): p. 153-202.
256. Bakker, J., et al., *Serial blood lactate levels can predict the development of multiple organ failure following septic shock*. *The American journal of surgery*, 1996. **171**(2): p. 221-226.

257. Parra, A., et al., *Design and characterization of a lactate biosensor based on immobilized lactate oxidase onto gold surfaces*. *Analytica Chimica Acta*, 2006. **555**(2): p. 308-315.
258. Wang, J., *Amperometric biosensors for clinical and therapeutic drug monitoring: a review*. *Journal of pharmaceutical and biomedical analysis*, 1999. **19**(1-2): p. 47-53.
259. Goodwin, M.L., et al., *Blood lactate measurements and analysis during exercise: a guide for clinicians*. *Journal of diabetes science and technology*, 2007. **1**(4): p. 558-569.
260. Meyerhoff, C., et al., *On line continuous monitoring of blood lactate in men by a wearable device based upon an enzymatic amperometric lactate sensor*. *Biosensors and Bioelectronics*, 1993. **8**(9-10): p. 409-414.
261. Pfeiffer, D., et al., *Amperometric lactate oxidase catheter for real-time lactate monitoring based on thin film technology*. *Biosensors and Bioelectronics*, 1997. **12**(6): p. 539-550.
262. Shinbo, T., M. Sugiura, and N. Kamo, *Potentiometric enzyme electrode for lactate*. *Analytical Chemistry*, 1979. **51**(1): p. 100-104.
263. Wu, F., Y. Huang, and C. Huang, *Chemiluminescence biosensor system for lactic acid using natural animal tissue as recognition element*. *Biosensors and Bioelectronics*, 2005. **21**(3): p. 518-522.
264. Omole, O.O., et al., *High-performance liquid chromatographic assay of (\pm)-lactic acid and its enantiomers in calf serum*. *Journal of Chromatography B: Biomedical Sciences and Applications*, 1999. **727**(1-2): p. 23-29.
265. Galban, J., S. de Marcos, and J.R. Castillo, *Fluorometric-enzymatic lactate determination based on enzyme cytochrome b2 fluorescence*. *Analytical chemistry*, 1993. **65**(21): p. 3076-3080.
266. Ren, J., A. Dean Sherry, and C.R. Malloy, *Noninvasive monitoring of lactate dynamics in human forearm muscle after exhaustive exercise by ^1H -magnetic resonance spectroscopy at 7 Tesla*. *Magnetic resonance in medicine*, 2013. **70**(3): p. 610-619.
267. Broder, G. and M.H. Weil, *Excess lactate: an index of reversibility of shock in human patients*. *Science*, 1964. **143**(3613): p. 1457-1459.
268. Yang, Q., P. Atanasov, and E. Wilkins, *Needle-type lactate biosensor*. *Biosensors and Bioelectronics*, 1999. **14**(2): p. 203-210.
269. Faridnia, M.H., et al., *Amperometric biosensor for determination of lactate in sweat*. *Analytica chimica acta*, 1993. **278**(1): p. 35-40.
270. Marquette, C.A. and L.c.J. Blum, *Luminol electrochemiluminescence-based fibre optic biosensors for flow injection analysis of glucose and lactate in natural samples*. *Analytica Chimica Acta*, 1999. **381**(1): p. 1-10.
271. Marquette, C.A., A. Degiuli, and L.J. Blum, *Fiberoptic biosensors based on chemiluminescent reactions*. *Applied biochemistry and biotechnology*, 2000. **89**(2): p. 107-115.

272. Garjonyte, R., et al., *Prussian Blue-and lactate oxidase-based amperometric biosensor for lactic acid*. Sensors and Actuators B: Chemical, 2001. **79**(1): p. 33-38.
273. Claver, J.B., M.V. Mirón, and L. Capitán-Vallvey, *Disposable electrochemiluminescent biosensor for lactate determination in saliva*. Analyst, 2009. **134**(7): p. 1423-1432.
274. Lamas-Ardisana, P.J., et al., *Disposable amperometric biosensor based on lactate oxidase immobilised on platinum nanoparticle-decorated carbon nanofiber and poly (diallyldimethylammonium chloride) films*. Biosensors and Bioelectronics, 2014. **56**: p. 345-351.
275. Yao, Y., et al., *An electrochemiluminescence cloth-based biosensor with smartphone-based imaging for detection of lactate in saliva*. Analyst, 2017. **142**(19): p. 3715-3724.
276. Chen, M.-M., et al., *Construction of a flexible electrochemiluminescence platform for sweat detection*. Chemical science, 2019. **10**(25): p. 6295-6303.
277. Antonio M. Gotto, J.C.L., Donald Hunnighake, Scott M. Grundy, Peter W. Wilson, Thomas B. Clarkson, Joel W. Hay, DeWitt S. Goodman, < *The Cholesterol Facts .pdf*>. AHA Medical/Scientific Statement, 1987.
278. Arya, S.K., M. Datta, and B.D. Malhotra, *Recent advances in cholesterol biosensor*. Biosensors and Bioelectronics, 2008. **23**(7): p. 1083-1100.
279. Narwal, V., et al., *Cholesterol biosensors: A review*. Steroids, 2019. **143**: p. 6-17.
280. Amiri, M. and S. Arshi, *An overview on electrochemical determination of cholesterol*. Electroanalysis, 2020. **32**(7): p. 1391-1407.
281. Markas, A., *Fabrication and characterization of a screen-printed, disposable, amperometric cholesterol biosensor*. Analyst, 1994. **119**(11): p. 2331-2336.
282. Charpentier, L. and N. El Murr, *Amperometric determination of cholesterol in serum with use of a renewable surface peroxidase electrode*. Analytica Chimica Acta, 1995. **318**(1): p. 89-93.
283. Yao, T. and K. Takashima, *Amperometric biosensor with a composite membrane of sol-gel derived enzyme film and electrochemically generated poly (1, 2-diaminobenzene) film*. Biosensors and Bioelectronics, 1998. **13**(1): p. 67-73.
284. Brahim, S., D. Narinesingh, and A. Guiseppi-Elie, *Amperometric determination of cholesterol in serum using a biosensor of cholesterol oxidase contained within a polypyrrole-hydrogel membrane*. Analytica chimica acta, 2001. **448**(1-2): p. 27-36.
285. Singh, S., A. Chaubey, and B. Malhotra, *Amperometric cholesterol biosensor based on immobilized cholesterol esterase and cholesterol oxidase on conducting polypyrrole films*. Analytica chimica acta, 2004. **502**(2): p. 229-234.
286. Dey, R.S. and C.R. Raj, *Development of an amperometric cholesterol biosensor based on graphene- Pt nanoparticle hybrid material*. The Journal of Physical Chemistry C, 2010. **114**(49): p. 21427-21433.

287. Zhang, M., et al., *A biosensor for cholesterol based on gold nanoparticles-catalyzed luminol electrogenerated chemiluminescence*. *Biosensors and Bioelectronics*, 2012. **32**(1): p. 288-292.
288. Stewart, A.J., et al., *A cholesterol biosensor based on the NIR electrogenerated-chemiluminescence (ECL) of water-soluble CdSeTe/ZnS quantum dots*. *Electrochimica Acta*, 2015. **157**: p. 8-14.
289. Cooney, M.J., *Kinetic measurements for enzyme immobilization*. *Enzyme Stabilization and Immobilization*, 2017: p. 215-232.
290. Ahmed, E.M., *Hydrogel: Preparation, characterization, and applications: A review*. *Journal of advanced research*, 2015. **6**(2): p. 105-121.
291. Hoffman, A.S., *Hydrogels for biomedical applications*. *Advanced drug delivery reviews*, 2012. **64**: p. 18-23.
292. Kawaguchi, H., *Thermoresponsive microhydrogels: preparation, properties and applications*. *Polymer International*, 2014. **63**(6): p. 925-932.
293. Liu, W., et al., *Microcryogels as injectable 3-D cellular microniches for site-directed and augmented cell delivery*. *Acta Biomaterialia*, 2014. **10**(5): p. 1864-1875.
294. Rizwan, M., et al., *Effect of sterilization treatment on mechanical properties, biodegradation, bioactivity and printability of GelMA hydrogels*. *Biomedical Materials*, 2020. **15**(6): p. 065017.
295. Eigel, D., C. Werner, and B. Newland, *Cryogel biomaterials for neuroscience applications*. *Neurochemistry International*, 2021. **147**: p. 105012.
296. Razavi, M., Y. Qiao, and A.S. Thakor, *Three-dimensional cryogels for biomedical applications*. *Journal of Biomedical Materials Research Part A*, 2019. **107**(12): p. 2736-2755.
297. Gun'ko, V.M., I.N. Savina, and S.V. Mikhlovsky, *Cryogels: Morphological, structural and adsorption characterisation*. *Advances in colloid and interface science*, 2013. **187**: p. 1-46.
298. Bhat, S., A. Tripathi, and A. Kumar, *Supermacroporous chitosan–agarose–gelatin cryogels: in vitro characterization and in vivo assessment for cartilage tissue engineering*. *Journal of the Royal Society Interface*, 2011. **8**(57): p. 540-554.
299. Singh, D., V. Nayak, and A. Kumar, *Proliferation of myoblast skeletal cells on three-dimensional supermacroporous cryogels*. *International journal of biological sciences*, 2010. **6**(4): p. 371.
300. Srivastava, A. and A. Kumar, *Thermoresponsive poly (N-vinylcaprolactam) cryogels: synthesis and its biophysical evaluation for tissue engineering applications*. *Journal of Materials Science: Materials in Medicine*, 2010. **21**(11): p. 2937-2945.
301. Bencherif, S.A., et al., *Injectable preformed scaffolds with shape-memory properties*. *Proceedings of the National Academy of Sciences*, 2012. **109**(48): p. 19590-19595.

302. Kumar, A., et al., *Cryogels: Freezing unveiled by thawing*. *Materials Today*, 2010. **13**(11): p. 42-44.
303. Tosh, S.M., et al., *Aging dynamics in gelatin gel microstructure*. *Food Hydrocolloids*, 2003. **17**(4): p. 503-513.
304. Koshy, S.T., et al., *Injectable, porous, and cell-responsive gelatin cryogels*. *Biomaterials*, 2014. **35**(8): p. 2477-2487.
305. Fassina, L., et al. *Use of a gelatin cryogel as biomaterial scaffold in the differentiation process of human bone marrow stromal cells*. in *2010 Annual International Conference of the IEEE Engineering in Medicine and Biology*. 2010. IEEE.
306. Rodrigues, S.C., et al., *Preparation and characterization of collagen-nanohydroxyapatite biocomposite scaffolds by cryogelation method for bone tissue engineering applications*. *Journal of biomedical materials research Part A*, 2013. **101**(4): p. 1080-1094.
307. Razavi, M., S. Hu, and A.S. Thakor, *A collagen based cryogel bioscaffold coated with nanostructured polydopamine as a platform for mesenchymal stem cell therapy*. *Journal of Biomedical Materials Research Part A*, 2018. **106**(8): p. 2213-2228.
308. Jurga, M., et al., *The performance of laminin-containing cryogel scaffolds in neural tissue regeneration*. *Biomaterials*, 2011. **32**(13): p. 3423-3434.
309. Kathuria, N., et al., *Synthesis and characterization of elastic and macroporous chitosan–gelatin cryogels for tissue engineering*. *Acta biomaterialia*, 2009. **5**(1): p. 406-418.
310. Ak, F., et al., *Macroporous silk fibroin cryogels*. *Biomacromolecules*, 2013. **14**(3): p. 719-727.
311. Murphy, A.R. and D.L. Kaplan, *Biomedical applications of chemically-modified silk fibroin*. *Journal of materials chemistry*, 2009. **19**(36): p. 6443-6450.
312. Van Vlierberghe, S., P. Dubruel, and E. Schacht, *Biopolymer-based hydrogels as scaffolds for tissue engineering applications: a review*. *Biomacromolecules*, 2011. **12**(5): p. 1387-1408.
313. Bloch, K., et al., *Functional activity of insulinoma cells (INS-1E) and pancreatic islets cultured in agarose cryogel sponges*. *Journal of Biomedical Materials Research Part A: An Official Journal of The Society for Biomaterials, The Japanese Society for Biomaterials, and The Australian Society for Biomaterials and the Korean Society for Biomaterials*, 2005. **75**(4): p. 802-809.
314. Tripathi, A. and A. Kumar, *Multi-featured macroporous agarose–alginate cryogel: Synthesis and characterization for bioengineering applications*. *Macromolecular bioscience*, 2011. **11**(1): p. 22-35.
315. Hwang, Y., N. Sangaj, and S. Varghese, *Interconnected macroporous poly (ethylene glycol) cryogels as a cell scaffold for cartilage tissue engineering*. *Tissue Engineering Part A*, 2010. **16**(10): p. 3033-3041.

316. Eigel, D., et al., *Cryogel scaffolds for regionally constrained delivery of lysophosphatidylcholine to central nervous system slice cultures: A model of focal demyelination for multiple sclerosis research*. *Acta Biomaterialia*, 2019. **97**: p. 216-229.
317. Azhar, M.Y., *Synthesis and Characterization of Cryogel Microcarriers for Sustained Local Delivery of Anticancer Therapeutics to Glioblastoma multiforme*. 2019.
318. C. Qi, J.Z., X. Chen, J. Wan, J. Wang, P. Zhang and Y. Liu, *Hypoxia stimulates neural stem cell proliferation by increasing HIF-1 α expression and activating Wnt/ β -catenin signaling*. *Cellular and Molecular Biology*, 2017. **63**(7).
319. M. Bakhshpour, N.I., I. Perçin and A. Denizli, *Biomedical applications of polymeric cryogels*. *Appl. Sci.*, 2019. **9**: p. 1-22.
320. Blackburn, G.F., et al., *Electrochemiluminescence Detection for Development of Immunoassays and DNA Probe Assays for Clinical Diagnostics*. *Clin. Chem. Clinical Chemistry*, 1991. **37**(9): p. 1534-1539.
321. Martin, A.F. and T.A. Nieman, *Chemiluminescence biosensors using tris (2, 2'-bipyridyl) ruthenium (II) and dehydrogenases immobilized in cation exchange polymers*. *Biosensors and Bioelectronics*, 1997. **12**(6): p. 479-489.
322. Maier, R.M. and T.J. Gentry, *Physiological Methods*, in *Environmental Microbiology*. 2015. p. 213-243.
323. Hercules, D.M. and F.E. Lytle, *Chemiluminescence from reduction reactions*. *Journal of the American Chemical Society*, 1966. **88**(20): p. 4745-4746.
324. He, L., K.A. Cox, and N.D. Danielson, *Chemiluminescence detection of amino acids, peptides, and proteins using tris-2, 2'-bipyridine ruthenium (III)*. *Analytical letters*, 1990. **23**(2): p. 195-210.
325. Ruppert, R. and E. Steckhan, *Efficient photoelectrochemical in-situ regeneration of NAD (P)⁺ coupled to enzymatic oxidation of alcohols*. *Journal of the Chemical Society, Perkin Transactions 2*, 1989(7): p. 811-814.
326. Downey, T.M. and T.A. Nieman, *Chemiluminescence detection using regenerable tris (2, 2'-bipyridyl) ruthenium (II) immobilized in Nafion*. *Analytical chemistry*, 1992. **64**(3): p. 261-268.
327. Komoschinski, J. and E. Steckhan, *Efficient indirect electrochemical in situ regeneration of NAD⁺ and NADP⁺ for enzymatic oxidations using iron bipyridine and phenanthroline complexes as redox catalysts*. *Tetrahedron letters*, 1988. **29**(27): p. 3299-3300.
328. Deng, L., et al., *Electrochemiluminescence detection of NADH and ethanol based on partial sulfonation of sol-gel network with gold nanoparticles*. *Biosensors and Bioelectronics*, 2009. **24**(7): p. 2273-2276.
329. Chen, X.-m., et al., *Recent advances in electrochemiluminescent enzyme biosensors*. *TrAC Trends in Analytical Chemistry*, 2011. **30**(5): p. 665-676.
330. Belenky, P., K.L. Bogan, and C. Brenner, *NAD⁺ metabolism in health and disease*. *Trends in biochemical sciences*, 2007. **32**(1): p. 12-19.

331. Lee, W.-Y., *Tris (2, 2'-bipyridyl) ruthenium (II) electrogenerated chemiluminescence in analytical science*. *Microchimica Acta*, 1997. **127**(1): p. 19-39.
332. Theorell, H. and J. McKinley McKee, *Mechanism of action of liver alcohol dehydrogenase*. *Nature*, 1961. **192**(4797): p. 47-50.
333. Sanghani, P.C., et al., *Human glutathione-dependent formaldehyde dehydrogenase. Structures of apo, binary, and inhibitory ternary complexes*. *Biochemistry*, 2002. **41**(35): p. 10778-86.
334. Morgan, M.Y. and J.A. Levine, *Alcohol and nutrition*. *Proceedings of the Nutrition Society*, 1988. **47**(2): p. 85-98.
335. Park, J.-K., et al., *Determination of breath alcohol using a differential-type amperometric biosensor based on alcohol dehydrogenase*. *Analytica chimica acta*, 1999. **390**(1-3): p. 83-91.
336. Kanoh, Y., et al., *Structural insight into glucose dehydrogenase from the thermoacidophilic archaeon *Thermoplasma volcanium**. *Acta crystallographica. Section D, Biological crystallography*, 2014. **70**(Pt 5): p. 1271-1280.
337. Martin, A.F. and T.A. Nieman, *Glucose quantitation using an immobilized glucose dehydrogenase enzyme reactor and a tris (2, 2'-bipyridyl) ruthenium (II) chemiluminescent sensor*. *Analytica chimica acta*, 1993. **281**(3): p. 475-481.
338. Guo, G., Q. Chen, and X. Chen, *Electrochemiluminescence glucose biosensor based on glucose dehydrogenase functionalized Ru (bpy) 3 2+ doped silica nanoparticles*. *Science China Chemistry*, 2011. **54**(11): p. 1777-1781.
339. Spriet, L.L., R.A. Howlett, and G.J. Heigenhauser, *An enzymatic approach to lactate production in human skeletal muscle during exercise*. *Medicine and science in sports and exercise*, 2000. **32**(4): p. 756-763.
340. Suzuki, M. and H. Akaguma, *Chemical cross-talk in flow-type integrated enzyme sensors*. *Sensors and Actuators B: Chemical*, 2000. **64**(1-3): p. 136-141.
341. Suman, S., et al., *Development of a lactate biosensor based on conducting copolymer bound lactate oxidase*. *Sensors and Actuators B: Chemical*, 2005. **107**(2): p. 768-772.
342. Trojanowicz, M., et al., *Biosensors based on oxidases immobilized in various conducting polymers*. *Sensors and Actuators B: Chemical*, 1995. **28**(3): p. 191-199.
343. Marzouk, S.A., et al., *A conducting salt-based amperometric biosensor for measurement of extracellular lactate accumulation in ischemic myocardium*. *Analytical chemistry*, 1997. **69**(14): p. 2646-2652.
344. Park, T.-M., et al., *Sol-gel based amperometric biosensor incorporating an osmium redox polymer as mediator for detection of L-lactate*. *Talanta*, 1997. **44**(6): p. 973-978.
345. Haccoun, J., et al., *Reagentless amperometric detection of L-lactate on an enzyme-modified conducting copolymer poly (5-hydroxy-1, 4-naphthoquinone-*

- co-5-hydroxy-3-thioacetic acid-1, 4-naphthoquinone*). Biosensors and Bioelectronics, 2004. **19**(10): p. 1325-1329.
346. Disch, J.S., et al., *Discovery of Thieno[3,2-d]pyrimidine-6-carboxamides as Potent Inhibitors of SIRT1, SIRT2, and SIRT3*. Journal of Medicinal Chemistry, 2013. **56**(9): p. 3666-3679.
347. Allen, M.P. and H.J. Jeong, *Non-instrumented cholesterol assay*. 1992, Google Patents.
348. Anaokar, S., M.J. Crispino, and E.P. Crabtree, *Test strip for determining concentration of multiple analytes in a single fluid sample*. 2008, Google Patents.
349. Fang, C., J. He, and Z. Chen, *A disposable amperometric biosensor for determining total cholesterol in whole blood*. Sensors and Actuators B: Chemical, 2011. **155**(2): p. 545-550.
350. Arya, S.K., et al., *Application of octadecanethiol self-assembled monolayer to cholesterol biosensor based on surface plasmon resonance technique*. Talanta, 2006. **69**(4): p. 918-926.
351. Suman Singh, A.C., B. D. Malhotra, *Preparation and Characterization of an Enzyme Electrode Based on Cholesterol Esterase and Cholesterol Oxidase Immobilized onto Conducting Polypyrrole Films*. Journal of applied polymer science, 2003. **91**(6): p. 3769-3773.
352. M.A. De Paoli, W.A.G., *Electrochemistry, polymers and opto-electronic devices: A combination with a future*. Chemical Society Reviews, 2002. **13**: p. 410-424.
353. S. Yong, W.K., H. Kazuhito, *Hydroxylated and aminated polyaniline nanowire networks for improving anode performance in microbial fuel cells*. Journal of Bioscience and Bioengineering 2011. **112**: p. 63-66.
354. Inzelt, G., *Conducting Polymers-A New Area in Electrochemistry*. Springer. 2008, Berlin.
355. A.M. Kumar, Z.M.G., *In situ electrochemical synthesis of polyaniline/f-MWCNT nano-composite coatings on mild steel for corrosion protection in 3.5% NaCl solution*. Progress in Organic Coating, 2015. **78**: p. 387-394.
356. G.G. Wallace, P.R.T., G.M. Spinks, L.A.P. Kane-Maguire, *Conductive Electroactive Polymers, 3rd edn.*, ed. T.F. Group. 2009, Boca Taton.
357. Hussain, A. and A. Kumar, *Electrochemical synthesis and characterization of chloride doped polyaniline*. BULLETIN OF MATERIALS SCIENCE, 2003. **26**: p. 329-334.
358. B.B. Berkes, G.I., E. Vass, *Electrochemical nanogravimetric study of the adsorption of 4-aminoindole and the surface layer formed by electrooxidation in aqueous acid media*. Electrochimica Acta, 2013. **96**: p. 51-60.
359. M. Hosseini, M.M.M., M. Faraji, *Electrochemical fabrication of polyaniline films containing gold nanoparticles deposited on titanium electrode for electro-*

- oxidation of ascorbic acid*. Journal of Material Science, 2010. **45**: p. 2365-2371.
360. M.M. Gvozdenović, B.Z.J., J.S. Stevanović, T.L.J. Trišović, B.N. Grgur, *Electrochemical Polymerization of Aniline, Electropolymerization*. ed. by E. Schab-Balcerzak, ed. InTech. 2011, Rijeka.
361. H. Okamoto, T.K., *Structure and properties of polyaniline films prepared via electrochemical polymerization. I: Effect of pH in electrochemical polymerization media on the primary structure and acid dissociation constant of product polyaniline films*. Polymer, 1998. **39**: p. 4349-4358.
362. G. Fomo, T.T.W., P.G. Baker, E.I. Iwuoha, *Electrochemical deposition and properties of polyaniline films on carbon and precious metal surfaces in perchloric acid/acetonitrile*. International Journal of Electrochemical Science 2016. **11**: p. 10347-10361.
363. M.M. Gvozdenović, B.Z.J., J.S. Stevanović, B.N. Grgur, B.N. Hemijis, *Electrochemical synthesis of electroconducting polymers*. Hemijska Industrija, 2014. **68**: p. 673-684.
364. T. Hatano, A.H.B., M. Takeuchi, N. Fujita, K. Kaneko, H. Ihara, M. Takafuji, S. Shinkai, *Helical superstructure of conductive polymers as created by electrochemical polymerization by using synthetic lipid assemblies as a template*. . Angewandte Chemie International Edition., 2004. **116**: p. 471-475.
365. L.H. Mascaró, A.N.B., L. Micaroni, *Electrochemical synthesis of polyaniline/poly-o-aminophenol copolymers in chloride medium*. International Journal of Electrochemistry, 2011: p. 1-8.
366. M. Magnuson, J.H.G., S.M. Butorin, A. Agui, C. Sâthe, J. Nordgren, A.P. Monkman, *The electronic structure of polyaniline and doped phases studied by soft X-ray absorption and emission spectroscopies*. Journal of Chemical Physics, 1999. **111**: p. 4756-4761.
367. Y. Diamant, E.F., A. Landau, J.P. Lellouche, A. Zaban, *Electrochemical polymerization and characterization of a functional dicarbazole conducting polymer*. Electrochimica Acta, 2003. **48**: p. 507-512.
368. A. Eftekhari, Y.B., *Morphological effects of Ni nanostructures on electropolymerization of aniline*. Journal of applied polymer science, 2011. **122**: p. 1579-1586.
369. G.L. Zhang, J.H.X., X. Pang, H. Yang, Y. Wang, K. Ding, *Preparation and characterization of polyaniline (PANI) doped-Li₃V₂(PO₄)₃*. International Journal of Electrochemical Science, 2012. **7**: p. 830-843.
370. T.H. Le, T.N., L.H. Nguyen, H.B. Nguyen, V.A. Nguyen, T.D. Nguyen, *Electrosynthesis of polyaniline–multiwalled carbon nanotube nanocomposite films in the presence of sodium dodecyl sulfate for glucose biosensing*. . Advances in Natural Science: Nanoscience and Nanotechnology 2013. **4**.

371. N. Bicak, B.K., *Polymerization of aniline by copper-catalyzed air oxidation*. Journal of polymer science, 2006. **44**: p. 6025-6031.
372. R. Yue, F.J., Y. Du, J. Xu, P. Yang, *Electrosynthesis of a novel polyindole derivative from 5-aminoindole and its use as catalyst support for formic acid electrooxidation*. Electrochimica Acta, 2012. **77**: p. 29-38.
373. Y. Lee, S.C., H. Tu, S. Yau, L.L. Fan, Y. Yang, W.P. Dow, *In situ STM revelation of the adsorption and polymerization of aniline on Au (111) electrode in perchloric acid and benzenesulfonic acid*. Langmuir, 2010. **26**: p. 5576-5582.
374. Perc, S., *Electrochemical synthesis of poly(2-iodoaniline) and poly(aniline-co-2-iodoaniline) in acetonitrile*. Journal of applied polymer science, 2003. **89**: p. 1652-1658.
375. G. Nie, T.C., S. Zhang, Q. Bao, J. Xu, *Electrodeposition of poly(indole-5-carboxylic acid) in boron trifluoride diethyl etherate containing additional diethyl ether*. Electrochimica Acta, 2007. **52**: p. 7097-7106.
376. Y. Sahin, A.A., Y.A. Udum, K. Pekmez, A. Yildiz, *Electrochemical synthesis of sulfonated polypyrrole in FSO₃H/acetonitrile solution*. Journal of applied polymer science, 2004. **40**: p. 526-533.
377. J.M. Pringle, J.E., P.C. Howlett, J. Efthimiadis, D.R. MacFarlane, A.B.. Chaplin, S.B. Hall, D.L. Officer, G.G. Wallace, M. Forsyth, *Electrochemical synthesis of polypyrrole in ionic liquids*. . Polymer, 2004. **45**: p. 1447-1453.
378. Mu, S., *Pronounced effect of the ionic liquid on the electrochromic property of the polyaniline film: Color changes in the wide wavelength range*. . Electrochimica Acta, 2007. **57**: p. 7827-7834.
379. M.L. Schwuger, K.S., R. Schomaecker, *Microemulsions in technical processes*. Chem. Rev., 1995. **95**: p. 849-864.
380. K. Imanishi, M.S., Y. Yasuda, R. Tsushima, S. Aoki,, *Solvent effect on electrochemical polymerization of aromatic compounds*. Journal of Electroanalytical Chemistry, 1988. **242**: p. 203-208.
381. C. Lagrost, M.J., J. Tanguy, S. Aeiych, J.C. Lacroix, K.I. Chane-Ching, P.C. Lacaze, *Bithiophene electropolymerization in aqueous media: A specific effect of SDS and β -cyclodextrin*. . Electrochimica Acta, 2001. **46**: p. 3985-3992.
382. M. Kanungo, A.K., A.Q. Contractor, *Studies on electropolymerization of aniline in the presence of sodium dodecyl sulfate and its application in sensing urea*. Journal of Electroanalytical Chemistry, 2002. **528**: p. 46-56.
383. K. Karon, M.L., *Carbazole electrochemistry: A short review*. Journal of Solid State Electrochemistry, 2015. **19**: p. 2601-2610.
384. K. Matyjaszewski, T.D., *Handbook of Radical Polymerization*, ed. Wiley. 2002, Hoboken.
385. R. Lazzaroni, J.R., J.J. Verbist, L. Christiaens, M. Renson, *Electrochemical synthesis and preliminary characterization of poly(thieno[3,2-b]pyrrole)*. Journal of chemical society, Chemical Communications, 1985: p. 999-1000.

386. V. Gupta, N.M., *Large-area network of polyaniline nanowires prepared by potentiostatic deposition process*. . Electrochemistry Communications, 2005. **7**: p. 995-999.
387. J. Heinze, B.A.F.-U., S. Ludwigs, *Electrochemistry of conducting polymers persistent models and new concepts*. Chemical Reviews, 2010. **110**: p. 4724-4771.
388. Korent, A., et al., *A Correlative Study of Polyaniline Electropolymerization and its Electrochromic Behavior*. Journal of the Electrochemical Society, 2020. **167**.
389. S. Yong, W.K., H. Kazuhito, *Hydroxylated and aminated polyaniline nanowire networks for improving anode performance in microbial fuel cells*. . Journal of Bioscience and Bioengineering, 2011. **112**: p. 63-66.
390. M.K.L. Coelho, J.D.F.G., A.T.M. Da Silva, C.R.T. Tarley, K.B. Borges, A.C. Pereira, *Development and application of electrochemical sensor based on molecularly imprinted polymer and carbon nanotubes for the determination of carvedilol*. . Chemosensors, 2016. **4**: p. 1-15.
391. S. Nambiar, J.T.W.Y., *Conductive polymer-based sensor for biomedical application*. Biosens. Bioelectron., 2011. **26**: p. 1825-1832.
392. P.N. Bartlett, J.M.C., *Journal of Electronalytical Chemistry*. 362, A review of the immobilization of enzyme in electropolymerized films.: p. 1-12.
393. Cosnier, S., *Biosensors based on electropolymerized films: New trends*. . Anal. Bioanal. Chem., 2003. **377**: p. 507-520.
394. Cosnier, S., *Recent advances in biological sensors based on electrogenerated polymers: A review*. . Anal. Lett., 2007. **40**: p. 1260-1279.
395. M. Gerard, A.C., B.D. Malhotra, *Application of conducting polymers to biosensors*. Biosens. Bioelectron., 2002. **17**: p. 345-359.
396. R. Saraswathi, M.G., B.D. Malhotra, *Characteristics of aqueous polycarbazole batteries*. Journal of applied polymer science, 1999. **74**: p. 145-150.
397. T. Kawai, T.K., S. Wang, K. Yoshino, *Secondary battery characteristics of poly(3-alkylthiophene)*. . Jap. J. Appl. Phys., 1990. **29**: p. 602-605.
398. D. McQuade, A.E.P.T., T.M. Swager, *Conjugated polymer-based chemical sensors*. Chem. Rev., 2000. **100**: p. 2537-2574.
399. Gertrude Fomo, T.W., Usisipho Feleni, Priscilla Baker, and Emmanuel Iwuoha, *Electrochemical Polymerization*. Functional Polymers, 2019: p. 105-131.
400. D. Albrecht, T.W.J., *Luminol-enhanced chemiluminescence induced in peripheral blood-derived human phagocytes: obligatory requirement of myeloperoxidase esocytosis by monocytes*. Journal of leukocyte biologi, 1928.
401. Hajime. Obata, H.K., and Eiichiro. Nakayama, *Automated determination of iron in seawater by chelating resin concentration and chemiluminescence detection*. Anal. Chem., 1993. **65**: p. 1524-1528.
402. Chen, G.-F.Z.-Y., *Studies of polyluminol modified electrode and its application inelectrochemiluminescence analysis with flow system*. Analytica Chimica Acta, 2000. **419**: p. 25-31.

403. Leca-Bouvier, A.S.L.c.J.B.B.a.D., *Electrogeneration of polyluminal and chemiluminescence for new disposable reagentless optical sensors*. Anal Bioanal Chem, 2008. **390**: p. 865-871.
404. Ching Hao Wang, a.S.M.C.a.C.M.W., *Co-immobilization of polymeric luminol, iron(II) tris(5-aminophenanthroline) and glucose oxidase at an electrode surface, and its application as a glucose optrode*. The analyst 2002. **127**(11): p. 1507-1511.
405. Sassolas, A., L.J. Blum, and B.D. Leca-Bouvier, *New electrochemiluminescent biosensors combining polyluminal and an enzymatic matrix*. Anal Bioanal Chem, 2009. **394**(4): p. 971-80.